UNIVERSIDAD COMPLUTENSE DE MADRID
FACULTAD DE ÓPTICA Y OPTOMETRÍA

TESIS DOCTORAL

Aberraciones cromáticas, monocromáticas y diseños multifocales: interacción e impacto en la visión

Chromatic and monochromatic aberrations and multifocal designs: interaction and impact on vision

MEMORIA PARA OPTAR AL GRADO DE DOCTORA

PRESENTADA POR

Clara Benedí García

DIRECTORES

Susana Marcos Celestino
María Viñas Peña

Madrid

UNIVERSIDAD COMPLUTENSE DE MADRID
FACULTAD DE ÓPTICA Y OPTOMETRÍA

TESIS DOCTORAL

Aberraciones cromáticas, monocromáticas y diseños multifocales: interacción e impacto en la visión

MEMORIA PARA OPTAR AL GRADO DE DOCTOR

PRESENTADA POR

Clara Benedí García

DIRECTOR

Susana Marcos Celestino
María Viñas Peña

CHROMATIC AND MONOCHROMATIC ABERRATIONS AND MULTIFOCAL DESIGNS: INTERACTION AND IMPACT ON VISION

Aberraciones cromáticas, monocromáticas y diseños multifocales: interacción e impacto en la visión

Memoria presentada para optar al grado de Doctor en Óptica por la Universidad Complutense de Madrid por:

Clara Benedí García

Dirigida por:

Susana Marcos Celestino

María Viñas Peña

Laboratorio de Óptica Visual y Biofotónica
Instituto de Óptica "Daza de Valdés"
Consejo Superior de Investigaciones Científicas

Facultad de Óptica y Optometría
Universidad Complutense de Madrid

A mis padres, Angelines y Luciano, y a mi hermano, Daniel

Cambiar de respuesta es evolución. Cambiar de pregunta es revolución.
Jorge Wagensberg

72kilos.com

Acknowledgments

Dicen que es de bien nacidos, ser agradecidos. Y yo he llegado a este día gracias a mucha gente. Estoy escribiendo estas palabras como acompañante en una habitación de hospital, y después de todas las veces que he pisado una durante los años de mi tesis, cobra especial importancia agradecer a todas las personas con las que he compartido este tiempo, que me han ayudado, acompañado, aguantado y hecho feliz.

Empezaré por mis directoras, Susana Marcos y María Viñas.

Recuerdo el día que conocí a Susana. Me enseñó los laboratorios y yo sólo podía pensar: "Cómo puede estar todo esto en un sótano y nadie nos lo ha contado antes. ¡Qué barbaridad!". Ese día se me abrió un mundo nuevo y comenzó la aventura. Desde entonces, formar parte de Viobio me ha permitido aprender un montón de cosas, estar en contacto con los últimos avances en la óptica visual e incluso conocer nuevos lugares y culturas (algunas sin salir de la 3ª planta). Gracias, Susana, por acogerme en un grupo tan enriquecedor.

María, gracias por todos tus consejos y tu tiempo, siempre sacando un hueco para ayudar por muy hasta arriba que estés y gracias por pensar en mí en tantos proyectos, como el libro o el área de mujeres. Hemos compartido mucho y de ti nunca se deja de aprender tanto dentro como fuera del laboratorio.

Y gracias también al resto de gente de Viobio.

Magic, la de horas que hemos compartido a oscuras. Si te cansas de la ciencia y decides montar una pastelería, avísame que yo iré la primera. Gracias tus detalles y por tu bondad. Y resto del AO-Team, Carmen, Shrilekha, Ana y Merche, por todas las veces que me habéis ayudado, y Carlos, siempre con ideas para nuevos análisis. Dani, de pequeña solía decir "mi papá lo arregla todo, todo y todo". No sabes cuántas ves he pensado en esa frase hablando contigo: siempre una idea, una solución. Menudo crack eres. Nohelia y Elena, ayudando con todos los papeles y aguantando cada vez que hago mal el 14A o el 16B…

Elena, la coherencia y la cordura del pasillo. La que se cree que mañana estará mala. La que me trae vino a casa. La chica culta que empezó con Roadl Dahl. La fan de los pingüinos, pero no de los pandas. Gracias por no sacar esa silla de tu despacho. Has llegado para quedarte. Edu, empezamos en el despacho mano a mano y el día que te cambiaste, nos quedamos en silencio. Aunque nunca nos encontraremos en Zaragoza, me siento orgullosa de ser tu amiga. Xoana, que me descubriste las vacas blancas con manchas negras, gracias por tenderme la mano cuando he necesitado levantarme. Víctor, te conocí chipado en Alaska y aunque te gano con la canoa y en boxeo, en ciencia eres una bala, ¡¡keep paling!! 🤗

Y resto de gente del VioBio, ¡¡¡un millón de gracias por dejaros torturar en el AO!!! James, Rocío y sus mensajes de ánimo, Alberto y su "dime si te puedo ayudar", Andrés, Geethika, Andrea, Lupe, Pilar, Amal, Enrique, Lucie y un largo etc que seguro que me dejo.

Carlos, que nos encontramos a mitad de este camino y a poco te gano. Entre tupper y tupper hablamos de burpees y planos conjugados. Gracias por tu ingenio, que tantas veces me ha ayudado.

Quiero agradecer al IOSA por todas las oportunidades que me ha brindado de hacer tantas cosas bonitas. Hemos organizado charlas, mesas redondas, hemos ido a coles, museos, hospitales, plazas de pueblos… pero, sobre todo, hemos despertado la curiosidad en muchos niños y más de un padre. Hemos currado mucho pero también no llevamos grandes recuerdos y muchas celebraciones. Y al IOSA lo hacen sus gentes: James, Rocío, Andrés, María, Mario, Sara, Víctor, Francesca, Carmen, Pilar, Carlos, Ana, Xoana, Juan Luis, Iván, Merche y un larguísimo etc.

Me quiero acordar también de los que pasaron por el instituto. Mario, la persona más graciosa de Tetuán. Aunque hemos acabado siendo vecinos, también has sido amigo en la distancia. Muchas muchas muchas gracias por tantas cosas. Miriam, la primera persona con la que me arremangué en el laboratorio, de ti aprendí mucho. Iván, la de cañas y chismes que hemos compartido, y espero que aún nos queden muchas más!! Pablo, alguna vez me has dicho que eres el abuelo cebolleta. Ni confirmo ni desmiento, pero diré que me encanta hablar contigo y me encantas tú (y tu familia). Vero, me gusta mucho que seas mi vecina y tus frases random porque patatas. Francesca, no cambies esa caña que le metes a Juanlu. Aishu y Meng Chan, que os arrastré a Zaragoza. Tracy, how could I forget you! I hope to visit you soon.

Gracias también a esos profesores motivantes que he tenido al principio del camino, especialmente Amparo y Jorge, y por los que llegué al punto de partida.

No puedo olvidarme de Amanda y Marina. Que estáis cada una en un sitio, pero siempre a una llamada de teléfono. Las dos me habéis aguantado mucho, a veces sin entender muy bien de qué iba la historia. Gracias a las dos, porque sois la encarnación de la palabra amistad.

Y, por último, mi familia. A mis padres tengo muchísimo que agradecer. Vosotros habéis sido ejemplo durante toda mi vida de trabajo, constancia, curiosidad, inquietud. Gracias por todos los sacrificios que habéis hecho para darme siempre lo mejor. Y mi tato, que eres mi hermano pequeño, pero yo de mayor quiero ser como tú. Sin vuestro apoyo (y soporte técnico), esto no hubiera sido posible.

Funding

The work performed in this thesis would have not been possible without the funding received from public and private institutions.

- Research Collaboration Agreement between Essilor International SA and IO-CSIC "New insights into vision under induced astigmatism". 01/06/2015 – 31/12/2016. IP: Susana Marcos.

- ERC Advanced Grant. Bio-inspired optical corrections of presbyopia. Ref. 294099. 01/05/2012 – 31/05/2018. IP: Susana Marcos.

- Master Clinical Research Agreement between Johnson & Johnson Vision Care, Inc. and IO-CSI. 01/02/2016 - 31/10/2020. IP: Susana Marcos.

- FIS2017-84753-R. Nuevas tecnologías ópticas para entender y tratar la miopía. Funding body: Ministerio de Economía y Competitividad. 01/01/2018 - 31/12/2020. IP: Susana Marcos.

Keywords

Aberrations
Aberrometry
Accommodation
Adaptation
Adaptive Optics
Astigmatism
Blur
Cataract
Chromatic Aberrations
Crystalline Lens
Cuvette
Deformable Mirror
Hartmann Shack
HOAs
Intraocular lens
Laser
LCA
Matlab
Monochromatic Aberrations
Neural adaptation
Optical quality
Optics
Optics
Optometry
Phase Plate
Presbyopia
Presbyopia Correction
PSF
Psychophysics
Retinal Image
SimVis
SLM
Visual Acuity
Visual Perception
Visual Simulators
Wave Aberrations
Wavefront
Zemax
Zernike Polynomials

Summary of the thesis

Introduction

An important part of the information that we receive from the world is through the sense of vision: the eye projects images on the retina, which transforms them into nerve impulses that reach the neuronal cortex, where these impulses are interpreted. However, the images projected onto the retina are not perfect, as they are affected by diffraction, scattering, and aberrations, which degrade contrast and decrease the resolution limit of the eye.

To understand the effect of aberrations on vision, it is necessary to develop technologies and experiments that allow objectively and subjectively assess their interaction. In this sense, Adaptive Optics (AO) has played an important role in increasing our knowledge about the neural processes of vision, since AO can be used to measure, correct and induce aberrations. Understanding what role aberrations play and what their impact is on vision will help to develop better correction designs for the eye.

The manipulation of the wavefront using AO also allows to induce a certain visual correction, so it can be used as a basis for visual simulators. As AO allows studying a new lens design or comparing across different lens designs even before they are manufactured, this is an excellent tool to test and improve optical corrections before they are implanted in the eye of a patient. Different technologies including deformable mirrors (DM), spatial light modulators (SLM), or temporal multiplexing by an optotunable lens (SimVis), are currently being validated and launched into the clinical practice.

In this thesis, AO technologies have been implemented and used both to study the effect of aberrations and to cross-validate different simulator modalities.

Methods

In this thesis, we have used two different AO based systems, further developed from set-ups designed and developed in previous projects in the laboratory. In particular, a new channel has been designed, implemented and validated in both systems to project intraocular lenses with different powers to the patient's pupil, thus increasing their simulation capabilities. Custom-developed psychophysical tools have been implemented to test visual performance and visual perception under different combinations of monochromatic and chromatic aberrations, astigmatism, and presbyopic corrections.

AO systems have been used in this thesis, on the one hand, to explore some aspects of the basic fundamentals of vision. Specifically, the interaction of chromatic and monochromatic aberrations and their perception have been studied through psychophysical experiments. The blurring discrimination threshold has also been measured, using various blurring pedestals as a reference, using convoluted images and optically blurred images. Lastly, the perceptual impact of inducing astigmatism has been studied in presbyopic subjects, who are naturally exposed to astigmatism due to the

induced by its correction in progressive lenses, and it has been compared with a group with this previous visual experience.

AO has also been used as a platform for different visual simulation technologies. In this sense, an SLM has been compared objectively (via through focus (TF) images of a Snellen letter E) and subjectively (through a visual acuity (VA) test) with surfaces specifically manufactured (phase plates) with six different multifocal designs. On the other hand, two commercially available IOLs were simulated using SLM and SimVis technologies, and compared with the real lens immersed inside a tray and projected to the patient's pupil. Again, the comparison was made objectively and subjectively, using through focus one-step and double-pass images series, as well as through focus VA test respectively.

Finally, the new cuvette channel implemented was validated objectively (TF of one pass) and subjectively (with a VA test) with three commercial designs of intraocular lenses.

Results and Conclusion

In this thesis, performing different experiments in an AO environment has allowed us to gather knowledge on the interaction and influence of optical aberrations.

The presence of monochromatic ocular aberrations produces a lower impact on vision than that corresponding defocus due to chromatic aberration, influenced by neural adaptation mechanisms. It has been found that monochromatic aberrations play also a role in blur discrimination, which is highly related to the optical quality of the subject. The influence of a particular monochromatic aberration, astigmatism, has been explored in presbyopes wearing progressive lenses and it was found that they are adapted to astigmatism induced by their visual correction, experimenting a lower reduction of VA when astigmatism is induced as well as a shift of best focus upon induced astigmatism.

Finally, different AO based on active optical technologies have been tested as visual simulators. Perceived visual quality was similar when comparing the same optical correction in an SLM and phase plates. Also, the performance of visual simulators has been compared with the real IOL on the same individual patients and finally, a newly implemented channel of a non-0D cuvette has been implemented and validated on-bench and *in-vivo*.

Summary of the thesis in Spanish

Introducción

Una importante parte de la información que recibimos del mundo lo hacemos a través del sentido de la visión: el ojo proyecta las imágenes en la retina, la cual las transforma en impulsos nerviosos que llegan hasta el córtex neuronal, donde se interpretan estos impulsos. Sin embargo, las imágenes proyectadas en la retina no son perfectas, ya que están afectadas por la difracción, la dispersión y las aberraciones, que degradan el contraste y reducen el límite de resolución del ojo.

Para entender el efecto de las aberraciones en la visión es necesario desarrollar tecnologías y experimentos que permitan valorar objetiva y subjetivamente su interacción. En este sentido, la Óptica Adaptativa (AO) ha jugado un papel importante en el incremento de nuestro conocimiento acerca de los procesos neuronales de la visión, ya que la AO se puede utilizar para medir, corregir e inducir aberraciones. Comprender qué papel juegan las aberraciones y cuál es su impacto en la visión, ayudará a desarrollar mejores diseños de corrección para el ojo, sin embargo, aún no se entiendo completamente.

La manipulación del frente de onda mediante AO permite, además, inducir una cierta corrección visual, por lo que se puede utilizar como base de simuladores visuales. Estudiar un nuevo diseño o comparar varios diseños entre ellos antes incluso de que sean fabricados, plantea la AO como una excelente herramienta para probar y mejorar una corrección antes de que sea implantada. Para ello, diferentes tecnologías como los espejos deformables, los Moduladores Espaciales de Luz (SLM), la multiplexación temporal inducida por una lente optoajustable (SimVis), están siendo en la actualidad validados y lanzados a la práctica clínica.

En esta tesis se ha utilizado la AO tanto para estudiar el efecto de las aberraciones como comparar diferentes simuladores visuales.

Métodos

Para el desarrollo de esta tesis, se han utilizado dos sistemas de AO diferentes, ambos diseñados y desarrollados en proyectos anteriores en el laboratorio y con diferentes capacidades de simulación. Además, se ha diseñado, implementado y validado en ambos sistemas un nuevo canal para proyectar lentes intraoculares con diferentes potencias a la pupila del paciente, incrementando así sus capacidades de simulación.

Los sistemas de AO se han utilizado, por un lado, para explorar algunos aspectos de los fundamentos básicos de la visión. En concreto, se ha estudiado la interacción de las aberraciones cromáticas y monocromáticas y su percepción a través de experimentos psicofísicos. También se ha medido el umbral de discriminación del emborronamiento,

con varios pedestales de emborronamiento como referencia, a través de imágenes convolucionadas e imágenes emborronadas ópticamente. Por última, se ha estudiado el impacto perceptual de inducir astigmatismo en sujetos présbitas, que están naturalmente expuestos al astigmatismo debido al inducido por su corrección en lentes progresivas, y se ha comparado con un grupo son esta experiencia visual previa.

La AO también se ha utilizado como plataforma para diferentes tecnologías de simulación visual. En este sentido, se ha comparado objetiva (mediante imágenes a través del foco (TF) de la letra E de Snellen) y subjetivamente (mediante un test de agudeza visual (AV)) un Modulador Espacial de Luz con superficies específicamente fabricadas con seis tipos diferentes de diseños. Por otro lado, se compararon dos diseños comerciales de lentes intraoculares en el SLM y con el SimVis, con la lente real inmersa dentro de una cubeta y proyectada a la pupila del paciente. Nuevamente la comparación se hizo objetiva y subjetivamente, mediante imágenes TF de un paso y de doble paso y mediante un test de AV respectivamente.

Finalmente, el nuevo canal de cubeta implementado fue validado objetiva (con imágenes TF de un paso) y subjetivamente (con un test de AV) con tres diseños comerciales de lentes intraoculares.

Resultados y conclusión

En esta tesis, la realización de diferentes experimentos en un entorno de AO nos ha permitido mejorar el conocimiento sobre la interacción e influencia de las aberraciones oculares.

La presencia de aberraciones monocromáticas produce un menor impacto visual subjetivo que el desenfoque debido a la aberración cromática, influenciada por los mecanismos de adaptación neuronal. Se ha descubierto que las aberraciones monocromáticas también juegan un papel en la discriminación de borrosidad, que está muy relacionada con la calidad óptica del sujeto. La influencia de una aberración monocromática en particular, el astigmatismo, ha sido explorada en présbitas que usan lentes progresivas y se encontró que están adaptados al astigmatismo inducido por su corrección visual, experimentando una menor reducción de AV cuando se induce astigmatismo, así como un desplazamiento del mejor foco hacia el astigmatismo inducido.

Por otro lado, los sistemas de AO se han probado como simuladores visuales. Se ha demostrado una alta correlación en la calidad visual percibida comparando la misma corrección visual en un modulador espacial de luz y placas de fase. Además, se ha comparado el rendimiento de los simuladores visuales con una LIO real en los mismos pacientes y, finalmente, se ha implementado un nuevo canal de cubeta para lentes diferentes a 0D y se ha validado en el banco óptico e *in vivo*.

Table of Contents

Chapter 1. Introduction

The eye is an optical instrument that projects scenes of the visual world onto the retina. However, the human eye is far from being a perfect optical system, and, therefore, diffraction, scattering and ocular aberrations obscure the images projected on the retina. Retinal images are blurred by ocular aberrations, which reduce image contrast, limiting the available spatial frequencies for more visual processing levels, and greatly impacting the visual function.

Multiple technologies have been developed in the last years that allow the measurement and correction of ocular aberrations. In consequence, important knowledge has been obtained on the contribution of the different components of the eye to the degradation of image quality. Its understanding and correction are essential to explore the limits of human spatial vision and to design and optimize new alternatives of correction of presbyopia and more complex individualized refractive corrections. However, the effects of the ocular aberrations on vision are not yet well understood.

In the first chapter of this thesis, a brief revision of the state-of-the-art of the field of research and technologies, the goals of the thesis, motivation and hypothesis are presented. In particular, we revise the human visual process, the optical quality of the eye and its measurement, and the relation between retinal image and perceived image quality. Presbyopia, the gradual loss of capability of the crystalline lens of the eye to focus dynamically is briefly discussed, as some of the applications in this thesis address that condition.

1.1. Motivation

The fact that the retinal image is degraded by both chromatic and monochromatic aberrations is well known [1]–[3]. Also, work from our laboratory and others have shown that the visual system is naturally adapted to its optical imperfections [4]–[7]. However, there are still open questions regarding the interaction of chromatic and monochromatic aberrations and their impact of perception. Besides the fundamental understanding of the optics and perception, addressing questions such as the visual effect of optical aberrations, neural adaptation and the role of previous visual experience has also important practical implications in the future design of optical corrections, in particular presbyopic corrections.

One of the goals of this thesis is the study of the visual adaptation to the blur caused by monochromatic aberrations (i.e. astigmatism) by chromatic aberrations, and by interactions between high order monochromatic aberrations. This thesis makes use of a custom-developed Adaptive Optics system and dedicated psychophysical experiments to address these questions.

Further developments of visual simulators, including the implementations in an Adaptive Optics platform developed and validated in this thesis are critical in the consolidation of visual simulating technologies in the clinic. These systems allow giving patients the experience of vision with different corrections (for example progressive lenses or multifocal IOLs), therefore holding promise as a useful tool to select the most suitable correction of a patient.

Finally, the thesis aim at demonstrating the capability of these systems to simulate different corrections, from commercial IOL designs (i.e. multifocal or extended-depth-of-focus) to prospective designs not yet manufactured, both in on-bench and *in vivo* in patients. The validation channel (IOL in cuvette) developed in this thesis is a fundamental piece in the validation pipeline of the simulating technologies of real lenses.

1.2. The visual process

There is a long and complex pathway from the light entering the eye until the information is processed by the brain. The visual process comprises three differentiated stages: optical, retinal and cortical [8]. The light arriving from an object enters the eye and is focused on the retina, where the light is transformed on neural signals, which arrive at the visual cortex of the eye through the nerve optic and optical radiation, where they are perceived and interpreted. The following sections describe in detail the three stages of the visual process.

1.2.1. The optical stage of vision

The first stage of vision if the optical projection of the image onto the retina. A schematic diagram of the optics of the eye and the optical stage of the visual process is shown in Figure 1.1.

The light enters the eye through the pupil, the limiting aperture defined by the iris, which has the ability to contract and expands in order to modify the pupil size, in response to the amount of light arriving at the eye.

The light is focused on the retina by the two lenses of the eye: cornea and crystalline lens. The cornea is an inhomogeneous cellular and fibrillar structure, composed of 5 layers that nourish it and give support (Epithelium, the Bowman's Membrane, the Stroma, the Descemet's membrane and the Endothelium) and it is covered by the tear film, which preserves corneal optical proprieties. The cornea is around 20 D while the crystalline lens, with the shape of a biconvex lens, is around 40 when it is relaxed, thus the eye has a total power of 60D [3]. In an emmetropic eye, the power of the optical system is such that its focal length matches the axial length of the eye (around 23mm). In addition, the crystalline lens is suspended by the ciliary muscle, which gives it the capability of changing its shape to focus objects dynamically, in a process known as accommodation.

With age, the crystalline lens suffers changes that prevent its functionality. By around 45 years old the elasticity of the crystalline lens is highly reduced, resulting in a loss of the accommodation capacity (presbyopia). Generally, later in life, the proteins of the crystalline lens denaturalize, resulting in a loss of transparency (cataract). Whereas presbyopia can be compensated with refractive corrections, cataracts must be removed with surgery and the crystalline lens is, therefore, replaced by an intraocular lens (IOL).

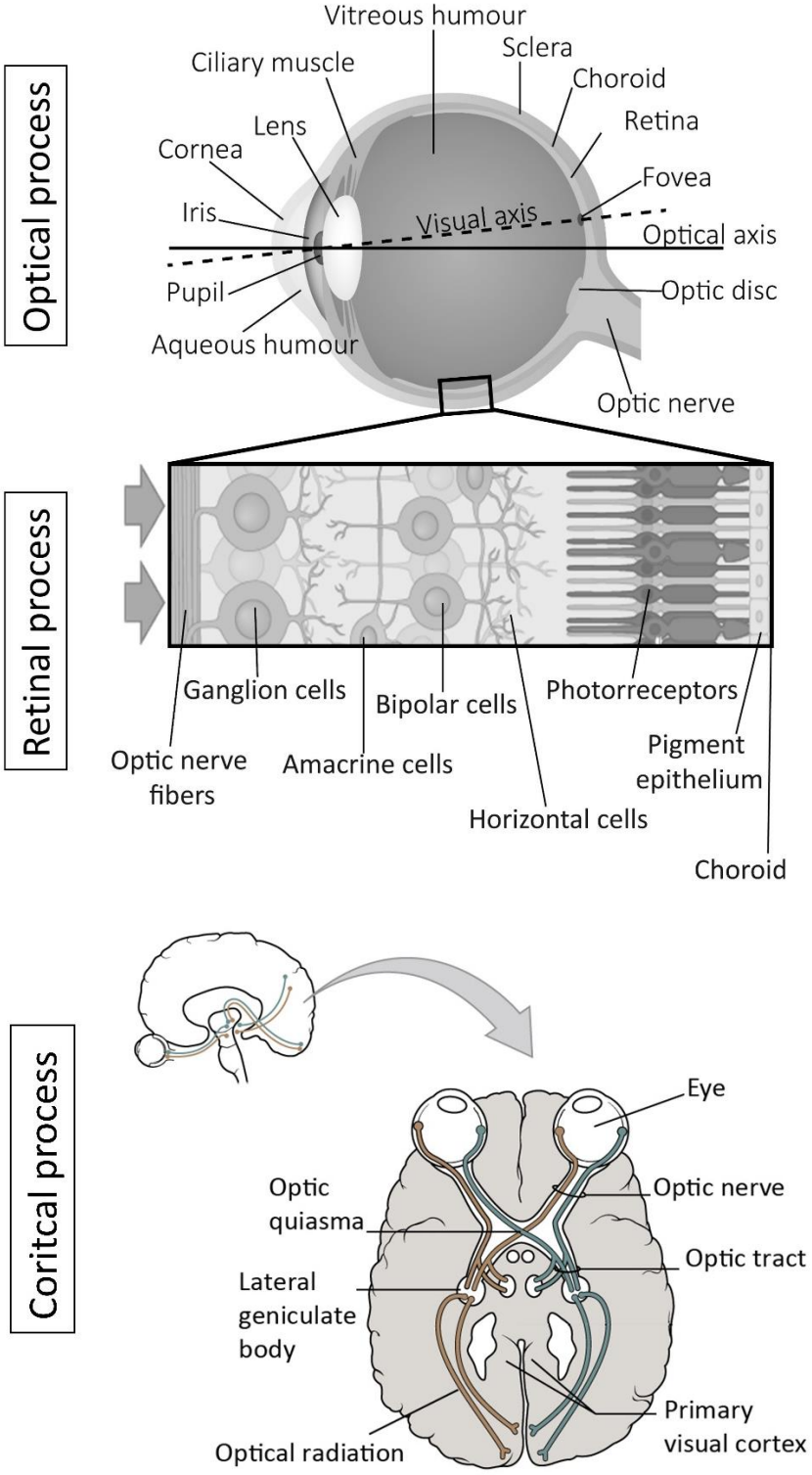

Figure 1.1. Schematic drawings of the three steps of vision process: optical process, retinal process and of a section of the human eye and an enlargement of the layers of the retina. Arrows indicate light direction. Visual pathway from the retina to the primary visual cortex. Adapted from [9]–[11]

1.2.2. The neurosensory retina

In the second step, the retina transforms light into nerve impulses. In a healthy and emmetropic eye, rays coming from an object, focus on the photoreceptors of the retina, which is directly connected to the brain through the optical nerve. The retina is composed of multiple layers [12] including the retinal epithelium layer and nervous-sensory layers, which comprise among many others bipolar and ganglion layer cells. The neural processing involves neural signal transduction and some forms of image processing. A simplified schematic diagram of the retina is shown in figure 1.1.

Bipolar cells are in the intermediate zone of the retina and connect the photoreceptors with the ganglion cells. Ganglion cells form the superior layer of the retina and its axons, the optical nerve. In the retina, there is a second group of cells, horizontal and amacrines, which serve as support to the rest of the layers.

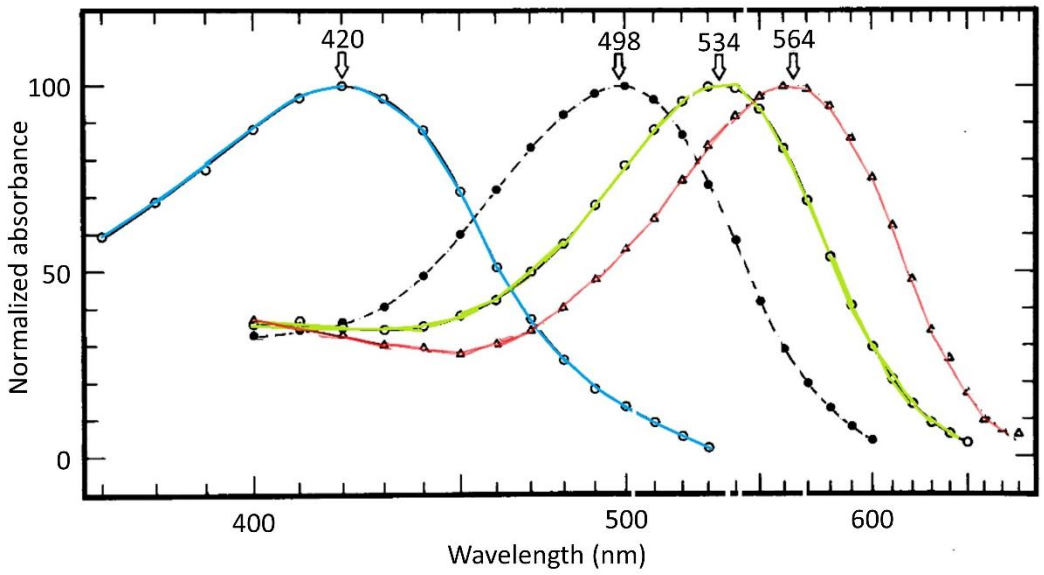

Figure 1.2. Normalized absorbance of rood cells (R) and cone cells (S, M & L). Modified from [13]

The neuroepithelial layers of the retina are formed by photoreceptors cells, which are the light-sensitive cells. There are two types of photoreceptors: rods and cones. Rods are cells sensitive to dark light while cones are sensitive to wavelengths. There are three types of cones: the S cones (short-wavelength, blue) with a sensitivity peak at 420 nm, the M cones (medium-wavelength, green) with a peak at 531 nm, and the L cones (long-wavelength, red) with a peak at 588 nm. Figure 1.2. shows the absorbance of the rods and the three types of cones, normalized to 100. The distribution of cones and rods on the retina is highly inhomogeneous: the fovea (lying around 5 degrees from the optical axis) is the area with the highest visual resolution containing only cones. In contrast, the density of rods increases towards the periphery, peaking at around 10-17 degrees [14], [15]. In addition, the sensibility of photoreceptors to light varies with the pupil position, being generally highest to rays coming near the center of the pupil (known as Stiles-Crawford effect) [16], [17] [17]. In the retina, there is also a zone, the optic disc, where the axons are collected

to form the optic nerve, and signals travel to higher steps in the visual processing. In the optic disc, there are not cones nor rods, thus, it is a blind zone.

1.2.3. The visual cortex

Once the information is converted into electrical impulses and following some initial processing at the retinal level, it travels to the visual cortex, in the occipital part of the brain, where it undergoes further high-level processing. In the optic chiasm, the nerve fibers from the nasal side of each eye cross between then, therefore the information from the left side of each eye arrives is mapped on the left side visual cortex and vice-versa. Other regions of the brain are also involved in the interpretation of color, movement, orientation, size, shape, motion analysis, pattern and object recognition, and integration of visual information with non-visual pathways and processing [12], [18].

1.3. The optical quality of the eye

It is attributed to Helmholtz one of the most famous cites regarding the optical quality of the eye, with the following quote: ‘‘Now, it is not too much to say that if an optician wanted to sell me an instrument which had all these defects, I should think myself quite justified in blaming his carelessness in the strongest terms, and giving him back his instrument.’’ [19]

Images formed in the retina are affected by diffraction, scattering and aberrations. A wave aberration is the phase departure from the ideal wavefront, as measured at the exit pupil [3]. As a result of those factors, the image of a point source (and therefore any image projected in the retina), is degraded. Aberrations differ across eyes, both in magnitude and distribution, and their pattern is unique to an eye and it changes with age [20]–[22]. A free aberrations system is limited by diffraction.

Aberrations can be mono- and chromatic aberrations. Figure 1.3 shows simulated images affected only by diffraction, and also by monochromatic and chromatic aberrations

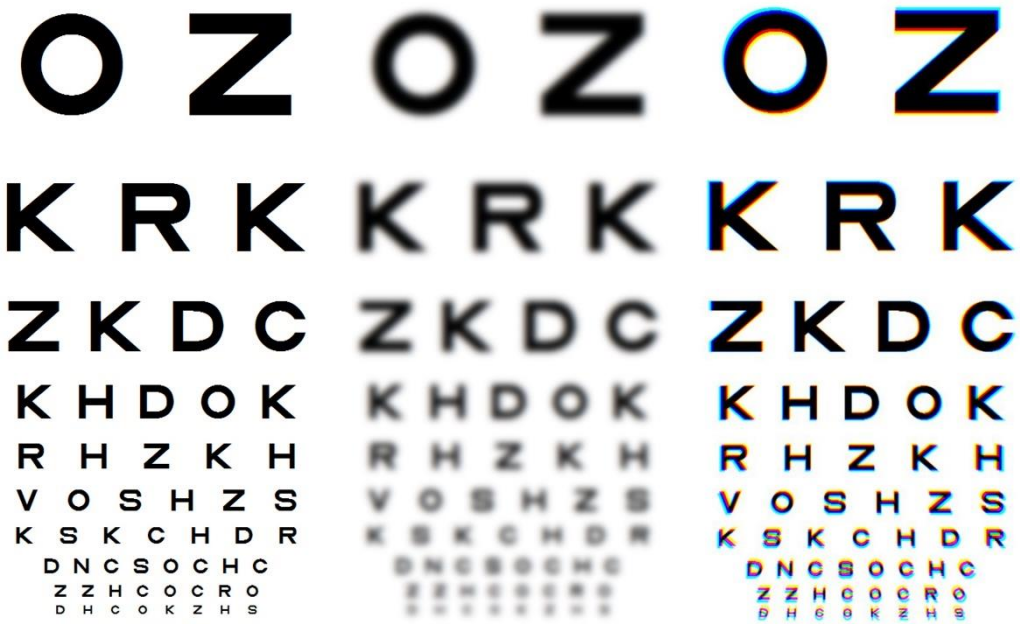

(a) (b) (c)

Figure 1.3. Simulated image projected by an optical system (a) limited by diffraction, (b) affected by monochromatic aberrations and (c) affected by chromatic aberrations. Simulated with photo-kako.com

The next sections describe both, mono- and chromatic aberrations, and the interaction between them, their possible manipulation and metrics used in this thesis to quantify the optical quality of the eye.

1.3.1. Monochromatic aberrations

Monochromatic aberrations affect the image in two ways: reduction of the contrast and limitation spatial frequencies available for further stages of the visual processing.

However, the influence of these effects on visual perception and adaptation to them have been studied. Part of these studies are collected on section 1.4.

Wave aberration can be described mathematically by a sum of simpler polynomials, called Zernike polynomials [23], and multiplied by a certain factor that indicates a weight of each polynomial, as in the following equation:

$$W(x,y) = \sum_{n,m} c_n^m Z_n^m(x,y) \quad [eq.\,1.1]$$

where W(x,y) is the wavefront expressed in Cartesian coordinates, c_n^m is the Zernike coefficient of order n and frequency m and $Z_n^m(x,y)$ are Zernike polynomial terms, also expressed in Cartesian coordinates. Zernike polynomials are an orthonormal basis on circular pupils. In this thesis, it was used the sing and order convention recommended by the Optical Society [24]. Figure 1.4 shows the Zernike polynomials terms up to the 6th order.

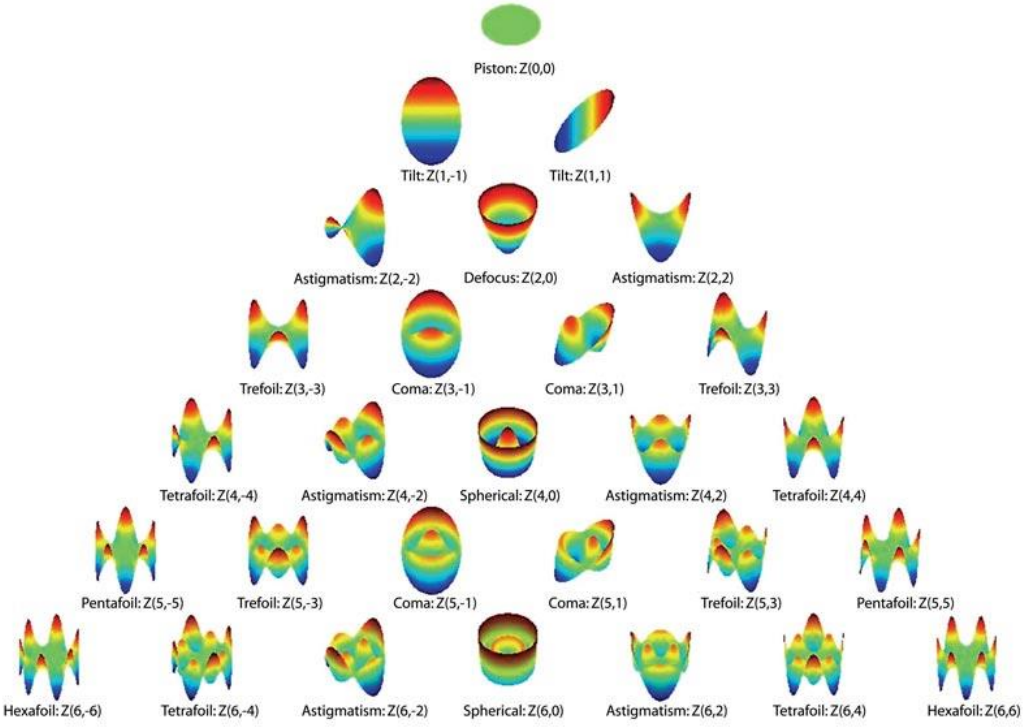

Figure 1.4. Representation of the wavefront of the Zernike polynomials up to 6th order. Source [25]

The optical quality of the eye is often described through the amount of monochromatic aberrations, which can be divided on Low Order Aberrations (LOAs) and Higher Order Aberrations (HOAs).

Second order of Zernike coefficients corresponding to LOAs, which correspond to defocus and astigmatism, and can be compensated with ophthalmic lenses (spectacles, contact

lenses, etc.). These second-order Zernike coefficients can be converted to a sphero-cylindrical prescription in power vector notation using (in a first approximation) equation 1.2 [26]

$$M = \frac{-c_2^0 4\sqrt{3}}{r^2}$$
$$J_0 = \frac{-c_2^2 2\sqrt{6}}{r^2} \qquad [eq.\,1.2]$$
$$J_{45} = \frac{-c_2^{-2} 2\sqrt{6}}{r^2}$$

HOAs also impact the magnitude of manifest refraction. Subjective refraction can be obtained from retinal image quality metrics, for example as the defocus term that maximizes retinal image quality [27].

The optical quality can be quantified using wave aberration metrics (described in section 1.3.5 of this chapter), such as the Root Mean Square (RMS) wavefront error or retinal image quality metrics, such as Visual Strehl [28].

Wave aberrations are measured using aberrometers [29], such as ingoing aberrometry systems based on measurements of ray deviations as the light goes into the eye or outgoing aberrometry systems, based on measurements of the wavefront emerging from the eye. Examples of ingoing aberrometers are the Laser Ray Tracing (LRT) [30], and the Spatially Resolved Refractometer (SRR) [31], while the Hartmann-Shack is an example of outgoing aberrometry [32]. In this thesis, we used a custom-developed Hartmann-Shack wavefront sensor, described below in section 1.5.4.2.

1.3.2. Chromatic aberrations

Natural vision is not monochromatic, given that the eye is sensitive to several wavelengths. Optical systems suffer from chromatic aberration as a result of the dependence of refractive index on the wavelength (dispersion). Chromatic aberrations in the eye were described by the first time by Newton [33]. There are two types of chromatic aberrations: Longitudinal Chromatic Aberration (LCA) and Transverse Chromatic Aberration (TCA).

The LCA refers to the chromatic difference of focus, as short wavelengths (blue) focus in front of long wavelengths (red), as shown in figure 1.5.a [34] and expressed in equation 1.3.:

$$LCA = L\,(\lambda_{Red}) - \,(\lambda_{Blue}) \quad [eq.\,1.3]$$

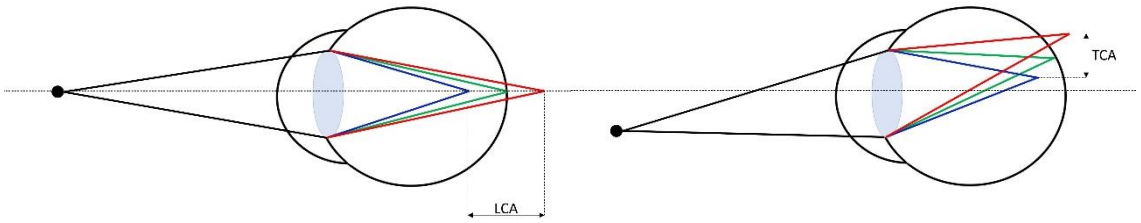

(a) (b)

Figure 1.5. (a) Longitudinal Chromatic Aberration in the eye. (b) Transversal Chromatic Aberration in the eye. Adapted from [3]

Typically, LCA is considered to be around 2 D along with the visible range with subjective techniques. However, this number varies depending on the measurement technique and the spectral range considered. LCA can be measured objectively and subjectively with psychophysical and reflectometric methods respectively. Several studies [34]–[37] report LCA in the eye, with discrepancies arising from differences in the measured spectral ranges, method or sample. Our group reported LCA measured in the same subjects and the same spectral ranges using both objective and subjective techniques and a wide spectral range [38]. LCA was found to be 1.84 D between 450 and 700 nm and 1.52 in the range 480-700 nm, from psychophysical measurements.

Objective measurements (based on HS or double-pass) consistently underestimated psychophysical measurements. In addition, it was demonstrated that the magnitude of LCA was independent of the presence of HOAs and speculated that differences across methods may be due to different spectral reflectivities of the retina's layers. Figure 1.6 shows a review of the estimated LCA in the literature using both psychophysical and reflectometric methods. In both graphs, a theoretical estimation of LCA using a model eye Indiana Chromatic Eye [39],.

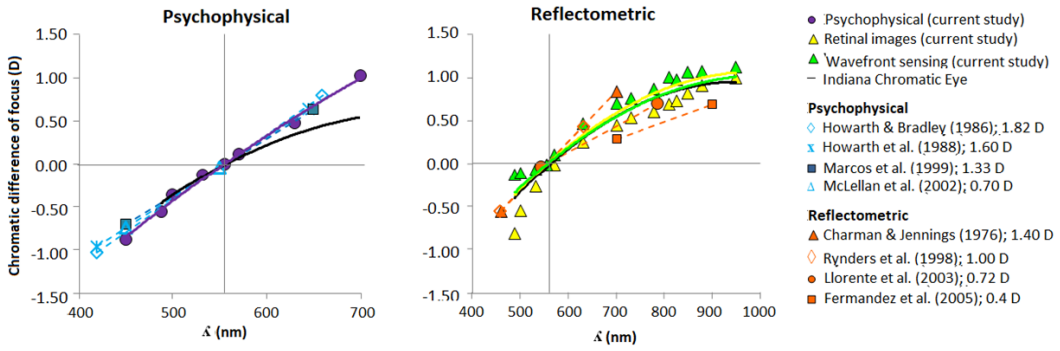

(a) (b)

Figure 1.6. Longitudinal chromatic aberration measured in the eye with two different methods: (a) psychophysical and (b) reflectometric techniques (DP, aberrometry, etc). [38].

Today, measurement of the LCA of the eye has experienced a renovated interest, like lenses with different materials (and different material properties) can modify the native LCA.- and new designs of IOLs (for example diffractive multifocal IOLs) modulate chromatic aberration Perez-Merino and colleagues [40] found statistical differences of focus in two groups of pseudophakic eyes implanted with IOLs of different materials, consistent with the Abbe number of the IOL materials (0.46 and 0.75 D, respectively), in the 532-787 nm range. Previous studies in our group report LCA measurements in. pseudophakic patients implanted with either monofocal IOLs or trifocal diffractive IOLs of hydrophobic and hydrophilic materials [41] [42]

The Transverse Chromatic Aberration (TCA) arises from the misalignment of the optical components, producing a lateral shift for different wavelengths [43]. This effect is represented in figure 1.5.b. TCA is generally measured using psychophysical methods [36], [43]–[45], finding a high variation across subjects and pupil sizes [46]. Recently, Aissati and colleagues found that both HOAs and Stiles-Crawford effect (SCE) interact with the TCA, reducing it in magnitude and changing its orientation [47]. These findings suggest that HOAs, LCA, TCA and SCE data from the patient may be considered in the assessments of the polychromatic image quality.

1.3.3. Interaction between aberrations

Exploring the impact of ocular aberrations is crucial to understanding visual performance and helps to improve optical designs for needed corrections.

Several studies have shown interactions between aberrations of low and high order. HOAs influence the amount of sphere and cylinder required to correct vision [27], [28], [48]–[50]. For example, it has been shown that certain combinations of defocus and spherical aberration provide better retinal quality over defocus alone. These findings bring out the convenience of compensating the average natural spherical aberration of the cornea with aspheric designs of IOL [51]. The impact of the combination of coma and astigmatism has been also studied [52]–[55]. It was found both computationally and experimentally that certain combinations of coma and astigmatism, over astigmatism alone, increase optical quality. These findings are also clinically relevant, as certain types of corrections attempt to correct totally or partially the aberrations of the eye. Numerous literature also demonstrates that the visual effect of manipulating the aberrations of the eye does not depend only on the optics, but also on prior visual experience. For example, the same degraded retinal image may appear to a subject as sharp or blurred depending on the patient's native aberrations. This has been proved clinically relevant in keratoconus patients, where customized contact lenses are being designed to correct substantial amounts of both, astigmatism and coma, in keratoconic eyes [56]. On other hand, it has been shown that the presence of astigmatism shifts the natural perceived best focus [57]–[59], with an influence of the previous visual experience. Understanding the role of these interactions as well as the role of neural adaptation is important in the clinical management with certain presbyopic corrections, such as progressive lenses, which are known to induced coma and astigmatism [60], [61]. In chapter 5 of this thesis, the author explores the adaptation to astigmatism in presbyopic subjects, with the previous visual experience of astigmatism due to progressive lenses.

The combination of monochromatic and chromatic aberration is not additive, and they may interact to improve image quality. The traditional explanation for the relatively low

perceptual impact for LCA, which is theoretically largest at short wavelengths, is attributed to two factors: the paucity of S-cones in the central fovea and the absorption of short wavelength light by the yellowish macular pigment. A previous paper [62] reported that invoking those with respect to M/L cones was large in diffraction-limited eyes (free of monochromatic aberrations) and that the presence of the eye's natural optical aberrations mitigated the differential impact of LCA on optical contrast for S-cones and M/L cones. In fact, optical simulations showed that the combination of natural monochromatic and chromatic aberrations boosted mechanisms may not be necessary and that the optical effect of the latter was minimal. Instead, it was found that, while the optical contrast reduction was produced by LCA in S-cones contrast for blue when the eye was focused in the green compared to an aberration-corrected eye. Aberrated optics, therefore, seemed to act as partial protection of the eye against chromatic blur. The perceptual impact of the interaction between chromatic and monochromatic aberrations has been studied in this thesis, and it is detailed in chapter 3.

Despite the degradation of the optical quality caused by aberrations, observers are not aware of the blur present in their retinal images, reflecting both the sampling properties of retinal neurons and the underlying neural adaptation to the native optical blur [5]. Neural adaptation to retinal blur is explained below in this chapter (section 1.4.2).

1.3.4. Manipulation of ocular aberrations

In the early 1960s, Smirnov introduced for the first time the possibility of manufacturing a lens that corrects the aberrations in the eye, [63]. The first non-military applications of aberration corrections occurred in astronomy, where deformable mirrors couple with ground-based telescopes to correct the effects of atmospheric turbulence. In 1989, Dreher et al. attempted for the first time to measure and correct monochromatic aberrations using an active mirror and provided improved depth resolution retinal images using scanning laser ophthalmoscope (SLO) [64]. Some studies demonstrated optical correction of high order aberrations. Burns et al. demonstrated improved contrast of scanning laser ophthalmoscopy images using phase-plates [65]. Yoon and colleagues [66] proved that the use of phase plates to correct HOAs in normal eye entails a reduction of RMS and increment of VA. The clinical adoption of Shack-Hartmann wavefront sensor to measure eyes wave aberration was first demonstrated in the early 90s [32] was key in the development at the University of Rochester of the first closed-loop adaptive optics systems for ophthalmology which, by means of a deformable mirror, could correct HOAs of the eye and achieve a supernormal vision and visualization of single cells in the human retina [67]. Vargas-Martin et al. [68] used instead of a spatial light modulator and showed that the spatial resolution of the limits the maximum correction attained. Also, changes in the eye optics [69] often place a limit on the efficiency of static corrections. More recently, some studies have presented wavefront aberration correction using computational methods [70]. The use of adaptive optics technologies for improved retinal imaging and visual simulation have expanded over the years, summarized by Marcos et al. in a recent review paper [71].

Correcting aberrations improves visual acuity in a wide range of luminances and both direct and reversed polarity [50], improves the visual performance of various tasks

involving natural images [72]. Several authors [73] have also shown improved contrast sensitivity for both white and monochromatic light when HOAs are corrected, although visual benefit does not appear as large as the optical benefit. Correcting HOAs in highly aberrated eyes (keratoconus) did not show drastic visual improvements in vision [74], suggesting an important role of neural adaptation to the prior visual experience.

While many studies have addressed the correction of high order aberrations, adaptive optics visual simulators are also capable of inducing high order aberrations, as a way to probe the effect of aberrations on vision or neural adaptation to high order aberrations. For example, Artal and colleagues [4] used Adaptive Optics to induced rotated versions of the subject's aberrations, or Sawides et al. induced scaled versions of the native aberrations to investigate the adaptation of visual system is adapted to the eye's own aberrations [5].

Ocular aberrations can be also manipulated to simulate a certain visual correction, for example, corrections aiming at treatment presbyopia (such as multifocal or extended-depth-of-focus lenses). Piers et al. assessed the possible benefits of IOLs with modified spherical aberration profiles simulated in adaptive optics [75]. Vinas et al. [76] mapped various types of refractive multifocal zonal designs (angular and radial), as well as commercial refractive bifocal and diffractive trifocal IOLs using Adaptive Optics [77]. A two-channel simultaneous vision simulator also developed at the Visual Optics and Biophotonics Lab allowed testing the impact of near add on pure simultaneous vision performance [78] or the impact of the ratio of energy in the far and near peaks and near add on neural adaptation to bifocality [79]. Radhakrishnan et al presented a portable binocular visual simulator based on the concept of temporal multiplexing allowing testing binocular presbyopia corrections [80], including bilateral bifocal or trifocal corrections, monovision or modified monovision.

In this thesis, we implemented Adaptive Optics technologies to both probes the impact of aberrations on vision, and to investigate vision with real or prospective optical corrections. A brief introduction to Adaptive Optics for visual testing is presented in section 1.5.4.1 in this chapter

1.3.5. Quantification of the optical quality

Different optical quality metrics can be derived from the measured wavefront aberrations either based directly on the wave aberration (pupillary metrics) or, following some Fourier Optics, on the retinal image quality of the eye [28], [54], [81].

1.3.5.1. Root Mean Square

The Root Mean Square (RMS) is a global metric of the ocular optics. RMS measures the deviation of the wavefront from a perfect wavefront (spherical or plane, for outgoing and incoming aberrometry respectively) and it is calculated following equation 1.4.

$$RMS = \sqrt{\sum_{n,m} {c_n^m}^2} \quad [eq.\ 1.4]$$

where c_n^m is the corresponding Zernike coefficient of order n and frequency m.

1.3.5.2. Retinal Image quality metrics

Retinal Image quality metrics rely on calculations (generally through Fourier Optics, knowing the wave aberration) of the image of an object on the retina. In the current thesis, retinal image quality is often used to evaluate and compare optical quality. Retinal image quality metrics include the cumulative effects of diffraction and wave aberrations (and potential interactions between terms -see section 1.3.3 of this chapter).

Point Spread Function and Line Spread Function

The image of a point through the optical system is called a Point Spread Function (PSF). The PSF is calculated as the squared magnitude of the inverse Fourier transform of the pupil function $P(x, y)$ [29], defined in equation 1.5. The pupil function $P(x, y)$ defines how light is transmitted by the optics of the eye.

$$P(x, y) = A(x, y) \exp\big(ikW(x, y)\big) \quad [eq. 1.5]$$

where k is the wave number (2π/λ) and $A(x, y)$ is an optional apodization function of pupil coordinates (x, y). Unless otherwise noted in this thesis, we omitted the apodization function (Stiles-Crawford effect) arising from the waveguide nature of cones. A narrow and peaky PSF is indicative of good optical quality, and this can be generally quantified by the maximum of the PSF (normalized to the diffraction-limited, no aberration, case).

At small pupil diameters, diffraction dominates in PSF, while at large sizes, aberrations contribute more to retinal blur. Figure 1.7 shows who PSF is for a normal eye and different pupil diameters, assuming full correction of high order aberrations (top) and with the natural aberrations of an eye. The PSF of a diffraction-limited of an optical system is the Airy disk [82].

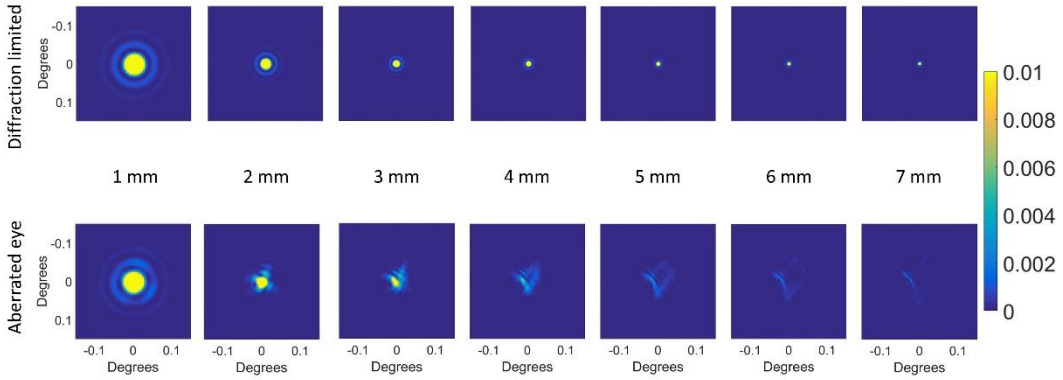

Figure 1.7. The effect of pupil size on PSF for a diffractive limited system (top) and a real human eye for different pupil diameters (bottom).

Since a line is just a sum of points, Line Spread function (LSF) can be simply defined as the line integral of the point spread function (eq. 1.6):

$$LSF(x) = \int_{-\infty}^{+\infty} PSF(x,y)dy \quad [eq.1.6]$$

Convolution of the PSF

Simulations of the retinal image are usually achieved through the convolution operation (⊗) of the PSF with a given image [83] as expressed in equation 1.7:

$$Retinal\ image = PSF \bigotimes Original\ Image \quad [eq.1.7]$$

To our knowledge, the convolution was first used to study the quality of the retinal image was by Flamant in 1955, who used Fourier theory to convolve a slit target with the eye's LSF [84]. The use of convolution to represent retinal images, and for example, the effect of certain aberrations on image quality is ubiquitous [85] [86],[48]. Several studies used convolved images to evaluate the effects of multifocal intraocular lenses on vision [87], the minimum amount defocus, astigmatism and spherical aberration that produces just-noticeable differences [88] or to study the adaptation to the blur produced by HOAs or astigmatism [5], [58], [89], among others.

Convolved images have been used in this thesis in order to induce spatial blur in the experiment that is described in chapter 4.

Strehl Ratio

Strehl Ratio (SR), computed in the spatial domain, is typically defined with respect to the peak of the PSF, rather than the coordinate origin [28].

SR can be defined as the relation between the maximum peak of the PSF and the maximum peak of a diffraction-limited PSF. SR is computed as equation 1.8

$$SRX = \frac{(PSF)}{(PSF_{DL})} \quad [eq.1.8]$$

where PSF_{DL} is the diffraction limited PSF for the same pupil diameter. Thus, SR would be a relationship between the maximum peak of the PSF of the actual system and the maximum for diffraction-limited one (figure 1.8). A value of 1 for the SR would mean a high quality of the image while the lower the value, worse image quality represents.

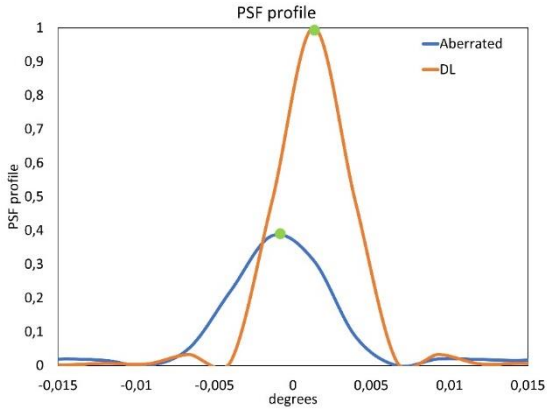

Figure 1.8. PSF profile of a diffraction-limited system (orange) and a real eye (blue) for 6mm pupil size. In green, the points used for the calculation of SR.

Optical Transfer Function

The Optical Transfer Function (OTF) measures the loss of contrast and any shift of the phase in the image of a sinusoidal target [28]. OTF is obtained as the Fourier Transform of the PSF (eq. 1.9):

$$OTF = FT(PSF) \quad [eq. 1.9]$$

Modulation Transfer Function and Phase Transfer Function

The Modulation Transfer Function (MTF) is the variation of image contrast with spatial frequency for an object with 100% contrast. MTF is mathematically defined as the modulus of the OTF. Figure 1.9 shows the MTF of a diffraction limited system as well as the MTF for the same set of aberrations as in figure 1.8.

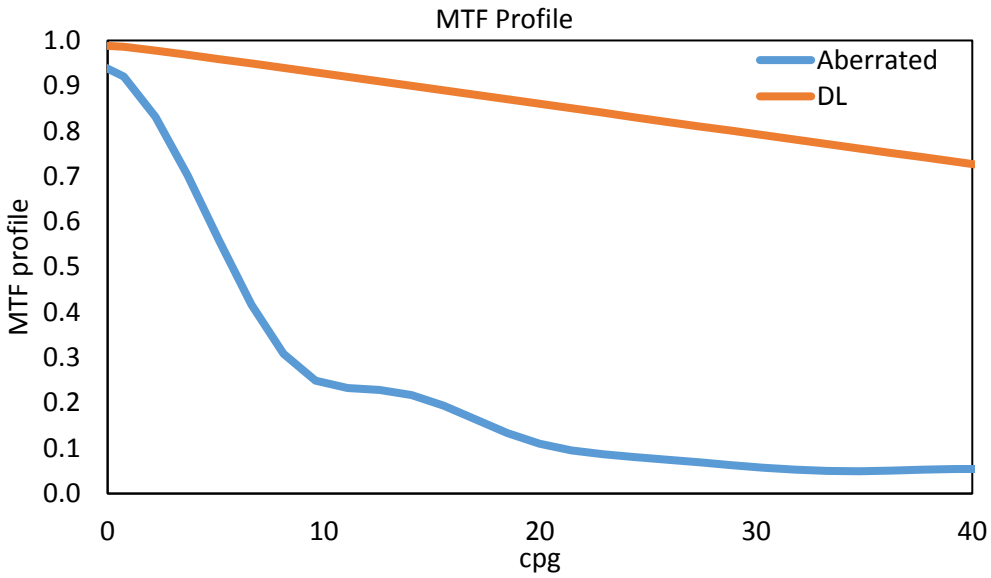

Figure 1.9. MTF radial profile of a Diffraction Limited eye at 6mm pupil diameter MTF radial profile for the same eye shown in Figure 1.8 at 6mm pupil diameter (Blue).

Phase Transfer Function (PTF) is the phase of the OTF. PTF describes the shift in the phase, primarily produced by asymmetric aberrations, such as coma or astigmatism.

In general, the amount of contrast attenuation and the amount of phase shift vary with spatial frequency. Since an object is a sum of gratings of various spatial frequencies, contrasts, phases and orientations, the eye's optical system can be considered a low-pass filter. Thus, good visual quality is defined by high MTF values and low PTF values, PTF becoming zero if the corresponding LSF is symmetrical.

1.3.5.3. Polychromatic image quality

All previous metrics are applicable are described for a single wavelength (which scales both the modulus and phase of the pupil function). However, as it was explained in section 1.2.1 of this chapter, the visual world is polychromatic and, the presence of LCA and TCA, alters the retinal image quality with respect to that in monochromatic light.

The interactions between measured monochromatic and chromatic aberrations can be accounted for computationally in the calculations of retinal image quality. Generally, wavefront aberration maps are shown independently for each wavelength as wavefronts of different wavelengths as they are mutually incoherent and do not interfere with each other. For this reason, wavefront quality metrics are not easily generalized to accommodate polychromatic light.

Different approaches have been developed to calculate the polychromatic image quality. Van Meeteren [90] used typical values of both chromatic and monochromatic aberrations (assumed to be wavelength-independent) from literature to measure Optical Transfer Functions (OTFs) for the average human eye for white light of equal intensity.

Marcos et al. [91] measured the wavefront aberrations at six different wavelengths (from 450 to 650 nm) in real subjects, using a spatially resolved refractometer. From these measurements, they extracted the LCA and TCA and computed the polychromatic PSF of an individual eye, weighted by the spectral content of the light source and spectral sensitivity of the retina (V(λ)). Thibos et al. [28] introduced weighted monochromatic optical quality metrics by V(λ), in order to calculate the polychromatic metric, as expressed in equation 1.10:

$$Metric_{poly} = \int V(\lambda) Metric(\lambda)\, d\lambda \quad [eq.1.10]$$

Ravikumar [92] used a model of average levels of LCA, which were constant cross eyes, as a reference to examine the impact of different levels of monochromatic aberrations and TCA, which were variable across the population.

The measurement of chromatic aberration and the calculation of the polychromatic PSF becomes particularly relevant when comparing the optical quality of pseudophakic eyes implanted with IOLs of different materials (and therefore Abbe numbers [93]). Chromatic aberrations have been measured *in vivo* in eyes implanted with IOLs [40] and it has been studied *in vivo* the interaction of monochromatic and chromatic aberrations [94], both demonstrated in our lab. In particular, in diffractive multifocal intraocular lenses [95], it has been shown that the diffractive design modulates chromatic aberration in each focus [42].

1.4. Visual perception and adaptation

As retinal images vary dynamically with time, the visual system incorporates a recalibration mechanism that keeps perception of the image constant overtime. While neural adaption (probed by shifts in the perceived image following short periods of exposure to a given blur), perceptual learning operates at longer scales and refers to the improvement in repeated vision tasks.

1.4.1. Adaptational processes in the eye: neural adaptation

A definition of visual adaptation was given by Clifford [96]: "The term visual adaptation describes the processes by which the visual system alters its operating properties in response to changes in the environment. These continual adjustments in sensory processing are diagnostic as to the computational principles underlying the neural coding of information and can have profound consequences for our perceptual experience."

Neural adaptation occurs in a range of time scales from just milliseconds to lifetimes [97]. Short-term adaptation happens with temporal changes [98] like, for example, the change of blur in a natural scene, while long-term adaptation recalibrates the visual system to changes in the environment or the observer. In addition, it has been demonstrated that neural adaptation depends on previous experience [99]–[101].

Some examples of visual adaptation are adaptated to contrast [102], color [103], [104] or changes of the visual system [105]–[107].

It is possible to evaluate visual perception and how an observer performs a particular task thanks to the Psychophysics theory [108]. Psychophysical methods are useful to find a threshold (for example, VA estimation) or carry out a decision task (for example, scoring measurement) and they are explained in section 2.3 of chapter 2. Psychophysical methods have some limitations: it is important that the observer is a cooperative subject and must understand clearly the task, thus instructions must be very precise. Perceptual learning is another factor to have account when a psychophysical method is performed.

For the observer, visual context is constantly changing well due to external elements such as color contrast, luminance, distance, etc., or well due to the intrinsic conditions of the observer, such as a disease, new refractive correction, etc. Neural adaptation is the capability of the visual system to adjust and recalibrate itself in order to maintain constant the perception and handle these changes. Thus, visual coding is a dynamic process, adapting continuously.

There are different ways to modify the appearance of the stimulus for the observer: using optical methods (by lenses, for example) or simulated images (computationally altered to induce blur or sharpness). Adaptive Optics (explained below, in section 1.6 of this chapter) are a powerful tool for the study of neural adaptation. Below are some examples of studies of visual adaptation. In particular, adaptation to blur, to chromatic blur and to astigmatic blur, which are particularly relevant to the thesis, as the studies presented in Chapters 3, 4 and 5 specifically entail adaptation to those blur features.

1.4.2. Neural adaptation to spatial blur

Despite the retinal image being subject to significant amounts of blur produced by high order aberrations (even in eyes habitually corrected for defocus and astigmatism), observers are not aware of such blur.

Several studies demonstrate that the eye is in fact adapted to its native aberrations is an already demonstrated fact. Artal and colleagues [4] performed an experiment in which subjects observed a stimulus through Adaptive Optics, either through their own aberrations and under the same aberrations pattern but rotated. They found that the stimulus judged as sharper was consistent that viewed through the natural optics. Chen and colleagues [6] also used Adaptive Optics to find the amount of aberrations that produced the best subjective image and found that this was not the full correction of aberrations. Sawides et al. [5] also used Adaptive Optics at the VioBio Lab to study the relationship between perceived blur and retinal image blur. Observers judged the quality if a series of images blurred with the aberrations of 128 different eyes, from very mildly to highly aberrated. They found a high correlation between the best perceived focus and the subject's own retinal blur, suggesting that spatial vision is calibrated for the specific blur levels of each individual's retinal image and that this adaptation at least partly reflects how spatial sensitivity is normalized in the neural coding of blur.

Several studies looked into the effect of adaptation/perceptual learning to lower aberrations (defocus and astigmatism). For example, Pesudovs and Brennan [109] studied the performance of low myopic subjects in two different sessions, with and without their refractive correction and the found a change in VA performance, but not in the refractive error, suggesting an adaptation mechanism. In a similar way, Man-Williams and colleagues [110] explored the neural compensation to blur in myopic subject after a period without their refractive correction. In the same line, Rosenfield et al. [111] studied the improvement of VA on myopes after long-term blur exposure. Also, the importance of prior visual experience has been demonstrated in other studies [111], [112], where myopes showed a lower reduction of visual acuity than emmetropes when myopic blur was induced.

Adaptation to astigmatism has been also studied and explained below in a dedicated section (1.4.4.).

Uncorrected presbyopes can be regarded as chronically exposed to blur at near. Besides, presbyopes wearing presbyopic corrections appear to adapt to the new visual experience produced by a presbyopic correction, to both blur in simultaneous vision images [79] as well as to distortions and to the presence of asymmetric aberrations produced by progressive lenses [113], in consistency with reported mechanisms of spatial neural adaptation [5]. Chapter 5 in this thesis presents a study suggesting neural adaptation processes in presbyopes, and in particular those wearing progressive lenses.

It has been also studied the adaptation to blur produced by surgical processes [114], which produce new patterns of HOAs and to blur produced by corneal disease such as keratoconus, which causes a local thinning of the corneal surface generally resulting in highly asymmetric optical blur [115].

Two specific types of blur, chromatic blur and astigmatic blur, are detailed in the two following sections.

1.4.4. Adaptation to astigmatic blur

Astigmatism is a common low order aberration, in which the power profile dependent on the meridian. Astigmatism can be corrected with toric surfaces, like cylindrical lenses or contact lenses.

Adaptation to natural or induced astigmatism has been studied in depth by VioBio Lab and others. In particular, Sawides and colleagues [58] studied the shift of the best perceived focus after brief periods of adaptation to astigmatic images. Furthermore, images blurred along an axis were perceived isotropic by astigmatic subjects with a consistent astigmatic axis [59]. In addition, there is adaptation to the natural axis of astigmatism [55], magnitude [5] and orientation [116]–[118]. Thus, the amount of astigmatism for perceived neutral point depends on the previous adaptation as well as the refractive profile of the patient. For example, Marcos and colleagues [57] found that, under the induction of astigmatism, the shifts are consistent with a bias towards vertical and horizontal blur, indication adaptation to native astigmatism. The fact that the same best focus shift trends were found when AO was used to correct aberrations, indicates that this shift is primarily a result of prior adaptation. Adaptation to astigmatic defocus and the axis of astigmatism has also been demonstrated for both simulated and real defocus [119].

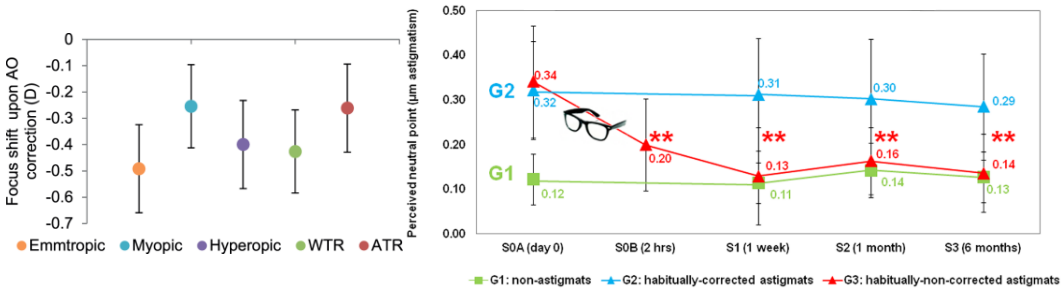

(a) (b)

Figure 1.10. Neural adaptation to astigmatism in two different studies: (a) Average difference between the best-focus setting with AO-corrected aberrations and the best-focus setting under natural aberrations for each group: emmetropic (orange), myopic (blue), hyperopic (purple), myopic astigmats with-the-rule (WTR, green) and against-the-rule (ATR, red). Source [57] *(b) . Perceived neutral point variation along sessions (2 hrs, 1 week, 1 month and 6 months) for each group: non-astigmats (green squares), habitually-corrected astigmats (blue triangles) and habitually-non-corrected astigmats (red triangles). ** indicates statistically significant shifts (p<0.01), from the first session to other measurement sessions for habitually-non-corrected astigmats group. Source* [59]. *In both cases, error bars stand for inter-subject variability (standard deviation).*

Vinas et al. [59] studied the neural adaptation to the clinical correction of astigmatism. They found that habitually-non-corrected astigmats shifted their perceived neutral point towards isotropy shortly (around 2h) and it reminds constant after that. In addition, upon induction of astigmatism, astigmatic subjects appear to be less sensitive to the reduction of VA than non-astigmatic subjects [53], especially if the axis of induced astigmatism coincides with the natural axis of astigmatism [55].

De Gracia et al. found that, in comparison with astigmatism alone, certain combinations of astigmatism and coma increase optical quality through focus [52], although the benefit of combining astigmatism and come in habitually uncorrected astigmats appeared to be much lower environment [53], [55]. Cheng and colleagues demonstrated with computationally-aberrated letters that VA was diminished and extended depth of focus increased by spherical aberration, coma and secondary astigmatism, however, the presence of coma does not affect cylindrical refraction [54]. On other hand, de Gracia et al. found that inducing coma to astigmatism resulted in a clear increase of VA, while Vinas et al. found that orientation of induced astigmatism has an impact on VA. Both studies were performed in an Adaptive Optics environment [53], [55].

Despite extensive research on adaptation to astigmatism (including the effect of previous visual experience, the axis of adaptation, refractive profile and correction, combination with other HOAs), the great majority of studies have been done on young subjects. There is a knowledge gap on the effect of astigmatism induction/correction on presbyopic subjects (i.e. subjects that do not or minimally accommodate and need presbyopic correction). Given that progressive lenses being a highly popular correction for presbyopia are progressive lenses, and those have a large impact on astigmatism [60], [120] the author explored the adaptation to astigmatism in presbyopic subjects (Chapter 5 in this thesis).

1.4.3. Neural adaptation to chromatic blur

As said above, LCA in the eye causes different wavelengths of light to be differentially focused on the retina. The retinal image is different for the different types of photoreceptors (long- (L), middle- (M) and short- (S) cones). The chromatic defocus between the wavelength of the maximum sensitivity of S and M/L cones is around 1.5 D [38], equivalent to a 26 arcmin blur circle approximately for a 5 mm pupil [121].

Despite the high sensitivity of the visual system, an important unresolved issue is why perception doesn't seem to be degraded by the huge amount of defocus produced by chromatic aberration. Understanding how the visual system handles the impact of LCA is relevant to many visual processes: it plays a role in emmetropization during eye's growth and on the reshaping of the crystalline lens during accommodation [122], [123]. During cataract growth, adaptation to chromatic blur may also take place as well after cataract surgery, when the crystalline lens is replaced by an intraocular lens (IOL), since the implanted IOL's chromatic aberration depends on the material [40], [41] and therefore, the chromatic aberration of the crystalline lens and the IOL differ.

The relatively lower optical contribution of the LCA to perception, which is theoretically largest at short wavelengths, is traditionally attributed to two factors: the paucity of S-cones in the central fovea and the absorption of short wavelength light by the yellowish macular pigment. Previously, it has been reported by McLellan and colleagues [62] that,

while the optical contrast reduction produced by LCA in S- cones with respect to M/L cones was large in diffraction-limited eyes (free of monochromatic aberrations), the presence of the eye's natural monochromatic aberrations mitigated the differential impact of LCA on optical contrast for S-cones and M/L cones. In fact, optical simulations showed that the combination of natural monochromatic and chromatic aberrations boosted contrast for blue stimuli when the eye was focused in the green compared to an aberration-corrected eye. Therefore, the interaction between chromatic and monochromatic aberrations seems to reduce the perceptual impact of chromatic blur. Figure 1.11 represents the finding of the study in Nature.

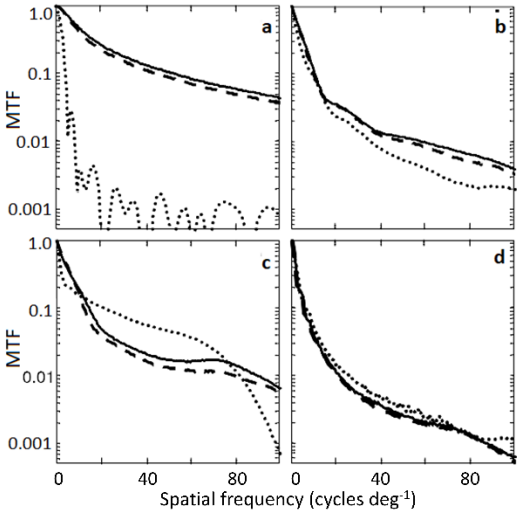

Figure 1.11. Polychromatic MTFs computed for a theoretical model eye, diffraction limited case (a) and three measured subjects (b-d) with 6 mm pupil size for L-cones (dashed lines), M-cones (solid lines) and S-cones (dotted lines). Source [62]

Webster and colleagues studied the adaptation and the neural adjustments to chromatic blur. They examined how adapting to the characteristic color distributions of natural images could influence color sensitivity and appearance [103]. In another study, they found that both the luminance and the chromatic mechanisms respond to changes in the blur level [124]. They also investigated the effects of adaptation on the sensitivity of the luminance and color contrast threshold; and they found that spatial sensitivity for color variations can be influenced strongly by adjusting the stimulus to the spatial structure.

The subjective perception of LCA and its interaction with HOAs has been studied in this thesis, and details can be found in chapter 3.

1.5. Ageing processes in the eye: Presbyopia

The optical quality of the eye changes with age [21], [22], due to physiological changes that take place with aging. One of the most challenging modifications is the loss of the ability to focus near and far objects, known as presbyopia. In the following sections, accommodation, presbyopia and its correction are further described.

1.5.1. Definition of accommodation and presbyopia

In an emmetropic eye, corrected for refractive error, rays coming from far focus on the retina. In the young eye, the crystalline lens has the capability to reshape to focus near objects, in a process known as accommodation. The first reference to accommodation is from Descartes in 1677 [125] but it was Thomas Young who demonstrated, in 1801, the changes in the crystalline lens curvature through the variations of the Purkinje's images [126].

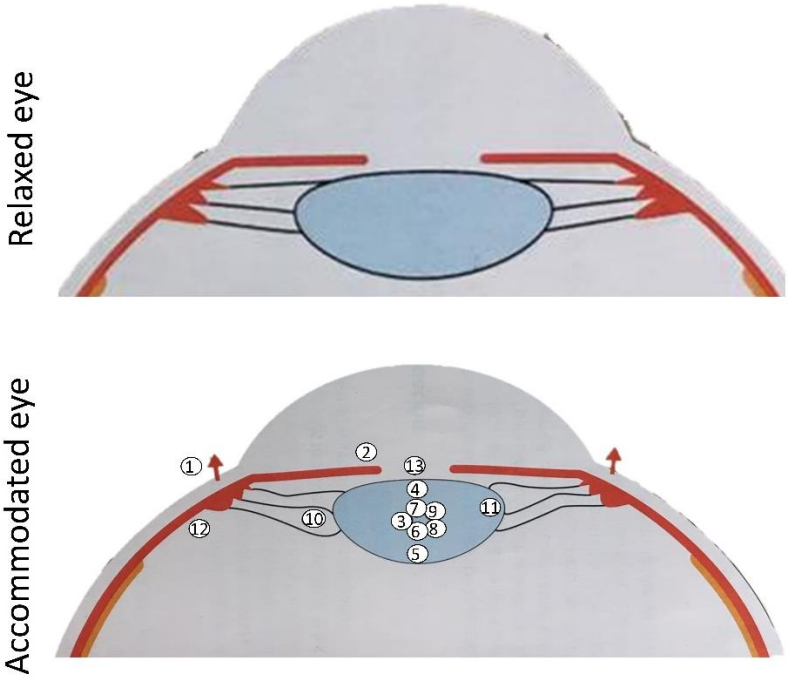

Figure 1.12.Changes in the eye during accommodation, adapted from [127]. *(1) Ciliary muscle moves inward and forward, (2) Iris' edge and anterior surface of crystalline lens move forward around 0.3 mm , (3) Peripherical part of anterior and posterior surfaces of crystalline lens flatten, (4) Anterior surface of the crystalline lens increases its curvature , (5) Posterior surface of the crystalline lens increases its curvature fewer than the posterior surface, (6) Central thickness of the crystalline lens increases from 0.36 to 0.58 mm, (7) Equatorial diameter of the crystalline lens decreases around 0.4 mm, (8) Refractive index increases from 1.421 to 1.426 for 7 D of accommodation, (9) Spherical aberration of crystalline lens decreases, (10) Zonular fibers are completely relaxed when accommodation is maximum, (11) Because of zonular fiber's relaxation, crystalline lens falls down around 0.3mm due to gravity (12) Choroid moves forward around 0.5 mm, (13) Pupil diameter reduces. Adapted from* [127]

The reshaping of the crystalline lens it is possible is produced by the forces exerted radially by the ciliary muscle and the zonulae, which connects the ciliary muscle with the capsular bag, around the equator. The most accepted theory of the accommodation process was postulated by Helmholtz in 1855. According to his theory, when the eye is des-accommodated, the ciliary muscle is relaxed, the fibers of the zonule are tensed and the crystalline lens is flattened and thin. Conversely, when the eye is accommodated, the ciliary muscle contracts, the zonular fibers relaxed and the curvature of the crystalline lens increases in both sides, it becomes more spherical, its equatorial diameter reduces and the thickness growths.

With age, there is a physiological loss of the natural elasticity of the crystalline lens (primarily), and to a much less extent, of the muscular tone of the ciliary muscle, resulting in the loss of the capability of accommodation. Thus, the eye is not able to focus near objects and the accommodative amplitude is gradually reduced. The loss of accommodation is called presbyopia. Conventionally, the onset of presbyopia is taken when the subjective amplitude of accommodation is lower than 3 D [128].

Presbyopia starts in the fourth decade of life, and it is typical to refer difficulty to read at the habitual distance, headache and visual fatigue. Presbyopia is an irreversible condition, but there exists a wide number of solutions for correcting presbyopia that can be adapted to the need of the patient, although to date none of them are fully satisfactory. They are described in the next section.

1.5.2. Types of correction for presbyopia

Solutions for presbyopia aim at providing the eye with visual functionality at near. That can be achieved with external solutions providing added optical power, such us spectacles or contact lenses [129], or by surgical intervention, modifying the cornea (i.e. PresbyLASIK or corneal implants), and (more often) implanting a multifocal or Extended-Depth-of-Focus (EDOF) IOL [130], [131].

It is possible to correct presbyopia with single vision (vision is corrected for just one distance) or multifocal designs. Instead of producing independent focus, it is also possible to extend the depth of focus of the lens through increasing certain combination of monochromatic aberrations, such as spherical aberration.

1.5.2.1. Types of strategies for presbyopia correction

There are different approaches to compensate presbyopia and provide the eye a clear image for near vision using multifocality: alternating vision, simultaneous vision or monovision.

Alternating vision

In alternating vision solutions, different optical zones in the form of spectacles correct for different distances. According to the optical zone that the gaze's direction selects, there is a clear image at a certain distance. Alternating vision solutions are always prescribed in spectacles with different designs: bifocal, trifocal, progressive alternative lenses (PALs) or occupational lenses.

In progressive lenses, the upper part of the lens compensates for the optical refraction at far, and progressively increases the optical power to provide a near add in the lower part of the lens, with an optical corridor for intermediate distances in the center of the lens. This change of optical power results in aberrations in the peripheral regions of the lens,

in particular in astigmatism [60], [61]. The distribution of astigmatism along the lens depends on the design, as shown in figure 1.14., and follows the equation (equation 1.11) described by Von Minkwitz in 1963:

$$\frac{Astigmatism}{\Delta x} = 2\frac{Addition\ Power}{\Delta y} \quad [eq.\ 1.11]$$

In general, PAL wearers adapt to distortions and to the presence of asymmetric aberrations produced by progressive lenses [113], although the previous visual experience plays a role in adaptation [132].

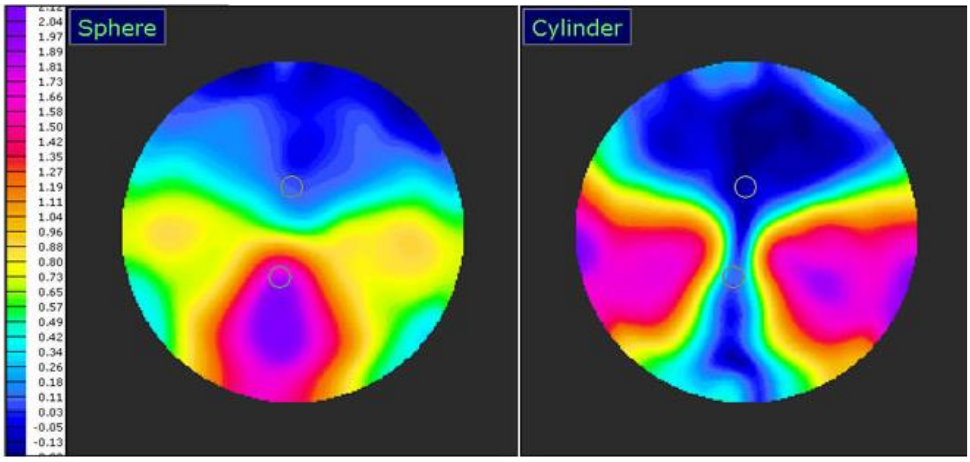

Figure 1.14. Distribution of spherical (left) and cylindrical power along a progressive commercial lens [133].

Simultaneous vision

Presbyopia corrections based on the principle of simultaneous vision have increased substantially in the last few years, either in the form of contact lenses, intraocular lenses or corneal treatments. In simultaneous vision, the eye is corrected for different working distances at the same time. Thus, a focused and a defocused image of the same object is projected simultaneously on the retina.

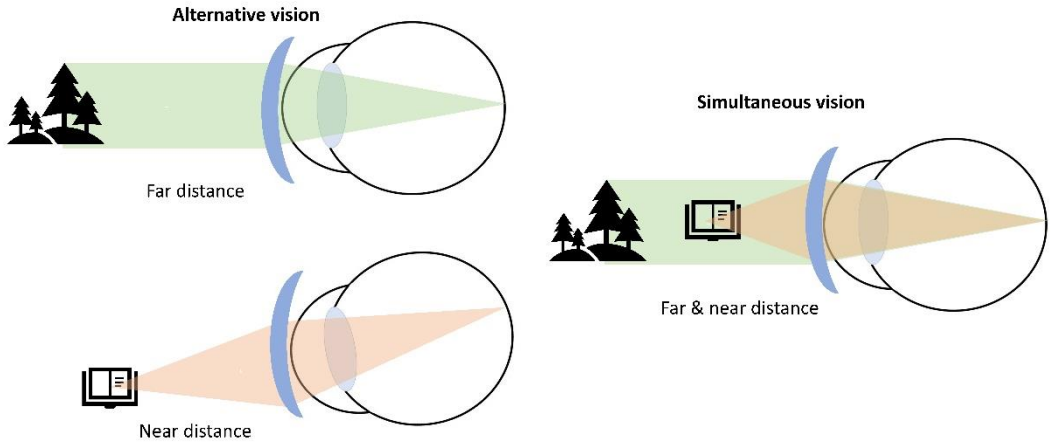

Figure 1.15. Schematic diagrams of various presbyopic corrections: (a) alternating vision and (b) simultaneous vision principles.

Monovision

Monovision consists of correcting one eye for far (usually the dominant eye) and the other one for near distance. A modification of this solution is to correct the second eye for intermediate and near vision through a multifocal design. It is very common to use contact lenses to apply monovision, although intraocular lenses are also an option for monovision correction [134].

1.5.2.2. Multifocal designs types

Multifocal corrections (presented in contact lenses or multifocal intraocular lenses) obtain multifocality through different optical principles: refraction, diffraction.

Refractive multifocal lenses have zones with different refractive index, producing a different correction for each zone. Zones are incorporated as two or more rings (radial design) or zones (angular design) [135]. Chapter 6 of this thesis will go in describe in depth these designs, which are tested in an Adaptive Optics system. An important characteristic of refractive multifocal lenses is that their optical performance is generally pupil-dependent.

Diffraction is a characteristic phenomenon of light that occurs when the wave finds an obstacle with a size of the same magnitude order than the wavelength, and light diverts. Diffractive lenses have diffractive rings that produce two or more foci, resulting in multifocality. Due to its nature, halos' presence is higher with diffractive lenses. Diffractive are not as sensitive to decentration as refractive lenses are, however as the design is only specific to one wavelength chromatic artifacts are produced (although some designs use chromatic shift as an advantage for creating intermediate vision or correcting longitudinal chromatic aberration)

Some IOL designs combine both refraction and diffraction principles (hybrid).

1.6. Adaptive Optical Visual Simulators

In this section, the principles of operation of Adaptive Optics systems, their main components and their use as visual simulators are introduced. Adaptive Optics allow to manipulate ocular aberration, therefore resulting in a powerful tool to study different aspects of vision: studying the optics of the eye, performing psychophysical tests to investigate the effects of optical changes on visual perception and neural adaptation, simulating new optical designs for presbyopia or allowing patients to experience non-invasively prospective corrections before surgery.

1.6.1. Adaptive Optics

Adaptive Optics systems allow measure, control and modulation of the wave aberration. Adaptive Optics (AO) started with astronomy [136]. Astronomical images taken from the earth are affected by the turbulence of the atmosphere. In 1953, Horace W. Badcock proposed to improve the captured image by using an active adaptive optical element, which would correct the captured images in real time. Today AO is applied in most of the important ground-based telescopes of the world. Figure 1.16 shows an example of the image quality improvement of a stellar object with Adaptive Optics. Subsequent developments of AO in other fields include microscopy [137] and ophthalmology. AO was first applied in the eye in a closed-loop in 1990's [32] and current applications include high-resolution imaging of retinal images [138], visual testing [71] and vision simulators [77], [139].

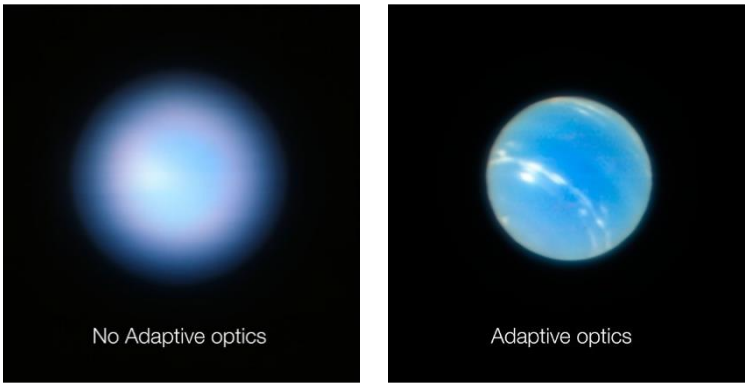

Figure 1.16. Planet Neptune during the testing of the Narrow-Field Adaptive Optics mode of the MUSE/GALACSI instrument on ESO's Very Large Telescope. (Credit: ESO/P. Weilbacher (AIP))

1.6.2. Adaptive Optics based visual simulators

There are three major steps in an Adaptive Optics instrument (1) An active modulator of the wavefront (2) A wavefront sensor (3) A computer control of the sensor (which measures the amount of aberration, and the optical component to modify its shape (. This process is repeated on a closed-loop until the wavefront sensor measures the desired

wavefront: either a corrected wavefront or a pattern of aberrations to be induced. Figure 1.17 represents the general principle of operation of AO.

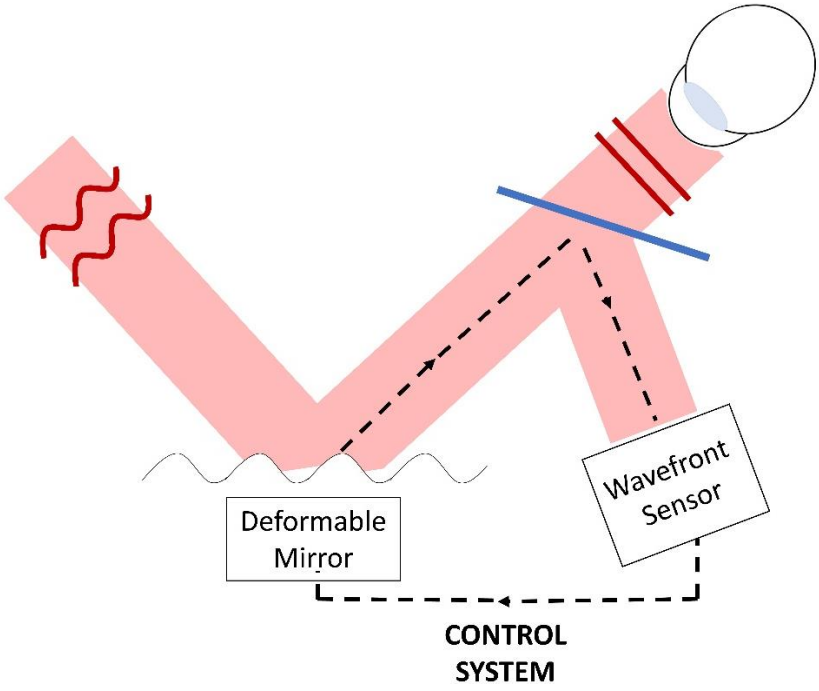

Figure 1.17. Basic schema of AO process.

Wavefront sensing

Different wavefront sensors have been used to measure the aberrations of the eye [29, Ch. 3], [140]: Spatially Resolved Refractometer (SRR) [31], Laser Ray Tracing (LRT) [30] or Hartmann-Shack (HS) wavefront sensor [32]. While spatially resolved refractometer is a subjective method, the other two are objective methods. The HS outgoing aberrometer; LRT and SRR are outgoing aberrometers. Both AO systems used in this thesis, contain HS wavefront sensors, and their technical specifications are described in detail in section 1 of chapter 2. HS is composed of an array of microlenses, all of them with the same diameter and focal length. The wavefront is sampled by the lens lets into many individual beams, which focus onto a CCD placed on the focal plane of the microlens array. The differences in the centroids of the spots from a perfect eye and the eye under measurement are estimated and are proportional to the derivatives of the wave aberration at each pupil location. Figure 1.18 shows a schematic diagram of the operation of a HS.

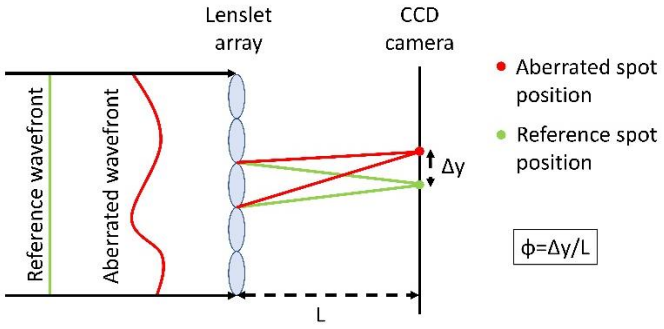

Figure 1.18. Schematic diagram of the operation of a Hartmann-Shack wavefront sensor

Phase modulators and wavefront correctors

Different elements can be incorporated on an AO system in order to modify wavefront incident to the eye. In the following sections, some of these elements are described: Deformable Mirrors (DM), Spatial Light Modulators (SLM), SimVis technology or cuvettes. Although a cuvette is not an active optical element, it can be used to induce a certain pattern on an AO environment.

Computer control

In AO, a control system by computer connects both wavefront sensor and the active optical element and facilitates the closed-loop operation

The function of the control system is to transform the measurement of wavefront aberrations taken by the wavefront sensor onto the need units for the corrector element in order to obtain the desired performance of the AO system, well to correct that wavefront aberration or well to induce a different pattern of aberrations. In the case of the Deformable Mirror, it is necessary to know the voltage to apply to each actuator, after a calibration process [101], [141]

1.6.3. Active optical elements for visual simulation

1.6.3.1. Deformable Mirrors

Deformable mirrors (DM) are composed by a reflective membrane, which is deformed by a series of (electromagnetic, in this thesis) actuators. Actuators push or pull the membrane according to the applied voltage. Commonly, DMs work in a closed loop with a wavefront sensor, which allows calibrating the amount of voltage needed to obtain the membrane's shape that corrects or induces a certain wavefront.

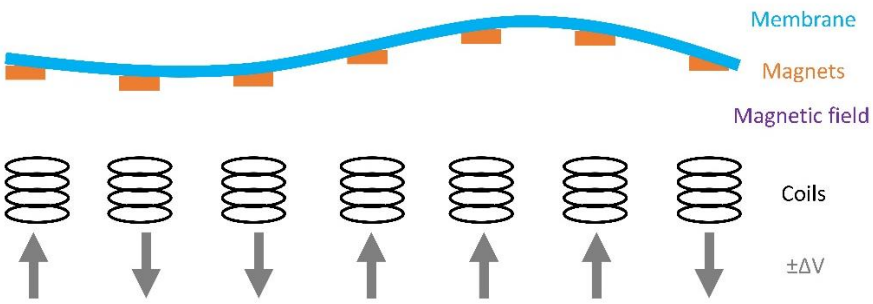

Figure 1.19. Schematic operation of a deformable mirror

In this thesis, electromagnetic DMs have been used in two different AO systems. They are described in section 1 of chapter 2. DM-based simulators are useful to induce a specific wavefront, in particular, to reproduce lenses with smooth varying profiles, due to the physical limitations of the membrane, as well as to correct the aberrations of the eye.

1.6.3.2. Spatial Light Modulators

Another active optical element used in AO systems is the Spatial Light Modulators (SLM) [29], [142], [143]. The most used SLM are LCoS (Liquid Cristal on Silicone) [144]. It is possible to apply different voltage to each pixel of the SLM, thus a different change in the refraction index is produced for every single pixel and, therefore, a phase local changes are induced.

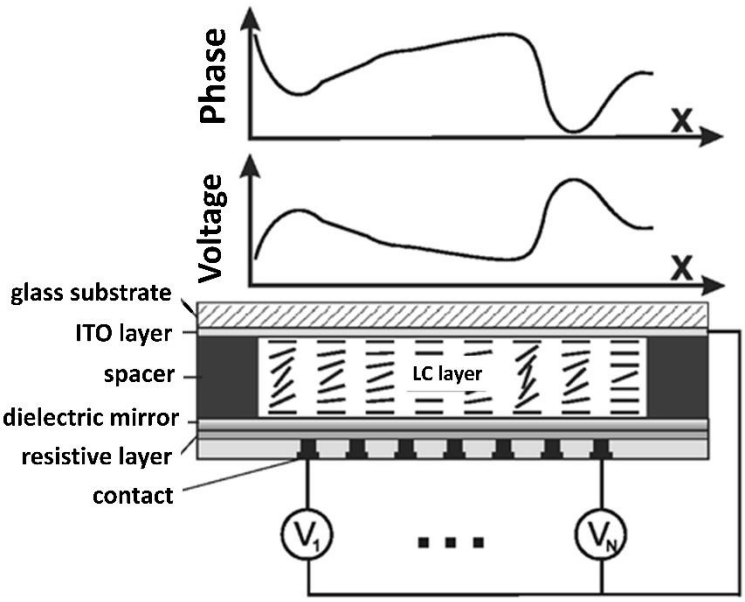

Figure 1.20. Design and principle of operation of the liquid crystal SLM. Adapted from [142]

During this thesis, we have used the SLM to represent different multifocal designs. The technical specifications of the used SLM are described in detail in chapter 2. SLMs are well suited to represent zonal refractive lenses of diffractive multifocal lenses.

1.6.3.3. SimVis technology

Alternatively to the DM and SLM-based simulators, simultaneous vision simulators combine images focused at near and at far. A development of SimVis uses two channels provided with Badal systems, in some configurations in combination with a transmission spatial light modulator which splits the areas of the pupil devoted for near and far [145], [146]. An alternative way to simulate multifocal lenses is by temporal multiplexing of optotunable lenses, changing their optical power in response to an electric signal [147] at high speed. In these simulators the lenses are simulated by sets of temporal coefficients which dictate the amount of time that the optotunable lens stays at a certain focus to reproduce the through-focus performance of the lens [148], [149], projecting onto the retina multifocal images of static appearance.

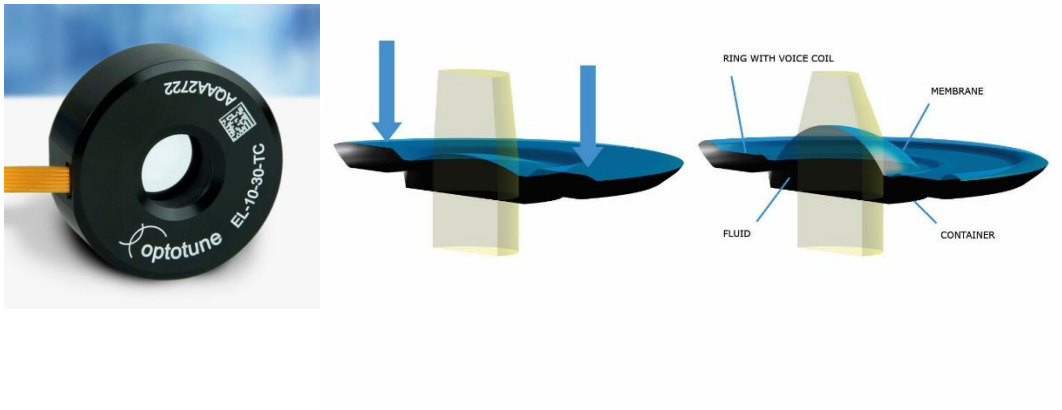

(a) (b)

Figure 1.21. (a) Optotunable lens. (b) Diagram of functioning of optotunable lens. Source [150]

Figure 1.21 shows a diagram of optotunable lenses in two different power states. In chapters 7 and 9 of this thesis, we demonstrate the simulation of real commercial intraocular lenses with a Spatial Light Modulator as well as with SimVis technology.

1.6.4. Static optical elements for visual simulation

1.6.4.1. Manufactured phase plate

Phase plates are a light single component and consist of a plate that changes the phase of light upon transmission. Phase plates can be produced by microlithography using UV light and photoresists to engrave the desired phase map. This technique has been utilized in the past to correct wavefront aberrations of the eye [65], [151]. Alternatively, profile-varying phase-plates featuring the multifocal component of a presbyopic correction can be obtained using lathe technology. The latter has been used in this thesis to simulate different multifocal patterns in chapter 6.

16.4.2. Projecting the real IOL in the pupil's eye

An alternative to programmable simulators (such as AO-based visual simulators) are devices that project the IOL onto the pupil plane of the patient's eye, inserting the lens in

a cuvette. While this type of simulation loses the option to dynamically try different lenses (for example to compare different options), and of course requires having the physical lenses available (unlike the programmable simulators that allow testing lenses prior to manufacturing), IOL projection systems do have the advantage of a direct test of the lens, in principle, without relying on assumptions or limitations of the simulating technology. For this reason, some studies in this thesis utilize phase plates (chapter 6) or real IOLs of 0D (i.e. only bearing the multifocal, and not the refractive component of the lens) inserted in a cuvette (chapter 7) as gold-standards to evaluate the accuracy of other simulators devices, like SLM and SimVis-based simulators. However, most often, standard power IOLs are available.

The literature describes optical systems specifically designed to project the IOL on the eye's pupil plane whole at the same time cancels out the power of the IOL. The system is called Rassow telescope [152] and consists of a 4F system with a magnification x1, with the IOL acting as one of the lenses in the system, and a +20 D achromatic lens acting as the second lens, compensating 20 D of the optical power of the IOL. Schaeffel et al describe the implementation and use of a Rassow to evaluate real IOLs [153]. A new channel for non-0D IOLs cuvette has been developed during this thesis, and it is described in depth in chapter 8.

1.6.5. Visual simulators in the clinic

Visual simulators are a good tool since a prospective correction can be tested on a non-invasive procedure. In addition, visual simulators are useful to identify if a patient is a suitable candidate for a given optical solution, such as multifocality, and provide him/her a personalized treatment.

Most AO Visual Simulators are laboratory prototypes (see [71], [154] for reviews). However, some clinical visual simulators, based on the previously described technologies, have been developed (figure 1.22).

(a) (b) (c)

Figure 1.22. Commercial visual simulators: (a) Crx1 by Imagine Eyes. (b) VAO by Voptica. (c) SimVis Gekko by 2EyesVision.

For example, DM-based has been launched commercially (i.e crx1 by ImagineEyes [155]). Most DM-based simulators are monocular, although there have been reports of binocular laboratory systems [156]. There is an SLM-based binocular simulator commercialized by Voptica, with a device called VAO [157]–[159]. A commercial product that makes used of SimVis technology (SimVis Gekko, by 2EyesVision) has been launched [160]. It is as wearable, binocular, see-through, and fully programmable and remotely operated device.

Two commercial systems were launched commercially based on the Rassow telescope or small variations of it (figure1.23): VirtIOL [161] and ACMIT [162]. In both cases, a manufactured IOL is inserted in a cuvette and projected onto the patient's pupil plane. In the ACMIT instrument, the IOL is inserted into an eye model based on the Liou and Breannan's model eye [163].

(a) (b)

Figure 1.23. Commercial simulators which project the real IOL onto the pupil eye: (a) Virtiol and (b) Acmit.

1.7. Open questions

Gaining knowledge on the interaction between mono- and chromatic aberrations and their impact on vision, as well as on the interaction of aberrations with multifocal designs, will help to improve the design of new intraocular and contact lenses, and their customized prescription in patients.

In this thesis, we have implemented new paradigms in custom-developed Adaptive Optics and carried out a series of experimental studies to respond to the following questions:

1. **To what extent previous visual experience plays a role in adaptation to astigmatism?** In particular, what is the effect of prior astigmatism on the perception of best focus (with and without induced astigmatism) in young subjects and presbyopic progressive lens wearers?

2. **Is the visual system adapted to blur due to chromatic aberrations?** Do monochromatic and chromatic aberrations interact favorably, both optically and perceptually? What is the effect of correcting monochromatic aberrations for green and blue targets (optics, perceived visual quality and visual acuity?

3. **Is it possible to predict visual performance with a particular visual correction using an ideal observer that operates on optical grounds?**

4. **Are visual simulators capable of replicating before surgery post-operative vision with a multifocal IOL?** How different visual simulator technologies compare both in bench and *in vivo*?

1.8. Goals of this thesis

The goal of this thesis is to understand the interaction chromatic, monochromatic aberrations and multifocal designs, and their impact on vision.

The specific goals are:

- To understand the adaptation to blur due to monochromatic aberrations, such as astigmatism, and to chromatic aberrations.

- To design and implement new simulation capabilities in an Adaptive Optics simulator, allowing to test optical performance (on-bench) and visual performance of physical and simulated IOLs.

- To explore on-bench and *in vivo* the performance of multifocal designs to correct presbyopia.

1.9. Hypotheses

The hypotheses of this thesis are:

- There exists an interaction between chromatic and monochromatic aberrations. Specifically, the presence of monochromatic aberrations attenuates the visual impact of chromatic aberrations.

- Due to adaptation to natural aberrations, blur threshold is dependent on the subject's native aberrations.

- Previous visual experience determines adaptation to monochromatic aberrations, particularly to astigmatism.

- Visual simulators, such as Spatial Light Modulators and SimVis are replicate accurately the optical and visual performance of physical multifocal lens designs (phase-plates or real IOLs).

1.9. Structure of the thesis

The content of this thesis is organized in the following chapters:

Current **chapter 1** details the state of art regarding vision, aberrations, optical quality, presbyopia and its correction, as well as the motivation of this thesis.

Chapter 2 describes the two experimental set-ups used during the development of this thesis, as well as the new implementation in the systems carried out by the author. The chapter also describes the psychophysical paradigms implemented in the systems and the corresponding experimental protocols.

Chapter 3 presents a study of the fundamentals questions of the interaction between chromatic and monochromatic aberrations, through tests of perceived image quality of gray-scale, green and blue natural images, with and without monochromatic aberrations, corrected with adaptive optics.

Chapter 4 reports measurements of the blur threshold for different pedestal references. Blur was induced by convolved images with the PSF of each subject or optically by using a Badal system to defocus the stimulus, under optical corrections of high order aberrations in an adaptive optics system.

Chapter 5, we present a study that explored the perceptual impact of astigmatism induction in presbyopes. We performed best focus search and visual acuity tasks (Snellen E) in a group of young emmetropic subjects, a group of presbyopic subjects and a group of presbyopic subjects wearing Progressive Addition Lenses under different amounts and angles of astigmatism.

Chapter 6 presents a comparison of two different simulators for multifocal designs in an Adaptive Optics platform: Spatial Light Modulator and lathe-manufactured multi-zone surfaces. Scoring and visual acuity were performed with both simulators for six different multifocal designs on subjects and compared with optical predictions. Also, on-bench through focus images of an E letter through each pattern were taken and compared across simulators.

Chapter 7 presents a comparison of two different simulators, Spatial Light Modulator and SimVis, with the real intraocular lens, immersed on a cuvette. This comparison was made objectively on-bench and subjectively (through focus visual acuity) on five simulated presbyopic subjects.

Chapter 8 presents the design and implementation of a new channel in the polychromatic AO system in order to measure real IOLs. We explored the capability of this new channel to measure on-bench and *in vivo* measurements of optical quality for 3 different designs of IOLs.

Chapter 9 summarizes the conclusions of the thesis.

Chapter 2. Methods

This chapter describes the experimental techniques used during the course of this thesis: two experimental set-ups based on AO, with different capabilities and used for different types of experiments, as well as general experimental procedures both for the psychophysical experiments and the optical quality quantification. Specific implementations and developments for each particular study are described in the corresponding chapter.

The two set-ups used in this thesis were an AO System of 1st generation (VioBio lab AOI) and an AO System of 2nd generation (VioBio lab AOII). VioBio lab AOI was designed, implemented, calibrated and validated between 2008 and 2015, and was the core of two PhD theses at VioBio Lab (Lucie Sawides and Enrique Gambra) [101], [164], also described in detail in previous papers [50], [58], [72]. VioBio lab AOII was designed and implemented between 2015 and 2020, and was the core of Maria Vinas' thesis [141], also described in detail by Vinas et al. [41], [76]. As it was said, both systems have different capabilities and have been used according to the requirements of each experiment:

1) VioBio lab AOI had been previously used to study the impact of HOAs on visual acuity at different luminances and polarities [50], on real-life tasks such as facial expression or familiar face recognition, on accommodation [165], the neural adaptation to blur [5], [89], or adaptation to astigmatism [52], [55], [57] and its correction (Vinas 2013).
2) VioBio lab AOII, polychromatic AO simulator had been previously used in measurements of longitudinal chromatic aberration [38] and transverse chromatic aberration [47] and their impact of monochromatic aberrations on those; vision testing with different multifocal patterns [76] or longitudinal chromatic aberration in patients implanted with monofocal and multifocal IOLs [41], [42].

The author of this thesis has worked on the two AO systems, providing alignment and calibration when needed. She also designed, implemented, calibrated and validated new channels in both systems, giving them new capabilities and conditions of simulation. One of the implementations allows to measure and testing real IOLs immersed in a cuvette in an adaptive optical platform, for cross-validations of other simulating methods. Other of the implementations offers the capability of performing experiments in white light, which makes it possible, on the one hand, to study vision in a more natural environment, and, on the other hand, to complement the studies addressing chromatic vision and chromatic aberration.
The author also participated in the development of the routines to control the AO systems, modifying existing programs to adapt them to the new needs of the experiments. In addition, she worked on the new developments and expansion of psychophysical routines for measurements of visual acuity and perceived visual quality, blur threshold detection and perception of best focus.

2.1. Adaptive Optics Systems in VioBio lab

In what follows, the main components and operation of the two AO systems utilized during this thesis are described in detail. Both systems feature two principal components: a deformable mirror and a Harman-Shack wavefront sensor. Some initial daily routines must be performed in order to calibrate the AO loop in both AO systems: interaction matrix acquisition, command matrix construction and close-loop correction [101], [141], [164].

However, channels of each one of the AO systems are different conferring them different capabilities. Descriptions of both systems can also be found in review articles [71], [154].

2.1.1. General description of VioBio lab AOI

VioBio lab AOI is composed of five differentiated channels, depicted on a schematic diagram in Figure 2.1.a: (1) Illumination channel, with a superluminescent Diode. (2) AO-control channel, with a Hartmann-Shack wavefront sensor and an electromagnetic deformable mirror (DM). (3) Badal system channel. (4) Testing channel, where real IOLs can be tested. (5) Psychophysical channel, with a CRT. (6) Pupil monitoring, consisting of a CCD camera. Image 2.1.b shows the configuration of the VioBio lab AOI.

- *Channel 1:* Illumination channel is used for wavefront measurements. It is composed by a superluminescent Diode coupled to an optical fiber, with a lambda of 827 nm. The beam of the diode (1 mm of diameter) enters the eye collimated and slightly off-centerd (around 1 mm) to avoid corneal reflexions. Reflected light from the eye passes through the Badal system and the deformable mirror, and it is finally focused on the Hartmann-Shack.

- *Channel 2:* The AO-control channel comprises a Hartmann-Shack wavefront sensor and a deformable mirror. Both are placed on a conjugate pupil plane, with a magnification of x0.5 and x2, respectively. The Hartmann–Shack wavefront sensor (HASO 32 OEM, Imagine Eyes) consists of a matrix of 32×32 microlenses (of 160 microns each one) and with 3.65 mm effective diameter and a CCD camera on the focal plane of the lenslet. Since magnification in the Hartmann-Shack plane is x0.5, subject's pupil diameter up to 7-mm can be measured. The DM (MIRAO, Imagine Eyes, France) has 52 actuators, a 15 mm effective diameter membrane with high quality reflection (>98% for 830 nm wavelength), and 50-µm stroke (maximum generated wavefront amplitude). The angle of the incident and reflected beam is 15 degrees.

- *Channel 3:* The Badal system is composed of 2 mirrors and 2 lenses (focal length=125 mm) and mounted on a motorized stage (VXM-1, Velmex). The Badal system is used both for compensating for spherical refractive error of the subjects and for inducing different vergences for testing distances. To induce different vergences, the mirrors are moved changing the distance between the two lenses of the Badal; when the mirrors are in a position such that the distance between lenses is the sum of their focal distances, while if the distance is longer than the sum it induces positive defocus and if it is shorter it induces negative defocus. A displacement of 7.81 mm on the rail was equivalent to a focus shift of 1 D. The

system corrects on a range of ±6 D, with a resolution of 0.125 D. Inducing different vergences with the Badal system doesn't change the magnification.

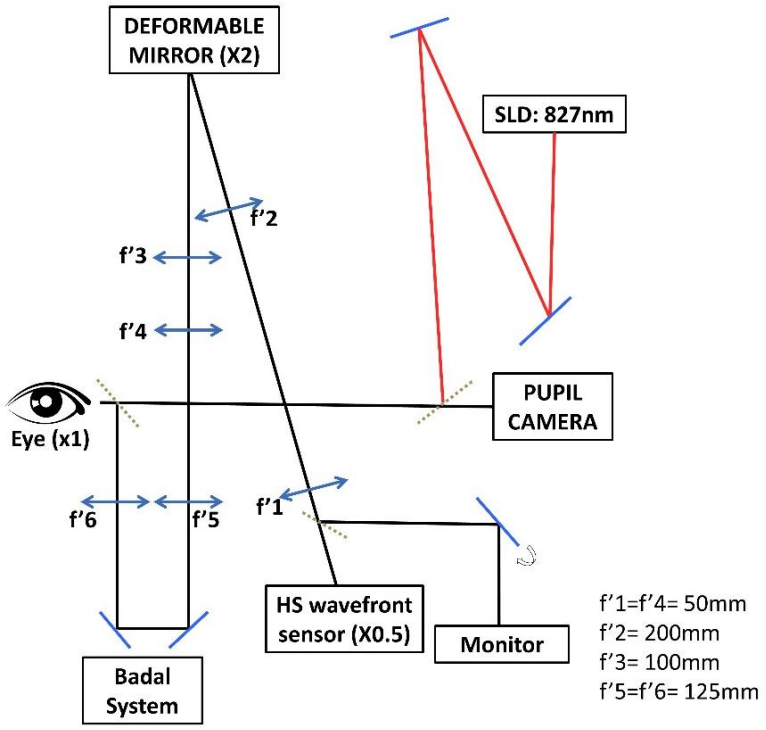

(a)

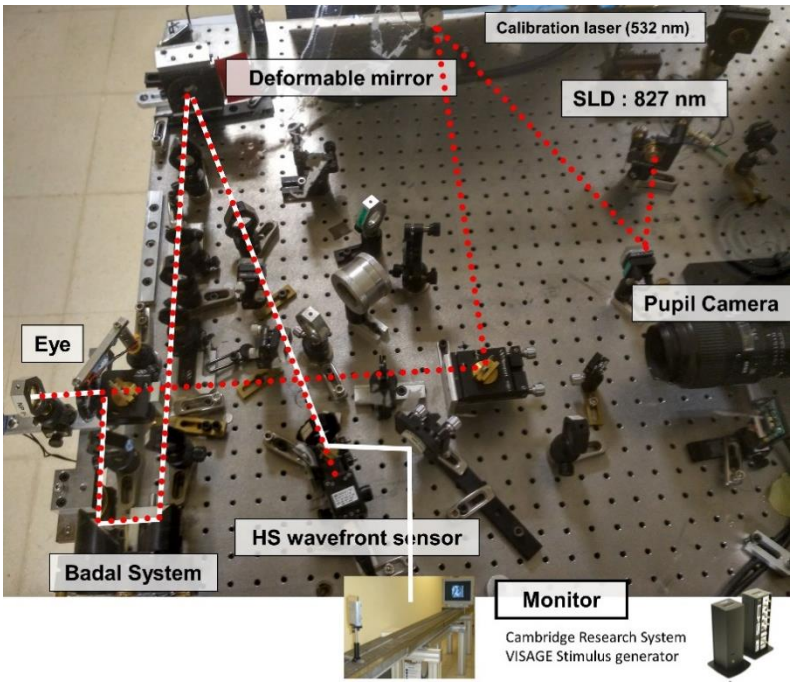

(b)

Figure 2.1. (a) Schematic diagram of the VioBio lab AOI. (b) Image of the VioBio lab AOI and its main components.

- *Channel 4:* During this thesis, a new channel has been developed to perform experiments with real IOLs placed at a conjugate pupil plane with x1 magnification. This new channel is described in detail in section 2.1.5.

- *Channel 5:* The psychophysical channel, to perform all the psychophysical experiments, is composed of a CRT monitor (Mitsubishi Diamond Pro2070). In the experiments described in this thesis, 480 pixel-size images were projected on the CRT, subtending 1.98º. The effective luminance of the white lines of the stimulus (after light losses in the system) is 50 cd/m, although it can be modified in order to perform mesopic or scotopic experimental conditions. The CRT is controlled by a programmable computer graphics system for psychophysical stimulus generation (ViSaGe, Cambridge Research System, United Kingdom).

- *Channel 6:* By using a plate beam splitter, a CCD camera (TELI, Toshiba) is inserted in the system in order to monitor the pupil of the subject. Subjects are stabilized by means of a bite bar and aligned to the system (using an *x*– *y*– *z* stage) using the line of sight as a reference. A ring of LEDs illuminates the pupil of the subject.

A custom-built software was developed [101], [164], programmed in Visual Studio C++ to control most of the devices of the system (Hartmann-Shack, Deformable Mirror and the Badal system). This software moves the motor of the Badal system, capture Hartmann–Shack images, and manage the deformable mirror, correcting or inducing different pattern of aberrations.

During this thesis, the study described in chapter 3 required to largely adapt the control program. In those measurements, subjects were asked to score random images under certain conditions: AO or NoAO correction and different Badal system's positions. The author of this thesis implemented the changes in the program in order to perform the experiment: the program randomly charged different deformable mirror states while the Badal system was moved. In that chapter, changes in the program are described in detail.

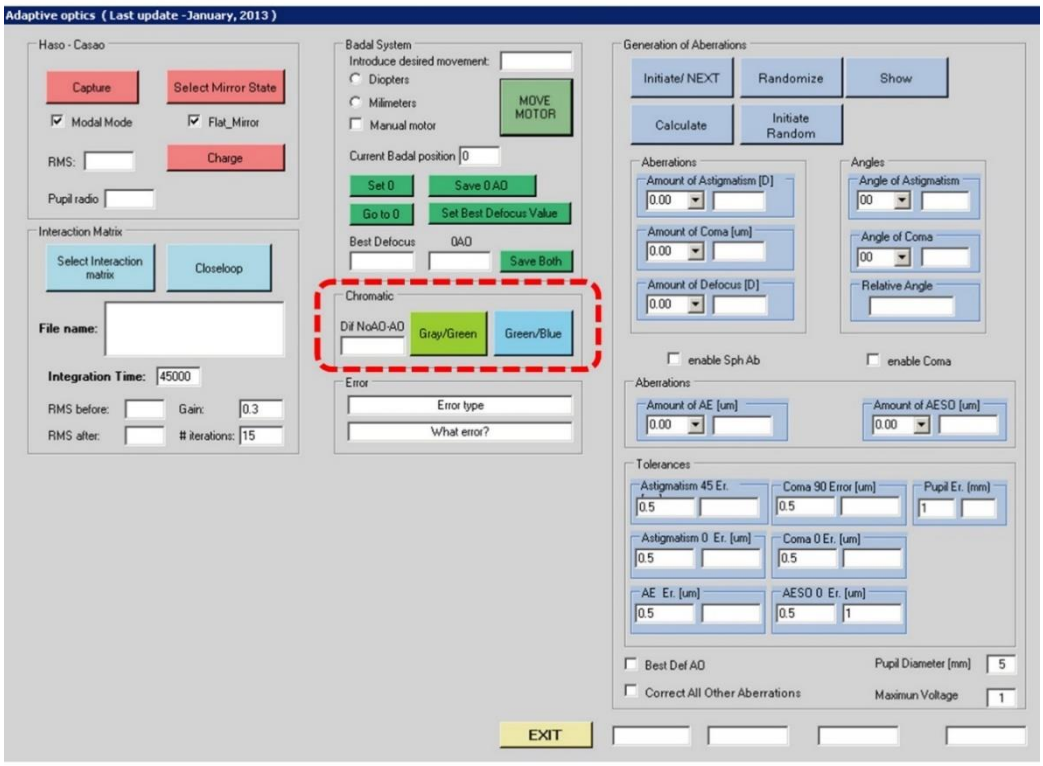

Figure 2.3. Custom-made software to control the VioBio lab AOI system: Badal system control, aberrations' measurement, correction and induction. Buttons outlined in red were specifically implemented for the experiment shown in chapter 3

A second program, software programmed in VB.Net 2005 (Microsoft), allows to monitor the size and centration of the pupil and to move the Badal system.

2.1.2. General description of VioBio lab AOII

VioBio lab AOII was designed, implemented, calibrated and validated in previous thesis [141]. The different stages of development are described in different publications [38], [47], [77], [166], [167].

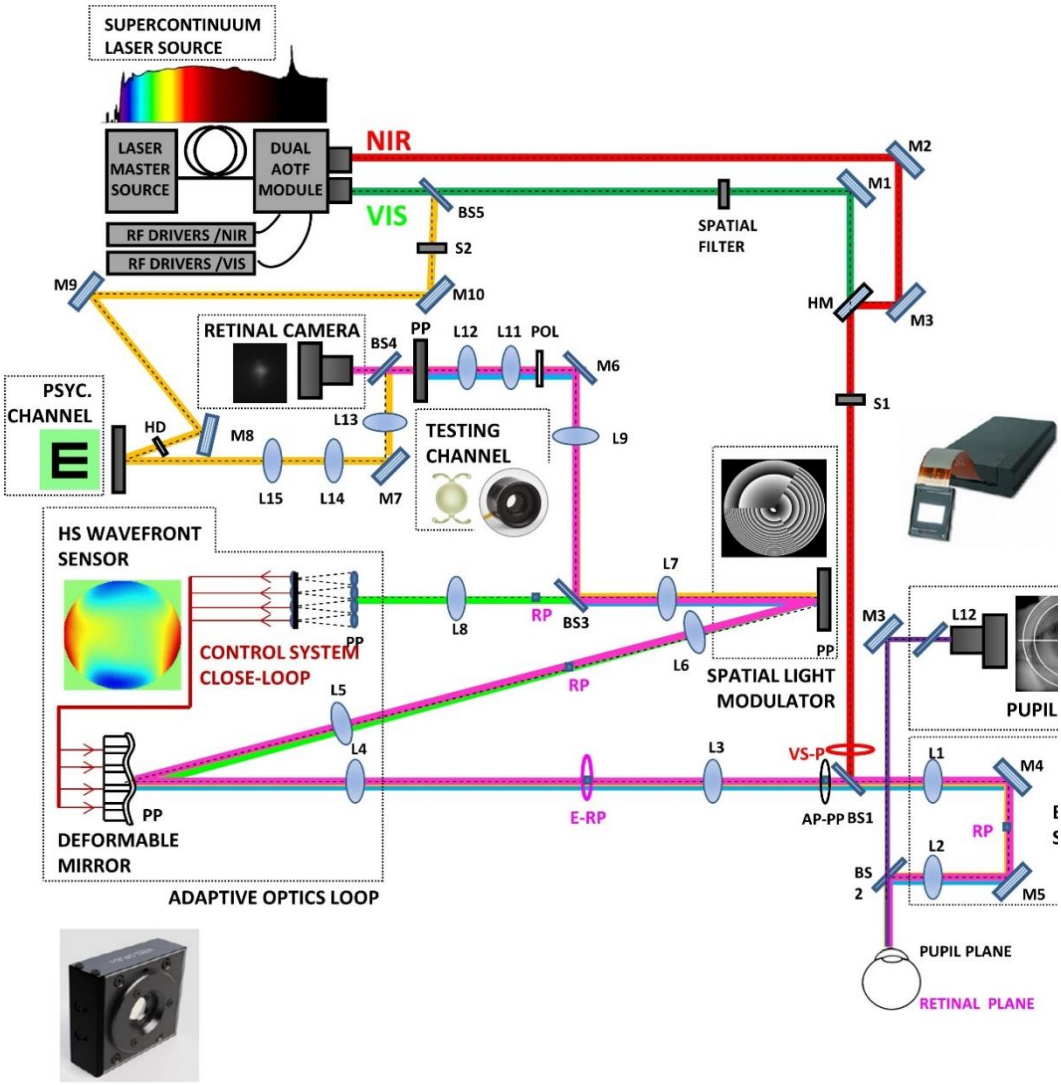

Figure 2.3. Schematic diagram of the VioBio lab AOII. In red NIR path; in green, Visible path; in green, AO channel; in blue, SLM and testing channel; in pink, retinal camera channel; in yellow, psychophysical channel; in purple, pupil camera channel. [77]

Figure 2.4 shows the VioBio lab AOII system. The system has (1) illumination channel, composed by a Supercontinuum Laser Source (SCLS). (2) AO-control channel composed by a Hartmann-Shack wavefront sensor and an electromagnetic deformable mirror. (3) Badal system. (4) Spatial Light Modulator (SLM) channel. (5) Testing channel. (6) Psychophysical channel, with a DMD. (7) A double pass retinal imaging channel. (8) Pupil monitoring channel.

- *Chanel 1:* The illumination channel is formed by a SCLS (SC400 femtopower 1060 supercontinuum laser, Fianium Ltd, United Kingdom). The SCLS emits in a range from 450 nm to beyond 1100 nm (according to our device settings). SCLS works in combination with a dual acousto-optic tuneable filter (AOTF) module (Gooch & Housego, United Kingdom), which is controlled by Radio Frequency drivers, and selects the appropriate wavelengths in visible or near infrared light automatically

(450, 488, 500, 532, 555, 570, 633 & 700 nm in the VIS light and 730, 780, 810, 827, 850, 880, 950 & 1020 nm in the NEAR-IR). The spectral bandwidth is 2-4 nm for VIS light and 3-6 nm for the NIR, on average. The beam is collimated and attached to two different multimode fibers, one for VIS light and the other one for NIR light. Laser path is splited to illuminate two different channels: AO channel (NIR and VIS) and psychophysical channel (VIR). After alignment of the illumination channel and before performing experiments on the eye, the laser power measured at the corneal plane for each wavelength on a range from 0.5 to 50 µW. Each time the laser was realignment, it was set a maximum permissible exposure according to the own parameters of the laser source and measurements (peak power, pulse duration) to avoid ocular damages [168]–[170].

- *Chanel 2:* The AO channel consists of a Hartmann-Shack wavefront sensor (HS) and an electromagnetic deformable mirror (DM). HS (HASO 32 OEM, Imagine Eyes, France) is composed of an array of 40x32 microlenses. The 2-mm diameter beam that penetrates the eye is marginally decenterd (1 mm) in comparison to the 3.6-mm effective diameter and centerd at 1062 nm the pupil center to avoid a corneal reflex in the Hartmann-Shack images. The DM (52 actuators, a 15-mm effective diameter and a 50-µm stroke; MIRAO, Imagine Eyes, France) works in closed-loop to correct the system's and eye's aberrations, as well as to induce aberrations. HS and DM are placed on conjugated pupil planes, with a magnification with respect the pupil's eye of x0.5 and x2 respectively. An artificial pupil (AP), placed in conjugate pupil plane, ensures constant pupil diameter in the measurements, with a different aperture according to the experiment.

- *Chanel 3:* The VioBio Lab AOII contains a Badal system which allows to compensate for the spherical error of the eye as well as for induce near distances without changing the magnification. The Badal system consists of two mirrors (M1 & M2) and two lenses (L1 & L2), mounted on a motorized system. It can be controlled by the scientific automatically or by the subject with a keyboard.

- *Chanel 4:* The SLM-Channel consists of a reflective phase-only LCoS-SLM (PLUTO-VIS; Holoeye Photonics 0AG, Germany; Resolution: 1920 × 1080; 0.7" diagonal; Pixel pitch: 8.0 µm; Image frame rate: 60 Hz; max. resolution: 62.5 lines/mm; 8 bits). The SLM is placed in a conjugate pupil plane with x1 magnification and allows to modify, by applying a voltage, the phase of a wavefront pixel by pixel. Thus, it is possible to simulate multifocal designs, even when the change of the phase is abrupt. To ensure the optimum output, a linear polarizer (POL) must be put in front of the SLM at the calibrated angle.

- *Chanel 5:* This is Testing-Channel, with a conjugate pupil plane with x1 magnification, where several devices can be tested. In this plane, a cuvette with a 0D real IOL immerse in water was placed, as it is described in chapter 7. Also, lathe-manufactured multi-zone multifocal surfaces were tested and compared with the performance of the same designs in the SLM, as described in chapter 6. Finally, also the simultaneous vision simulator (SimVis technology) has been implemented in this plane and compared with the real IOL and the SLM (chapter 7).

- *Chanel 6:* The psychophysical channel contains a Digital Micro Mirrors device (DMD, DLP® Discovery™ 4100 0.7 XGA, Texas Instruments Incorporated, USA), which is a rectangular array of moving micro-mirrors. The dimensions of the array are determined by the resolution of the particular DMD. DMD is located in a retinal plane and controlled by a programmable computer graphics system for psychophysical visual stimulus generation (ViSaGe, Cambridge research system). Images presented on the DMD are high resolution gray-scale and monochromatic light from SCLS illuminates the DMD. The visual stimulus subtends 1.62 degrees on the retina. To obtain a uniform stimulus illumination, a holographic diffuser (HD) is placed in the beam path to break the coherence of the laser. The luminance of the stimulus was 20-25 cd/m2 across the spectral range tested psychophysically (450-700 nm), therefore in the photopic region at all wavelengths.

- *Chanel 7:* The retinal imaging channel is implemented on the system with a 70/30 beam splitter. Images of the beam spot are projected on a scientific-grade CCD camera (Retiga 1300, CCD Digital Camera, 12-bit, Monochrome; QImaging, Canada; 6.7x6.7 µm pixel size, 1024x1280 pixels) by means of a collimating lens (L9, 50-mm focal length)and a camera lens (L16, 135-mm focal length). The laser beam is filtered before entering the eye by means of a spatial filter composed of a microscope objective (20x), a 25 µm-pinhole and a 50 mm lens. This channel acts as a "one-and-a half pass", with the aerial image being the autocorrelation of the image of the laser spot with a 2-mm entry beam and that with a 1-mm exit beam.

- *Chanel 8:* The natural pupil monitoring system consists of a camera (DCC1545M, High Resolution USB2.0 CMOS Camera, Thorlabs GmbH, Germany) conjugated with the eye's pupil by means of an objective lens (L12, 105-mm focal length). It is inserted in the system with a plate beam-splitter and is collinear with the optical axis of the imaging channel. Subjects are aligned to the system (using an x-y-z stage moving a bite bar) with the line of sight as a reference while viewing the natural pupil on the monitor.

Two different computers, with commercial and costumed-built software programs in visual C++, C# and Matlab, are used to control the devices in the VioBio Lab AOII system. The first computer controls the AO channel (DM and HS) using commercial software, as well as custom-built software (figure 2.5) which controls different channels: the pupil monitoring channel, the Badal system channel, the illumination channel (power and wavefront selection). The second computer controls the SLM, as well as with a costumed-built programmed in C++, as well as with Matlab routines. Psychophysical channel is also controlled with Matlab routines from the second computer

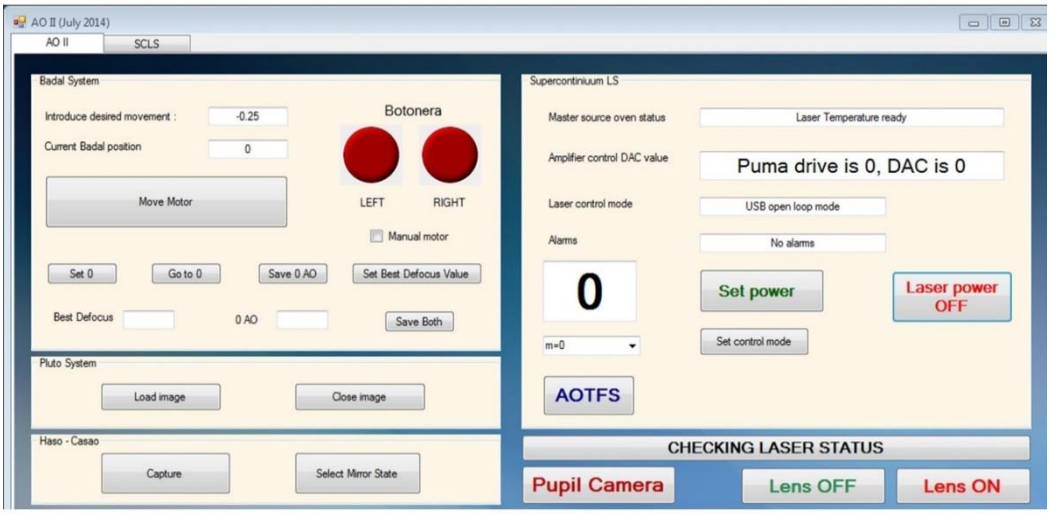

Figure 2.5. Custom-made software to control the VioBio lab AOII system. Software controls Badal system, illumination channel and pupil camera.

2.1.3. Experimental implementations during this thesis

For some of the experiments performed in this thesis, new implementations have been necessary in both AO systems. The following sections briefly describe these implementations and the capabilities that confer to the systems.

2.1.3.1. Implementation of a new channel for 0D IOLs testing within both AO simulators

During the development of this thesis, a new channel to testing real intraocular lenses was designed and implemented. A custom-developed cuvette was used to place real IOLs inside. Figure 2.6 shows the process of improvement of the cuvette for testing 0D IOLs. Several designs were tested (figure 2.6.a) until the final version of the cuvette (Figure 2.6.b-d), which was watertight.

The last version of the cuvette for 0D-IOL was composed of two assembled metal pieces with transparent windows and internal support to mount the real IOL in the proper plane and orientation. Expansion joints provided a watertight seal so that the cuvette can be filled with distilled water.

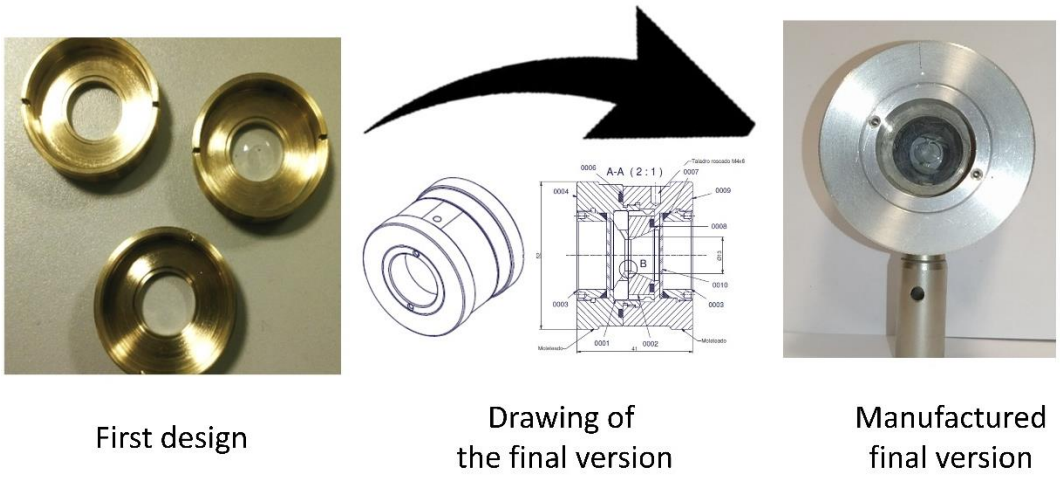

Figure 2.6. (a) First design of the 0D-IOLs cuvette. (b) Final version of the 0D-IOLs cuvette with an IOL mounted inside. (c) Draw of the general view of the last version of the 0D-IOLs cuvette. (d) Draw of the profile view of the last version of the 0D-IOLs cuvette.

Inserting the cuvette in a conjugate pupil plane allows measuring real IOL with 0D power. The 0D-IOL cuvette was implemented in both VioBio lab AO systems. To incorporate the 0D-IOLs cuvette in the VioBio lab AOI, it was necessary to generate a new conjugate pupil plane. The green line of Figure 2.7 shows the new path developed in the VioBio lab AOI to replicate the conjugate pupil plane.

Two lenses of 100mm of focal length were used in order to keep x1 magnification in the new pupil plane. Two flip-up mirrors allowed to select one or the other path.

Once the cuvette was developed and tested in the VioBio lab AOI system, it was moved to VioBio lab AOII system and placed on the conjugate pupil plane of the testing channel (Figure 2.3). In VioBio Lab AOII, real intraocular lenses were compared with other simulators (SLM and SimVis) by using the 0D-cuvette [77]. This comparison is described in the chapter 7.

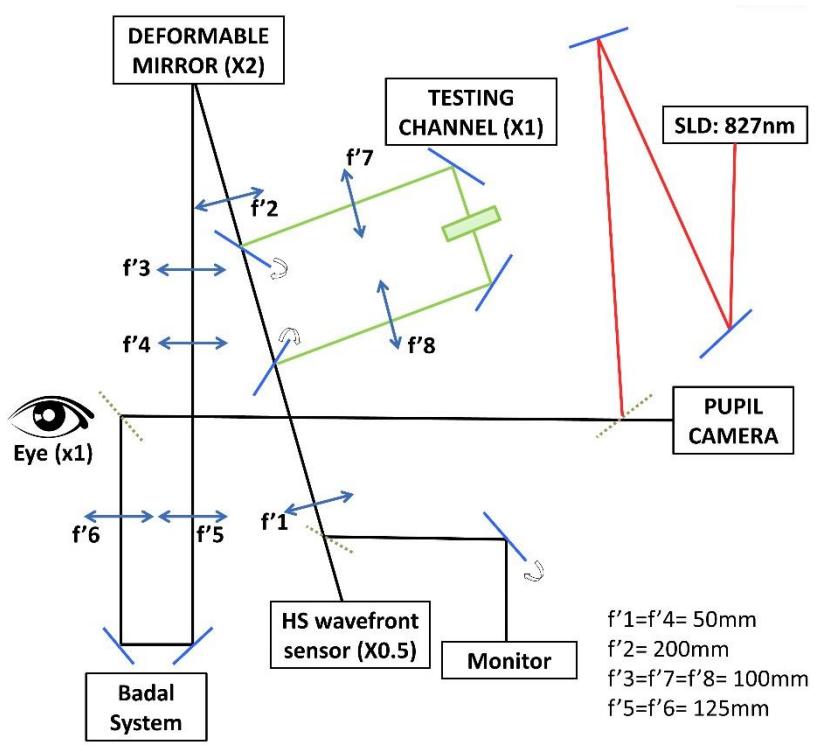

(a)

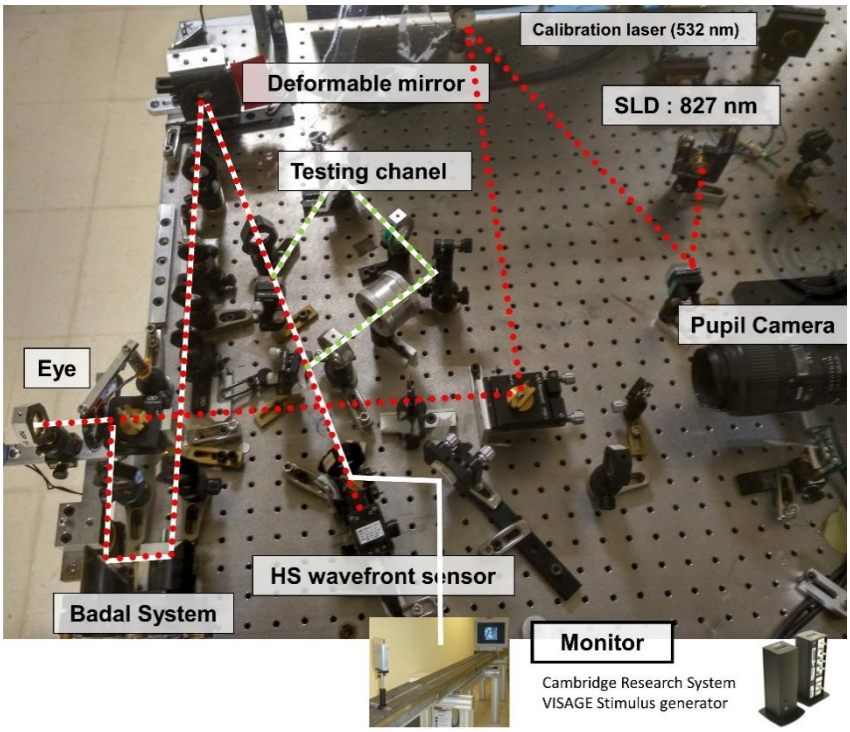

(b)

Figure 2.7. (a) Schema of the generation of a new conjugate pupil plane in VioBio lab AOI with magnification x1 for the placement of 0D-IOLs cuvette. In green line, new implemented channel. (b) Image of the VioBio lab AOI after implementation of new channel for 0D-IOLs cuvette.

2.1.3.2. Implementation of a new channel for real IOLs testing within both AO simulators

The previous cuvette design provides the capability of measuring 0D IOLs. However, it is interesting to expand this capability to non-0D IOLs, of different powers. A new type of cuvette and a new channel were designed and implemented with this goal.

The second design of the cuvette was developed making use of a Rassow system. The Rassow system is a telescope 4F system [152] (relay system) with x1 magnification, in which one of the lenses is the IOL and the other one, is an achromatic doublet which compensates the 20D of the power of the IOL (Newport, PAC043 Achromatic Doublet Lens, 63.5 mm EFL). The IOL is immersed on a cuvette, composed of metallic support where the IOL is placed and a transparent container (Lambda-X, Nivelles, Belgium) filled with distilled water (n=1.33). The distance between the cuvette which contains the IOL and the Rassow lens is 120mm, two times the focal length of the Rassow lens, as well as the distance between the Rassow lens and the following pupil plane. The Rassow system had been previously used to evaluate real IOLs [153].

Before the implementation of the Rassow system, optical simulations were performed with Zemax (Zemax–EE Optical Design Program © 1990-2005). Figure 2.8 shows the schematic diagram of the design simulated in Zemax: real values of a 20D IOL immersed in a cuvette with distilled water, the Rassow lens (lens which compensates the 20D of the IOL) at a distance of two times the focal length, the first lens of the Badal system at the distance of two times the focal length plus the focal length of the first Badal lens, the second lens of the Badal at a distance of the sum of the focal length of both Badal lenses and, finally, a paraxial lens to collimate rays in the image plane, which is at a distance of the focal length of the paraxial lens.

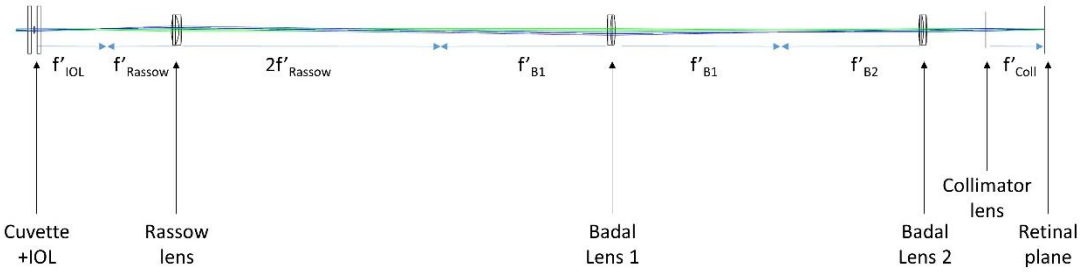

Figure 2.8. Schema of the Rassow system with Zemax.

After Zemax simulations, the Rassow system was implemented in both VioBio lab AO systems. For implementation in VioBio lab AOI, the previous new path for 0D-IOL cuvette was removed and we took advantage of the two flip-up mirrors to build the new path for non 0D-IOL cuvette (figure 2.9).

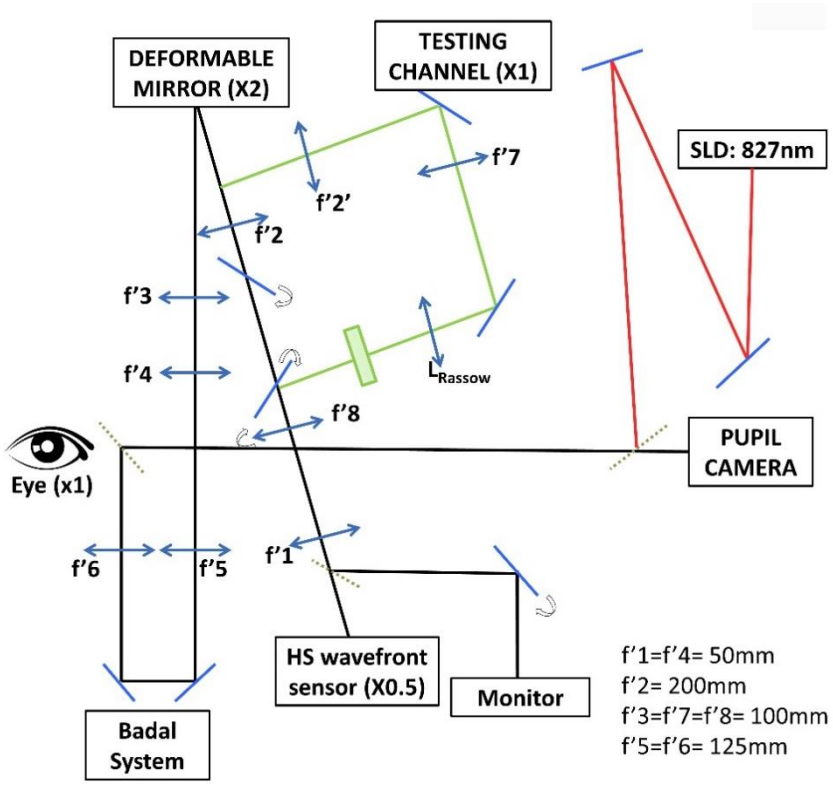

(a)

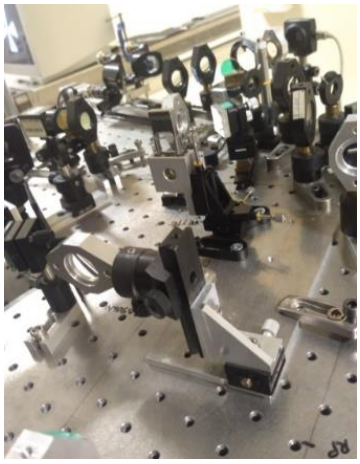

(b)

Figure 2.9. (a) Schema of the implementation of the non 0D-IOL cuvette in VioBio lab AOI. In green, the new path. (b) Image of the implementation of the cuvette in the VioBio Lab AOII.

The implementation of the cuvette in the VioBio lab AOII was made through the built of a second floor, in order to maintain the conjugate pupil plane of the testing channel, because it is used to evaluate phase maps and SimVis technology.

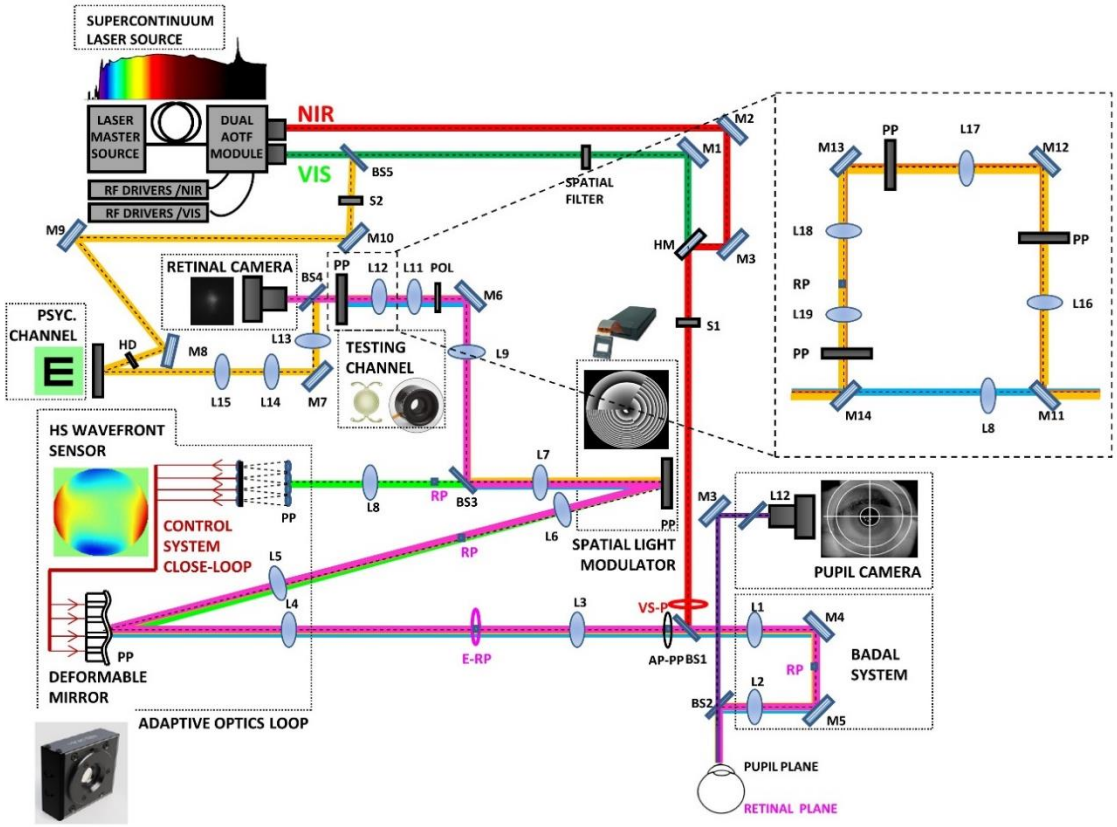

(a)

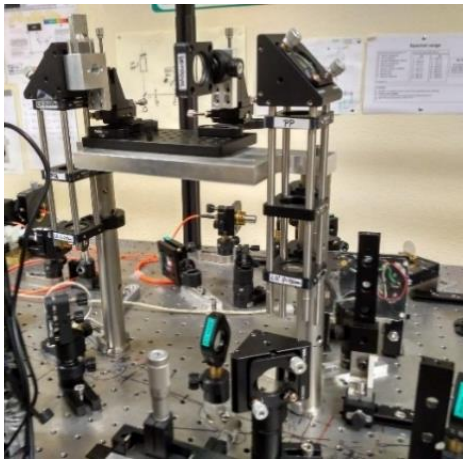

(b)

Figure 2.10. (a) Schema of the implementation of the non 0D-IOL cuvette in VioBio lab AOII. (b) Image of the implementation of the cuvette in the VioBio Lab AOII.

Measuring IOLs with refractive powers different from 20D is possible by compensating the power difference with the Badal system. With this needed system, it is possible to measure IOLs from +16 to +23 D. The power magnitude to compensate the power difference was estimated with Zemax simulations and also experimentally calculated in both set-ups VioBio lab AOI (Figure 2.11, b) and AOII. A linear correlation was found experimentally, as shown in Figure 2.11, a.

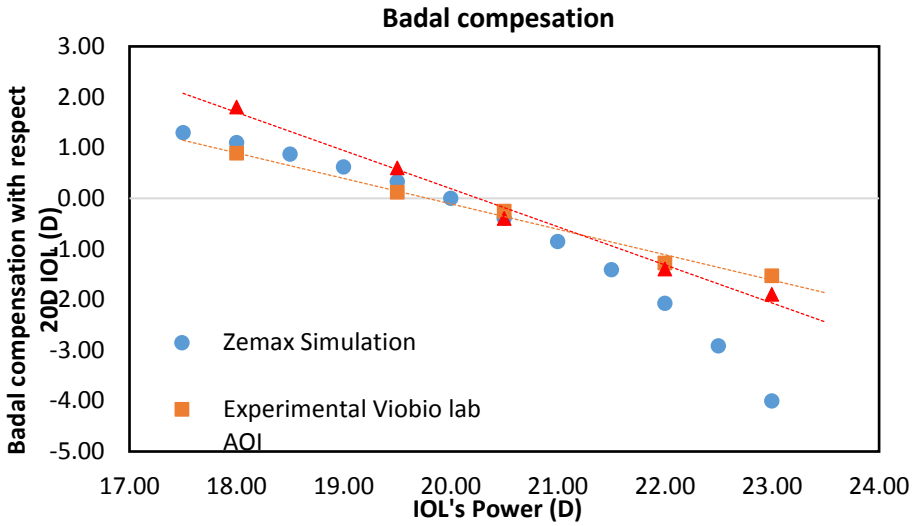

(a)

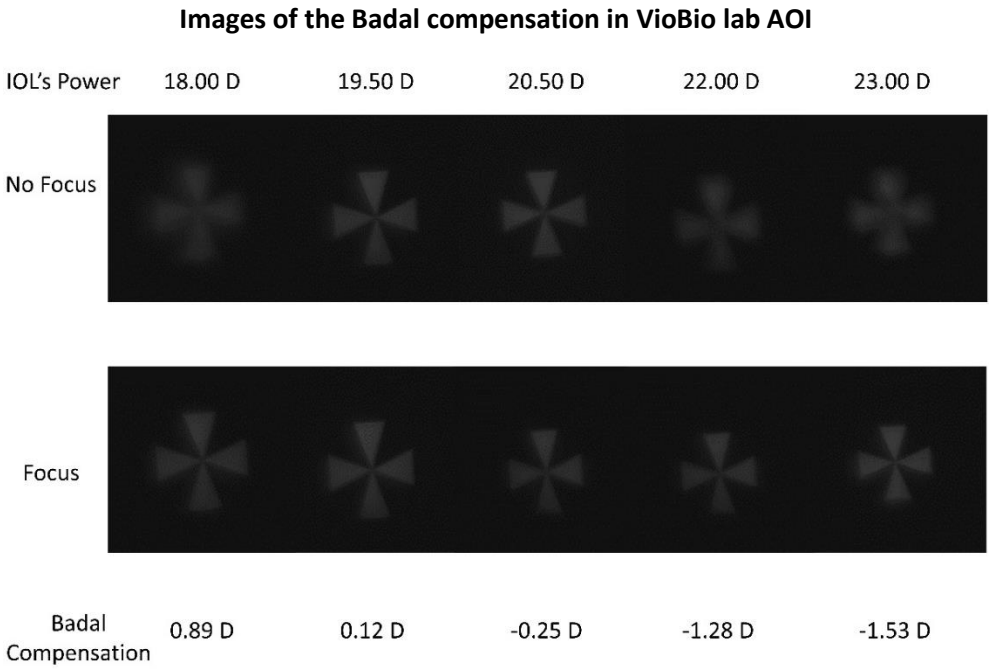

(b)

(c)

Figure 2.11. (a) Amount of needed diopters to compensate the power of an IOL different from 20D. Blue circles are for Zemax simulations, orange squares are for experimental measurements of VioBio lab AOI and red triangles are for experimental measurements of VioBio lab AOII. (b) Example of images of the Badal compensation in VioBio lab AOI. (c) Image of the non-0D cuvette with a mounted IOL.

2.1.3.3. Implementation of white illumination for the psychophysical channel of VioBio Lab AOII

A halogen fiber optic illuminator (150 W, 3200 K Halogen Bulb, Thorlabs Mod. OSL2) was incorporated to the psychophysical channel. The implementation on the VioBio lab AOII was in front of the holographic diffuser of the DLP, and following the same path that the supercontinuum laser source does.

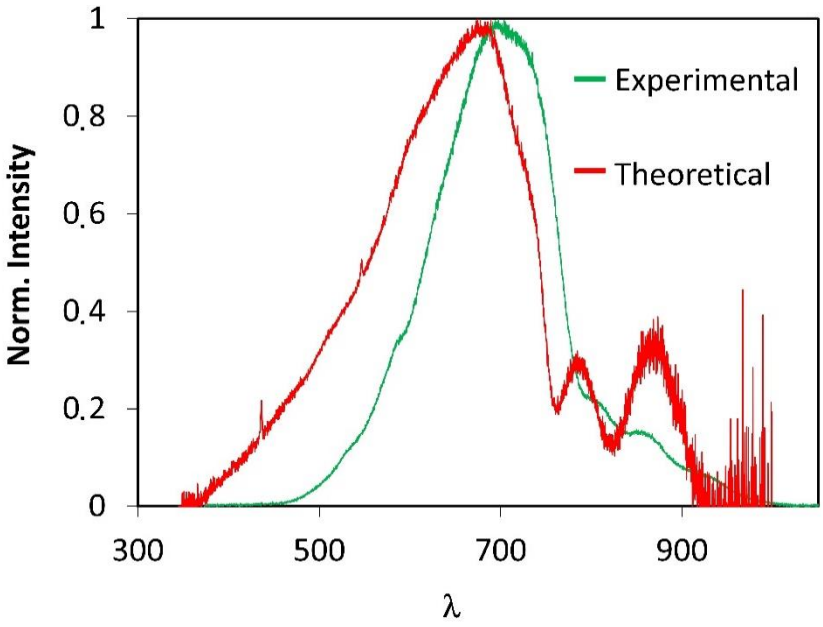

(a)

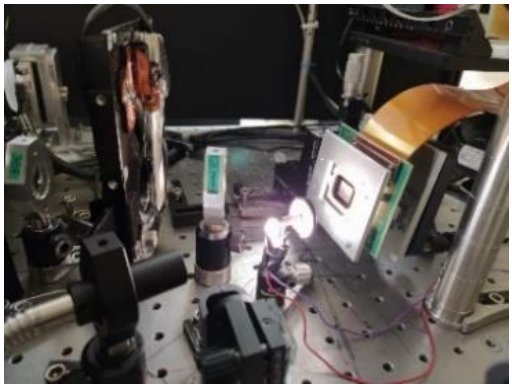

(b)

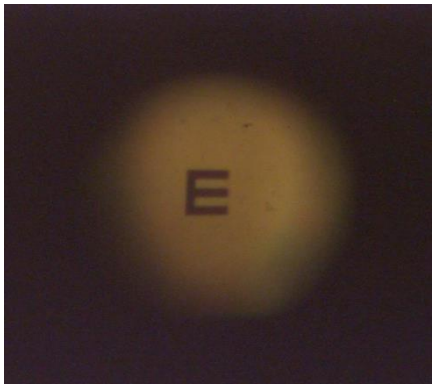

(c)

Figure 2.12. (a) Spectrum of the implemented white light source. Data were measured in the VioBio lab AOII (in green) and provided by Thorlabs (in red). (b) Halogen fibre optic illuminator implemented in the system and illuminating the DLP. (c) Image of E Snellen stimulus through the system, illuminated with the white light source and taken with a camera placed on the artificial eye position.

Figure 2.12 shows the implementation of the illuminator in the VioBio lab AOII system and the spectrum of the source. Using white light allows performing optical measurements in a more realistic environment. An example of this is the experiment described in chapter 3. It should be noted that the SLM is subject to chromatic aberration, and this must be corrected for each wavelength.

2.1.3.4. Development of new routines for chromatic experiments with both AO simulators.

The luminance of the CRT at the subject's pupil plane is 23 cd/m2. Experiments involving the use of different wavelength required adjustments by the luminous efficiency function or luminosity function $V(\lambda)$ [171] represented in figure 2.13, a to compensate the differences in sensitivity to the different wavelengths and equate perceived luminance of the different wavelengths, through brightness matching.

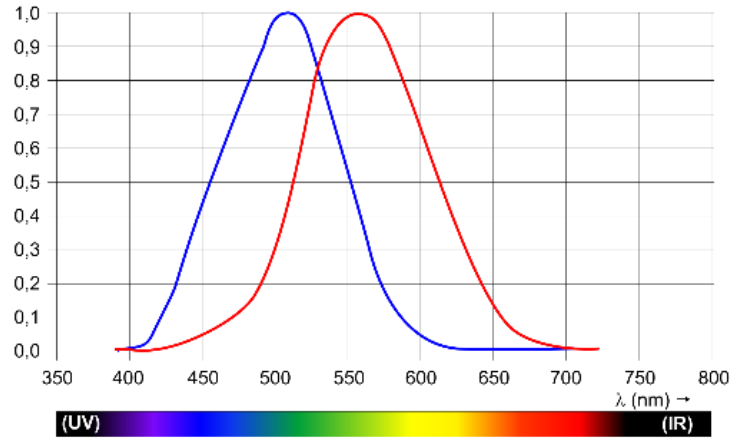

(a)

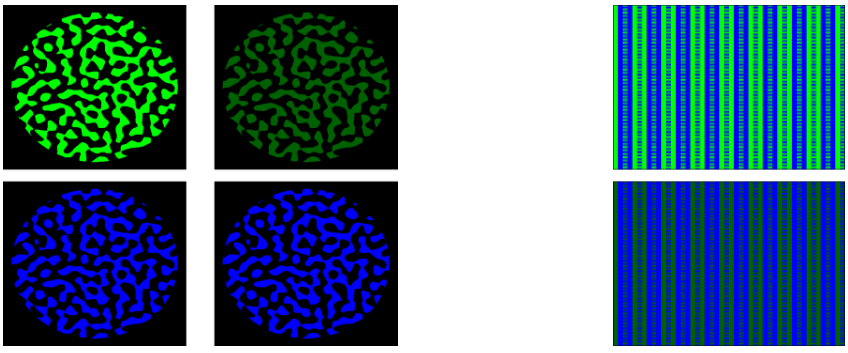

(b) (c)

Figure 2.13. (a) Luminosity functions V(λ) for photopic (red) and scotopic (blue) human vision. (b) Example of the noise stimulus used to equalize blue and green luminances. Blue and green stimuli were alternatively presented (minimum motion technique). On the left column, the stimuli at the beginning of the experiment and right column at the end of the experiment, once luminances were subjectively equalized. (c) Stimulus presented to equalize luminances of green and blue light, where both colors were simultaneously seen. Up, the stimulus at the beginning of the experiment and down, once that both luminances were equalized.

This was done through various strategies.

In VioBio lab AOI, subjects manually adjusted the illumination of the stimulus presented in the CRT. The minimum motion technique [172] with 16 sectors was used to measure the equiluminance balance of the blue and green channels of the screen in the experiment described in chapter 3. That balance was then checked with heterochromatic flicker fusion experiment [173] using the blue and green versions of the noise images used in the experiment (figure 2.13, b). A second method was developed to double-check the results. In this case, luminances were compared in the same image simultaneously and the subject manually adjusted green color until the same perceived luminances were obtained (figure 2.13, c).

In VioBio lab AOII, a manual control of the power laser by the subject was not possible. In this set-up, the change of luminance is done by increasing the gray level of the projected image on the DLP while the laser power remains constant. In this way, the subject has control over the level of gray that increases to the most luminous wavelength while the examiner controls the wavelengths which illuminate the stimulus. This method was used to perform the experiment described in chapter 3.

2.2. Experimental protocols

These two AO systems were used to perform experiments both on-bench and *in vivo*. General procedures were common to all human subjects, both regarding ethics and measurements, as described in this section. Specific protocols for each study are presented in each specific chapter.

2.2.1. General protocols with human subjects

2.2.1.1. Ethics statement

A total of 70 subjects, with different inclusion criteria depending on the study, participated in the different studies of this thesis. All of them knew the nature and possible consequences of the study and gave their written informed consent before enrolling in the study. All protocols complied with the principles of the Declaration of Helsinki and had been previously approved by the Bioethics Committee of the National Research Council (CSIC).

2.2.1.2. Optometric and Ophthalmologic evaluation

The subjects who participated in the different experiments followed an exhaustive optometric evaluation in the Clinic of the Faculty of Optometry of the Complutense University of Madrid (UCM). Subjects implanted with IOL received a complete ophthalmological evaluation, in most cases followed by surgery before enrollment in the study at IOA Madrid Innova Ocular (Madrid, Spain) (chapter 3). Before the AO measurements, subjects underwent additional standard optometric measurements on site, including autorefraction (ARK1, Nidek), which allowed an initial adjustment of the correction of defocus in the Badal system.

2.2.2. Measurement with the VioBio lab AO systems

2.2.2.1. Pupil dilation

In all described experiments during this thesis, subjects were instilled with Tropicamide 1% in order to paralyze accommodation and to dilate the pupil. The aperture of the system is therefore limited by the artificial pupil, guaranteeing the same pupil diameter for all the subjects across the measurements. Drops were instilled according to the following dose: Before starting the experiment, 2 drops 10 minutes apart, and during the experiment, 1 drop every 1 hour.

2.2.2.2. Alignment of the subjects with the pupil camera

With the help of a camera, the subject's pupil was monitored during the whole experiment, controlling focus and centration. The subject was asked to look at the center of a Maltese cross projected on the CRT or on the DMD (in the VioBio lab AOI or AOII, respectively). A dental impression mounted on a xyz linear stage ensured that the subjects kept proper alignment during the experiment.

2.2.2.3. Compensation of the refractive error

The subject was asked to adjust his/her best subjective focus (from a myopic blur) by controlling the Badal system with a keyboard while observing a high-contrast Maltese cross in the CRT or DMD (in the VioBio lab AOI or AOII, respectively). Spherical error was corrected with Badal system instead of with the deformable mirror, as the range of the mirror was saved to correct astigmatism and high order aberrations. The best subjective focus was obtained for the different states of aberration correction, because for example, the presence/absence of aberrations plays a role in the best focus setting.

2.2.2.4. Measurements, induction and correction of HOAs

After alignment of the subject and once that the Badal position is in the best subjective focus of the subject, a wavefront measurement is saved and used as a baseline measurement of the natural aberrations of the subjects (using a “flat mirror” of the system previously charged in the DM which accounts for the aberrations of the system). In those experiments in which the natural aberrations of the subjects have to be compensated (described in chapters 3, 4, 5 and 6) or any kind of aberration has to be induced (chapter 5), a closed-loop correction is performed. The mirror state obtained after a closed-loop correction is saved and used during the measurements, with initial verifications (and subsequent verifications throughout the experiment) to confirm that this mirror state actually corrects the natural aberrations of the subject or induces the desired aberration, An AO correction is considered satisfactory if the residual aberration (RMS for a 6-mm pupil) is less than 0.2 microns. In most cases, the residual RMS is around 0.1 µm. A closed-loop correction (at a speed of 13 Hz) is typically achieved in 15 iterations. The control of the pupil and wavefront aberration with the proper mirror state was done before and after the psychophysical measurement to confirm correct centration and AO correction/induction. The duration of the experiments reported in this thesis ranged from to 2 to 10 hours.

All the studies performed in this thesis involved measurements and manipulations of the aberrations of the eye in the AO systems and psychophysical measurements in subjects under manipulated aberrations. The next section describes psychophysical paradigms used in the experimental studies of this thesis.

2.3. Psychophysical experiments

Psychophysical experiments allow measuring the quantitative relationship between physical stimulus properties and the perceptual experience [174] in order to describe perceived visual quality and visual function under a certain visual correction[174].

2.3.1. Visual stimuli and manipulation of retinal blur

The different psychophysical tasks in the experiments of the thesis entailed different. Some examples can be found on figure 2.14.

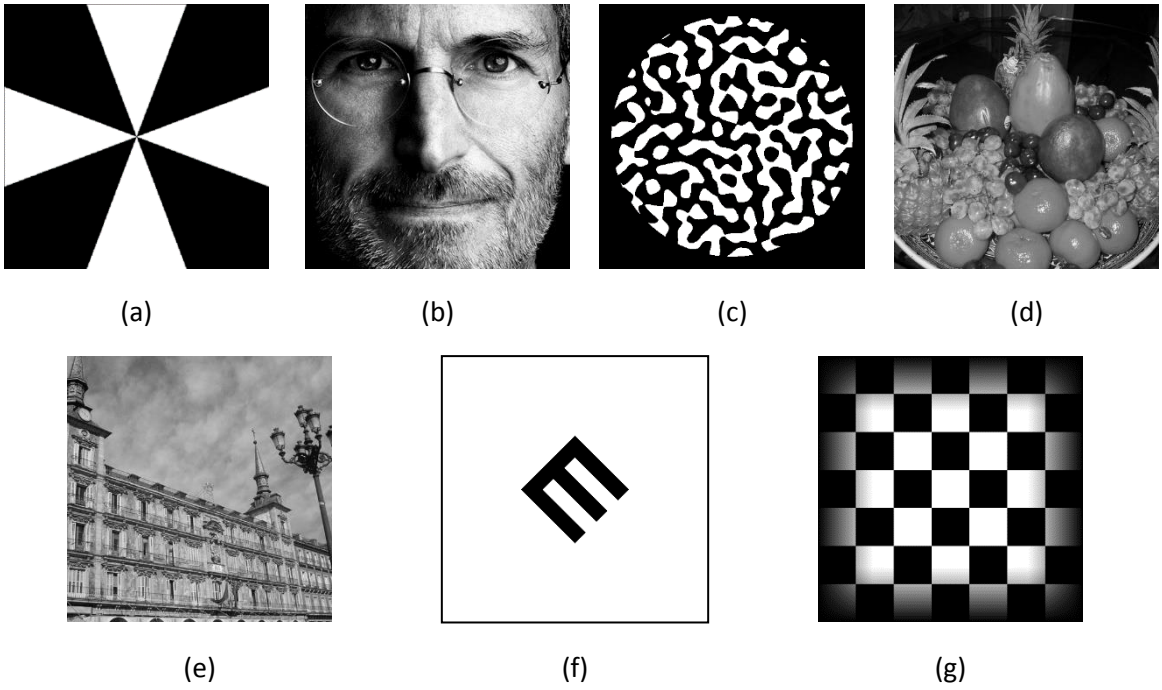

Figure 2.14. Example of stimuli used in the experiments of this thesis. (a) Maltese Cross. (b) Steve Jobs' face. (c) Binary noise. (d) Fruit bowl. (e)Plaza Mayor, Madrid's square. (f) Snellen E (used in different orientations, 4 or 8). (g) Checkerboard Square. Edges are smoothed with cosine function

Stimuli were presented on the CRT of VioBio Lab AOI or the DLP of VioBio AOII. In the VioBio lab AOI, stimuli subtended 1.98 degrees while in the VioBio lab AOII, stimuli subtended 1.62 degrees.

Manipulation of the retinal blur was done with different methods, depending on the experiment:

- Using AO elements such as the deformable mirror, the SLM or the testing channel (Phase Maps, Cuvette, SimVis). The deformable mirror is used in chapters 3, 4, 5 and 8; the SLM in chapters 6 and 7 and the testing channel in chapters 6, 7 and 9.

- Using convolved images. In this case, the deformable mirror corrects the subject's aberrations and the retinal blur is produced directly on the image, guaranteeing

that subjects have the same retinal images projected on their retina, thus, any difference in function/perception will arise from their own neural processing and their prior neural adaptation. This method is used in chapter 4. To calculate the convolution, subject's aberrations (LOAs and HOAs) must be previously measured. The PSF is calculated with Matlab using Standard Fourier optics techniques [83] Fast Fourier Transform, and scaled to match the pixel size of the original image. All computations were performed for a constant pupil diameter (5mm pupil). The Stiles–Crawford effect was not considered, as for typical ρ values (ρ< 0.1; [175]) its effect was negligible for the purposes of our studies.

2.3.2. Visual Psychophysical paradigms

The following psychophysical paradigms were used in the studies of this thesis, all programmed with the Psychtoolbox Package in Matlab [176], [177].

2.3.2.1. QUEST method

QUEST (QUick Estimation by Sequential Testing) procedure is the first Bayesian method developed for estimating the psychophysical threshold [178]. QUEST is an adaptive procedure that estimates the slope in the stimulus in each trial: after each response, the values of the parameters that maximize the probability of the set of responses that have been obtained are calculated, given the set of stimuli that have been presented. These values are used to determine the location of the next stimulus.

Figure 2.X.a. shows an example of how QUEST graphs converge to the tested threshold. During this thesis, QUEST method has been used to determinate two different parameters:

- Visual Acuity (VA) was measured using a high contrast tumbling Snellen E letter. The thickness of the lines and gaps of the E letter are 1/5 each one. Subjects must have identified the orientation of the E letter, using an 8 (chapters 5, 6 and 7) or 4 (chapters 3 and 9) Alternative Forced Choice (8AFC, 4AFC), according to the number of orientations (8 orientations: pointing up, down, left, right, oblique up-right, oblique-up- left, oblique-down-right, oblique down-left. 4 orientations: pointing up, down, left, right.). QUEST method estimated the threshold of the minimum recognizable size letter for VA measurement.

- Amount of blur threshold (chapter 5). Subjects must have to answer if they appreciate any blur difference between the stimulus and a given reference, which are presented in random order. This was a Yes/No 2 Alternative Forced Choice experiment (2AFC).

A QUEST (QUick Estimate by Sequential Testing) algorithm was programmed in Matlab with Psychtoolbox [177] to select the size of each E letter or the blur difference and optimize the estimation of the spatial resolution threshold.

2.3.2.2. Up-down staircase procedure

Up-down staircases are designed to approximate thresholds by adjusting the stimulus variable up or down after integer numbers of correct or error responses at certain specified probabilities of a correct answer [174]. During this thesis, a truncated staircase procedure was used to determine subjective best focus chapter 5).

The truncated staircase refers to a 1/1, or 1-up and 1-down, a staircase that converges on 50% correct (or "yes") responses [179]. The 1/1 adaptive staircase increases the manipulated variable, after every "no" response and decreases the variable after every "yes" response. It is also possible to perform transformed staircases (2/1, 3/1, or 4/1), which increase difficulty after 2, 3 or 4 consecutive correct answers after each mistake. These staircases converge with a 70.7%, 79.4% and 84.1%, of probability respectively.

In this thesis, the manipulated variable was a certain amount of defocus, induced with the Badal system. The maximum number of trials in each staircase was 40 and the best focus was selected after a maximum number of 20 reversals. The four interleaved staircases started at different initial values and the best focus was defined as the average of the last 8 reversals.

Fig 2.15.b shows an example of a staircase measured during this thesis, compared to QUEST procedure.

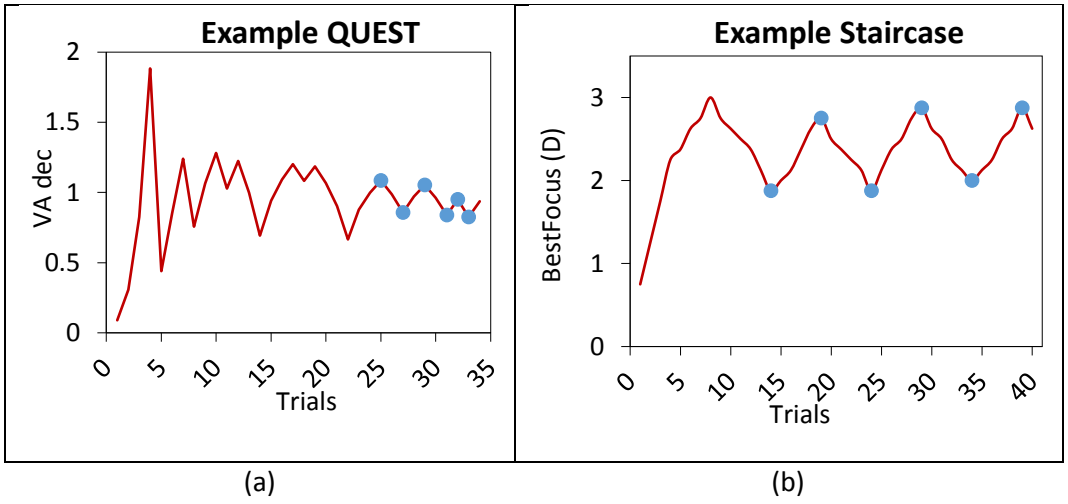

Figure 2.15. Real examples obtained from the same subject S#2-G3 of the experiment described in chapter 5 (a) from Quest method and its corresponding graph and (b) for Staircase procedure and the obtained graph

2.3.2.3. Scoring algorithm

With the scoring method, subjects evaluate an image under a certain condition indicating the level of confidence. In this thesis, a scoring task was used in two different experiments (reported in chapters 3 and 6). In both cases, subjects had to grade the image quality with 6 levels of confidence with a numerical keyboard from very sharp to very blurred in a 6-point scale using corresponding keys in a response system (1-very blurred, 2-blurred, 3-not so blurred....). A score, of 0 to 5, was posteriorly assigned, based on the grading. In each experiment, subjects evaluated the stimulus under different conditions:

- With or without chromatic shift, compensating or not of HOAs. Subjects had to judge three different images (binary noise, fruits picture and city picture) with the correction or not of HOAs and with or without chromatic induced shift with the Badal system (gray or green images) or inherent in the image (blue/green images) Images were presented during 1.5 seconds. (Experiment described in chapters 3).

- Stimulus is viewed under different multifocal corrections (lathe-manufactured or SLM simulated) projected to the pupil of the subject. The stimulus was a binary noise pattern with sharp edges at random orientations, generated for each trial, 60 in total, and presented for 0.5 seconds. (Experiment described in chapter 6).

2.4. Optical quality analysis

The experimental measurement of the aberrations with the Hartmann-Shack sensor allows us to study the optical quality of the retinal image of the subject and compare it with the perceptual response of the subject. There are different metrics to quantify the optical quality of the retinal image: RMS, PSF, MTF or Strehl Ratio, already described in chapter 1.

In this thesis, the most frequently used metric is Visual Strehl (VS), previously reported as a metric that best correlates with visual function. Thus, while SR (chapter 1) includes frequencies that are not relevant to the visual system, VS is scaled by the neural contrast sensitivity function, CSF_N [28]. Equation 2.1 describes the calculation of the VS, being CSF_N the Neural Contrast Sensitivity Function, OTF the Optical Transfer Function of the aberrated system, OTF_{DL} the OTF of a limited by diffraction system and (fx, fy) are the spatial frequency coordinates.

$$VS = \frac{\int_{-\infty}^{\infty}\int_{-\infty}^{\infty} CSF_N(f_x, f_y) \cdot OTF(f_x, f_y) df_x df_y}{\int_{-\infty}^{\infty}\int_{-\infty}^{\infty} CSF_N(f_x, f_y) \cdot OTF_{DL}(f_x, f_y) df_x df_y} \quad [eq.\ 2.1]$$

A correlation between VS and subjective acuity testing in the clinic has been previously reported [81]. We used this metric to build an “ideal observer” to predict performance purely based on optical grounds.

2.4.1. Building an ideal observer from the optical quality

MTF and Visual Strehl are metrics that describe the optical quality of the eye. In this thesis, they have been used to predict the response of the subjects and build an “ideal observer”, purely responding on optical grounds to the same psychophysical test performed on subjects [76]. Using an ideal observer, it is possible to correlate the optical quality of the subjects and their psychophysical responses. Note that “ideal observer” is not referred here to sophisticated classical models that attempt to reproduce the performance of the entire visual process [180].

This procedure is used in two different studies of this thesis

- In the study described in chapter 3, the ideal observer was calculated from the MTF. Optical wave aberrations of each subject were measured and fitted by a Zernike polynomial expansion up the 6th order, obtained as the average of 3 repeated measurements. The MTF was calculated replicating the different conditions of the experiments and the optical responses of the ideal observer were obtained from the normalized volume under each MTF. Psychophysical responses were also normalized to 1, in order to compare them with the optical responses.
- In chapter 6, the responses of an ideal observer were calculated. Through focus VS normalized to the maximum VS value was calculated for each eye and condition. From VS curves, three different values were obtained: (1) Area under VS curves in a 6.0 D dioptric range; (2) Dioptric range above a certain threshold

(0.06); (3) VS at far, intermediate and near distance (0 D, + 1.5 D and + 3.0 D, respectively). Taking this account, the responses of an ideal observer were estimated for each subject, distances and conditions. Scores were ranked from 0 to 5, using a similar approach to the psychophysical paradigm for perceptual scoring.

2.4.2. Correlation metric

As it was explained in the previous section, it is possible to predict the psychophysical performance of a subject through an ideal observer, built from the optical quality of the subject. To study the objective performance of a certain design, with 1-pass on-bench images, it is possible to compare how similar are two images through correlation metric, which following eq. 2.2:

$$corr = \frac{\sum_n (X_n - \overline{X_n})(Y_n - \overline{Y_n})}{\sqrt{\sum_n (X_n - \overline{X_n})^2 \sum_n (Y_n - \overline{Y_n})^2}} \quad [eq.\ 2.2]$$

In this thesis, the correlation metric has been used to compare through focus images obtained for a certain design with a reference image, which would be perfect. The correlation metric is used in experiments described in chapters 6, 7 and 8.

Chapter 3. Understanding the interactions between chromatic and monochromatic aberrations

This chapter presents a study about the interaction between chromatic and monochromatic aberration and its influence on visual performance.

This chapter is based on the paper by Benedi-Garcia et al. "*Vision is protected against blue defocus with or without (im)perfect optics*" submitted to Scientific Reports in 2020. The co-authors are Maria Vinas, Carlos Dorronso, Eli Peli, Stephen Burns and Susana Marcos. This study was also described in the review paper by Marcos et al. "VioBio lab AO: technology and applications by women vision scientists" [154]

The work was presented as a poster contribution in the IX Workshop on Adaptive Optics for industry and medicine in 2018 by Benedi-Garcia under the title "*Impact of the interactions between mono- and chromatic aberrations on visual function*". Same year was presented as a poster contribution in ARVO by Susana Marcos with the title "*Visual benefit of correcting Higher Order Aberrations in blue or green light: an optical effect?*". Preliminary results were presented in IONS on 2017 as an oral contribution by Benedi-Garcia under the title of "*Impact of the interactions between mono-and chromatic aberrations on visual function*".

The author of this thesis designed the experiment in collaboration with the rest of the authors, implemented the experimental protocol in collaboration with Maria Vinas, performed the experimental measurements on subjects, collected and analyzed the data in collaboration with the rest of the authors and prepared the manuscript in collaboration with Susana Marcos.

3.1. Introduction

Despite the degradation of the optical quality caused by aberrations, observers are not aware of the blur present in their retinal images, reflecting both the sampling properties of retinal neurons and the underlying neural adaptation to the native optical blur [5]. This neural adaptation, a recalibration process in the visual system that hide the retinal images blur, is ubiquitous in vision, as the visual system adapts to changes in the optics and the environment over time, using similar strategies across different stimulus domains (contrast, spatial frequency, face perception or color) [7].

The physical defocus of the retinal image caused by the LCA of the eye is potentially high. The chromatic defocus between the wavelength of the maximum sensitivity of S and M/L cones is ~1.5 D, equivalent to a ~26 arcmin blur circle for a 5 mm pupil [121]. Yet, the visual system is sensitive to blur as small as 1 arcmin, although this is dependent on the context of the blur [181]. An important unresolved issue is why perception of images is not severely degraded by the chromatic defocus. While the visual impact of the LCA on polychromatic image quality is largely decreased by the spectral sensitivity of the retinal photoreceptors [36], [182]–[184], the effect of LCA on monochromatic targets when the eye is focused in the middle of the spectrum is of importance. Understanding how the visual system copes with LCA is relevant to many visual processes [91]. For instance, chromatic aberration has often been invoked as a polarity cue for eye growth during emmetropization and for reshaping the crystalline lens during accommodation [122], [123]. The process of adaptation to chromatic blur may also occur during cataract development and may play a role in the adaptation to replacement of the eye's lens with an intraocular lens (IOL) following cataract surgery, since the magnitude of chromatic aberration of the crystalline lens and IOL differ depending on the lens material [40], [41]. With the development of new diffractive multifocal IOL designs, it is also possible to modulate chromatic aberration independently for the far, intermediate or near foci, cancelling LCA for at least some distances [42]. However, the visual impact of removing LCA remains an open question [122].

The relatively lower optical contribution of the LCA, which is theoretically largest at short wavelengths, is traditionally attributed to two factors: the paucity of S-cones in the central fovea and the absorption of short wavelength light by the yellowish macular pigment. Two decades ago, some of the authors of the current study reported in *Nature* that invoking those mechanisms may not be necessary, and that the optical effect of the latter was in fact minimal [62]. Instead, it was found that, while the optical contrast reduction produced by LCA in S- cones with respect to M/L cones was large in diffraction-limited eyes (free of monochromatic aberrations), the presence of the eye's natural monochromatic aberrations mitigated the differential impact of LCA on optical contrast for S-cones and M/L cones. In fact, optical simulations showed that the combination of natural monochromatic and chromatic aberrations boosted contrast for blue stimuli when the eye was focused in the green compared to an aberration-corrected eye. Aberrated optics therefore seemed to provide the eye partial protection of against chromatic blur.

The interaction between monochromatic aberrations occurs because the presence of aberrations increases the depth-of-focus of the eye [185]–[187], and consequently improves the eye's modulation transfer function out of focus [188]. Depth-of-focus has also been invoked as a factor limiting the evolution of visual pigments and trichromatic

color vision [189]. However, the potential perceptual consequences of the optical interactions between LCA and high order monochromatic aberrations have not been investigated to date.

AO, is now commonly used to compensate for the monochromatic aberrations of the eye, both in eye fundus imaging and in psychophysical experiments[71]. This has provided a tool for probing neural adaptation to new aberration patterns[5], [89], [190]. Thus, AO enable testing the hypothesis that increased depth-of-focus arising from the optical interactions of LCA and monochromatic aberrations is the main reason for the relative insensitivity in human vision to chromatic blur in short wavelength components of a polychromatic image, or if instead, other perceptual (adaptation) mechanisms play a role. The question is timely as intraocular lens (IOL) manufacturers embark on the developing of new designs to reduce LCA. These developments will lead to patients fitted with IOLs that alter the balance of monochromatic/polychromatic aberrations, which may be needed to perceptually recalibrate to a new spatial/chromatic environment.

3.2. Methods

An AO system consisting on an optical channel to measure and correct the optical aberrations of the eye and a psychophysical channel to present visual stimuli (monochromatic and polychromatic blue or green stimuli, as well as broadband gray scale) was used. Observers viewed stimuli with natural (NoAO) or fully corrected (AO) monochromatic aberrations, in three experiments that evaluated the visual effect of chromatic defocus.

3.2.1. Subjects

Ten subjects with good visual health participated in the study (ages ranging from 22 to 45 years old, (31±9); average spherical error: -1.23±2.28 D, cylinder: -0.20±0.23 D). The pupil was dilated, and the accommodation was paralyzed using Tropicamide 1% (2 drops instilled at the beginning of the session and re-instilled every hour). The study was explained to the subject; before they were asked to sign informed consents. The study met the tenets of the Declaration of Helsinki, and the protocols were approved by the CSIC Institutional Review Board. All participants were acquainted with the nature and possible consequences of the study and provided written informed consent.

3.2.2. Visual stimuli

Visual stimuli were natural images displayed on a CRT monitor: a city scene and a fruit platter as well as binary noise (figure 3.1.e). These images were generated in polychromatic grayscale, green and blue versions. Stimuli's size was 480x480 pixels. Colors were produced by cancelling the other channels ((0, G, 0) for green and (0, 0, B) for blue). The emission of the CRT phosphors was characterized using a Minolta Spectroradiometer (CS-1000). Peaks were found at λ=450 nm (56-nm bandwidth) for blue images and at λ=550 nm (77-nm bandwidth) for green images. The CRT green luminance was 23 cd/m^2. Mirrors and beam splitters produced 48% attenuation. Isoluminant green and blue stimuli were generated by adjusting the green color in a luminance matching psychophysical procedure.

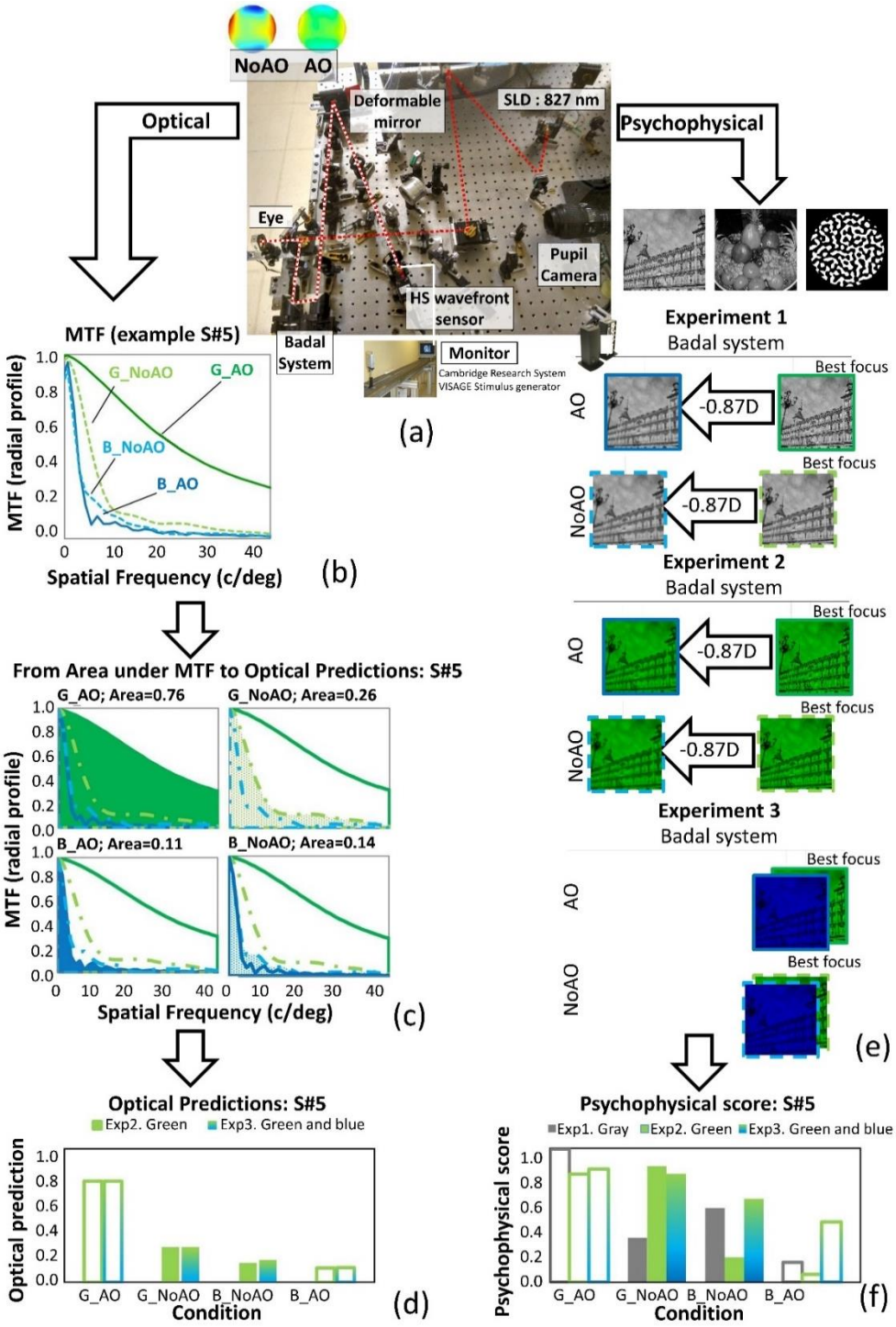

Figure 3.1. Methods overview. Example of Optical predictions (left) and Psychophysical scores (right) for S#5 from experimental measurements in the AO system (with natural and AO-corrected aberrations, (a)). MTFs were obtained from the measured HOAs at best focus for Green (NoAO, dotted line and AO, solid line) and for a defocus corresponding to the chromatic difference of focus for Blue (c). Optical quality predictions are estimated computing the normalized area under the MTF (0-40 c/deg range). The patients score the perceived quality of natural images of gray-scale images (in focus, and defocus by -0.87 D), green images (in focus, and defocus by -0.87 D), and green and blue images (in the best focus of green), both with NoAO and AO, illustrated in (e). Psychophysical scores are obtained from the perceptual judgment of natural images (0-5) as seen in 4 conditions (G_AO, G_NoAO, B_NoAO) and normalized to 1 (f).

3.2.3. Psychophysical experiments

Subjects scored the perceived image quality of the visual stimuli under different conditions (grayscale, green and blue images; in and out of focus; with natural aberrations and with AO-correction), in three different experiments (figure 3.1.e-f). The subjects were asked to score the images according to their perceived sharpness of the images on a scale from 0 to 5. Images were presented either at best focus or defocused by an amount equivalent to the chromatic difference of focus between green and blue (-0.87 D [38]). Three experiments were conducted:

- Experiment 1: Grayscale images were viewed at the subject's best subjective focus (selected separately under natural aberrations and under AO-correction), and defocused by -0.87 D from best focus in each condition. In this experiment, we studied the effect of blue chromatic defocus level (induced as pure optical defocus) on multi-wavelength images.
- Experiment 2: Green images were viewed at the subject's best subjective focus (under natural aberrations and AO-correction), and defocused by -0.87 D from best focus in each condition. In this experiment, we studied the effect of blue chromatic defocus (induced as pure optical defocus) on green images.
- Experiment 3: Equi-luminant green and blue images were viewed at the subject's best subjective focus obtained in green (under natural aberrations and under AO-correction), without shifting focus for blue. In this experiment, we studied the natural chromatic defocus on blue images. The green images in this experiment are identical to those in experiment 2.

G_AO and G_NoAO means best focus of gray-scale images in Exp 1 and best focus for green in Experiment 2 and 3, for AO and NoAO conditions, respectively, and B_AO and B_NoAO means -0.87 D from the best focus of gray-scale images and green images, for Experiment 1 and 2, respectively, and best focus of green (with blue stimuli) in Experiment 3.

The three experiments were conducted in the same order in a single experimental session, which typically lasted 2 hours. In each experiment, images were presented to the subject for 1.5 seconds, and scoring of perceived quality (a score of 0-5, on a keyboard) was made following an auditory cue. In each experiment, subjects scored the quality of 3 images, 9 repetitions in each condition. In each experiment, each condition consisted of a given focus position in the Badal system and a status of the deformable mirror. The condition of best focus in green or gray is labeled G. The condition out-of-focus in gray or green, or blue with non-additional defocus in the Badal optometer is labeled as blue (B). The conditions in which the subject's aberrations are corrected or left uncorrected are labeled AO or NoAO, respectively. Within a condition, images were randomly interleaved and the quality judgements were made 9 times for each of the 3 images. Each condition consisted therefore of 27 scores (3 images x 9 repetitions/image), and each experiment involved 108 trials (4 conditions x 27 scores/condition). The maximum possible score for each condition is 135 (27 scores x 5 maximum score). Total scores were normalized to 1 by dividing by 135.

3.2.4. Control experiments in the polychromatic AO set-up

Two control experiments were performed in the VioBio lab AOII set up to complete findings from the general experiments:

- Replication of experiments 2 and 3 using a narrow band. The replication of the experiment was performed in the VioBio lab AOII, in which the stimuli are generated using narrow blue and green lines (spectral bandwidth of 5 nm). As it was explained in methods chapter (chapter2 2), illumination comes from a supercontinuum laser source (SCLS, SC400 femtopower 106 supercontinuum laser, Fianium Ltd, United Kingdom) that works in combination with a dual acousto-optic tunable filter (AOTF). A 5-mm artificial pupil is placed at a conjugate pupil plane.
  Two subjects from the original experiment (S2, high HOAs, and S9, low HOAs) scored the same 3 stimuli in three different conditions (corresponding to Experiments 2 and 3) under natural aberrations (NoAO): (1) Illumination with green light (λ=550 nm) for the best subjective focus in green light; (2) Illumination with blue light (λ=450 nm) for the best subjective focus in green light.; (3) Illumination with green light (λ=550 nm) for an induced defocus of -0.87D from the best subjective focus in green light. As in the original experiment, the power of the green and blue laser beams was adjusted so that they produced equal perceived luminance. As for the main study, the experiment was performed with natural aberrations (NoAO) and the aberrations corrected by the deformable mirror (AO).
- Measurement of subjective Best Focus (BF) and Visual Acuity (VA) at different wavelengths. Best focus and Visual Acuity (VA) were measured in the VioBio lab AOII using monochromatic light, as well as a white light source. Differences in the best focus setting and VA across subjects and wavelengths were evaluated.
  Best focus searching consisted on subjectively focus a Maltese Cross by using a numerical keyboard, connected to the Badal system. Best focus was searched with the stimulus illuminated at different wavelengths: 480 nm, 546 nm, 650 nm, 700 nm and white light. Best subjectively best focus was set as the average of three trials per wavelength. LCA was estimated as the difference between best focus found at 700 nm and best focus found at 480 nm.
  A tumbling E-letter (black letter on colored background) test was used to measure Visual Acuity (VA). The task of the subject was to indicate the orientation of the E letter which was presented at 4 random orientations. The size of the E-letter was changed in the subsequent presentation, depending on the response of the subject using a quaternion estimation algorithm. A run consisted of 32 trials and 10 reversals, and the visual acuity was measured as the mean of the last 10 reversals. VA was measured with two different Badal positions: the best focus found at 546, with the stimulus illuminated at 480 nm, 546 nm, 650 nm and white light; and the best focus found at 480, with the stimulus illuminated at 480 nm and 546 nm.

BF Measurements	VA Measurements	
λ	**BF**	**λ**
480 nm 546 nm 650 nm 700 nm White Light	480 nm	480 nm 546 nm
	546 nm	480 nm 546 nm 650 nm White Light

Table 3.1. Resume of the conditions tested in both psychophysical experiments.

Both experiments were performed monocularly under cycloplegia a pupil size limited at 3 mm and natural aberrations. The group of subjects was formed by ten subjects (39 ± 12 years old) with spherical error of -1.5 ±2.3 D and astigmatism -0.5 ±0.3 D. Measurements were performed on the eye with best VA.

The wavelengths employed in this experiments were subjectively equalised in terms of luminance by three external and experimental subjects before starting the experiment, and the average from the three trials was fixed for all the subjects. Maltese cross was the illuminated stimulus employed for the task.

Luminance of the four wavelengths, 480, 546, 650 and 700 nm was manually changed until obtain a subjectively equal luminance between them. Once the luminance for 546 nm was determined, it is proceeded with white light source. White light source's luminance was computationally changed, modifying the level of grey of the stimulus with a numerical keyboard. The change of luminance of white light source to compare with green light was from darkness (20% of the total) to brightness, since white light was much more brightness than monochromatic light. Brightness was increased until 85% of luminance, when both white and green light are matched.

3.2.5. Optical predictions

Optical wave aberrations of each eye were measured before and after AO correction, and expressed by a Zernike polynomial expansion up the 6th order, obtained as the average of 3 repeated measurements. MTFs were calculated from the measured wave aberrations (natural and AO-corrections) for 5-mm pupil diameters, for green (550 nm) and blue (450 nm) wavelengths (figure 3.1.b). Since HOAs are effectively independent of wavelength[91], high order Zernike coefficients measured at 827 nm were used in the MTF calculations. The wavelength was introduced as a scaling factor in the pupil function (both in the modulus and phase). Defocus was introduced in the phase of the pupil function as a defocus Zernike term. Chromatic defocus between 550 and 450 nm was assumed to be -0.87 D[38]. Visual Strehl (VS) was estimated as the normalized volume under the MTF (progressively truncated by the neural contrast threshold) [191], [192]. Best focus in green was estimated as the defocus producing the largest VS. Radial profiles for figure 3.2 were obtained by averaging the MTF across all meridians. Optical quality

prediction was estimated in all conditions replicating Experiments 2 and 3 (AO, NoAO, in focus and defocused by chromatic defocus, 5-mm pupil, figure 3.1.c-d) normalized area under the MTF radial profile (0-40 c/deg range).

3.2.6. Statistical analysis

A one-way ANOVA test showed no statistical differences between perceptual scores assigned to the different images (noise, fruits and city) for a similar condition (p=0.58), and therefore data was pooled across images.

To comparatively evaluate the weight of each effect, a Mixed Model Analysis with two fixed factors (condition and experiment), and subject as random factor in repeated measures was used for each type of result (optical and psychophysical). For each type of result (optical and psychophysical) and experiment we used a Mixed Model Analysis with one fixed factor (condition) and a random factor (subject).

3.3. Results

3.3.1. Ocular optical quality

Figure 2 shows the optical quality for each measured eye in terms of the MTF radial profile, in green and blue light with natural aberrations (dotted lines: NoAO) and with AO correction of the monochromatic aberrations (solid lines: AO), for 5-mm pupils. The color maps on top of each graph show the corresponding wave aberrations at the pupil for NoAO (left) and AO (right). The MTFs in green are calculated for the focus which maximizes optical quality in green (both for NoAO and AO: G_NoAO and G_AO). The MTFs in blue are calculated for a chromatic defocus of -0.87 D (450-550 nm)[38] from the corresponding best focus in green (B_NoAO & B_AO). Subjects are labeled according to increasing optical quality of their natural optics (G_NoAO), from lower (S#1) to higher (S#10), in terms of Visual Strehl (VS[191]). Figure 3.2 represents the conditions tested in Experiment 2.

As expected, AO improved image quality in green, more for subjects with lower optical quality than for subjects with higher optical quality: MTF G_AO/G_NoAO: 3.11-5.25 (S#1-S#5) vs 6.92-7.09 (S#6-S#10). The opposite occurred for the blue, subjects with poorer optics experienced a relatively higher MTF in blue with natural aberrations than with AO-correction: MTF B_NoAO/B_AO: 2.42-1.34 (S#1-S#5) vs 0.92- 0.73 (S#6-S#10).

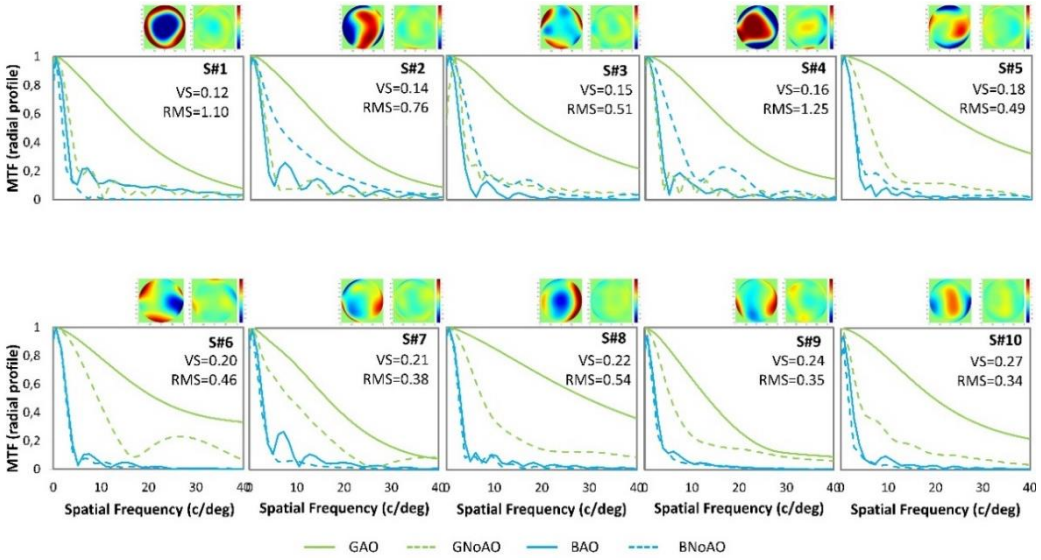

Figure 3.2 MTFs in all eyes, computed from individual measurements of wave aberrations. With natural aberrations (NoAO, dashed lines) and AO-corrected monochromatic aberrations (solid lines). MTFs are for best focus in green (G. 550 nm) and for the corresponding chromatic difference of focus (-0.87 D, 450 nm) in blue. The maps above each graph represent monochromatic wave aberrations with no defocus with natural aberrations (left) and AO-corrected aberration (right). Subjects are ordered according to increasing Visual Strehl (VS) value for 5-mm pupil diameters for the G_NoAO condition. VS and RMS values (for the natural aberration condition) are shown in each panel under the subject's label, unitless and μm units, respectively).

3.3.2. Optical quality & Psychophysical scores

Subjects scored [76] the perceived quality of monochromatic grayscale and green images in focus and out of focus and blue images (for best focus in green), projected in a visual display viewed through AO. Figure 3.3 compares measured optical quality and psychophysical scores. Optical quality –top panels- are normalized area values (from Exp 2 and 3). The psychophysical scores in the bottom row of panels represent the normalized perceived image quality responses in the four evaluated conditions (G_AO, G_NoAO, B_AO and B_NoAO) for experiments 1, 2 and 3. For this scale, a value of 1.0 represents the highest perceived image quality. Left panels represent average data across subjects, and the middle and right panels represent data from individual subjects: S#1-S#5, (more aberrated, i.e. poorer optics; Middle) and S#6-S#10 (less aberrated, i.e. better optics; Right).

Optically (top panels), the effect of correcting natural aberrations in green (at best focus) is quite dramatic, with the optical quality (VS) improving on average from 0.28 (NoAO) to 0.62 (AO), i.e. by x2.21 consistently in both Exp 2 and Exp 3. As expected, the relative improvement is larger for the more aberrated subjects (x2.77, top middle panel, Exp 2 and 3) than for the less aberrated subjects (x1.84, top right panel, Exp 2 and 3), due to the lower natural MTF in the more aberrated subjects.

On the other hand, correcting natural aberrations in grayscale or green images (in focus-bottom panels) had little impact on the perceptual scores (from 0.71 to 0.76, on average across the three experiments). Some subjects, particularly the more aberrated subjects in fact judged image quality to be better without AO correction despite the large improvement in the MTF. The average perceptual score changed from 0.77 to 0.68 in the more aberrated subjects (middle) and from 0.65 to 0.83 on average in less aberrated subjects (right panel), upon correction of their natural aberrations.

For blue images, or green images defocused by an equivalent (blue) chromatic defocus, perceived image quality is consistently higher with natural aberrations (0.15 and 0.17, Exp 2 and 3, respectively) than with AO-correction (0.12 and 0.13, Exp 2 and 3, respectively). The improvement of the perceptual score with natural aberrations in blue (B_ NoAO/B_AO ratio) is larger in the more aberrated group. Interestingly, while the results are similar for the three perceptual experiments for gray or green images in focus, perceptually blue images (with inherent chromatic defocus) are judged consistently shaper than the gray or green images defocused by an equivalent amount of defocus (0.60 vs. 0.43-0.41, under natural aberrations; 0.55 vs. 0.33-0.34, under AO-correction). The improvement in perceived image quality of blue images, defocused by chromatic aberration, is largest in the more aberrated group.

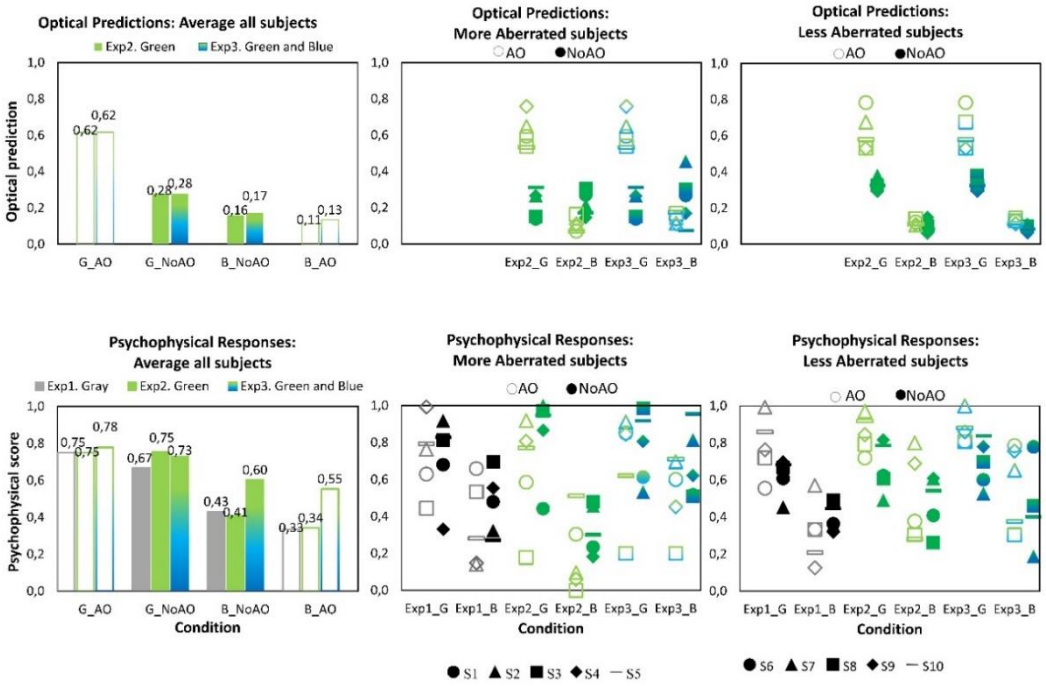

Figure 3.3. Results summary. Optical image quality (top panels) and Psychophysical scores (bottom panels). Left panels represent average data across all subjects. Middle panels represent data of individuals with more aberrations (S#1-S#5; VS<0.2), and right panels data of individual less aberrations (S#6-S#10; VS>0.2). Open bars represent results under corrected monochromatic aberrations (AO) and filled bars under natural aberrations (NoAO). Gray bars represent results for grayscale images (Exp 1), Green bars for green images (Exp 2) and graded green-blue bars for green and blue images (Exp 3). In the middle and right panels, open symbols stand for results under corrected monochromatic aberrations (AO) and closed symbols for results under natural aberrations (NoAO). Black symbols correspond to Exp 1, green symbols to Exp 2 and green&blue symbols to Exp 3.

Mixed two-way ANOVA analysis of differences across conditions indicated similarities across optical measurements and the three psychophysical experiments. Optically, a significant main effect ($p<0.001$) of conditions (G_AO, G_NoAO, B_AO, B_NoAO) was found while psychophysically, both the conditions and the three experiments (different chromatic content) main effects were significant ($p<0.001$, and 0.017, respectively). Also optically, the quality for green stimuli for corrected aberrations (G_AO) is significantly higher ($p<0.05$) than for natural aberrations (G_NoAO) for all subjects. On the other hand, the quality of blue stimuli (or green stimuli with equivalent chromatic defocus) for corrected aberrations (B_AO) is significantly lower ($p<0.05$) than for natural aberrations (B_NoAO) in the group of subjects with lower optical quality (higher aberrations), which means that the described effect is stronger in subjects with poorer optics.

3.3.3. Control experiments using a polychromatic AO set-up

3.3.3.1. Replication of experiments 2 and 3

In the control experiment one of the subjects from the more aberrated group (S2) and one from the less aberrated group (S9) repeated the experiment on the polychromatic AO system. As in the main experiment, the higher scores (0.88, on average) were found for the green stimulus in focus (G_NoAO). However, the scores for the defocused green images (equivalent to B_NoAO in Experiment 2) was lower (0.44, on average) than the score for blue images (B_NoAO in Experiment 3), 0.44 on average. Psychophysical scores for these two subjects with the narrow spectral band stimuli are shown in figure 3.4.

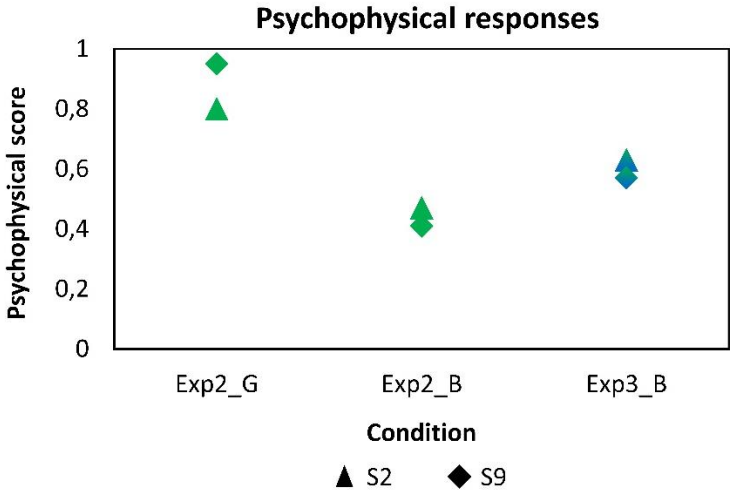

Figure 3.4. Results from the control experiment using narrow spectral bandwidth stimuli. Normalized psychophysical score of the perceived quality of natural images (555 nm for G, 480 nm for B, 5-nm spectral bandwidth), for experiments equivalent to Exp 2 and Exp 3. Exp2_G stands for green stimuli at best focus, Exp 2_B stands for green stimulus defocused by -0.87 D with respect to the best focus in G, and Exp3_B stands for blue stimulus at the best focus in G. Data are for two subjects (S2, S9)

3.3.3.2. Subjective best focus and Visual Acuity

Figure 3.5.a shows the subjective best focus found in the ten subjects for the four tested wavelengths (480, 546, 650 and 700 nm) and white light. Figure 3.5.b shows the LCA

stimated as the difference of subjective best focus with the stimulus illuminated at 700 and at 480 nm. The averaged subjective LCA of all subjects is 1.31 D, in good agreement with previous studies [39], [41], [193].

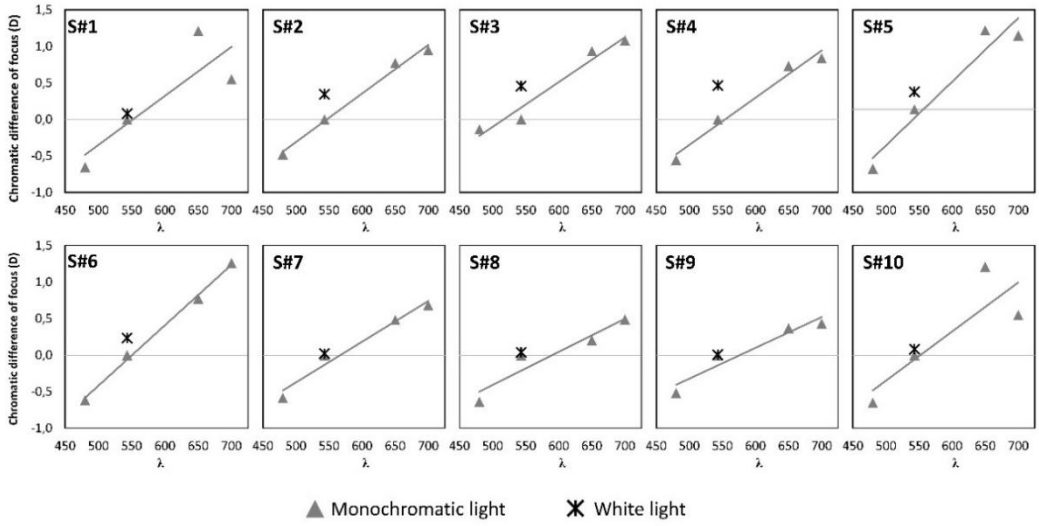

(a)

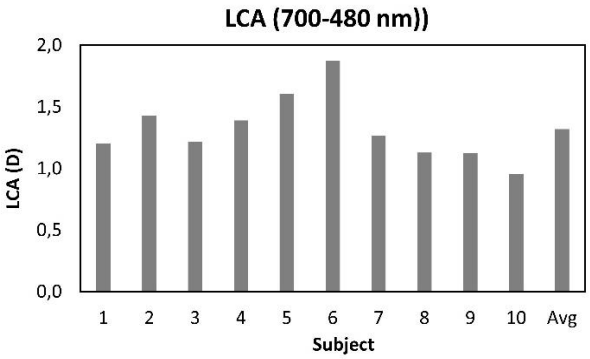

(b)

Figure 3.5 Results of subjective best focus. (a) Best subjectively search focus for the four monochromatic lights tested (triangles) and white light (asterisk) (b) LCA calculated as the difference of best subjectively search focus between 700 and 480 nm at far distance.

Figure 3.6 shows the VA measured with the stimulus illuminated at 480, 543, 650 nm and white light and the Badal position at the best focus found at 480 and 543 nm. In all cases, VA with green stimulus was higher than with blue stimulus when best focus was set at 543 nm. However, VA was higher with the stimulus illuminated in blue when best focus was set a 480 nm in three subjects and the same in two of them.

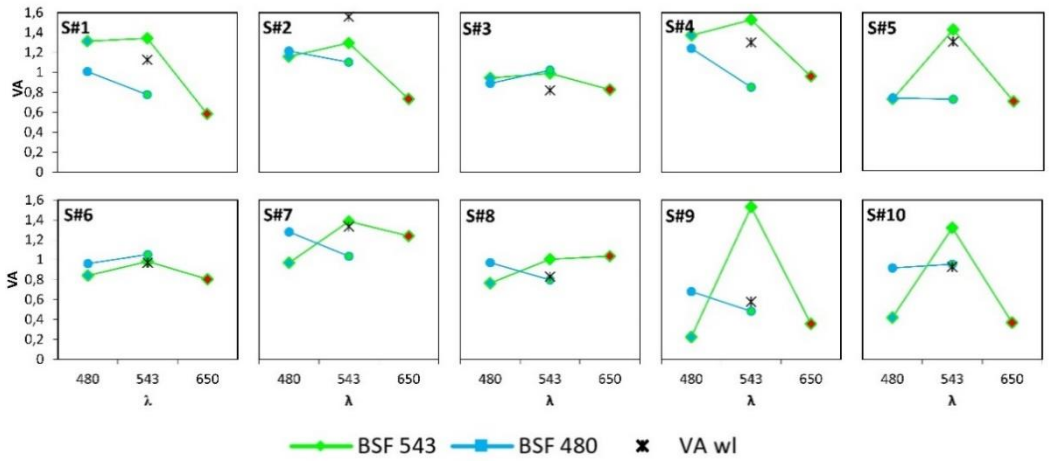

Figure 3.6 Decimal VA measured with Badal position of the best focus found at 543 nm (green lines) and the stimulus illuminated at 480 nm (blue inside marker), 543 nm (green inside marker) and 560 nm (red inside marker) as well as illuminated with white light, and with Badal position of the best focus found at 480 nm (blue lines) and stimulus illuminated at 480 nm (blue inside marker) and 543 nm (green inside marker). Measurements are for control group.

3.4. Discussion

The normal focus for the eye is in the middle of the spectrum[194] and under this condition, the eye's monochromatic and chromatic aberrations interact to improve optical quality at short wavelengths. We found that the degree of improvement varied widely across individuals, with the largest positive interaction occurring for eyes with larger monochromatic aberrations (poorer optics). This occurs because the eye's aberrations increase the eye's depth-of-focus, improving optical quality for out-of-focus stimuli compared to the diffraction-limited eye (perfect optics). This increase in depth-of-focus is largest for those eyes with larger amounts of aberrations, in the same way as inducing spherical aberration expands depth-of-focus in aberrated eyes. Our findings replicate and expand on a previous publication[62], which reported results on three eyes, demonstrating here a graded effect of the naturally occurring aberrations.

Surprisingly, there is a pronounced difference in the corresponding perceptual response to these variations in image quality. This finding seems to arise from the ability of individuals to adapt to their own aberrations[5], [190]. This adaptation causes individual variations in optical quality to be less perceptually important. Perceptual image quality scores tended to be higher for focused green images than for grayscale images, but only when the higher order monochromatic aberrations were corrected. This is consistent with a larger impact of LCA when monochromatic aberrations are corrected by AO. However, correcting high order monochromatic aberrations only improved perceived image quality by a factor of x1.07, on average. This finding that a large improvement in optical quality leads only to small improvements psychophysically is consistent with prior work. For example a previous study reported an average increase in the MTF by x8, whereas the CSF increased by only 1.35 times[195] with AO-correction. An attenuated visual benefit of correcting the eye's optics is not surprising given the neural adaptation to the subjects' native aberrations[5]. While subjects generally identify as sharper images viewed through

AO-corrected optics[89], previous work has shown that the amount of blur in the image that produces highest perceived image quality matches the level of blur (and blur orientation) produced by the native aberrations of their eyes[5],[190]. The evidence that it is a neural adaptation is supported by the fact that the native blur does not produce aftereffects (while scaled versions of that blur do [5]). Also in experiments where subjects judged images blurred with different individual's aberrations (from low to highly aberrations), the image judged as perceptually best corresponds to that blurred with the subject's own aberrations (or similar amounts of blur) [5].

Our results also reveal that, on average, out of focus images appear less blurred when the native aberrations are present than when they are corrected, in line with the optical findings [62]. However, perceived quality of blue images (when the eye is focused for green) is relatively high, either with or without high order monochromatic aberrations. And what is most relevant, blue images (naturally defocused by chromatic blur) are psychophysically judged as sharper than green (or monochromatic grayscale) images defocused by the same amount of equivalent blur (-0.87 D). The higher perceived quality of defocused blue images compared to defocused green or luminance-contrast (grayscale) images suggests that the visual system is calibrated based on the average chromaticity, and due to the univariance of the cones, the mechanism of adaptation might use color information to discount perceptual blur or loss of sharpness.

A potential reason for reduced sensitivity to defocus in blue may be associated with the reported increased psychophysical depth-of-focus in blue, not caused by the optics [196], as objective depth-of-focus does not vary across wavelengths [182]. The sparse sampling of S cones alone is unlikely to cause this effect. As the luminance contrast, determined by L and M cone signals, is similar for all three stimuli once the optical effect is accounted for. The spectral range of the blue images in the main experiment (CRT blue phosphor) strongly stimulates not only S but also M cones. This finding is consistent with the observation that the increase in perceived blur with increasing physical defocus is higher for luminance than for blue-yellow stimuli. This may explain the observation that compressing the color information in a natural scene (as done in JPEG compression [197]) produces little or no impression of blur, as opposed to a much higher blur sensitivity to changes in the luminance layer [198]. Although our stimuli are not based on chromatic contrast (green and blue stimuli provided luminance contrast and were matched in average luminance) higher spatial sensitivity for luminance than chromatic contrast variations may prevail in this effect. It is also important to note that the effect appears to be intrinsic to the peak wavelength, and not biased by the spectral bandwidth of the images, as a control experiment showed similar results using stimuli illuminated with narrow spectral bandwidth (5 nm) blue and green light.

3.5. Conclusions

We conclude that the observed higher perceived quality of defocused blue stimuli is influenced by neural adaptation mechanisms. The shift in psychophysical score for blue (as compared to the same defocus in green) may underlie contingent adaptation to blue and out-of-focus (as the blue component of images is normally out-of-focus). It may suggest that observers naturally adapted to both the blur produced by their native aberrations for stimuli where L and M cone signals are predominant (the middle of the spectrum) and to the effect produced by natural defocus in blue.

In summary, the presence of monochromatic optical aberrations protects vision against chromatic defocus, but adaptational mechanisms appear to be equally important in controlling contrast constancy and can work differentially across wavelengths.

In this chapter, we have studied he interaction between chromatic and monochromatic aberrations and concluded a potential adaption to chromatic blur in blue images. In the following chapter, we explore the adaptation to blur sensitivity in relation to blur produced by monochromatic aberrations.

Chapter 4. Adaptation to blur sensitivity in normal subjects with natural aberrations and under AO correction

As we showed in previous chapter, there exists an interaction between chromatic and monochromatic aberration that results on the conclusion that presence of monochromatic aberration attenuates the effect of chromatic aberration. In this chapter we are going to focus on the effect of monochromatic aberration itself, and the adaptation to blur sensitivity produced by natural aberrations.

This study was presented by Benedi-Garcia in the Reunión Nacional de Óptica (RNO) in 2018 as an oral presentation with Maria Vinas, Carlos Dorronsoro, Mike Webster and Susana Marcos as co-authors.

The author of this thesis implemented the experimental procedure in collaboration with Maria Vinas, performed the measurements on subjects, collected and analyzed the data and discussed them with the rest of the authors.

4.1. Introduction

As it was explained before, retinal image is degraded affected, among other things, by ocular aberrations. However, it exits a neural process after the retina, in which there is a recalibrations and an interpretation of the information.

Perception of blur is important, since it plays a role in the best VA that a subject obtain with his best correction of low order aberration [199]. Blur also takes part in accommodation process, thus it will be minimized when the eye focus to the viewed object [200]. In addition, blur must be had account to determinate the tolerance level of an optical instrument, so understanding the nature of blur perception will help to optimize optical instruments.

Due to blur is so important attribute for vision, its perception has been already studied in experimental research and theoretical modelling. However, many aspects of the experiments affect the results, such us the type of stimulus (natural image, sinusoidal image, single edge, …), the type of blur (Gaussian blur, realistic blurring functions), the way to generate it, contrast, luminance and chromatic of the image [201], … Watson and Ahumada collected and review the several studies that have analyzed blur perception and discrimination [181]. In their analysis, it is very common that dipper-shaped curves often accurately represent the relationship between the magnitude of a baseline or "pedestal" and a measurable change [202].

By other hand, it has been already proved that vision is adapted to its own visual quality [5], [190]. Artal and collages demostrated that the eye is adapted to the PSF inducing PSF's differently rotated with AO. Sawides and colleges proved that vision is adapted to the natural level of blur presenting images convolved with realistic blur of different amounts and forms. Not only there is an adaptation to the natural level of blur, but vision is capable to adapt to changes in the level of blur imposed by HOAs [89]. Besides, brief period of adaptation shift the subjective neutral point toward the sharpness of blur level of the adapting images [98].

In this study, we studied the discrimination of blur for a given blurred image of reference. Induced blur is directly related with the natural aberrations of the subject, using a multiplying factor in order to generate blur. We perform the experiment in an adaptive optic system, in order that we have full control of wave aberrations of the subjects.

4.2. Methods

The experiment consisted on compare the difference of blur between a reference image, called pedestal, and a second image with a bigger amount of blur (always positive blur). Both image, the reference and the tested images, where randomly showed and the blur of the tested image is calculated according to the previous answer using QUEST algorithm [178]. Between the two images to compare, as well as while the subject answered, a gray screen was presented with a cosine filter and a white circle in the middle in order to avoid afterimages. Figure 4.1 shows the sequence of presentation of the images.

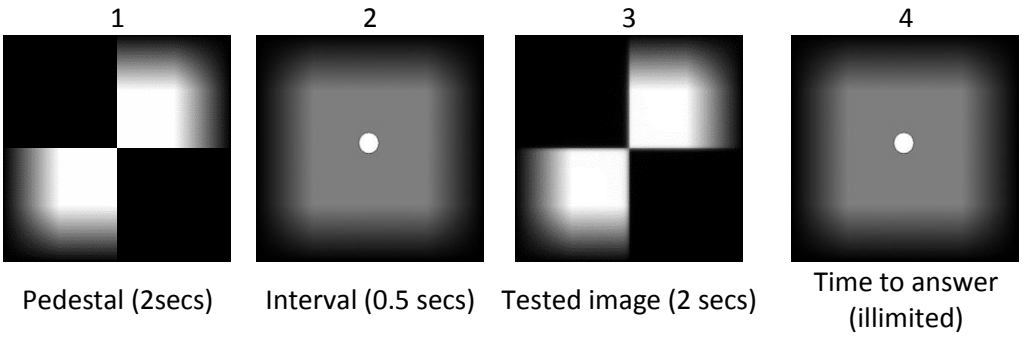

Figure 4.1. Sequence of presentation of the images in the experiment. Steps 1 and 3 are randomly exchanged.

The experiment was performed in the VioBio lab AOI with a pupil diameter of 5 mm. Accommodation was paralyzed with Tropicamide 1%. 5 subjects performed the experiment, with an averaged age of 38 years old and a refractive error of -0.70 sph -0.50 D on average.

4.2.1. Experiments

Blur in the images was induced in two different ways: with convolved images and optically. Two different experiments can differentiate according to these techniques.

Experiment 1: Convolved Images

Blur was generated through the convolution of the original stimulus with the PSF of the subject multiplied by different steps, from 0xPSF to 3xPSF in steps of 0.0125xPSF, with a total of 240 images. After convolution, a cosine filter was applied in order to smooth the edges. The shift showed on the VS was included on aberrations as a defocus term, thus the 0xPSF correspond to the best values of VS for each subject. Pedestals were also generated by convolution, with the following factors: PSFx 0 (AO condition), PSFx 0.25, PSFx 0.50, PSFx 0.75, PSFx 1 (No AO condition), PSFx 1.25, PSFx 1.50, PSFx 1.75, PSFx 2, PSFx 3 and PSFx 4. Mirror state was correction aberrations of the subject during the whole experiment and aberrations where measured before each pedestal to confirm the mirror state.

A second variant of this experiment was perform including adaptation. Adaptation was carried out with a jittering of the image to adapt during 60 seconds at the beginning of the experiment and 5 second between trials. In experiment 1.2, the jittered image was the pedestal PSFx0 while in experiment 1.3, it was PSFx1.5

Experiment 2: Optical blur

Blur was also induced optically with the Badal system of the AO system. In this case, the DM corrected wavefront aberrations in a first experiment (experiment 2.1, AO) and it didn't' in a second one (experiment 2.2, NoAO). Pedestals for experiment 2 were 0D, +0.25D, +0.75D, +1D.

4.2.2. The stimulus

Stimulus consisted on a checkered image, with two black squares and two white ones. Each square subtended 0.99º.

4.2.3. Scale change

The units that are used in these experiments (pixels for experiment 1 and diopters for experiment 2) were transform to arcmin, since a main bibliography about blur adaptation use it as unit of magnitude. For the change of scale was, we found a minimum radius of the circumference which contains the 50% of the energy of the PSF with a 5 mm pupil size [121]. For calculating the minimum circumference, it was developed a specific algorithm in which a circumference with gradual increasing radius traverse the PSF until find the 50% of the energy.

4.3. Results

4.3.1. Subject optical quality

Figure 4.2 shows the optical quality of the measured eye for each subjects. First image shows the wavefront map, the PSF and the MTF radial profile of the subjects, while the graph B shows the RMS of different Zernike terms (astigmatism and HOAs, only astigmatism, only HOAs, coma alone and Spherical aberration alone). The RMS goes from 0.76 for S1 microns to 0.25 for S4.

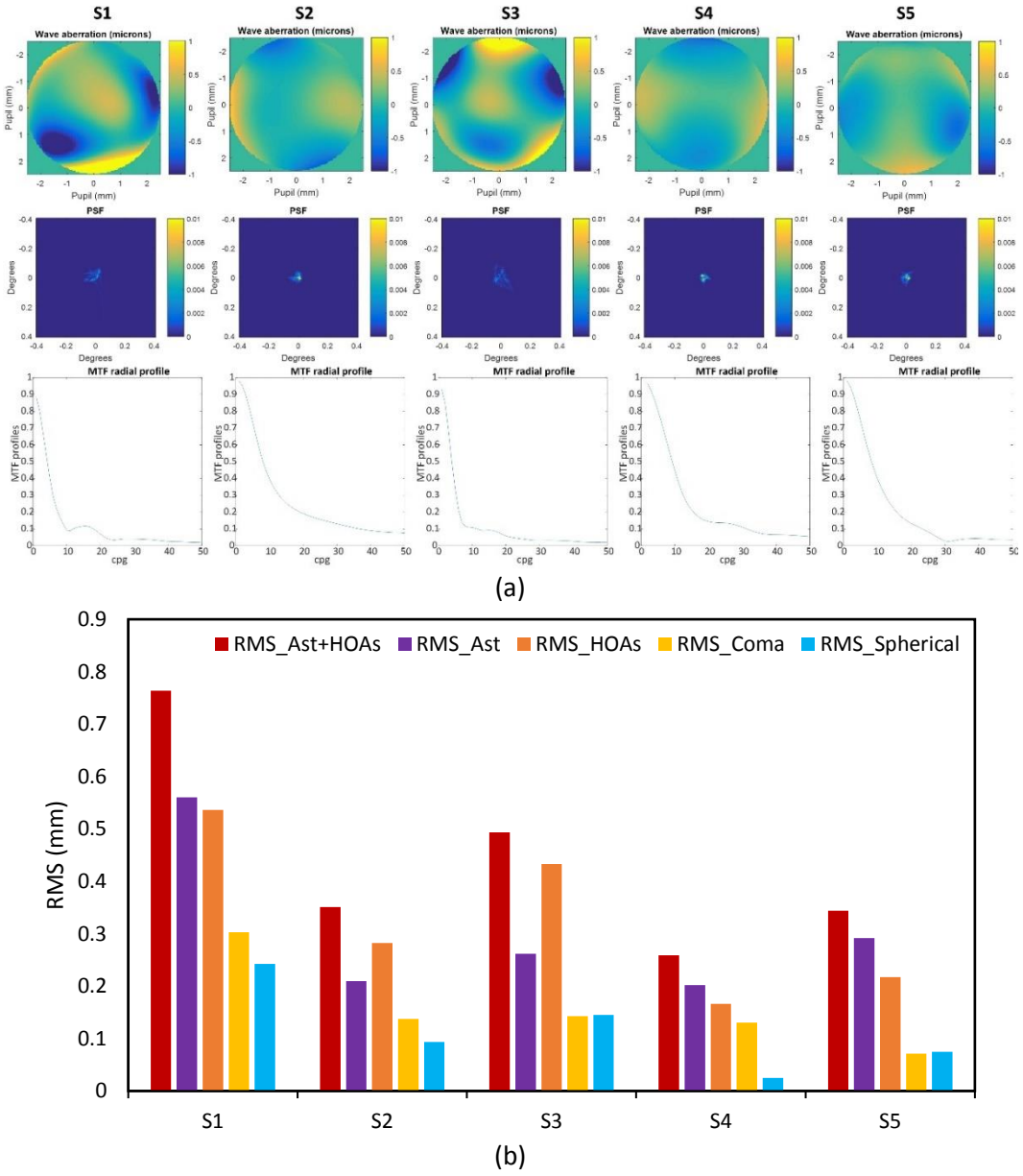

Figure 4.2. (a) Wavefront, PSF and MTF for the five subjects. (b) Optical quality of the five tested subjects in terms of RMS

4.3.2. Results of convolved images experiment

Figure 4.3. shows the results of experiment 1, in which blur was simulated with convolved images. Scale Y is logarithmic in figure 4.3.a in order to compare with literature. In figure 4.3.b, in which graphs are grouped in pedestals, it is clear that those subjects with the worst optical quality, S1 and S2, present a higher threshold when images are more blur than the natural condition (PSFx1).

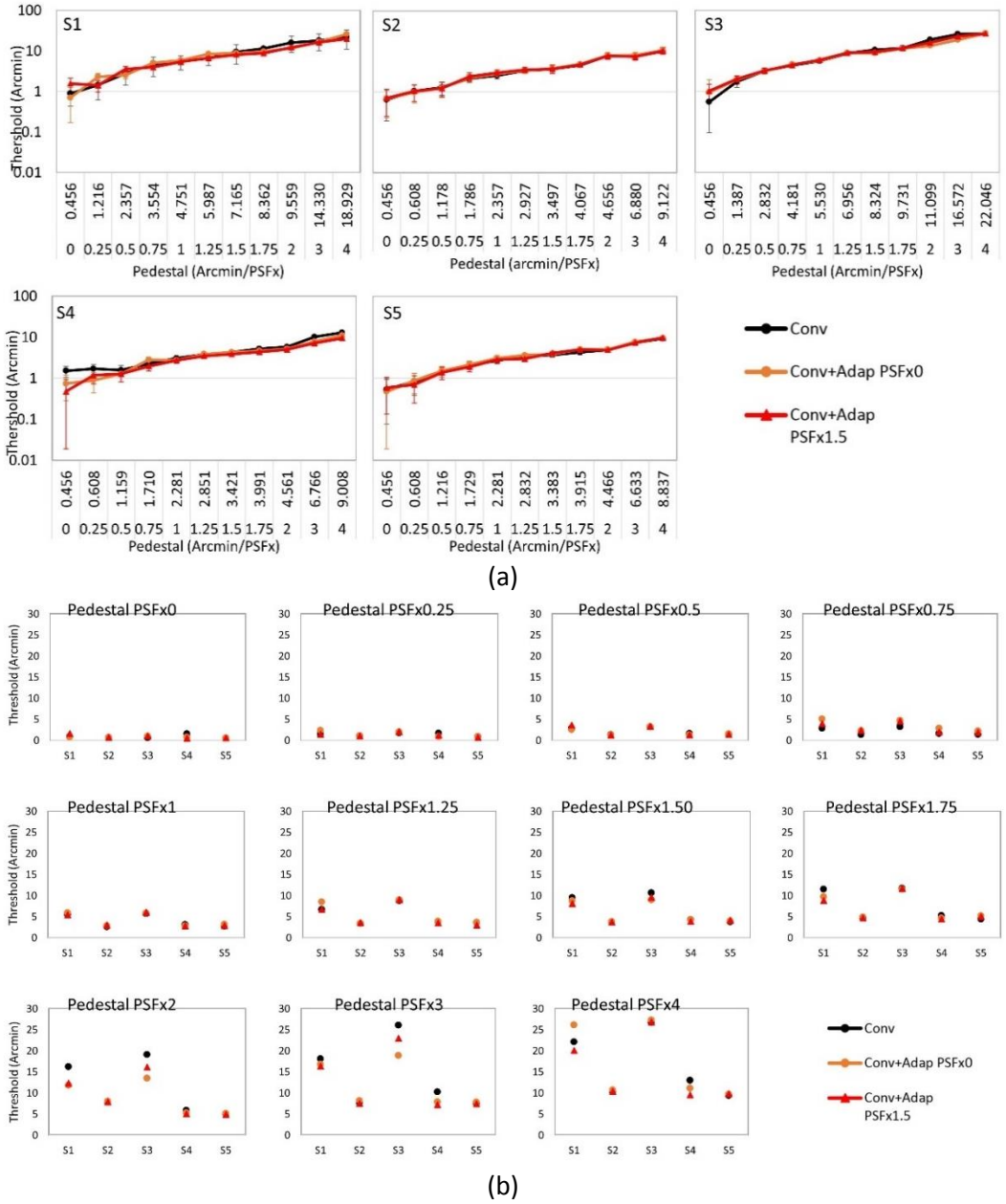

Figure 4.3. (a) Threshold in arcmin for the five subjects in each pedestal (PSFx 0, 0.25, 0.5, 0.75, 1, 1.25, 1.5, 1.75, 2, 3 and 4). (b)Threshold in arcmin for the five subjects grouped by pedestals. In both graphs, data are for convolved images (black lines or points), adaptation to pedestal PSFx0 (orange lines or points) and adaptation to pedestal PSFx1.5 (red lines or points).

Differences between adaptation and not adaptation are not evident in those subjects with better optical quality. In subjects S1 and S3 it is found a lower threshold when there is adaptation on those pedestals with bigger amount of blur, PSFx1.5 or more. On the other hand, S4, the subject with lower RMS, presents a reduced threshold in presence of adaptation in most of pedestals, while there is not difference between adaptation or not in S2 and S5.

4.3.3. Results of optical blur experiment

Figure 4.4 represents the found thresholds in experiment 2, in which blur was induced with the Badal system. In this case, there is a clear improvement when aberration are corrected for the pedestal without blur (0 D) in those subjects with higher RMS, S1 and S3, although this difference between correcting aberrations or not doesn't exits whenever pedestal is more blur.

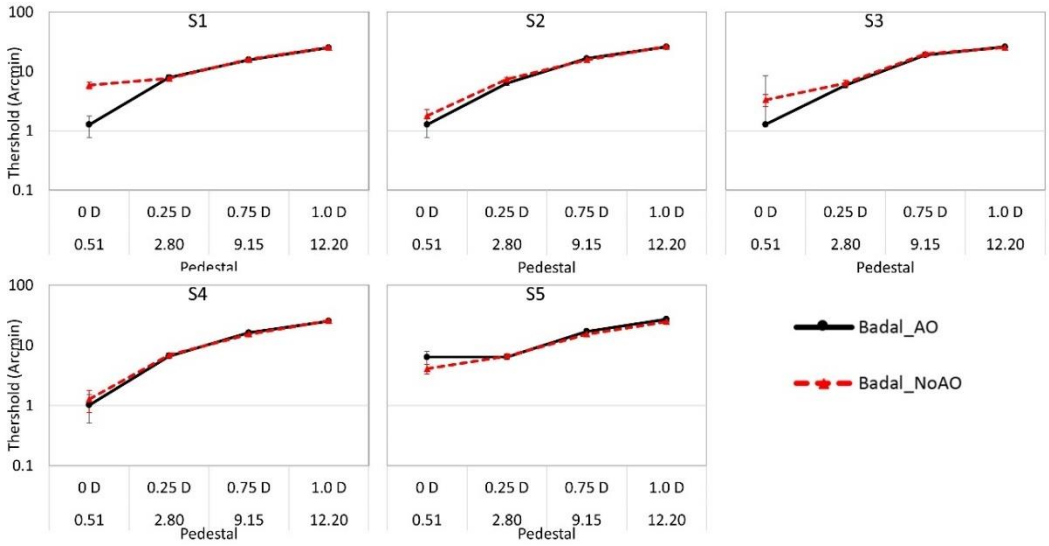

Figure 4.4. Threshold in arcmin for the five subjects in each pedestal (0, 0.25, 0.75 and 1 D) with aberrations corrected (solid black lines) and natural aberrations (dashed red lines).

4.4. Discussion

In this experiment we have studied the threshold of blur discrimination in five subjects. Blur was generated in two different ways: with convolved images and optically with the Badal system. A metric has been developed in order to compare results between experiments and with bibliography. In the first experiment, in which images were convolved, it was found that those subjects with worst optical quality presented a higher threshold than the rest of the subjects. Also, this subjects presented a lower threshold when they were adapted to a pedestal. In the case of the second experiment, in which blur was induced optically, it was found a lower threshold when aberrations are corrected for more aberrated subjects when the pedestal is not blur. All this suggest that the optical quality of the subject plays an important role in the visual performance facing blurred images. More aberrated subjects are more sensitive to adaptation or correction of aberrations.

Comparing both experiments, threshold is most of times bigger for experiment 2 (Badal) than for experiment 1 (Convolution) for the same level of blur (similar arcmin value). This could indicate that subjects are adapted to the asymmetry of their own aberrations.

4.5. Conclusions

The AO systems allow us to control and manipulate aberrations in order to study blur discrimination. We have found that exits a dependency of the threshold with the optical quality of the subject.

In next chapter, we are going to focus in the perception of one monochromatic aberration: astigmatism

Chapter 5. Perceptual impact of astigmatism induction in presbyopes

In this chapter we investigate in influence of astigmatism induction in best perceived focus and visual acuity in three group of subjects with different previous visual experience.

This chapter builds on the paper of Benedi-Garcia entitled "*Perceptual impact of astigmatism induction in presbyopes*" and published in Vision research on 2019. Co-authors are Miriam Velasco-Ocana, Carlos Dorronsoro, Daniel Pascual, Martha Hernandez, Gildas Marin and Susana Marcos.

A collaborative research project sponsored by Essilor International has provided support for the work that led to these findings.

This project was also presented by Benedi-Garcia on ARVO conference on 2019 as a poster contribution under the tittle "*Perceived best focus and visual performance upon induction of astigmatism in presbyopes*".

The author of this thesis implemented the experimental procedure in collaboration with Miriam Velasco, performed the measurements on subjects, collected and analyzed the data and discussed them with the rest of the authors and wrote the manuscript in collaboration with Susana Marcos. All authors revised the manuscript.

5.1. Introduction

5.1.1. Progressive lenses

With age, the capability of the crystalline lens to dynamically focus near and far is lost, thus optical solutions are needed to produce functional vision at different distances. Solutions for presbyopia include multifocal contact lenses (which work on the principle of simultaneous vision) and progressive ophthalmic lenses (which work on the principle of alternating vision) [203]. Multifocal contact lenses impose blur on the retinal image as they superimpose on the retina images focused at different distances. In progressive lenses, the upper part of the lens compensates for the optical refraction at far, and progressively increases the optical power to provide a near add in the lower part of the lens, with an optical corridor for intermediate distances in the center of the lens. This change of optical power results in aberrations in the peripheral regions of the lens, in particular in astigmatism [60], [116]. In general, presbyopes wearing presbyopic corrections appear to adapt to the new visual experiences, to both blur in simultaneous vision images [79] as well as to distortions and to the presence of asymmetric aberrations produced by progressive lenses [113], in consistency with reported mechanisms of spatial neural adaptation [5].

5.1.2. Changes in perceived best focus with astigmatism

In general, understanding how presbyopic lens designs can be improved, and even customized to the patient's refractive profile, requires understanding focus perception in presbyopic patients and to what extent visual perception with a new correction is affected by prior visual experience. Previous studies have shown adaptation to astigmatism [55], [57], [118], reflected by a strong bias in the perception of blur orientation.

There are several reports of changes in perceived best focus setting following changes in visual experience. In particular, we found that subjects shift their neutral best perceived focus following brief periods of adaptation to simulated astigmatic images [204]. Furthermore, naturally astigmatic subjects perceive as isotropic images that are blurred along their axis of astigmatism. Following correction of their natural astigmatism, the neutral best focus shifts towards isotropy [59]. In addition, young astigmatic subjects appear to be more sensitive to the reduction of visual acuity upon induction of astigmatism than non-astigmats [53], particularly when astigmatism is induced along the axis of their natural astigmatism [55]. Other studies have shown that subjects are not only adapted to their native astigmatism, but also to the magnitude [5] and orientation [116], [118], [204] of their own aberrations, and that the best perceived focus shifts following adaptation to HOAs [57]. Achieving optimal best focus is key to providing best optical quality with a correction. Defocus, astigmatism and HOAs interact optically, as demonstrated from optical simulations [49], and experimentally using AO [50]. These interactive effects across aberrations and their impact on subjective spherical error need to be considered when the correcting alternatives simultaneously induce astigmatism and HOAs, as it is the case with progressive lenses. Also, it has been observed that prior adaptation to astigmatism also plays a major role in the way certain optical corrections work, as well as in the selection of best focus. In a previous study we found that certain combinations of astigmatism and coma increase optical quality through focus (compared

to astigmatism alone) [52]. However, the benefit of the interactive effects of coma and stigmatism appears to be much lower in habitually non-corrected astigmats [53]. On the other hand, the best focus setting is shifted in the presence of astigmatism, and the actual shift depends on the refractive profile of the patient [57]. The fact that the same best focus shift trends were found when aberrations were corrected with AO indicates that this shift is primarily a result of prior adaptation. Those previous studies investigated adaptational effects to astigmatism, and the impact of astigmatism on visual function and on best focus setting in young subjects of different refractive profiles (emmetropes, myopes and hyperopes, non- astigmats or habitually/ non-habitually corrected astigmats) [57]. However, to our knowledge, these effects have not been investigated in presbyopic subjects (i.e. subjects that do not or minimally accommodate and need presbyopic correction).

5.2. Methods

Best focus and Visual Acuity (VA) were measured in three groups of subjects with different refractive profiles (pre-presbyopic emmetropic and emmetropic presbyopic and astigmatic presbyopes), under natural aberrations and under corrected aberrations with AO, upon induction of astigmatism (different amounts and orientation). Differences in the best focus setting and VA across subjects and conditions were evaluated. Measurements were performed in the VioBio Lab AOI.

5.2.1. Groups of subjects

A total of 28 caucasian subjects participated in the study. Subjects followed an optometric and ophthalmological evaluation at School of Optometry Clinic of the Universidad Complutense de Madrid (UCM). Subjects were classified in three groups, according to their age (pre-presbyopic subjects and corrected presbyopic subjects) and refractive profile (emmetropes or astigmats). Table 5.1 shows the patients' profile of the subjects in the three groups (G1): pre-presbyopic emmetropic group (n=10), spherical error −0.5 to+0.5 (0.1 ± 0.36 D on average); cylindrical error≤0.25D; age: 29.3 ± 6.5 years. (G2): emmetropic presbyopic group; (n=8); spherical error: −0.5 D to+1.5 (0.47 ± 0.7 D on average); cylindrical error≤0.25D; addition: 2.4 ± 0.35 D; age: 62.6 ± 6.3 years. (G3): astigmatic presbyopic group (n=10); spherical equivalent: −0.8 ± 1.84 D; cylinder -1.52 ± 0.4 D (S1, S9 & S10 against the rule, and the rest with the rule); addition: +2.28 ± 0.28 D; age: 56 ± 4 years. Presbyopic subjects used progressive ophthalmic lenses (PALs) to correct their presbyopia (having worn them between 6 months to 3 years by the time of participation in the study), and therefore exposed long-term to astigmatism induced by PALs. The experiment was performed on one eye (in bold in Table 1), with its refraction meeting the inclusion criteria. If both eyes were eligible, measurements were performed on the dominant eye. Protocols met the tenets of the Declaration of Helsinki and were

		Age	Days between sessions	OD			OS			Add
				Sph	Cyl	Axis	Sph	Cyl	Axis	
G1	**S#1**	23	2	**-0.5**	**-**	**-**	-0.5	-0.5	180º	-
	S#2	31	71	**0**	**-**	**-**	0	-	-	-
	S#3	24	57	**0.5**	**-**	**-**	0.5	-	-	-
	S#4	38	1	-0.25	-	-	**0.25**	**-**	**-**	-
	S#5	37	3	**0.25**	**-**	**-**	0.25	-	-	-
	S#6	24	14	**0.25**	**-**	**-**	0.25	-	-	-
	S#7	23	49	**0.5**	**-**	**-**	0.5	-	-	-
	S#8	36	81	**-0.5**	**-0.25**	**2º**	0	-0.75	13º	-
	S#9	34	96	-	-	-	**0**	**-**	**-**	-
	S#10	23	22	2.5	-	-	**0.25**	**-**	**-**	-
	Mean	**29.3**		**0.1**	**-0.03**					
	std	**6.5**		**0.36**	**0.08**					
G2	**S#1**	55	1	**0**	**-0.5**	**80º**	1	-	-	2.5
	S#2	67	9		-	-	**1.5**	**-0.5**	**105º**	2
	S#3	75	2	1	-	-	**0**	-	-	2.5
	S#4	61	3	1.25	-0.5	10º	**0.75**	-	-	2.5
	S#5	61	5	-1	-0.25	43º	**-0.25**	-	-	2.75
	S#6	65	30	**0**	-	-	0	0.75	90º	2.75
	S#7	60	32	**1.5**	-	-	1.5	-	-	2.5
	S#8	57	12	**0.25**	**-0.5**	**120º**	0.5	-1	80º	1.75
	Mean	**62.6**		**0.47**	**-0.19**					**2.4**
	std	**6.32**		**0.7**	**0.25**					**0.35**
G3	**S#1**	58	10	**0.25**	**-1.25**	**95º**	1	-1.25	85º	2.75
	S#2	56	3	**0.25**	**-1.5**	**180º**	-0.25	-1	169º	2.5
	S#3	54	2	**-1.25**	**-2**	**5º**	-1.5	-2	15º	2
	S#4	56	4	**0**	**-1**	**180º**	0.25	-0.5	180º	2
	S#5	51	2	**1.25**	**-1.5**	**18º**	1	-0.5	0º	2.25
	S#6	55	5	-2.5	-2.5	175º	**-2.75**	**-2**	**180º**	2.5
	S#7	62	5	0.5	-2	10º	**0**	**-2**	**170º**	2
	S#8	50	9	**1.25**	**-1.75**	**5º**	1.75	-2.5	170º	2.25
	S#9	56	18	-3.75	-0.5	90º	**-3.75**	**-1**	**80º**	2
	S#10	62	2	**-3.25**	**-1.25**	**95º**	-3.5	-0.75	100º	2.5
	Mean	**56**		**-0.8**	**-1.53**					**2.28**
	std	**4**		**1.84**	**0.4**					**0.28**

Table 5.1. Participating subject's profile: age, days between sessions and refraction of both eyes (measured eye in bold)

approved by the Institutional Review Board. Subjects signed an informed consent following explanation of the nature of the study.

5.2.2. Experimental protocol: VA & BF at different amount and angles of astigmatism

Best focus was systematically searched using a staircase algorithm, based on four interleaved staircases with random initial position [57]. Focus shifts were achieved using a motorized Badal optometer, which allows adding positive or negative sphere power (in 0.125 D steps) until the optimal appearance of a natural grayscale image (consisting of a face) is reached, according to the subject's responses. The algorithm is based on a randomized-step efficient method, where the subject reports (using two buttons in a keyboard) whether the image presented in the display appears more blurred or sharper than the precedent image. The maximum number of trials in each staircase was 40 and best focus was selected after a maximum number of 20 reversals. The four interleaved staircases start in different initial values (−0.75, −0.50, +0.50 and +0.75 D) from an initial focus setting manually searched by the subject while looking at the Maltese cross stimulus. The best focus was defined as the average of the last 8 reversals.

A tumbling E-letter test was used to measure Visual Acuity (VA). Snellen E letters of varying size (white E-letters on a black background) were presented at 8 random orientations. The subject's task was to identify the orientation of the E letter. The size of the E-letter in the subsequent presentation was changed depending on the subject's response using a quaternion estimation algorithm. A run consisted of 50 trials and 20 reversals, and the visual acuity was measured as the mean of the last 10 reversals.

Measurements (best focus search and visual acuity) were performed in two different sessions (Table 5.2), conducted in two different days. Table 1 shows the difference between sessions for each subject. In the first session, the best focus was searched using the staircase procedure, for different amounts of induced astigmatism (0, 0.50, 1.5, 2.00 D at 180º); with natural HOAs (correcting astigmatism) and with all corrected HOAs using AO. Measurements were also performed for 1.00 D of induced astigmatism at 180º in the AO-correction condition (this condition was repeated in the second session).

Session A **Magnitude of induced astigmatism**		**Session B** **Angle of induced astigmatism**	
Nat	**AO**	**Nat**	**AO**
0.5D 180º BF 1.50D 180º BF 2.00D 180º BF	0.5D 180º BF 1.00D 180º BF 1.50D 180º BF 2.00D 180º BF	1.00D 180º BF +VA 1.00D 45º BF +VA 1.00D 22.5º BF	1.00D 180º BF +VA 1.00D 45º BF +VA 1.00D 22.5º BF
Duration: 120 min		Duration: 120 min	

Table 5.2. Conditions tested in each session

In a second session, best focus was search for 1-D astigmatism induced at 180º, 22º and 45º, and Visual Acuity was measured for 1-D astigmatism induced at 180º and 45º, with

natural aberrations and AO-correction. Best focus and visual acuity were also measured without induction of astigmatism (with and without aberration correction). Under induced astigmatism, Visual Acuity was measured with both the initial search focus and with the staircase-searched best focus.

5.3. Results

5.3.1. Optical quality of the subjects

Optical aberrations were measured before correction (Figure 5.1, natural aberrations), after closed-loop correction of HOA (Figure 5.1, AO-correction) and after induction of astigmatism. Maximum pupil diameters ranged from 5.17 to 4.08 mm. Data were re-scaled to the smallest pupil for averaging across subjects. On average, residual RMS following AO-correction was 0.11 ± 0.13 µm (for 4.08-mm pupil). There were no statistically significant differences across groups in the natural RMS wavefront error for HOAs (p=0.23), nor in the RMS of the residual aberrations after AO-correction (p=0.19). Natural spherical aberration was 0.027 (G1), 0.032 (G2) and 0.040 (G3) µm for 4.08-mm pupils. As expected [205], the presbyopic groups (G2 and G3) showed higher spherical aberration, although differences were not statistically different across groups (p-value= 0.51).

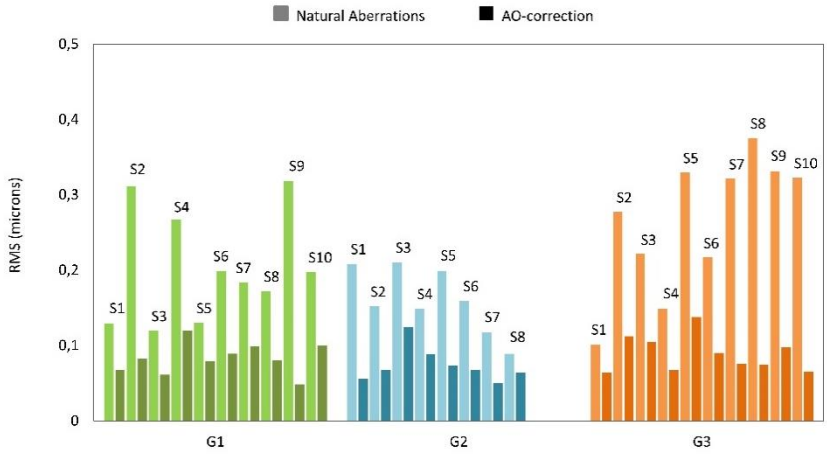

Figure 5.1. Root-Mean-Square (RMS) wavefront error of astigmatism and HOAs for all subjects of the study for natural aberrations (light bars) and AO-corrected aberrations (dark bars). Data are for 4.08-mm pupil diameters. G1: Pre-presbyopic emmetropic group; G2: Presbyopic emmetropic group; G3: Presbyopic astigmatic group.

The attempted astigmatism magnitude was induced with an accuracy of 3% (on average across subjects and the four induced magnitudes) and the attempted angle was induced within 10% (on average across subjects and the three induced orientations). Figure 5.2 shows the difference in the best focus when HOAs are corrected in comparison with the best focus found with Natural aberrations.

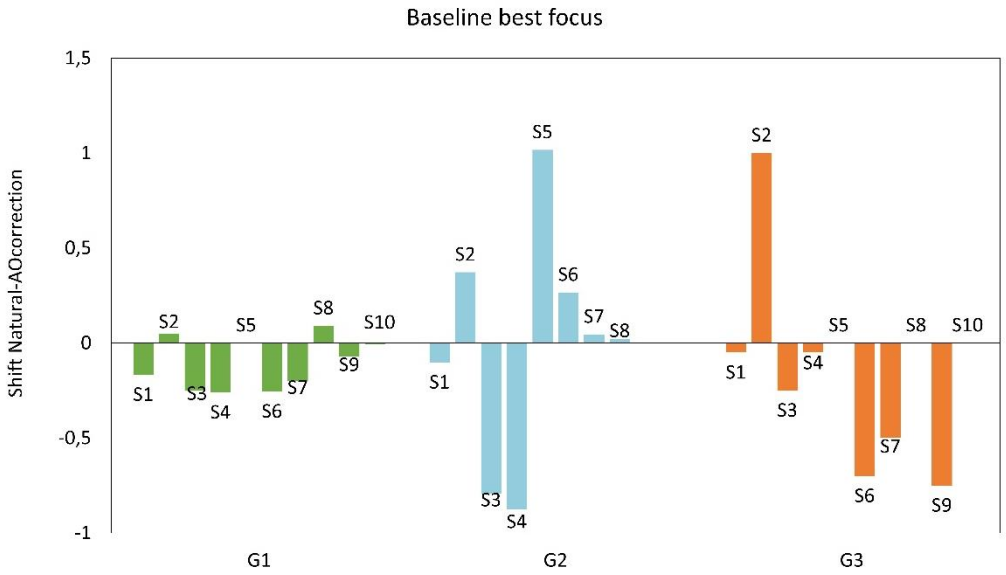

Figure 5.2. Baseline (no astigmatism) best focus point for all subjects, relative to the best focus point in the presence of natural aberrations. The values shown in graph represent the focus shift when HOA are corrected.

5.3.2. Best focus shift with induced astigmatism

In the majority of subjects, there was a shift in the best focus position upon correction of HOAs, and also upon induction of astigmatism. When astigmatism and HOA aberrations were corrected with AO, best focus shifted by 0.05 D (G1), −0.19 D (G2) and −0.08 D (G3). Shifts in best focus for different amounts of induced astigmatism were measured with natural aberrations and AO-correction, relative to the respective best foci without induced astigmatism. Figure 5.3.a-f shows the shift in best focus for all subjects in each group: G1 (a, b); G2 (c, d) and G3 (e, f) as a function of the magnitude of induced astigmatism, with natural aberrations (a, c, e) and AO-correction (b, d, f). Each symbol represents the average of four repeated focus settings for each individual subject. The average standard deviation across repeated measurements across all subjects was 0.28 D (natural aberrations) and 0.26 D (AO-correction).

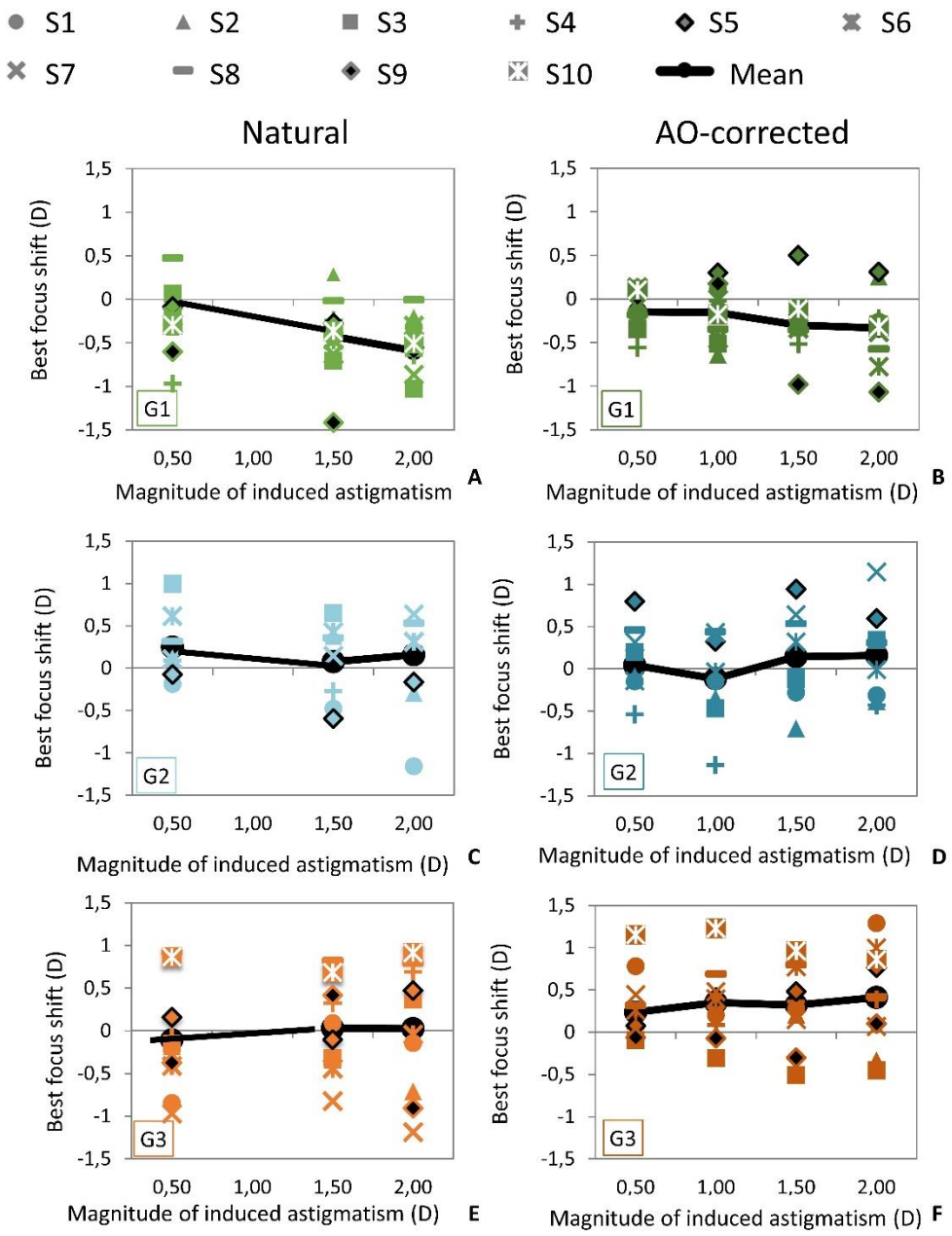

Figure 5.3. Shift of best focus setting as a function of induced astigmatism (with respect to the not-induced astigmatism condition), for all subjects in G1 (a, b), G2 (c, d) and G3 (e, f). Left: Natural correction; Right: AO-correction. A positive shift indicates a focus shift towards horizontally oriented blur in the retina, and a negative shift towards vertically oriented blur in the retina.

In pre-presbyopic emmetropic subjects (G1), there was a consistent shift towards negative defocus, which tended to be higher, the higher the magnitude of induced astigmatism. Best focus values shifted towards less negative defocus (emmetropic presbyopes, G2) or towards predominantly positive defocus (astigmatic presbyopes, G3). The shift in best focus produced by astigmatism in G1 was statistically different from G2 when aberrations were corrected, for all magnitudes of induced astigmatism ($p < 0.04$ for 0.50D of astigmatism induced; $p < 0.015$ for 1.00D, 1.50D and 2.00D). S7 of emmetropic presbyopes group (G2), presents a slightly higher best focus shift in the condition of 2.00

D of astigmatism induction with HOA correction, that may be caused by furthest from strict emmetropia in this group. One condition (1.00D 180° AO-corrected) was repeated in both sessions. An inter-session variability analysis showed no statistical differences between these repeated measurements in any group. However, we found statistical differences in the best focus setting across groups upon induction of astigmatism: best focus in general significantly shifted towards more negative values in G1 (both under natural and AO-corrected aberrations), towards less negative values (under natural aberrations) or even positive values (under AO-corrected aberrations) in G2, and towards more positive values (under AO corrected aberrations) in G3. Statistical significance values are shown in Figure 5.4.

In general, the best focus shift was independent of the angle at which astigmatism was induced for measurements performed either under natural aberrations or under AO-correction (Figure 5.5). Only astigmatism induced at 180° resulted in slightly higher shift in G1. The best focus shift was more positive in the presbyopic groups than in the prepresbyopic group at all angles, with the astigmatic presbyopes (G3) exhibiting the more positive shifts. The shift in best focus produced by astigmatism in G1 was statistically different from G2 at all angles ($p < 0.015$, $p < 0.02$, for astigmatism induced at 180° and 22.5°, and 45° respectively).

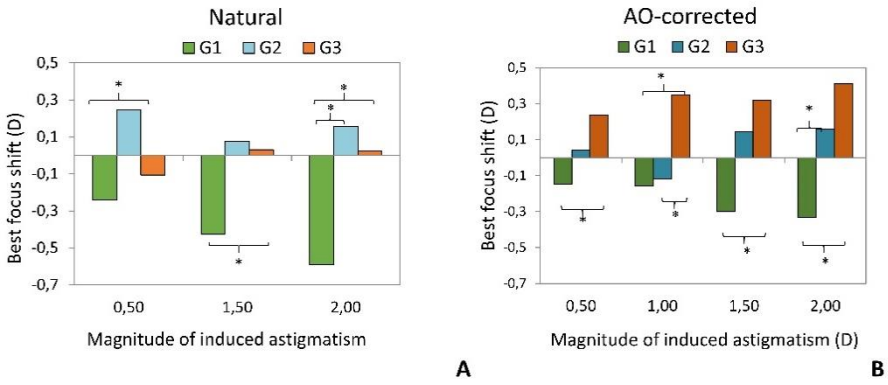

*Figure 5.4. Average best focus shift across subjects in each group upon induction of astigmatism. Left: Natural aberrations; Right: AO–corrected aberrations. *p-≤0.05. A positive shift indicates a focus shift towards horizontally oriented blur in the retina, and a negative shift towards vertically oriented blur in the retina.*

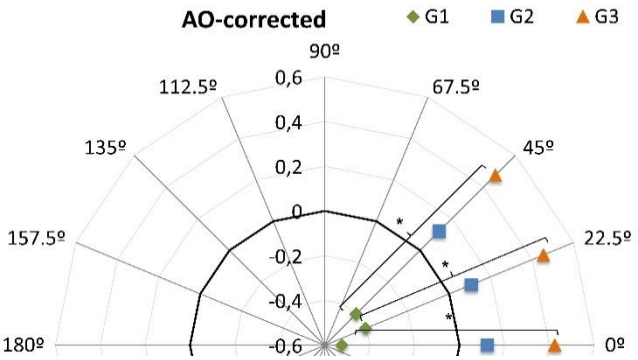

*Figure 5.5. Average mean best focus shift across subjects in each group upon induction of 1.00D of astigmatism at different angles, for AO–corrected aberrations. *p-values≤0.05.*

5.3.3. VA under induced astigmatism

Pre-presbyopic emmetropic subjects (G1) showed the highest VA, and the astigmatic presbyopic group (G3) the lowest VA, and the differences were statistically significantly different under AO-correction ($p < 0.01$). VA improved significantly ($p < 0.01$) in pre-presbyopic emmetropic subjects (G1) and in emmetropic presbyopes (G2) when astigmatism and HOA were corrected, but not in astigmatic presbyopes (G3). Induction of astigmatism produced the largest degradation of VA for G1, particularly when astigmatism was induced at 45°, and the lowest degradation of VA for G3, which appeared rather insensitive to induction of astigmatism, particularly at 180°.

Figure 5.6 shows decimal VA under natural aberrations (left columns) and AO-correction (right columns) without astigmatism and with astigmatism induced at 180° and 45°, for G1 (A), G2 (B) and G3 (C). Measurements were performed at the initial focus setting without astigmatism (Ini), which was different for the Natural and AO-corrected conditions, and the focus setting obtained following the staircase procedure (SC).

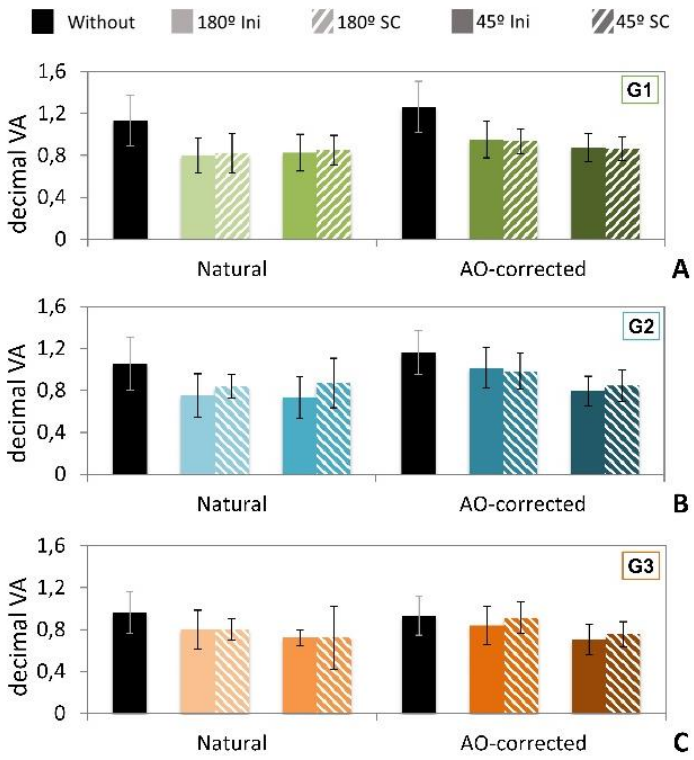

Figure 5.6. Decimal Visual Acuity without astigmatism induction (black bar) and for 1.00D of induced astigmatism (measured at the initial best focus setting, Ini, –prior to astigmatism induction, solid colored bars- and at the best focus setting following the staircase procedure, SC –upon astigmatism induction, dashed bars-). Lighter bars in each panel stand for 1D of astigmatism induced at 180° and darker bars for astigmatism induced at 45°. Data are for Natural Condition (left panels) and AO-correction (right panels for the three groups (A, G1, prepresbyopic emmetropes; B, G2, emmetropic presbyopes; C, G3, astigmatic presbyopes). Error bars are SDs.

Figure 5.7 shows the decrease in Decimal VA in terms of ratios of VA with induced astigmatism (at best focus)/VA without astigmatism, for all groups and conditions. The VA Ratio with/without induced astigmatism was higher in G2 and G3, indicating that presbyopes are less sensitive to the induction of 1D of astigmatism, both at 180° and 45°, especially when natural aberrations were corrected. All groups experienced a larger decrease in visual acuity when astigmatism was induced at 45° than at 180°, more remarkable under AO-correction.

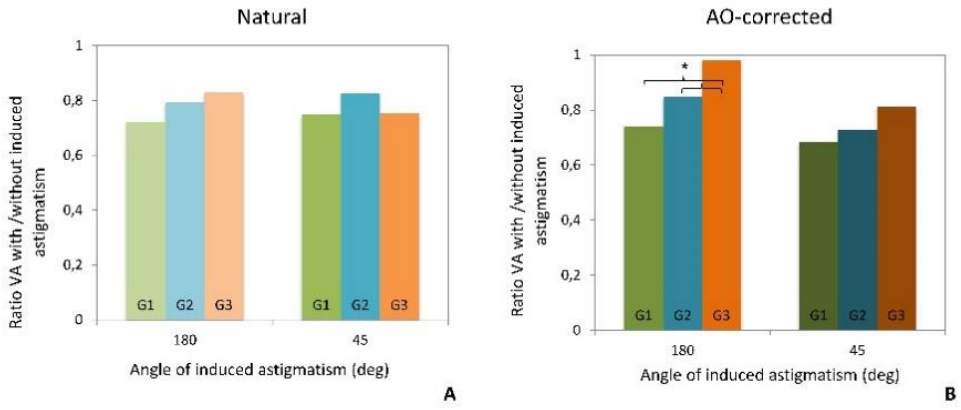

*Figure 5.7. Ratio VA with astigmatism/VA without astigmatism Ratios, for 1.00D of astigmatism induced at 180° or 45°, under natural aberrations (A, left panel) and AOcorrection of aberrations (B, right), for the three groups (G1, in green; G2 in blue; G3 in orange). *p-values≤0.05.*

5.4. Discussion

We measured the impact of inducing astigmatism in pre-presbyopic emmetropes and two groups of presbyopic patients, non-astigmats and astigmats. All patients in both presbyopic groups were PAL wearers, therefore exposed to a visual experience consistent with the presence of astigmatism produced by progressive power changes in their spectacle correction. The best focus setting in the presence of astigmatism as well as the Visual Acuity with induced astigmatism was compared to a control group of pre-presbyopic emmetropes. We found that presbyopes, most prominently those that were natural astigmats, showed significant differences in the impact of astigmatism induction on best focus setting and on Visual Acuity, compared to pre-presbyopic emmetropes. Since it was not possible to include an age-matched presbyopic group not wearing any presbyopic correction, given that the majority of the population of this age wears some sort of correction aid for their presbyopia, we cannot rule out that the predominant factor in the effect is age or the correction, and it is likely a combination of the two. Despite the relatively small number of subjects in each group, the groups are equality distributed and their variance is homogenous and follow a normal distribution, resulting in a statistical power of ~70%.

Similarly to our earlier reported on young astigmats [57], we found that presbyopes also shift their perceived best focus toward less negative defocus values (or positive) in the presence of astigmatism, with largest shifts occurring in the presbyopic astigmats. A positive shift is consistent with horizontally oriented blur in the retina, and a negative shift is consistent with vertically oriented blur in the retina. It should be note that the aberrations were corrected in monochromatic light, allowing for potential natural interactions between chromatic and monochromatic aberration to occur [62]. In any case, that the wavelength that is best focused when polychromatic targets are focused is close to 555 nm [206], suggesting that at least, in general best focus settings should not be biased by chromatic effects, although may be the cause behind some intersubject variation). The reasons for the consistent negative shift found in young emmetropes in all studies are not clear, but may be connected to a lower reduction in visual acuity with

vertical blur (as opposed to other orientations) found in emmetropes [55]. Interestingly, in the current study, which examined induction of astigmatism at various orientations, the largest shift in emmetropes occurred at 180° (when HOAs are corrected). On the other hand, while in the prior study the consistent positive shift in best focus upon induction of astigmatism at 180° was only found in ATR astigmats (explained by the fact ATR myopic astigmats would be naturally adapted to horizontal blur in the retina), in the current study a more positive blur is found regardless the axis of native astigmatism (i.e. both in ATR and WTR astigmats). These findings may be explained by the fact that older subjects have higher amounts of aberrations (although differences did not reach statistical significance in our cohort) or by adaptation effects produced by their habitual presbyopia correction, as progressive ophthalmic lenses may induce horizontal, vertical and oblique astigmatism (even for the non-natural astigmats of G2). Intersubject variabilities in this effect could not be associated to a particular characteristic (refraction or aberration magnitude), particularly as the range of spherical error was slightly higher in G3 than in the other groups. While the PAL induced astigmatism is mostly peripheral (intermediate corridor), and prior work has shown little effect of peripheral blur adaptation to central vision perception [207], the integrated vision at all distances in PAL wearers is likely more affected by astigmatism than in non-PAL wearers. Aberrations are expected to affect also foveal vision, as the eye looks through different parts of the lens [120]. Longer-term exposure to astigmatism in native astigmats may explain the larger best focus shifts differences in this group. Under corrected aberrations, the best focus shift was consistently positive for all magnitudes of induced astigmatism in all subjects of G3, except in two subjects (S3, a WTR astigmat, and S9, an ATR astigmat), for astigmatism induced at all different orientations. The clear difference on the axis-dependency of the best focus shift upon induced astigmatism between pre-presbyopic and presbyopic astigmats may be associated to age, presbyopia (accommodation not being able to scan through the Sturm interval in neither myopic nor hyperopic presbyopes) or potential differences between the astigmatic correction wear in non-presbyopic subjects and that of the habitual presbyopic correction in presbyopic subjects. It is also likely that the observation made in young astigmats [99] ¡that adaptation can be actually transferred to a long-term storage that can be instantly engaged when blur is reapplied, can also hold in older subjects wearing PALs. Measurements were made for a fixed pupil diameter. We can only speculate on the effects of the natural pupil size (and their influence on retinal bur) on adaptation, as to the best of our knowledge, this has not been systematically evaluated. The magnitude of the blur level and (to a lesser extent) the blur orientation depend on the pupil diameter. In a previous study [99] also pointed out to the potential learned ability of storing multiple transformations of the visual world, allowing observers to switch between different states of adaptation, which, regarding the pupil may correspond to different pupil diameters. Potential adaptation to astigmatism in presbyopic correction wearers and indications of a prior adaptation to astigmatism in native astigmat presbyopes is also evidenced by the different impact of astigmatism induction on Visual Acuity, found in the current study. As reported in recent studies, we found that emmetropes experienced the largest degradation (lower VA with astigmatism/without astigmatism Ratios) when astigmatism was induced. Astigmatism induced at 180° imposed less degradation than when it was induced at 45°, also as previously found (Vinas et al., 2013). On the other hand, astigmatic presbyopes were the least sensitive to the induction of astigmatism, with minimal degradation (Ratio with

astigmatism/without=0.98 in G3) for astigmatism induced at 180° (with aberrations corrected).

Differences between the native astigmatism angle and induced astigmatism (at 180°) ranged between 0–20 deg (7 subjects) and 80–90 deg (3 subjects). We did not find a systematic difference neither in the defocus shift or decrease in VA with induced astigmatism, as a function of angle difference. We only found higher variability in the measured best focus shift value in patients with native against the rule than in patients with the rule astigmats (1.80 D vs 0.63 D), but not a difference in the shift sign. Our results suggest then that it is rather the presence of astigmatism, rather than the sign (horizontal or vertical), the main contributor to the effect. In fact, the higher insensitivity of astigmats to the induction of astigmatism, regardless the angle of native and induced astigmatism, parallels findings by de Gracia et al. This paper reported that inducing 0.5 D of astigmatism at 45° in a young cohort of subjects produced a decrease in VA by 23% and in habitually corrected astigmatic subjects by 21%, whereas in habitually non-corrected astigmatic subjects (with astigmatism angles ranging from 30 to 180) the decrease was only 5%. In that study, the finding was attributed to accommodation possibly sweeping the retinal image in the Sturm interval, therefore allowing exposure and adaptation to retinal images blurred in range of orientations. We can speculate here that prior exposure to different retinal oriented blur in now a presbyopic group, in combination with the effects of the current presbyopic correction (which produces a similar, yet reduced bias in non-astigmats) could result in similar effects. The general effects of astigmatism on visual performance occurred both in the presence or absence of natural aberrations, although differences (and statistical significance) were more marked when the native aberrations of the subject were corrected, as previously found in young subjects (Marcos et al., 2015). The overall effect of correcting aberrations on visual performance appears to be significantly higher in the pre-presbyopic group (G1) than in the presbyopic groups (G2, G3). While for G1 VA improved from 1.14 to 1.30 when aberrations were corrected, the other two groups either experienced a minor improvement of VA (1.06 to 1.16, G2) or did not significantly improve VA when aberrations were corrected (0.96 to 0.93, G3). A comparison of ocular aberrations across groups showed only a small HOA RMS increase and spherical aberration positive-shift in the older groups (particularly G3), likely insufficient to explain the lower VA in the older group. The lack of benefit of aberration correction in the older groups suggests that the lower VA is in fact additionally affected by other optical effects (i.e. intraocular scattering) and neural effects. Interestingly, shifting focus to the best focus as identified in the presence of astigmatism did not improve VA, indicating that improved perceptual image quality is not necessarily associated to improved performance, although may result in higher visual comfort to the patient.

5.5. Conclusions

Presbyopes experience shifts in the best focus upon induced astigmatism and higher insensitivity to astigmatic induction, which is consistent to habitual exposure to higher aberrations and astigmatism. The effect was found in presbyopic patients wearing progressive lenses, whether they are native astigmats (where the effect is higher) or emmetropes. This study shows that the best focus correction in the presence of

astigmatism is dependent on the refractive profile of the patient, and can be optimized to the patient's preference, even if this only have a minimal impact on visual performance.

The use of AO helps to understand adaptation to astigmatism, in particular in presbyopic patients that are progressive addition lenses wearers. Alternative solutions to presbyopia are multifocal corrections, in the form of contact or intraocular lenses. In the next chapters we used visual simulators of multifocal corrections, and tested their accuracy in replicating real lens designs.

Chapter 6. Comparison of vision through surface modulated and SLM multifocal optics on simulated presbyopic subjects

In this chapter, we used an AO platform to study the performance of the Spatial Light Modulated and its comparison with a reference device, such as phase plates.

This chapter is based on the paper by Vinas et al. "*Comparison of vision through surface modulated and spatial light modulated multifocal optics*". Co-authors are Dorronsoro, Radhakrishnan, Benedi-Garcia, LaVilla, Schwiegerling; Susana Marcos and it was published on Biomedical Optics Express on 2017. The study was also collected in the review paper by Marcos et al. "VioBio lab adaptive optics: technology and applications by women vision scientists" [154].

The study was presented in ARVO 2016 by Vinas with the title "*Testing vision with physical and simulated multifocal corrections in an adaptive optics visual simulator*" as a poster contribution.

The author of this thesis collaborated in the characterization of the manufactured phase plates and the revision of the manuscript.

6.1. Introduction

Spatial Light Modulators (SLM) are increasingly used as active elements [208], [209] to simulate different optical corrections in AO visual simulators. As opposed to deformable mirrors (DM), liquid crystal on silicon (LCoS)-SLMs are capable of reproducing abrupt phase maps, through the use of wrapped phase representations, increasing the device effective stroke [144], [210]. On the other hand, LCoS-SLMs have a lower response speed, present artifacts due to diffraction effects, generally require the use of polarized light and their behavior is wavelength-dependent due to the dispersion properties of the liquid crystal and the phase wrapping [143], [144]. AO visual simulators based on SLMs have been used for sensing and compensating of optical aberrations in ophthalmic applications [68], [143], [209], [211]. One of the most interesting application of the AO visual simulators based on LCoS-SLMs is their possibility to simulate and test vision on patients at different distances under complex multifocal presbyopic refractive corrections, such bifocal and trifocal corrections [212], bifocal, trifocal and tetrafocal, angular and radially segmented corrections [76], simulation of corneal inlays [213], or spherical aberration inducing corrections [214], [215]. There have also been some attempts to simulate diffractive corrections using SLMs [216]. Two-channel Simultaneous Vision Simulators have also made use of SLMs (in transmission) to simulate bifocal corrections with angularly [217], radially and hybrid pupillary distributions for near and far [218]. Visual simulations using these systems have revealed significant differences in visual perception of patients with the different designs. Some lens design preferences were consistent across individuals (and to a large extent independent on the patient's eyes aberrations, as the preferences for particular designs remained similar when the eye's aberrations are AO-corrected [76]), whereas others were patient-specific (i.e. bias to particular orientations in bifocal angularly segmented designs [217].

These studies indicate the value of using visual simulators to select the multifocal design that is better suited for a patient before lenses are fitted or implanted in a patient's eye. They also allow investigating new multifocal lens designs and assessing the relative contributions of the native optics and neural effects on the performance of multifocal lenses at the patient level. A question often raised when using phase-only reflective SLMs to represent a certain design is the extent to what they truly represent a real lens. Differences may be expected arising from resolution limitations and diffraction artifacts in the SLM, and from manufacturing limitations in the physical lens. In this study, we compared visual perception and optical quality with lathe-manufactured multi-zone multifocal surfaces and through equivalent phase maps simulated with an LCoSSLM in a custom developed AO visual simulator.

6.2. Methods

6.2.1. Subjects

Five young subjects (ages ranging from 25 to 32 years, mean 28.5 ± 0.14 years) participated in the study. The spherical error was −1.4 ± 0.2 D, and the average astigmatism was −0.2 ± 0.1D.

All participants were acquainted with the nature and possible consequences of the study and provided written informed consent. All protocols met the tenets of the Declaration of Helsinki and were previously approved by the Spanish National Research Council (CSIC) Ethical Committee.

6.2.2. Designs of the lenses

Six different refractive multifocal designs were evaluated experimentally in the form of SLM-simulated phase maps and manufactured (freeform lathe) phase plates. The refractive multizone segmented phase designs consisted of N-zones with varying optical power ranging from 0 D to +3 D across the lens in equal steps between the zones. In Zernike terms, defocus varied sequentially and linearly across zones between 0 and −3.89 µm in a 6 mm pupil, equivalent to a dioptric power change from + 0 D for Far distance correction to + 3.0 D as near addition. The six multifocal designs are split into angular and radially segmented designs.

The angular lenses featured N = 2, 3 and 4 zones (2ANG, 3ANG and 4ANG, respectively) of varying power across equi-sized sectors. To replicate more realistic manufacturing conditions, a transition zone was incorporated to smooth the phase change between the different 3- and 4-angular segments (5 degrees). The radial lenses featured N = 2, 3 and 4 zones (2RAD, 3RAD and 4 RAD, respectively) of varying power, where the zones are equalarea concentric regions. The radial lenses also have a transition zone between the zones corresponding to the diamond tool radius. The diameter of each lens was 6 mm. The area of each zone was constant in all cases.

Matlab routines were used to numerically simulate the multizone segmented phase designs, which were later programmed in a reflective phase-only LCoS-SLM and manufactured in a freeform lathe.

6.2.3. Simulators: SLM-phase maps generation and surface manufacturing

SLM-phase maps generation: Each phase map was defined by the wavefront in each zone and a set of complementary masks (radial or angular, 2, 3 and 4 zones) that equals 1 in the corresponding zone and 0 elsewhere [135]. A wrapping process [219], [220] was applied to the phase patterns to achieve a maximum phase difference of 2π defined by the calibration of the SLM. The generated pattern is a grey-scale image, where each level of grey corresponds to a certain phase difference between 0 and 2π. Images were generated for a 6-mm pupil at the pupil plane where the SLM is placed.

Surface manufacturing: Phase plates were manufactured in a four-axis Nanocam 650 FG free-form lathe (Moore Nanotechnology Systems, Swanzey, NH). Polar coordinate sag tables of each of the lenses were generated in custom software and provided to the lathe [16]. Each lens was lathed into one PMMA blank using a diamond tool with a 0.5-mm tool radius. An optical profilometric microscope (PLµ, Sensofar, Barcelona, Spain) [221], mounted on a vibration-isolated table, was used to characterize the surface profile of the lathe-manufactured phase plates.

6.2.4. Psychophysical experiments: Scoring and VA

Perceived visual quality: Images generated by multifocal optics vary on more than one perceptually identifiable dimension [222], thus the use of global perception metrics [76], [79], [223] is well suited to characterize visual perception with multifocal designs. In this study, the psychophysical paradigm consisted on a perceptual scoring of the stimuli viewed through the different SLM simulated and the lathe-manufactured multifocal surfaces, in series of 60 trials. The stimuli consisted of a binary noise pattern with sharp edges at random orientations. The binary noise pattern was digitally produced from a uniform noise distribution spatially filtered with an annular filter in the frequency domain (inner radius: 3 cycles/deg; outer radius: 6 cycles/deg), that was later transformed to a binary image and smooth by means of a Gaussian function [76]. A new stimulus was generated on each trial with a different noise pattern, so that edges at all orientations were presented over the course of the experiment. Patterns and viewing distances were randomly selected. For each test stimulus presented (for 500 ms) the subject was instructed to grade the image quality from very sharp to very blurred in a 6-point scale using corresponding keys in a response system (1-very blurred, 2-blurred, 3-not so blurred....). A score, of 0 to 5, was posteriorly assigned, based on the grading. The measurements were repeated 3 times. This method has been used and shown to be useful in determining subjective visual quality with multifocal correction in previous studies [79], [223].

Visual acuity: Visual acuity (VA) was measured using an 8-Alternative Forced Choice (8AFC) [224] procedure with Tumbling E letters and a QUEST (Quick Estimation by Sequential Testing) algorithm programmed with the Psychtoolbox package [177] to calculate the sequence of the presented stimulus (letter size and orientation) in the test following the subject's response. Subjects had to determine the orientation of the letter E, through the SLM-simulated phase maps or the lathe-manufactured surfaces, while aberrations were AO-corrected with the deformable mirror. The QUEST routine for each VA measurement consisted of 40 trials, each one presented for 0.5 seconds, where the threshold criterion was set to 75%. The threshold, VA measurement, was estimated as the average of the 10 last stimulus values. Visual acuity was expressed in terms of decimal acuity (logMAR = $-\log_{10}$[decimal acuity]) [225].

6.2.5. Optical Quality metric: ideal observer

Through-focus optical quality for the different 6-zone angular and radial segmented phase designs was calculate from the wave aberration of each eye in all conditions (different multizone angular and radial segmented phase designs, with natural and AO-corrected aberrations). The measured residual aberrations after AO-correction of the five subjects, the phase map programmed in the SLM, and the phase-plate phase map, derived from profilometric data, were used in the optical simulations.

The Visual Strehl (VS) was used as an optical quality metric, estimated as the volume between the Modulation Transfer Function (MTF) of the system, and a general neural transfer function [81], [192]. The MTF was estimated from the pupil function using Fourier Optics. The following parameters were computed from the through-focus VS curves: (1) Area under VS curves in a 6.0 D dioptric range; (2) Dioptric range above a certain threshold (0.06); (3) VS at far, intermediate and near distance (0 D, + 1.5 D and + 3.0 D, respectively)

[76]. The response of an “ideal observer”, purely responding on optical grounds to the same psychophysical test performed on subjects, was calculated in all eyes, conditions and distances. Scores (ranging from 0 to 5) were based on the VS values, normalized to the maximum VS value, using a similar approach to that of the psychophysical paradigm for perceptual scoring. All calculations were performed for a 6-mm pupil diameter.

6.2.6. 1 pass TF images

The optical quality of both, lathe-manufactured surfaces and SLM-simulated phase maps, was evaluated on-bench in the same AO system, using an artificial eye provided with an objective lens (50.8 mm) and a CCD camera (DCC1545M, High Resolution USB2.0 CMOS Camera, Thorlabs GmbH, Germany) acting as a “retina”, in place of the subject’s eye. An E-letter (1.62-deg subtend) was displayed in the Digital Micro-Mirror Device (DMD), illuminated with 555 nm light from the SCLS. Series of through-focus images (+1.00 to −4.00 D, in 0.25D steps) of the stimulus were collected in the artificial eye with all patterns, while the aberrations of the system were AO-corrected, for 6-mm pupil diameter. The optical quality metric was the image correlation of the collected image with the reference image (same E-letter, through monofocal optics in focus). Through focus optical quality curves were compared across patterns and lens type (lathe-manufactured surface and SLM-simulated phase maps), and the values at near, intermediate and far were used to rank the patterns.

6.3. Results

6.3.1. Comparison SLM-simulated phase maps and manufactured phase plates

The six lathe-manufactured surfaces were characterized using non-contact microscopy-based optical microscopy (PLμ, Sensofar, Barcelona, Spain). Figure 6.1.a shows an example of a photograph of a 2ANG phase plate (top) and the corresponding optical profile across a horizontal half-meridian (bottom). For each lens, the optical profile was analyzed and the areas of the different zones were calculated and compared with the nominal values. The resulting phase map was obtained and compared with the SLM-simulated phase map. Figure 6.1.b shows the measured areas of the different lathe-manufactured surfaces for far (green solid bars), intermediate-3-segmented (red solid bars), intermediate-4-segmented (red dashed bars), and near distance (blue solid bars) zones, and of the corresponding nominal areas of those designs (black dashed bars). On average, discrepancies between experimental and nominal areas were below 2% in all cases. In terms of dioptric power, the averaged power for all zones falls within 0.1% of difference with respect to the nominal values for the same zones (figure 6.1.c).

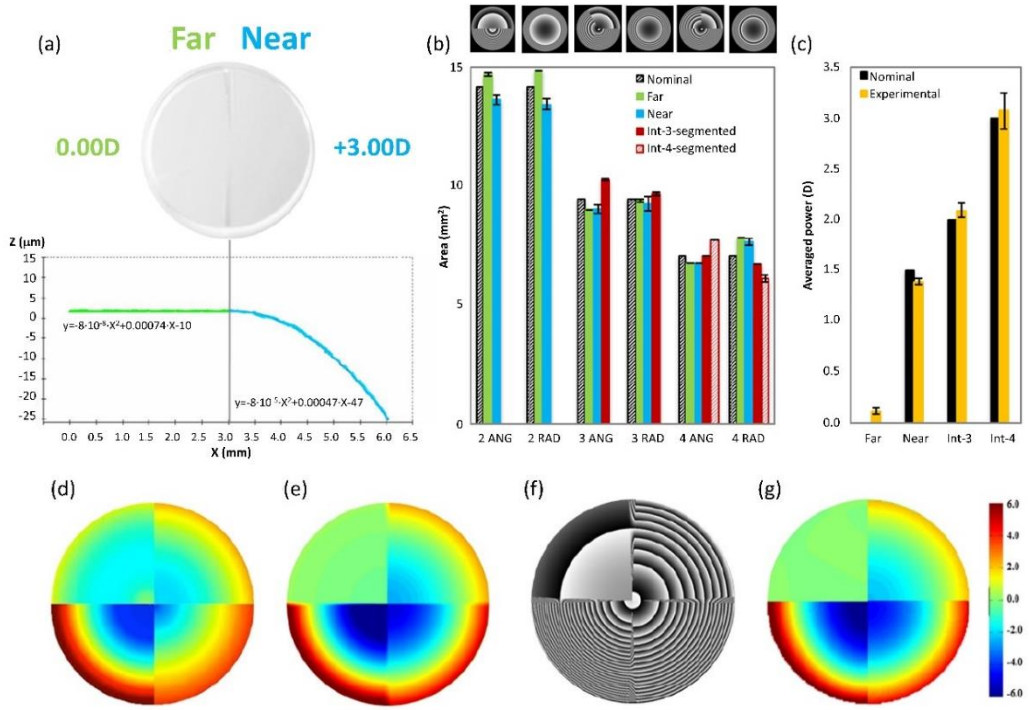

Figure 6.1. (a) 2ANG lathe-manufactured phase plate (top) and its corresponding lathemanufactured surface profile (bottom, measured with non-contact profilometry) for far (green) and near distance (blue). (b) Areas of the different lathe-manufactured phase plate for far (green solid bars), intermediate-3-segmented (red solid bars), intermediate-4segmented (red dashed bars), and near distance (blue solid bars) and for the nominal areas of those designs (black dashed bars). Error bars stand for experimental error during measurements with the profilometer. (c) Dioptric power of the different optical zones of the lathe-manufactured phase plate for far, near, intermediate for 3-segmented and intermediate for 4-segmented (yellow bars) and their corresponding nominal values (black bars). Error bars stand for experimental error during measurements with the profilometer. (d) Phase map obtained from profilometric measurements of an example surface-modulated plate (4ANG); (e) Intended phase map for 4ANG in the SLM (before wrapping); (f) Wrapped phase map in the SLM; (g) Measured phase map induced by the SLM (composite from Hartmann Shack measurements of equivalent pure defocus phase maps). Color bar scale is in microns. Data are for 6-mm pupil diameter.

Figure 6.1.d-g shows an example of the generated wavefront with either the lathemanufactured surface or the SLM-simulated phase map with 4ANG design. The figure shows the phase map obtained from profilometric measurements of the 4ANG phase plate (d), the intended phase map for the SLM (before wrapping) (e), the wrapped phase map for the SLM (f), the measured phase map induced with the SLM (composite from Hartmann-Shack measurements obtained for induced pure defocus of 0.0, + 1.0, + 2.0, and + 3.0 D) (g).

Figure 6.2 shows the results of on-bench optical quality measurements with surfaces and SLM-simulated phase maps. Figure 6.2.a shows an example of the through-focus image series obtained for 3ANG design in the form of surface-modulated plate (upper row) and mapped with the SLM (lower row). Figure 6.2.b shows the corresponding through-focus optical quality (image correlation metric) for the surface-modulated phase plate (green)

and the SLM (blue). Figure 6.2.c shows through-focus optical quality (image correlation) for all 6 designs with surface-modulated plates, and figure 6.2.d for the SLM-simulated phase maps.

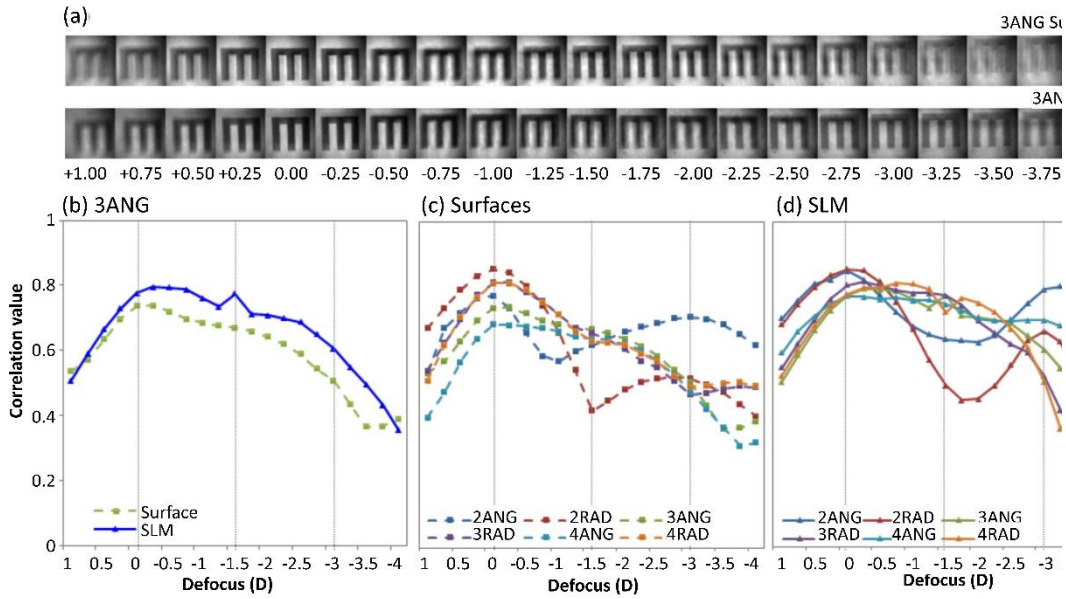

Figure 6.2. (a) Example of the through-focus image series obtained for 3ANG design in the form of lathe-manufactured surface (upper row) and SLM-simulated phase map (lower row). (b) Corresponding through-focus optical quality (image correlation metric) for those two series of images (blue for lathe-manufactured surface and green for SLM-simulated phase map). (c) Through-focus optical quality (image correlation metric) for all 6 designs with surfaces modulated plates. (d) Through-focus optical quality (image correlation metric) for all 6 designs with SLM-simulated phase maps. Data are for 6-mm pupil diameter.

6.3.2. Scoring

The results of the perceptual scoring from the five subjects are summarized in figure 6.3. Perceptual scoring obtained with lathe-manufactured surfaces (upper row, solid bars), with SLM-simulated phase maps (middle row, dashed bars) and the correlations between them (lower row) for far (green), intermediate (red) and near (blue) distance upon AO-correction of HOAs of the subjects. Similar general trends are found with lathe-manufactured surfaces and SLM-simulated phase maps.

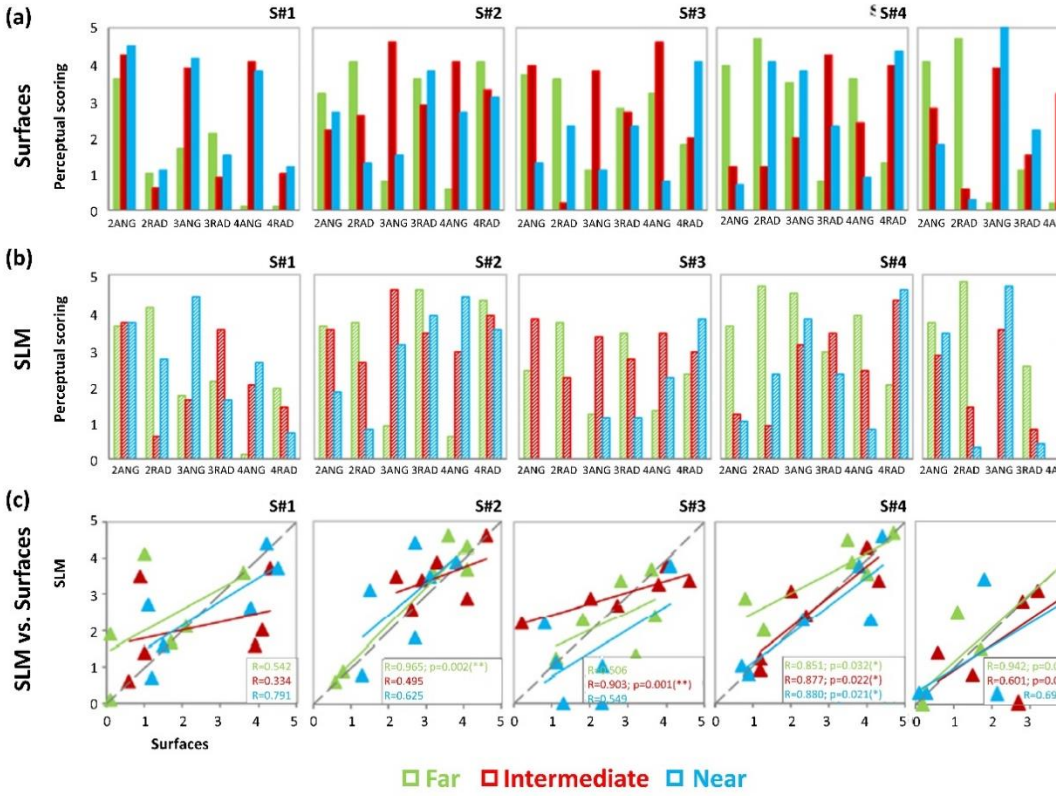

*Figure 6.3. Perceptual scoring with each multifocal pattern from all 5 subjects for far (green), intermediate (red) and near (blue) distance with (a) lathe-manufactured surfaces and (b) SLMsimulated phase maps. (c) Correlations between perceptual scores for lathe-manufactured surfaces and SLM-simulated phase maps for all subjects. Statistically significant correlations (*p < 0.05; **p<0.005) are noted in each graph.*

Figure 6.4 shows the correlation between the perceived visual quality with the SLM simulated phase maps and with the lathe-manufactured surfaces for all subjects and all designs (left), all angular designs (center) and all radial designs (right) for far (green), intermediate (red) and near (blue) distance. The correlations were statistically significant ($p<0.05$) for all conditions and all testing distances.

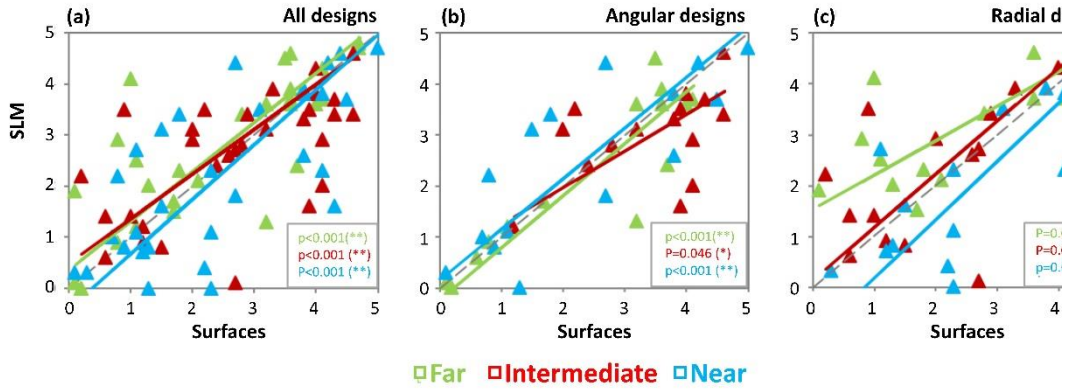

*Figure 6.4. Correlation between the relative perceived visual quality results obtained with the SLM-simulated phase maps and the lathe-manufactured surfaces for all subjects and all designs (left), all angular designs (middle) and all radial designs (right) for far (green), intermediate (red) and near (blue) distance, and calculated orthogonal regression (solid lines). Statistically significant orthogonal correlations (*p < 0.05; **p<0.005) are noted in each graph.*

Figure 6.5 shows the average (across 5 eyes) perceived visual quality (perceptual scoring) with lathe-manufactured surfaces (solid bars) and SLM-simulated phase maps (dashed bars) for far (green), intermediate (red) and near (blue) distance after AO-correction of HOAs of the subjects. Black bars show the difference between both conditions.

In general, there is good agreement between the relative perceived visual quality obtained with the lathe-manufactured surfaces and the SLM-simulated phase maps with similar trends across distances. The higher differences occurred for 2RAD (0.58), 3RAD (1.02) and 4RAD (0.60) for far vision; 2RAD (0.5) and 4ANG (0.92) for intermediate vision; and 2RAD (0.60), 3RAD (0.56) and 4RAD (0.58) for near vision.

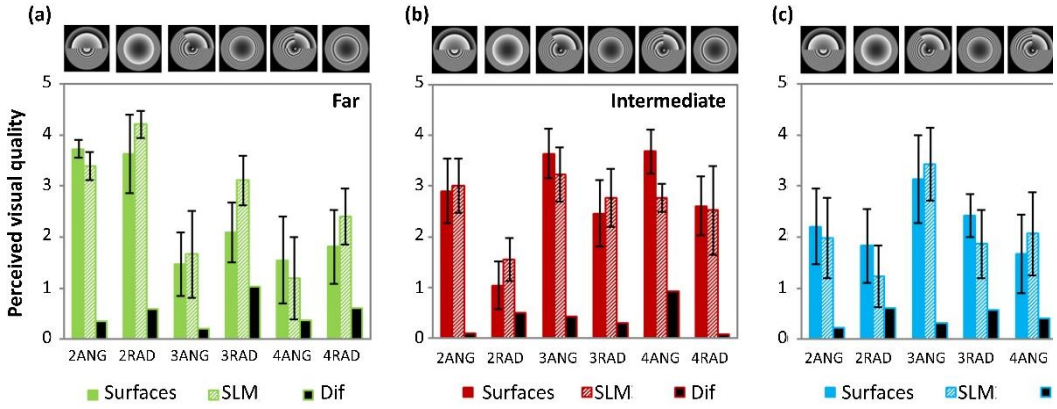

Figure 6.5. Average relative perceived visual quality (perceptual scoring) with lathe-manufactured surfaces (solid bars) and SLM-simulated phase maps (dashed bars) for far (green), intermediate (red) and near (blue) and their corresponding difference (black bars). Data average data across 5 subjects, for 6-mm pupils and AO-correction of the HOAs of the subjects. Error bars stand for standard deviation across subjects.

6.3.3. Scoring vs. optical quality

For comparison between optical (ideal observer and correlation metrics) and perceived visual quality with the SLM-simulated phase maps and lathe-manufactured surfaces, the six patterns were organized according to the average scored, from the least preferred to the most preferred pattern on average by the "ideal observer" with the lathe-manufactured surfaces and at far distance. The ranking was as follows: 2ANG was the most preferred followed by 2RAD, 3RAD, 4RAD, 4ANG and 3ANG (as illustrated by the images on top of the graphs in figure 6.6).

Figure 6.6 shows the ranking of patterns for the perceived visual quality test performed experimentally with lathe-manufactured surfaces (squares) and SLM-simulated phase maps (triangles), the corresponding optical predictions (circles) based on the responses of the "ideal observer" using the ideal patterns and measured residual aberrations, and the correlation metric from the through-focus series of on-bench images (dash symbols), for the 3 testing distances (far: green, intermediate: red and near: blue). In general, there is very good agreement between both, lathe-manufactured surfaces and SLM-simulated phase maps, responses for all distances (RMS ranking difference at Far: 0.21; Intermediate: 0.14; and Near: 0.18). The optical simulations predicted well the results of both lathe-manufactured surfaces (RMS ranking difference at Far: 0.24; Intermediate: 0.42; and Near: 0.58) and SLM simulated phase maps (RMS ranking difference at Far: 0.2; Intermediate: 0.38; and Near: 0.58). There are not statistically significant differences in the ranking between the phase plate and SLM-simulated phase maps. The only significant differences between the experimental results and those purely predicted on optical grounds occurred for the 2ANG at intermediate ($p = 0.241$) and near and 4RAD at near ($p=0.381$).

Image correlation metric for both, lathe-manufactured surfaces and SLM-simulated phase maps also follow similar trends than optical predictions (RMS difference in ranking for lathe-manufactured surfaces at Far, 0.64; Intermediate, 0.44; and Near, 0.57; RMS ranking difference for SLM-simulated phase maps at Far, 0.48; Intermediate, 0.44; and Near, 0.44).

Average standard deviation in the scores (averaged across patterns and subjects) was higher for the psychophysical measurements (0.622 for surface-modulated and 0.603 for SLM) than for the computations based on the ideal observer (0.007), which used the measured residual aberrations, but was relatively small compared to the 0-5 score scale (figure 6.6).

Similar trends in pattern ranking were found for the psychophysical experiments in subjects, simulations based on the ideal observer and on-bench optical data, particularly at Far and Intermediate. Psychophysical ranking for 2ANG patterns (both, for lathe-manufactured surfaces and SLM) outperform predictions from ideal observer simulations and from optical bench measurements at intermediate, and Psychophysical ranking for 2ANG and 2RAD underperform predictions at near. Difference in performance of surface-modulated plates and SLM only occurred for on-bench measurements of 4RAD and 4ANG.

Pattern ranking from on physical on-bench measurements showed high similarity between surface-modulated and SLM-simulated phase maps for the on-bench experiment (RMS difference = 0.17), and real psychophysical measurements with both

lathe-manufactured surfaces and SLM-simulated phase maps (RMS difference = 0.63 and 0.54, respectively), in a 0 to 5 range. The average RMS difference (across patterns, subjects and distances) between model (ideal observer) and psychophysical ranking results was 0.401 and 0.375 for lathe-manufactured surfaces and SLM, respectively, and between model and on-bench results was 0.548 and 0.419 for lathe-manufactured surfaces and SLM, respectively, in a range of 0-5. This indicates that, in general, the ideal observer metric (as well as the physical on-bench measurements) is a good predictor of the psychophysical performance.

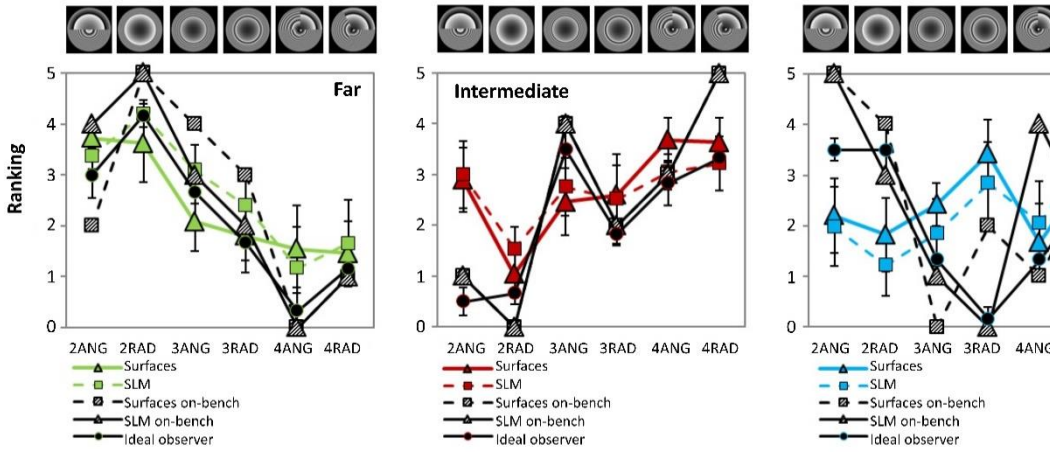

Figure 6.6. Average rankings of multifocal patterns for the 3 testing distances (far: green, intermediate: red and near: blue) from experimental results from lathe-manufactured surfaces (squares), SLM-simulated phase maps (triangles) and optical predictions (circles), and from on-bench measurements from lathe-manufactured surfaces (dashed black squares) and from phase maps (dashed black triangles). Error bars stand for standard deviation across subjects.

6.3.4. VA

Figure 6.7 shows the average decimal visual acuity (VA) across subjects for all designs with lathe-manufactured surfaces (solid bars) and SLM-simulated phase maps (dashed bars), for far (green bars) and near (blue) distance. There are not statistically significant differences between VA with SLM-simulated phase maps and lathe-manufactured surfaces at any distance (one-way ANOVA; $p>0.05$). Inter-subject variability is lower for lathe-manufactured surfaces than for SLM-simulated phase maps (Lathe-manufactured surfaces: Far, 0.014 ± 0.002; Near, 0.024 ± 0.003; SLM-simulated phase maps: Far, 0.028 ± 0.006; Near, 0.014 ± 0.003).

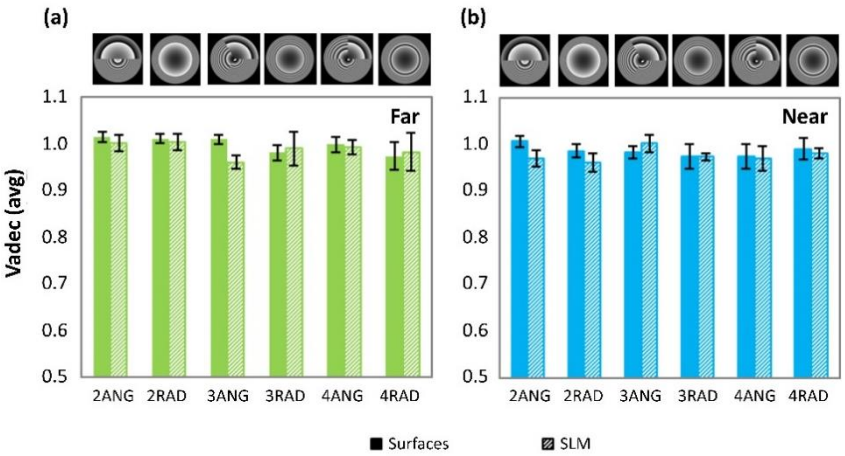

Figure 6.7. Average decimal visual acuity (VA) for all 5 subjects and all designs with lathe-manufactured surfaces (solid bars) and SLM-phase maps (dashed bars) and for far (green bars) and near (blue) distance. Error bars stand for standard deviation across subjects.

6.4. Discussion

AO visual simulators are increasingly used to simulate visual performance with multifocal lens designs [76], [212]–[215], [217], [218]. In particular, LCoS-SLMs allow representing diffractive and segmented refractive designs, although the correspondence of this simulation with that obtained from physically manufactured lenses tested on the same eyes, had not been, to our knowledge, demonstrated. In this study, we compared vision through real lathe-manufactured surfaces and SLM-simulated phase maps, in a custom-developed AO visual simulator, in terms of relative perceived visual quality (lens design ranking) and of visual acuity. The same angularly and radially segmented profiles presented in a previous study were selected [76].

Previous studies found consistent differences in perceived visual quality with segmented patterns, which depended both on the radial or angular distribution of the far-intermediate and near zones and the number of zones respectively [76], [135]. The findings are consistent with those of the current study (angular, and fewer number of zones generally preferred), both with SLM-simulated and surface-modulated phase maps, indicating that these differences in perceived visual quality across patterns are in fact associated to the design and not an artifact of the SLM simulation. As in previous works [217], we also found that a perceived visual quality test is more sensitive in detecting perceptual differences across designs that a high contrast visual acuity task.

On average there was a good agreement between the perceived visual quality obtained with lathe-manufactured surfaces and SLM-simulated phase maps at all distances (RMS ranking difference at Far: 0.21; Intermediate: 0.14; and Near: 0.18) (figure 6.6), and are only slightly larger for the radial than for the angular designs (averaged perceptual scoring: 0.54 vs. 0.36, respectively) (figure 6.5). For intermediate vision, surface-modulated angular designs (3- and 4-ANG) provided better perceived visual quality than radial designs (averaged perceptual scoring: 3.63 and 3.68 vs. 3.22 and 2.76 respectively).

The relatively higher perceived visual quality with angular compared to radial designs found for surface-modulated plates (Figure 6.5, Far), might be associated to manufacturing artifacts, arising from the diamond turning process during the phase plate lathing: the angular lenses needed to be cut at a much slower RPM so that that tool translation speed would be able to make the jump from each zone to the next as the lens is rotated. Slowing down the RPM increases the introduction of tool marks onto the lens [226]. These submicron surface grooves can introduce diffraction and scattering effects in the visual testing and therefore affect the perceived visual quality through the lenses. In our case, on average discrepancies in zones distribution between experimental and nominal values for the different areas are below 2% in all cases. However, discrepancies are slightly higher for 3- and 4- segmented angular than for radial designs (0.73% and 0.54% vs. 0.69% and 0.43%, respectively).

The optical simulations based on an ideal observer ranking the patterns according to a Visual Strehl metric predicts well the results of both lathe-manufactured surfaces (RMS difference in ranking at Far: 0.24; Intermediate: 0.42; and Near: 0.58) and SLM-simulated phase maps (RMS ranking difference at Far: 0.2; Intermediate: 0.38; and Near: 0.58) (Figure 6.6). The optical predictions matched well the experimental pattern ranking and scoring in most cases but underestimated perceived quality with 2ANG at intermediate and 4RAD at near, and overestimated 2ANG and 2RAD at far. We can speculate on the reasons for the discrepancy relating to the simplicity of the VS as an optical quality metric (which ignores orientational aspects) or neural factors (including neural adaptation effects which present orientation bias [117]). On-bench optical evaluation of surface-modulated plates and SLM simulated phase maps, expressed as rankings, is in close agreement with predictions from the ideal observer at far, intermediate and near, except for 4RAD surfaces and 4ANG SLM simulated phase maps at near. The reasons why the optical predictions are closer to the perceptual results for far than for intermediate and near are not known, but suggest that a true evaluation of the through-focus performance with different designs should not entirely rely on optical simulations.

6.5. Conclusions

The high similarity in perceived visual quality assessed in patients with real lathe manufactured surfaces and phase maps simulated with a Spatial Light Modulator demonstrates that visual simulators are excellent tools to test vision programing the designs on the SLM allowing rapid assessment of different designs before manufacturing. The current study addressed segmented designs, and used monochromatic stimuli. Future studies should address diffractive designs (also possibly mapped in the SLM), and real polychromatic stimuli, where limitations associated to chromatic and diffractive artifacts may result in discrepancies between real and SLM-simulated lenses, which should be quantified.

The following chapter presents a comparative study between the SLM and a second simulator, SimVis, with the real IOL immersed in a cuvette.

Chapter 7. Comparison of visual simulators with real IOL on simulated presbyopic subjects

In this chapter, we test visual performance of two commercial with two visual simulators, Spatial Light Modulator and SimVis Technology, with the 0D real IOL. The visual performance was evaluated on-bench and *in vivo*, with a though focus visual acuity test.

This chapter is based on the paper by Vinas published in Scientific Reports in 2019 and tittled "*Visual simulators replicate vision with multifocal lenses*". Other co-authors are Benedi-Garcia, Aissati, Pascual, Akondi, Dorronsoro and Marcos.

Results were presented in ARVO conference in 2017 by Marcos with the title "Visual simulations of real multifocal lenses in a multi-channel Adaptive Optics system" as an oral contribution. Results were also presented as an oral contribution on ECRS conference in 2017 by Dorronsoro under the tittle "*Pre-surgical visual simulations of real multifocal lenses with different optical methods*". Preliminary results were presented as an oral contribution by Vinas in Reunión Nacional de Óptica in 2015 with the title "Testing vision with angular and radial multi-zone multifocal designs using Adaptive Optics" and also presented as an oral contribution on Wavefront & Presbyopic Refractive Corrections conference in 2017 by Marcos with the title "*Wearable See-thru Binocular Simulator of Multifocal and Monovision Presbyopic Corrections*".

The author of this thesis carried out the cuvette used in the measurements, participated in the tune-up of the system and collaborated in the on-bench images collection as well as their analysis and the revision of the manuscript.

7.1. Introduction

AO, a technology originally developed to image stellar objects with ground-based telescopes eliminating the degrading effects of the atmospheric turbulence [227], has more recently expanded applications into microscopy [228] and ophthalmology [20], [71]. Fundus cameras and scanning laser ophthalmoscopes provided with AO have allowed imaging of individual photoreceptor cells and microscopic structures in the retina. Conversely, AO has allowed probing the visual system under manipulated optics [38], [59], [76], [217], either with fully corrected optical aberrations [50], through the optical aberrations of another subject or scaled versions of their own [4], or a phase pattern simulating a given correction (i.e. an intraocular lens, contact lens or a corneal treatment) [76], [166].

AO visual simulators are particularly attractive to test vision in patients with new optical designs [217], [218] prior to delivering surgical corrections to the patient or even manufacturing the lenses. Simulations of new corrections with AO primarily serve to investigate interactions between the patient's optics and a given correction, to investigate differences across corrections, and eventually to select the correction that optimizes perceived visual quality and performance in patients [76], [166], [223].

Providing patients the visual experience before implanting an intraocular lens or fitting a contact lens is particularly relevant for multifocal corrections for presbyopia (the age-related loss of the ability to dynamically focus near and far objects) [229]. Multifocal corrections work under the principle of simultaneous vision, projecting simultaneously focused and defocused images on the retina. These corrections generally provide multifocality at the expense of reducing optical quality at all distances. There are several multifocal designs, working on refractive or diffractive principles, including refractive bifocal concentric or angular designs, diffractive bifocal and trifocal designs, and extended depth of focus designs with smooth refractive profiles or hybrid refractive-diffractive designs [130]. Visual simulators allow undertaking systematic studies of visual performance testing multiple lens designs (programmable in the AO active element), which can be directly compared by the patient. As clinical instruments, AO visual simulators can help demonstrating the patient the experience of multifocality and can guide the patient and eye care practitioner in the selection of the most suitable correction.

In AO-based visual simulators, an active optical element (deformable mirror, spatial light modulator, or optotunable lens) reproduces the equivalent phase map of a certain optical design in a plane conjugate to the subject's pupil plane, while the observer is looking at a visual stimulus. Deformable Mirrors (DM) allow simulating smooth optical designs, or to induce certain amounts of aberrations, while controlling the aberrations of the subject. DMs have been used, for example, to evaluate the effects of inducing spherical aberration [214], [215], or combinations of astigmatism and coma on through-focus (TF) visual performance [52]. In contrast, spatial light modulators (SLMs) [76], [208], [209], [230], generally liquid crystal-based on silicon (LCoS)-SLMs devices, are capable of reproducing abrupt phase maps due to their high spatial resolution, and to increase the effective phase range through the use of wrapped phase representations [144], [210]. In prior work, we have studied perceived visual quality at far, intermediate and near distances with SLMs simulating bifocal, trifocal and tetrafocal, angular and radially segmented corrections [76],

[166], [212]. Other studies have also used SLMs to simulate the effect of corneal inlays [213] and to map diffractive optics [50], [216]. Reflective-DM or SLM-based visual simulators are mostly limited to experimental environments, given their relatively high complexity and dimensions, although some have made their way into commercial products [159], [231]. In these devices the visual experience is limited to stimuli projected in a display, subtending a relatively small (typically <2 degree) visual field, in many cases monocularly [71].

Ideal visual simulators in a clinical environment should be see-through, allowing a direct view of the real world and should display a larger visual field. Visual simulators of bifocal corrections, with two optical channels superimposing two images using a transmission SLM to simulate different pupillary masks, have been used on clinical subjects [218], but still remain in a laboratory setting. Deformable multi-actuator lenses have been recently released, which may be suitable to reproduce smooth surface-varying multifocal optics, although, to our knowledge, they have not been yet used in visual simulators [232], and won't be capable of mapping diffractive or segmented optics. An interesting novel approach to simultaneous vision simulation is the use of optotunable lenses working in temporal multiplexing mode, a technology developed by our group (SimVis technology), described in detail in previous publications [223], [233]. The tunable lens scans multiple foci to provide superimposed images on the retina, all of them with the same position and magnification, but corresponding to different planes in focus. These custom electronically driven lenses can produce fast periodic foci variations at speeds greater than the flicker fusion threshold of the human visual system, delivering seemingly static images on the subject's retina that emulate the effect of the multifocal correction. The simulation of multifocal corrections relies on evaluating the TF energy distribution of the correction, from the knowledge of the spatially varying pupillary power distribution, and programming in the optotunable lens the corresponding time-varying focus changes. The simulated multifocal correction is tuned to match the TF optical quality (in terms of Visual Strehl) [81] of real existing multifocal lenses. It is an optimization of the electrical input signal driving the tunable lens and, consequently, of the SimVis technology TF optical quality [233]. Real multifocal intraocular lens (M-IOL) designs are therefore temporally mapped by evaluating the corresponding temporal profile of the optical power of a tunable lens that results in a TF optical quality matching the TF optical quality of the M-IOL. While symmetric MIOL designs can be fully captured using a temporal pattern, some limitations are expected for asymmetric complex designs.

The goal of this study is to compare on real subjects, for the first time to our knowledge, TF optical and visual quality produced by real M-IOLs and visual simulations of those multifocal designs using two different active optical elements, a spatial light modulator (SLM) and temporal multiplexing with optotunable lenses (SimVis technology), all of them incorporated in a polychromatic AO Visual Simulator.

7.2. Methods

7.2.1. Devices for simulation

Real IOLs. Two 0-D M-IOLs with the Bi-R and Tri-D designs (provided by the manufacturers) were inserted in a cuvette filled with distilled water, placed in a conjugate pupil plane,

and projected on the eye's pupil of the subjects. Calculated TF curves (figure 7.1, right plots) show distinct bifocal and trifocal performance.

Spatial light modulator (SLM). The multifocal phase maps (Bi-R and Tri-D) were extracted in pseudophakic computer eye models from the knowledge of the surface height profiles of the lenses, provided by the respective manufacturers, as described in a previous publication [234]. Matlab routines were used to numerically simulate the multifocal phase designs, the Bi-R and Tri-D, which were later programmed in a reflective phase-only LCoS-SLM. The SLM addressable phase maps (Φ) were evaluated from the multifocal phase maps by performing 2π-wrapping such that, $\Phi = X \ [\mathrm{mod}\ 2\pi]$, where X represents the unwrapped phase map. and Φ is the wrapped phase map. The generated phase pattern is a grey-scale image, where each level of grey corresponds to a certain phase difference in the interval [0 2π] (figure 7.1, central plots). The images were generated for a 5-mm pupil.

SimVis technology & Temporal multiplexing. Both multifocal designs were mapped using SimVis technology with a temporal profile, as shown in figure 7.1. The TF optical quality of the two multifocal designs in terms of Visual Strehl (VS) [81] was estimated for a 5 mm pupil diameter at 555 nm. The corresponding SimVis temporal profile that provides an equivalent TF VS was determined [233]. The temporal profiles were addressed with SimVis technology as shown in figure 7.1, right plots.

7.2.2. Design of the lenses

Two M-IOLs (bifocal non-rotationally symmetric refractive, Bi-R, and trifocal diffractive, Tri-D) were projected on the eye's pupil, and also mapped in the SLM (as a spatial phase map) and on SimVis technology (as a temporal profile), shown in figure 7.1.

The bifocal non-rotationally symmetric refractive (Bi-R) IOL design mimics the Lentis MPlus LS-313 MF30 (Oculentis, Berlin, Germany), a multifocal acrylic refractive IOL, made out of hydrosmart, a copolymer consisting of acrylates with hydrophobic surface, UV absorbing (n = 1.46). The optical design consists of an aspherical surface with a posterior sector shaped near vision segment, which provides 2 useful focal distances: 0.0 D for far-vision, and +3.00 D addition for near-vision.

The trifocal diffractive (Tri-D) design corresponds to the POD F (FINeVision, PhysIOL, Liege, Belgium), a hydrophilic (26% hydrophilic acrylic) aspheric multifocal diffractive IOL built with a combination of two bifocal diffractive patterns, of which one is for far and near-vision and the other for far and intermediate-vision [235], [236]. The combination of the two diffractive structures provides 3 useful focal distances: 0.0 D for far-vision, +1.75 D addition for intermediate-vision and +3.50 D addition for near-vision [235].

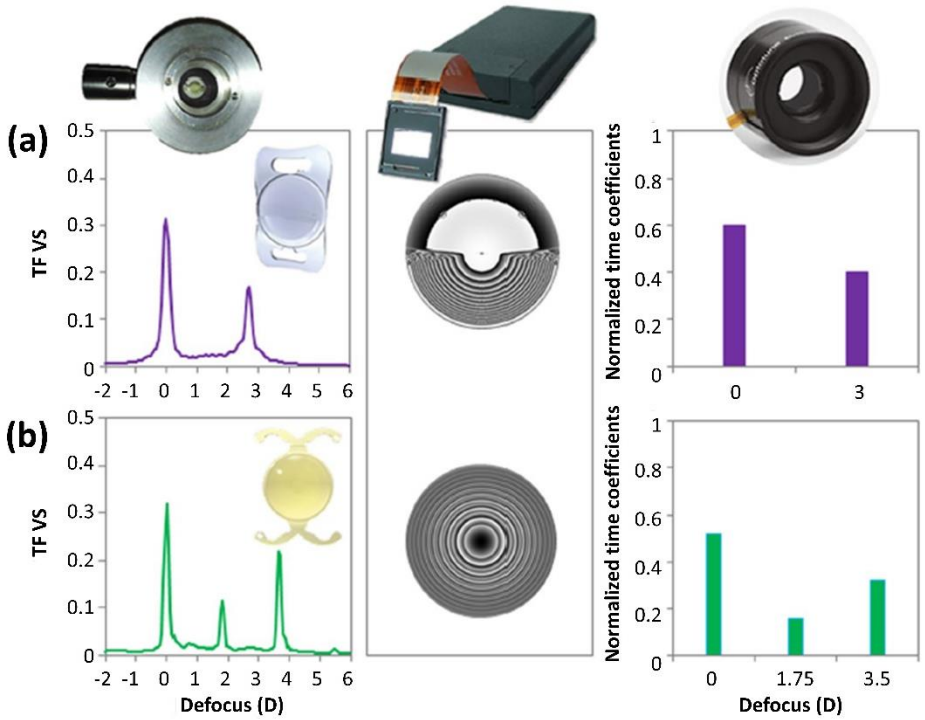

Figure 7.1. Multifocal designs evaluated in the study in terms of Visual Strehl (VS): (a) Bifocal non-rotationally symmetric refractive, Bi-R (MPlus, Oculentis); and (b) Trifocal diffractive, Tri-D (POD F FINeVision, PhysIOL), in the form of real IOLs (left), phase maps on a SLM (center) and temporal profile on an optotunable lens working on temporal multiplexing mode (right).

7.2.3. Experiment: TF VA

VA was measured using an 8-Alternative Forced Choice (8AFC) procedure with Tumbling E letters and a QUEST (Quick Estimation by Sequential Testing) algorithm programmed with the Psychtoolbox package to calculate the sequence of the presented stimulus (letter size and orientation) in the test following the subject's response. Measurements were performed at different positions of the Badal Optometer ranging from −1.00 to +4.00 D, for the two lenses and the SLM and SimVis technology simulations. After looking for their best subjective focus without a multifocal correction and prior to measurements, subjects were shown the whole TF range with the corresponding design, so that they could identify the approximate position of their best focus for the different visual distances (far, intermediate and near). After that, measurements were performed at different positions of the TF range with higher sampling around the identified foci, which varied for each subject. The QUEST routine for each VA measurement consisted of 40 trials, each one presented for 0.5 seconds, where the threshold criterion was set to 75%. The threshold, VA measurement, was estimated as the average of the 10 last stimulus values. Visual acuity was expressed in terms of decimal acuity (logMAR = $-\log_{10}$[decimal acuity]).

Variability of each VA measurement was obtained from the standard deviation of the 10-last stimulus values used to estimate the threshold in each measurement.

7.2.4. Patients

Seven subjects were monocularly tested in the system under cycloplegia. Subjects were non-presbyopic (35 ± 3 years old) and nearly emmetropic (spherical error: −0.85 ± 0.90 D, astigmatism <0.50 D in all cases). The RMS for 3rd and HOAs (5-mm pupil diameter) in the subjects ranged from 0.19 to 0.59 um.

All protocols met the tenets of the Declaration of Helsinki and had been previously approved by the Spanish National Research Council (CSIC) Bioethical Committee. All participants were acquainted with the nature and possible consequences of the study and provided written informed consent.

7.3. Results

TF optical quality (double-pass aerial retinal point images and E-letter stimulus images, on-bench) and visual acuity (VA), in 7 patients, were measured with two M-IOLs: a bifocal refractive segmented IOL, Bi-R, and a trifocal diffractive IOL, Tri-D. Those corrections, of complex design, were tested in a polychromatic AO visual simulator for 3 different conditions: the real lens, simulations in a SLM, and simulations using SimVis technology. All measurements were performed monocularly, in green light (555 nm) and for 5-mm pupils.

7.3.1. On-bench tests.

Figure 7.2.a-b shows TF double-pass (DP) aerial images and E-letter images (1P) obtained on-bench with the three simulating conditions, real IOL, SimVis technology and SLM, for (a) bifocal refractive segmented lens, Bi-R, and (b) the trifocal diffractive lens, Tri-D. Qualitatively, the replication of the images with the simulators is highest around the foci for both simulators. Also, the asymmetric bifocal design (Bi-R) produces an asymmetry in the PSF (reminiscent of vertical coma [234], which is apparent with real IOL and SLM, but cannot be reproduced with SimVis.

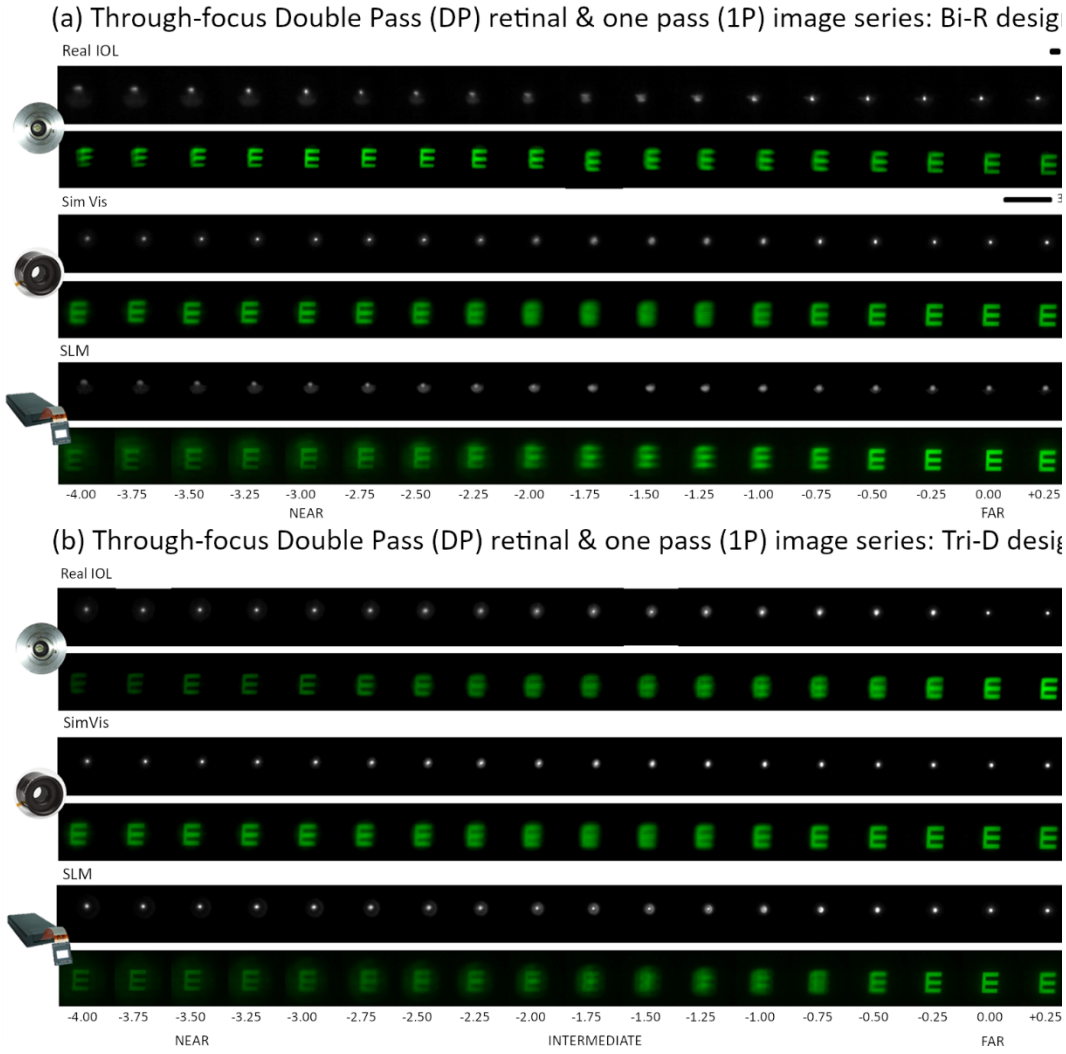

Figure 7.2. TF Optical quality on-bench testing. On-bench TF Double-pass (DP) aerial retinal point images and TF retinal images of an E-optotype (1P) through the bifocal refractive (a) and the trifocal diffractive (b) designs for all simulated conditions. Scale bars account for the angular extent of the images (6' for the DP and 32' for the 1P images).

Figure 7.3 shows TF optical quality metrics obtained from the on-bench images series: (a) full width at half-maximum (FWHM) for the double-pass images and (b) image correlation metric for the TF E-letter images, with the different multifocal designs (Blue lines: real IOL; red lines: SimVis; yellow lines: SLM)). In addition, the TF curve obtained from on-bench image series for a monofocal condition (no multifocal design) are shown (grey lines) for the TF DP and the 1P image series. TF DP images were normalized to the 0 D monofocal image series, so that FWHM = 1 at 0.0 D for the monofocal curve, while 1P image series were correlated to the image of 0.0 D of the monofocal TF range, where image correlation was 1 for the monofocal image at 0.0 D. There is a good correspondence between both the double-pass images and 1P image series across all simulating conditions in the position of best near and far focus (Bifocal: 0.0 D for far vision, +3.00 D addition for near vision; Trifocal: 0.0 D for far vision, +1.75 D addition for intermediate vision and +3.50 D addition for near vision).

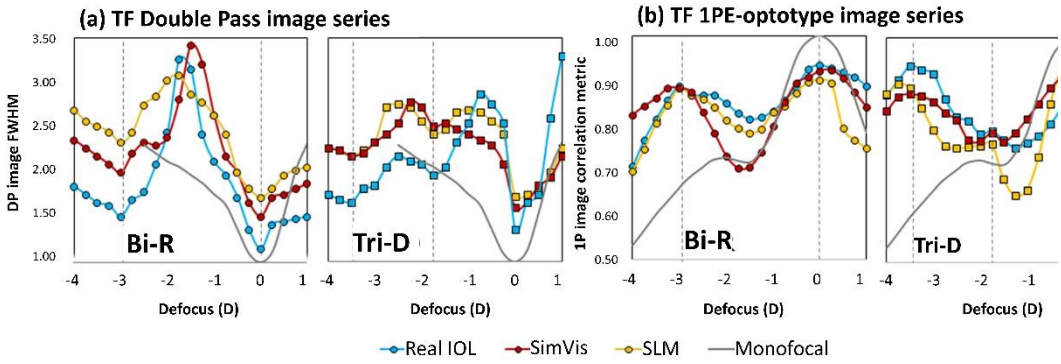

Figure 7.3. TF optical quality metrics. (a) TF double-pass optical quality (FWHM) for the bifocal refractive IOL (Bi-R) and the Trifocal diffractive IOL (Tri-D), gray line, for a monofocal lens (no IOL) as a reference; (b) TF image correlation metric, gray line, for a monofocal lens (no IOL) as a reference. Blue symbols represent the real IOL; Red symbols represent the SimVis technology simulation and yellow symbols represent the SLM Simulations.

RMS TF difference in the TF curves (5-D range) between the real multifocal IOL and the simulation was taken as a metric for the quality of the simulation. Figure 7.4 compares the RMS TF difference for SimVis technology (red bars) and SLM (yellow bars) for the two analyzed optical quality metrics: TF DP aerial retinal image curves (a) –data from figure 7.3.a, and for TF 1P E-optotype image (b) correlation curves –data from figure 7.3.b. In both cases, the RMS TF difference is below 0.07, and as low as 0.01-0.02 in some conditions. When comparing both simulating techniques, the RMS TF difference between SLM and SimVis technology TF curves is statistically significant only for Tri-D design with both TF optical quality metrics (paired-samples t-test: TF 1P, $t=2.70$, $p=0.014$; TF DP, $t=-2.90$, $p=0.008$). When comparing both designs, the RMS TF difference between Bi-R and Tri-D TF curves is significantly different for SLM (TF 1P; paired-samples t-test: $t=-4.10$, $p=0.01$) and for SimVis technology (TF DP; paired-samples t-test: $t=-2.40$, $p=0.025$), while there is no significant differences between them for SimVis technology (TF 1P) and SLM (TF DP).

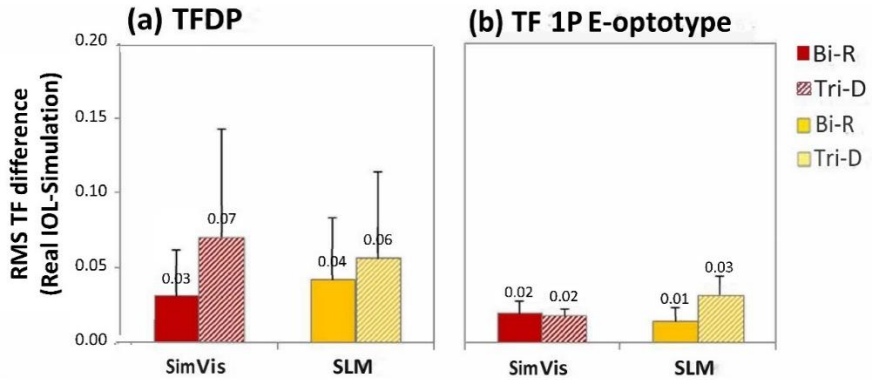

Figure 7.4. Comparison of TF optical quality metrics. RMS TF difference of the TF curves (5.0-D range) with respect to the real multifocal IOL, for SimVis technology (red bars) and SLM (yellow bars) (a) for TF Double-Pass curves, and (b) for TF 1P E-optotype image correlation curves. Solid bars are for the bifocal refractive IOL (Bi-R); Shaded bars are for the Trifocal diffractive IOL (Tri-D). Data are for 5-mm pupils.

7.3.2. Through focus visual acuity.

Figure 7.5 shows the TF decimal VA for the 7 subjects participating in the study and the 4 conditions measured (no lens, real IOL, SimVis technology, and SLM) for the two simulated designs: (a) Bi-R and (b) Tri-D in a 5.00 D range. The last plot in each panel represents the averaged data across subjects (bottom, right. VA measurements are highly repeatable (averaged standard deviation: 0.03 ± 0.005). TF VA curves showed individual similarity across simulations (either using SimVis technology or SLM) and real IOLs in all 7 subjects. VA obtained through the real IOLs correlated statistically with those obtained through SimVis technology ($r = 0.71$ and $r = 0.46$; $p < 0.05$ across subjects, for Bi-R and Tri-D, respectively) and SLM ($r = 0.46$ and $r = 0.56$; $p < 0.05$ across subjects for Bi-R and Tri-D, respectively). Averaged data showed a good agreement between the TF curves. A mixed model analysis for repeated measurements was performed to investigate differences in outcomes for the two simulation techniques in comparison with Real IOLs TF performance, for both designs (Bi-R & Tri-D). The analysis showed no significant differences for any of the simulators when using as factors the TF performance and the simulator for both designs (Bi-R $p = 0.911$ & Tri-D $p = 0.504$), indicating that while there may be differences between the curves point by point, the general shape of the TF curves is preserved.

Figure 7.6 shows the RMS TF difference between the TF curves for the real IOL and both SimVis technology and SLM. The average RMS TF difference of the simulated Bi-R design with respect to the real Bi-R IOL was 0.11 ± 0.02 for the SimVis technology & 0.11 ± 0.02 for the SLM. The average RMS TF difference for Tri-D was 0.13 ± 0.016 for the SimVis technology & 0.13 ± 0.02 for the SLM, respectively. The differences across simulators are not statistically different (paired-samples t-test: Bi-R, $t = -0.81$, $p = 0.46$; Tri-D, $t = -0.45$, $p = 0.67$). The differences between both designs (Bi-R and Tri-D) for real IOLs and the different simulations are statistically different for the SimVis technology (paired-samples t-test: $t = -2.29$, $p = 0.04$), but not for the SLM.

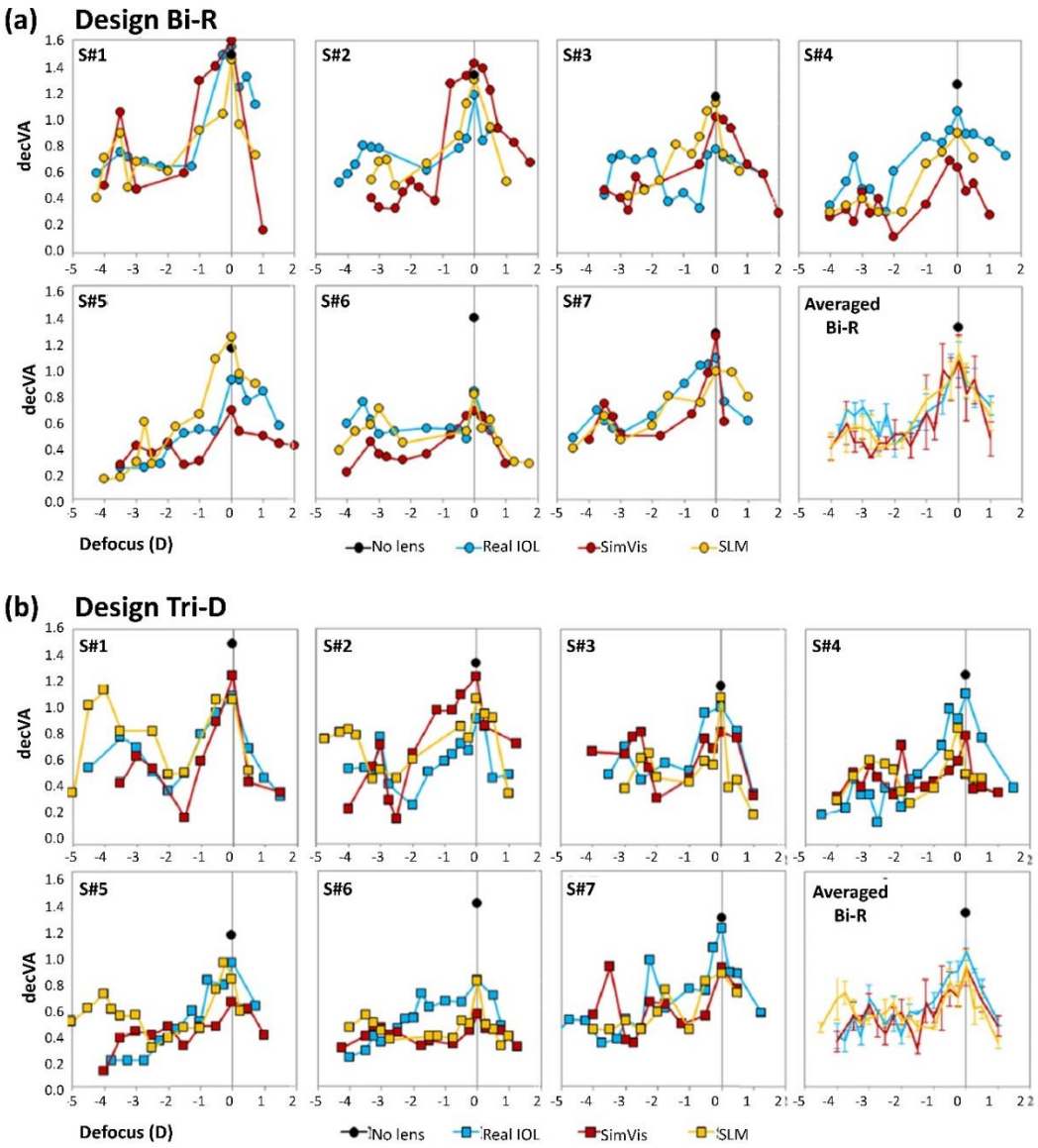

Figure 7.5. TF decimal VA on patients. TF decimal VA for all 7 subjects and all conditions (no lens, black dot; real IOL, blue line; SimVis technology, red line; SLM, yellow line) for the two simulated designs: (a) Bi-R (circles) and (b) Tri-D (squares). Averaged data across subjects is shown for both designs. Error bars stands for inter-subject deviation.

On average, RMS TF difference in subjects was higher for Tri-D than for Bi-R, in line with results from the on-bench measurements previously described. On the other hand, different multifocal designs produce different TF performances on the same subject (average RMS TF difference of 0.11 ± 0.01, 0.14 ± 0.04, and 0.12 ± 0.02 for real IOLs, SimVis technology and SLM, respectively between the two IOL designs).

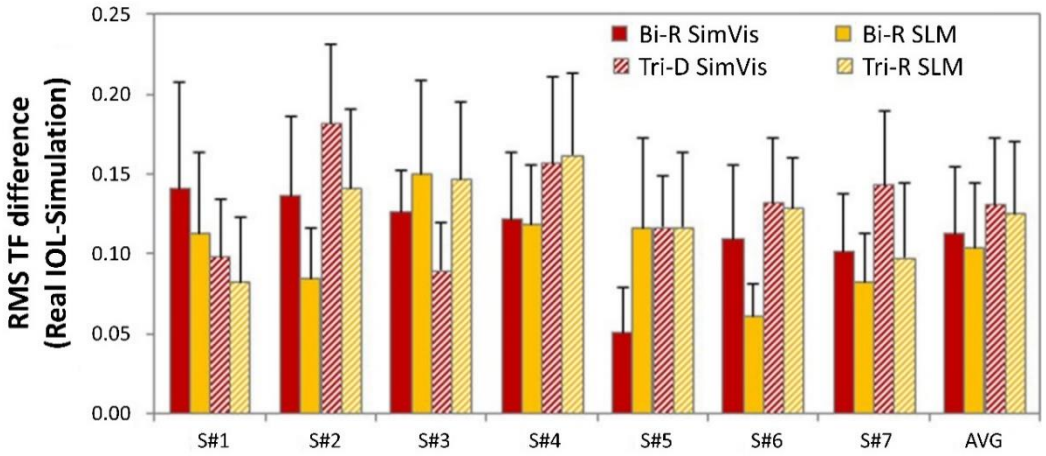

Figure 7.6. Comparison of TF VA across designs. RMS difference of TF VA curves (5.0-D range) for all subjects with respect to the real multifocal IOL, for SimVis technology (red bars) and SLM (yellow bars). Solid bars are for the bifocal refractive IOL (Bi-R); Shaded bars are for the Trifocal diffractive IOL (Tri-D). Error bars stand for inter-subject variability. Data are for 5-mm pupils.

7.4. Discussion

AO visual simulators based on different active optical elements are increasingly used to simulate vision through different multifocal lens designs. However, the correspondence of this simulation with the vision obtained through the physically manufactured real IOLs tested on the same eyes had not been, to our knowledge, demonstrated. In this study, we compared for the first time TF optical and visual quality produced by real M-IOLs with visual simulations using a spatial light modulator (SLM) or an optotunable lens working in temporal multiplexing mode (SimVis technology), in monochromatic light. We found a general good correspondence between the through-focus performance with the real and simulated M-IOLs, both optically (on-bench) and visually (measured VA in patients).

We did not find a bias for higher reproducibility of the TF performance towards a particular type of simulator, although the very different principles of operation may favor one or the other depending on the design of the lens or the stimuli. For example, the temporal patterns for SimVis technology are programmed using the TF Visual Strehl performance of the theoretical lens as a target, and the results on patients demonstrate that it captures adequately the TF visual performance (and the optical image quality using a FWHM metric). However, as SimVis technology is limited to represent symmetric patterns, the blur produced on the images is invariably symmetric, which may be the reason for the discrepancies in the appearance of the E-optotype images (particularly those between foci) in the SimVis technology simulation (showing symmetric, more degrading, blur) compared to the real IOL or the SLM (where the asymmetric blur appears to be less noticeable) Figure 7.2.a [233]. Also, measurements were performed monochromatically. While SimVis technology is not affected by chromatic aberration and the temporal patterns could be programmed to modify the effects of chromatic aberration on the TF visual Strehl curve that serves as a template for SimVis technology, SLMs are largely affected by chromatic artifacts [237], as the phase map is in fact only representative of one single wavelength. This is of great importance in novel diffractive

M-IOL designs, where chromatic aberration is used to generate the multifocal component of the lens [42], thus the SLM pattern and SimVis technology signal would need to be modified accordingly. Since capturing the specific chromatic effects of the diffractive lenses pose a challenge in SLM-based simulators, it is likely that measurements with polychromatic stimuli (instead of the green stimuli as used in this study) would result in lower performance for the SLM.

Our results also support the use of visual simulators in the clinic. TF performance with the same IOL largely varies across individuals, indicating that the visual experience of a multifocal correction is rather unique to the patient and therefore valuable to be demonstrated to a patient prior to implantation. We found lower differences in TF performance across patients with the same IOL (0.10 ± 0.02 RMS TF difference) than in different IOLs on the same patient (0.13 ± 0.02 RMS TF difference). Visual simulators can help identifying those patients whose visual quality will be largely affected by a multifocal correction. For example, patient S#6 experiences a large drop in VA with both multifocal corrections (44.6% for the Bi-R and 48.5% for the Tri-F compared to the monofocal performance at far), and while depth-of-focus is enlarged, VA remains low for a large range. On the other hand, most patients experience minimal changes in VA for far (average multifocal VA/monofocal VA at far, 1.05 for the Bi-R and 0.95 for the Tri-F) and exhibit functional VA at a near (average VA for near, 0.60 for the Bi-R and 0.53 for the Tri-F), and even an intermediate peak/range for the Tri-F.

The significant differences in TF performance of the same IOL across subjects are likely associated to the different interactions between the subjects native aberrations and the IOL optics [76], [217], and to a lesser extent, to neural factors and adaptation of the subject to native aberrations. While in the current study, measurements were done under natural aberrations (and these were not included as a variable in the study) it is interesting to note that the AO instrument in this study allows measurement and correction of these aberrations. An interesting open question is whether the TF performance would have been more similar across subjects had the native aberrations of the eye been corrected. On the other hand, despite the contribution of the subject's aberrations to the effective TF, there are clear observable features in the TF curves attributable to the lens design. For example, TF VA with the trifocal IOL in patient S#7 reveals clearly three best foci (both with the real and simulated IOL). The ability of visual simulators to capture the performance of the specific IOL designs supports their clinical utility not only to demonstrate multifocality to a prospective patient, but also to demonstrate differences across different commercial lenses.

The ultimate utility of the visual simulators relies on their application on patients prior to intraocular lens implantation. The tested intraocular lenses are designed to replace the natural crystalline lens. Visual simulators are designed generally to be used on phakic eyes, while a post-operative validation of the real IOL will not include the contribution of the crystalline lens (except for phakic IOLs). As the cornea is the major contributor to the ocular aberrations, we expect the crystalline lens contribution to pre-operative measurements to be secondary, particularly in the presence of a multifocal correction. Furthermore, a cataractous crystalline lens will produce an overall decrease of visual performance. While a direct pre- and post-operative comparison of TF visual quality with simulators and real IOL is only possible for clear crystalline lens, we expect (particularly with zonal segmented corrections) SimVis technology to be generally less affected by

opacities, as due to the temporal multiplexing the simultaneous image will be projected on the retina bypassing opacities [233].

7.4. Conclusions

The current study demonstrates that visual simulations in an AO system capture to a large extent the optical and visual performance obtained with real IOLs, both in absolute values and the shape of TF curves when compared, for the first time, on the same individual patients. Visual simulators based on different technologies (real IOLs, SLMs, SimVis technology) are useful programmable tools to predict visual performance with M-IOLs.

However, the cuvette used in this experiment to compare with other visual simulators was designed to operate with IOLs of 0 D. In the following chapter we describe the implementation and validation of a cuvette for testing real IOLs of more standard optical powers.

Chapter 8. Implementation and validation of a cuvette for testing real non-0D IOL on a polychromatic AO system

This chapter describes the design, implementation and validation of a new channel in the VioBio lab AOII to test non-0D real IOLs. Three commercial IOLs were tested on-bench and *in vivo* in the new channel, performing a though focus visual acuity test.

The study described in this chapter was presented at ARVO conference in 2020 by Benedi-Garcia as an oral contribution under the title "Optical and visual quality of real intraocular lenses physically projected on the patient's eye". Co-authors were Vinas, Lago, Dorronsoro and Marcos. The work was awarded with an ARVO International Travel Grant.

The author of this thesis developed, with the help of co-authors, the design and implementation of the new channel for the non-0D cuvette. She also performed the measurements and analyzed the data.

8.1. Introduction

A cataract is typically treated by replacement of the natural lens of the eye with an artificial IOL. The number of multifocal and extended-depth-of-focus (EDOF) IOLs designs has grown enormously in the last years. Yet, patients face the question of how the vision will look like with this type of corrections. Visual simulators allow the patients to experience multifocal vision before surgery, trying out different designs before implantation. In previous chapters it is presented the option of use adaptive optics as a tool for visual simulation [77], with technologies such as deformable mirrors [214], [215], [238], SLMs [166], [213], [216] or by temporal multiplexing of optotunable lens [147], [233]. The capability of visual simulators to reproduce optical performance of the subject after surgery has been already probed [167] and in the previous chapter, we have demonstrated the comparable performance of visual simulators with the real IOL of 0D.

An alternative to programmable simulators (such as AO-based systems or SimVis) are devices that project the IOL onto the pupil plane of the patient's eye, inserting the lens in a cuvette. While this type of simulation loses the option to dynamically try different lenses (for example to compare different options), and of course requires having the physical lenses available (unlike the programmable simulators that allow testing lenses prior to manufacturing), IOL projection systems do have the advantage of a direct test of the lens, in principle, without relying on assumptions or limitations of the simulating technology. For this reason, some studies, such as that by Vinas et al. used phase plates, or real IOLs inserted in a cuvette, as gold-standards to evaluate the accuracy of SLM and SimVis-based simulators, which each simulator type set-up in a different channel of a polychromatic AO visual simulator. In that study, IOLs of 0-D (i.e. only bearing the multifocal, and not the refractive component of the lens, were used as a reference. However, most often, standard power IOLs are available.

The literature describes optical systems specifically designed to project the IOL on the eye's pupil plane whole at the same time cancels out the power of the IOL. The system is called Rassow telescope [152] and consists of a 4F system with a magnification x1, with the IOL acting as one of the lenses in the system, and a +20 D achromatic lens acting as the second lens, compensating 20D of the optical power of the IOL. Schaeffel et al describe the implementation and use of a Rassow to evaluate real IOLs, who evaluated on-bench the contrast transfer of six monofocal and four multifocal IOLs [153]. Two commercial systems have been launched that are based on the Rassow telescope or small variations of it: VirtIOL [239] and ACMIT [162]. In both cases, a manufactured IOL is inserted in a cuvette and projected onto the patient's pupil plane. In the ACMIT instrument, the IOL is inserted into a model eye based on the Liou and Breannan's model eye [163].

In some configurations of the projection system such as in the Rassow telescope, the rays impacting the IOL are parallel, in contrast to the converging effect of the rays onto the IOL occurring in real eyes. This difference may be critical in the accuracy of the simulation, as it likely alters the imaging properties of the eye+IOL with respect to the natural (post-operative) configuration.

In this study, we implemented a new channel in an AO system that incorporated a Rassow telescope for the projection of a real IOL immersed on a cuvette to the pupil's plane of the patient. We calculated computationally and measured experimentally the spherical

aberration induced by the system. The through-focus optical and visual quality with three different types of lenses (monofocal, diffractive trifocal and refractive EDOF) was measured with the standard Rassow telescope.

8.2. Methods

8.2.1. Rassow system configuration.

The new channel for the non-0D cuvette was composed by a Rassow system, a 4F telescope explained in section 2.1.3.2. of this thesis. Figure 8.1 presents the new channel already implemented in the VioBio lab AOII system.

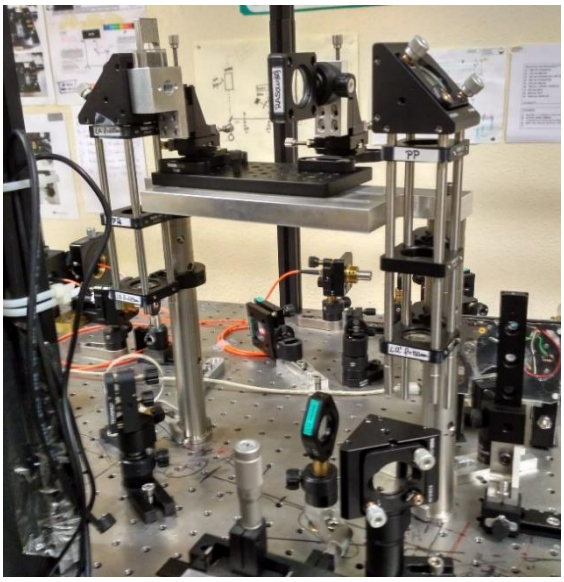

Figure 8.1. Rassow system implemented in the VioBio lab AOII system.

The functionality of the Rassow system is completed with the Badal system, an optometer which compensated the power of any IOLs different from 20 D, in a range of ± 4D. The system is composed of 2 lenses (125mm EFL) and 2 mirrors. These mirrors are mounted on a motorized stage that allows the distance between the lenses to be adjusted and the defocus added. The zero position was achieved when the distance between the lenses is equal to the sum of their focal lengths. When the distance is longer than the length of their focal lenses, Badal system induces positive defocus, while if the distance is shorter, rays induce negative defocus.

8.2.2. Optical computer simulations

Previous to its experimental implementation of the Rassow telescope, we performed optical simulations of the Rassow system and the Badal Optometer with Ray Tracing software (Zemax–EE Optical Design Program 2005, Zemax Development Corporation). A schematic diagram of the new channel was presented in section 2.1.3.2. of this thesis.

Ray tracing was performed with 5-mm pupil diameter and a wavelength of 555 nm. The calculated optical quality was expressed in terms of MTF, Spot Diagram and wavefront

map both on axis (0º) and at the maximum subtended angle in the AO system (2º). Optical quality was expressed in terms of phase maps and MTFs.

The compare the fidelity of the simulation with the Rassow telescope projection of the IOL onto the eye to reproduce the optical performance of the actual IOL, we probed the calculated optical quality, and spherical aberration (SA) for the following conditions (illustrated in figure 8.2: (a) the IOL alone, immersed in water, with parallel rays impacting the IOL; (b) a model eye with an aspheric cornea and the IOL virtually implanted behind the cornea; (c) difference of a model eye with an aspheric cornea and the IOL minus model with a paraxial lens behind the same cornea; (d) the IOL immersed in the cuvette with the Rassow telescope; (e) as case (d) but without the IOL . The potential impact of the cuvette on inducing SA was calculated from the difference of (d)-(e). The fidelity of the simulation was obtained by calculating the difference (b)-(d). Also, the IOL Phase Map was estimated as the difference of (b)-(c). This is the phase map that would be mapped in an SLM or DM to represent the lens. The corresponding SA was compared to that of (d)

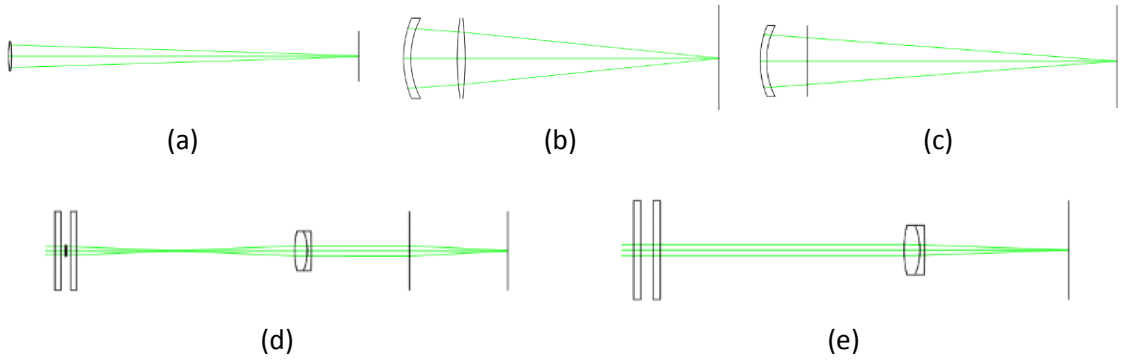

Figure 8.2. Conditions simulated using Zemax to study the influence of the SA. (a) the IOL alone, immersed in water, with parallel rays impacting the IOL; (b) a model eye with an aspheric cornea and the IOL virtually implanted behind the cornea; (c) a model eye with an aspheric cornea and a paraxial lens behind the cornea; (d) the IOL immersed in the cuvette with the Rassow telescope; (e) as case (d) but without the IOL .

8.2.3. Tested IOLs

Three commercial IOLs from PhysIOL were tested in the cuvette, projecting them on the eye's pupil of the subjects or the model eye: a monofocal IOL, an EDOF IOL and a trifocal IOL.

The monofocal IOL (20 D), is a biconvex, hydrophobic and aspheric monofocal IOL, aiming at correction a large proportion of the corneal SA (-0.11 µm SA). The extended-depth-of-focus IOL (21 D) is a refractive, hydrophobic, with smooth aspheric surfaces (described by the radius of curvature, and 4 conic constants per surface [240]). The trifocal IOL (19.5 D), is diffractive, hydrophilic and aspheric trifocal IOL [241]. The 3 foci of this lens are 0.0 D for far-vision, +1.75 D addition for intermediate-vision and +3.50 D addition for near-vision.

8.2.4. Measurement of spherical aberration

Wave aberrations were measured with the Hartmann-Shack wavefront sensor of the AO device (described above) using IR (820 nm) illumination, for on-bench and in patients. Aberrations were obtained in the following conditions: (1) Artificial eye with a IOLs placed in the cuvette (Rassow telescope, with two monofocal real IOLs immersed in the cuvette); (2) Artificial eye with a monofocal and EDOF IOL placed in the cuvette (Rassow telescope, with the cuvette filled in with water alone (no lens immersed). In this case, an aspheric lens was placed on a pupil plane in order to compensate for the IOL power.

Measured IOL Monofocal 1 is the design presented in section 8.2.3. Measured IOL Monofocal 2 is made from a high refractive index soft acrylic material that gently unfolds following implantation. The posterior aspheric surface was designed with negative spherical aberration to compensate for the positive spherical aberration of an average cornea. Measured IOL Isofocal is presented in the previous section, 8.2.3.

8.2.5. Through-focus on-bench optical quality

Through focus series of images of an E letter (1.62 deg angular subtend, 555 nm illumination) were taken on the artificial camera of an artificial eye for the three IOLs inserted in the cuvette. The artificial eye was composed by an objective lens (50.8 mm of focal length) and a CCD camera (DCC1545M, Thorlabs, Germany) placed on the retinal plane. The focus was scanned in 0.25 D steps using the Badal system.

All images for all lenses were taken for identical conditions of pupil diameter (4.5 mm), laser power and camera configuration, with the DM either correcting the aberrations of the system only.

The images were analyzed with a correlation metric. Each image of the TF series was correlated with the image obtained for 0 D with the monofocal IOL.

8.2.6. Through focus Visual Acuity measurements

Visual Acuity (VA) was measured using a tumbling E letter test an 8-Alternative Forced Choice (8AFC) procedure and a QUEST (Quick Estimation by Sequential Testing) [174] algorithm programmed with the Psychtoolbox package of Matlab [176], [177] to calculate the size and orientation of the following presented E letter according to the subject's response. E letter was presented for 0.5 seconds. VA was measured through focus, induced with the Badal system on a range of +2 to -5 D for the 3 real IOL on the cuvette. The best subjective focus without real IOL was set as zero. Each VA measurement consisted of 32 trials and 20 reversals. The visual acuity was estimated as the mean of the last 10 reversals and its variability, as the standard deviation of that 10 values.

VA measurements were performed under pupil dilation. The subject's eye pupil center was aligned with the optical axis of the system with an x-y-z stage and stabilized with a dental impression on a bite bar. Subjects found their best focus with the Badal system while looking at a Maltese Cross stimulus prior to performing the VA test. The psychophysical stimulus was presented on the DMD, illuminated at 555 nm and viewed

through the real IOL. Measurements were performed for the three IOLs inserted in the cuvette, with the DM either correcting the aberrations of the system only.

8.2.7. Subjects

Three subjects participated in the experiment. Ages ranged from 27 to 40 years old. Subjects were nearly emmetropic (Refractive error: -0.08±0.31 D, astigmatism < -0.08±0.07). All measurements were performed under paralyzed accommodation with Tropicamide (2 drops at the beginning of the session, and 1 drop every hour if required.

All protocols met the tenets of the Declaration of Helsinki and had been previously approved by the Spanish National Research Council (CSIC) Bioethical Committee. All participants were acquainted with the nature and possible consequences of the study and provided written informed consent.

8.3. Results

8.3.1. Optical simulations

The optical quality of the retinal image was estimated with Zemax simulations. Figure 8.3 shows the MTFs, the wavefront maps and the spot diagrams obtained for the system at 0º and 2º for a monofocal IOL immersed in the cuvette. There is a low spherical aberration at 0º (0.02µm). Out of axis, there is also astigmatism (0.05µm) and coma (0.02µm). Spot diagram of a grid image of 1.5mm for 0º (left) and 2º (right). AOII system would be able to project properly at the maximum field.

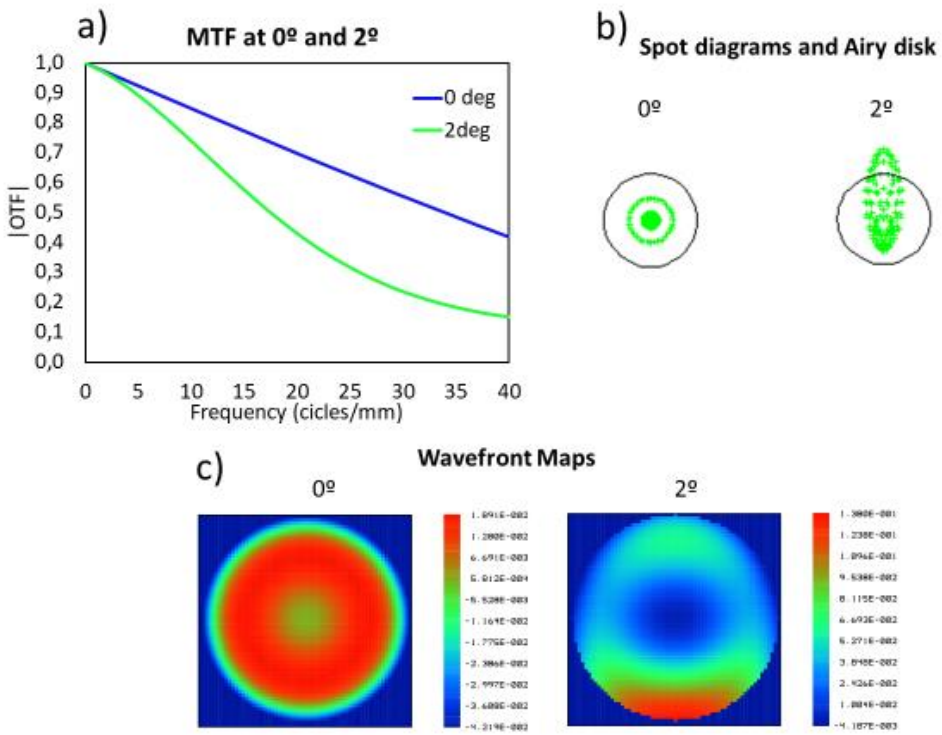

Figure 8.3. Computer simulations from Zemax Ray Tracing software of the optical quality in the image surface for 0 deg and 2 deg in terms of MTF (a), Spot diagram with the Airy disk as a reference (b) and wavefront maps (c).

Figure 8.4 shows the spherical aberration found in the 5 previously described cases: (a) the IOL alone, immersed in water, with parallel rays impacting the IOL; (b) a model eye with an aspheric cornea and the IOL virtually implanted behind the cornea; (c) difference of a model eye with an aspheric cornea and the IOL minus model with a paraxial lens behind the same cornea; (d) the IOL immersed in the cuvette with the Rassow telescope; (e) as the case (d) but without the IOL. Regarding the induction of SA by the cuvette alone, SA close to zero was found in Zemax simulations (case e). The theoretical induction of the SA alone, calculated as the difference between the IOL inside the cuvette and the IOL (case d-a) is also close to zero. The comparison of the IOL inside the cuvette (case d) and the Phase Map of the lens (case c), the found SA is the half in both monofocal lenses, probably due to the fact that rays are arriving parallel to the cornea instead of converging. The difference of SA for Monofocal 1, even being the half (0.05 μ), is lower than the minimum resolution of the experimental system, thus in the case of this lens, it would not be necessary to compensate the SA.

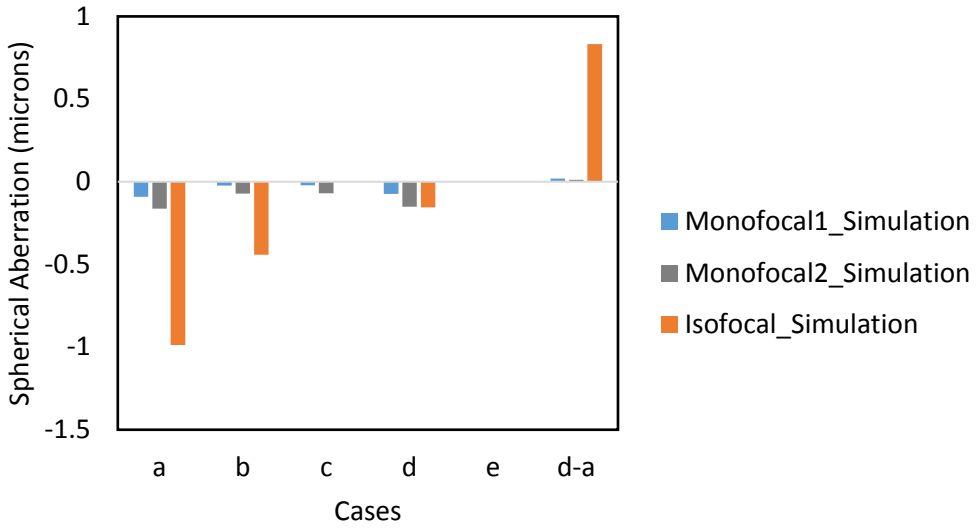

Figure 8.4. Spherical aberration in microns found with optical simulations in the described cases for a pupil size of 4.5 mm. Cases are: (a) the IOL alone, immersed in water, with parallel rays impacting the IOL; (b) a model eye with an aspheric cornea and the IOL virtually implanted behind the cornea; (c) difference of a model eye with an aspheric cornea and the IOL minus model with a paraxial lens behind the same cornea; (d) the IOL immersed in the cuvette with the Rassow telescope; (e) as case (d) but without the IOL.

8.3.2. Experimental Performance of Rassow telescope

The optical performance of the Rassow telescope was calibrated using monofocal IOLs of different powers (18.00D, 19.50D, 20.50D, 22D and 23.00D. We found that the optical relay produced by the Rassow telescope was maximized for lenses of optical power ~20 D. The Badal optometer allowed spherical compensation for other powers, linearly (R^2=0.99) in a 5 D range.

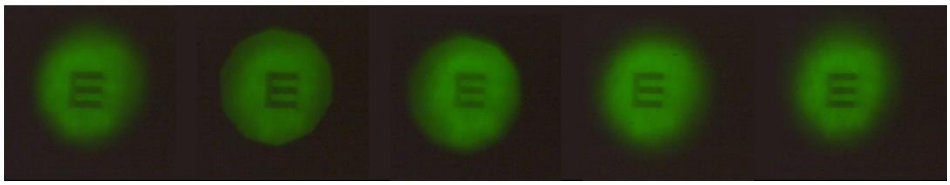

IOL's Power	18.00 D	19.50 D	20.50 D	22.00 D	23.00 D
Badal Compensation	0.89 D	0.12 D	-0.25 D	-1.28 D	-1.53 D
	(a)	(b)	(c)	(d)	(e)

Figure 8.5. On-bench images through monofocal IOLs of 18.00D (a), 19.50D (b), 20.50D (c), 22D (d) and 23.00D (e) and the needed amount of diopters to compensate with the Badal system in the VioBio lab AOI.

The same process with the same IOLs was repeated on VioBio lab AOII system. The results of both lenses and computer simulations are presented in figure 8.6. Both systems are perfectly aligned for the 20D-IOL, since the required compensation is 0D. In addition, the performance of both AO systems is linear (R^2=0.99 in both cases) and quite similar between them in the range in which it is possible to measure.

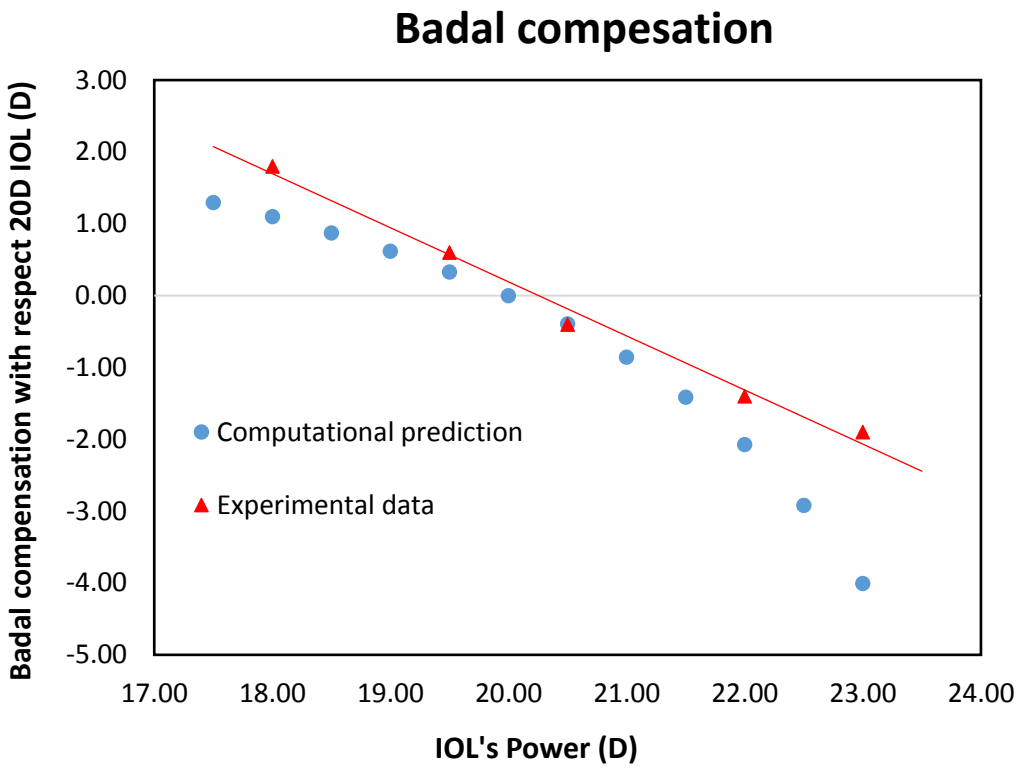

Figure 8.6. Comparison of the amount of diopters needed to compensate with the Badal system in Ray tracing software (blue dots), experimentally in the VioBio lab AOI (orange squares) and in the VioBio lab AOII (red triangles).

We also measured the spherical aberration induced by the Rassow telescope configuration and compared it with computational simulations, as shown in figure 8.7. Differences were < 20%

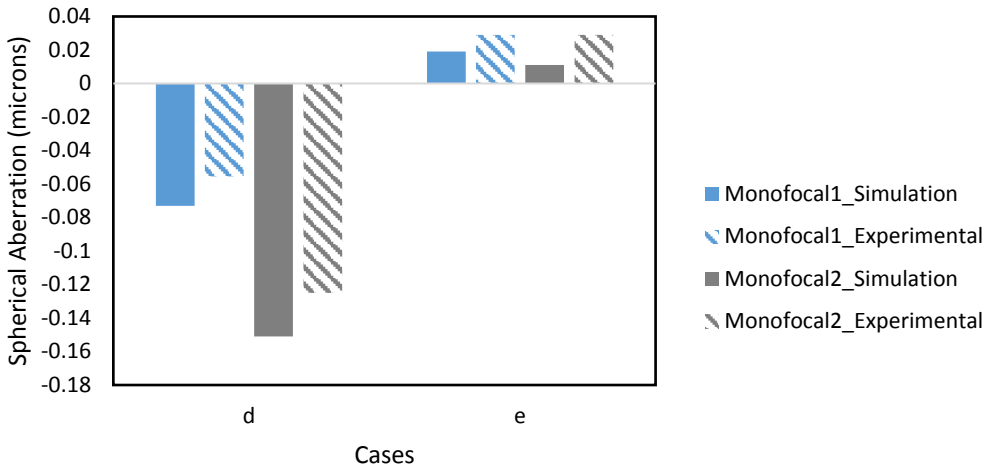

Figure 8.7. Comparison of spherical aberration in microns between optical simulations and experimental measurements for two different IOLs and pupil diameter of 4.5 mm. Tested cases are the IOL inside the cuvette (case d) and the cuvette alone (case e).

As found computationally (figure 8.4), we also found experimentally that the cuvette alone induces negligible spherical aberration. We also found a high correspondence between simulated and measured spherical aberration induced by the IOL immersed in the cuvette (figure 8.7). This value is higher (about double) than that induced by the IOL in the eye or that of the phase map representing the IOL. We found that the magnitude of the offset spherical aberration depended on the design of the IOL under test.

8.3.3. Through-focus on-bench optical quality

Figure 8.8 shows the TF on-bench images of an E letter obtained for three IOLs: Monofocal, Isofocal and Trifocal inserted in the cuvette. The upper rows correspond to images obtained with the standard Rassow configuration. The lower rows correspond to images obtained with the standard Rassow configuration and the compensatory spherical aberration in the DM.

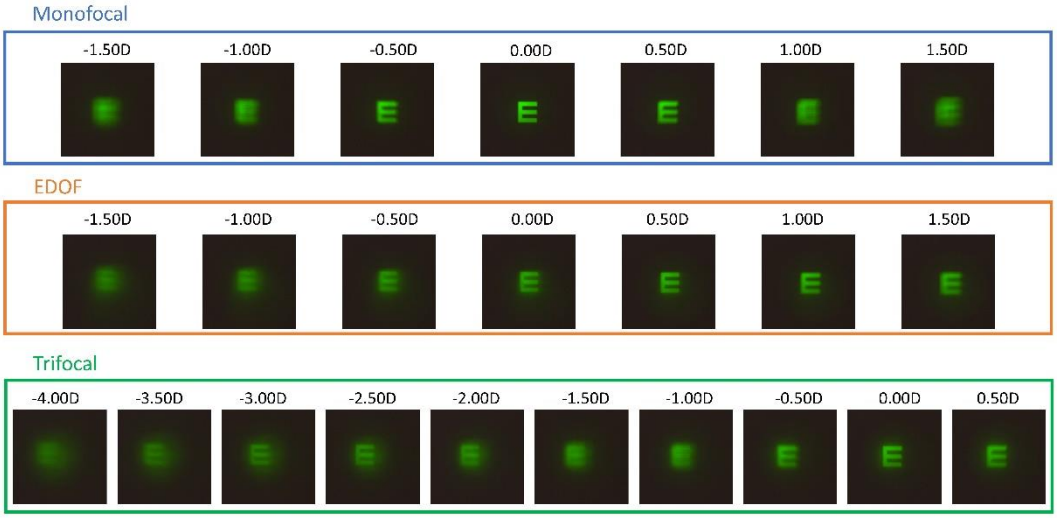

Figure 8.8. TF on-bench 1 pass images through the monofocal (blue), Isofocal (solid orange) and Trifocal (green) IOLs.

Figure 8.9 shows the TF optical quality on-bench using a correlation metric, using the image of the monofocal IOL at best focus as a reference. The optical quality of the images obtained through the Isofocal lens stays constant over a wider dioptric range than those obtained through the monofocal lens. The trifocal lens produces two peaks of higher quality and a relatively flat valley between the peaks.

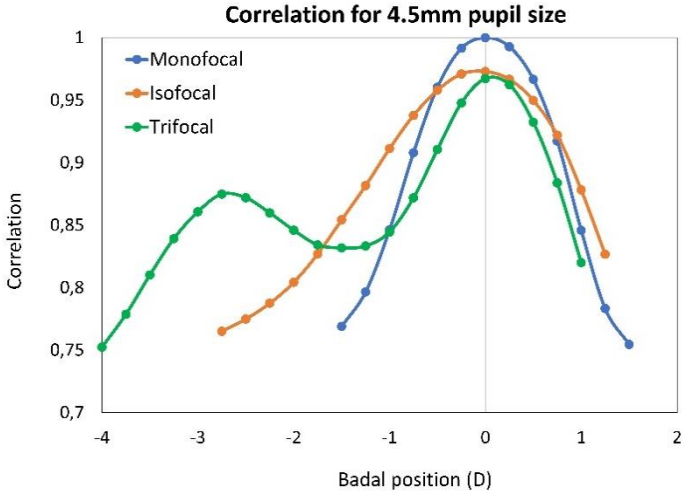

Figure 8.9. TF image correlation metric for the Monofocal (blue line), Isofocal (solid orange lines) and Trifocal (green line) IOLs.

8.3.5. Through-focus Visual Acuity

Figure 8.10 shows through-focus VA with the 3 IOLs immersed in the cuvette and projected on the pupil plane in 3 real patients. In the case of VA, it is also a smaller DOF for the monofocal IOLs and there are 2 peaks in the trifocal lens.

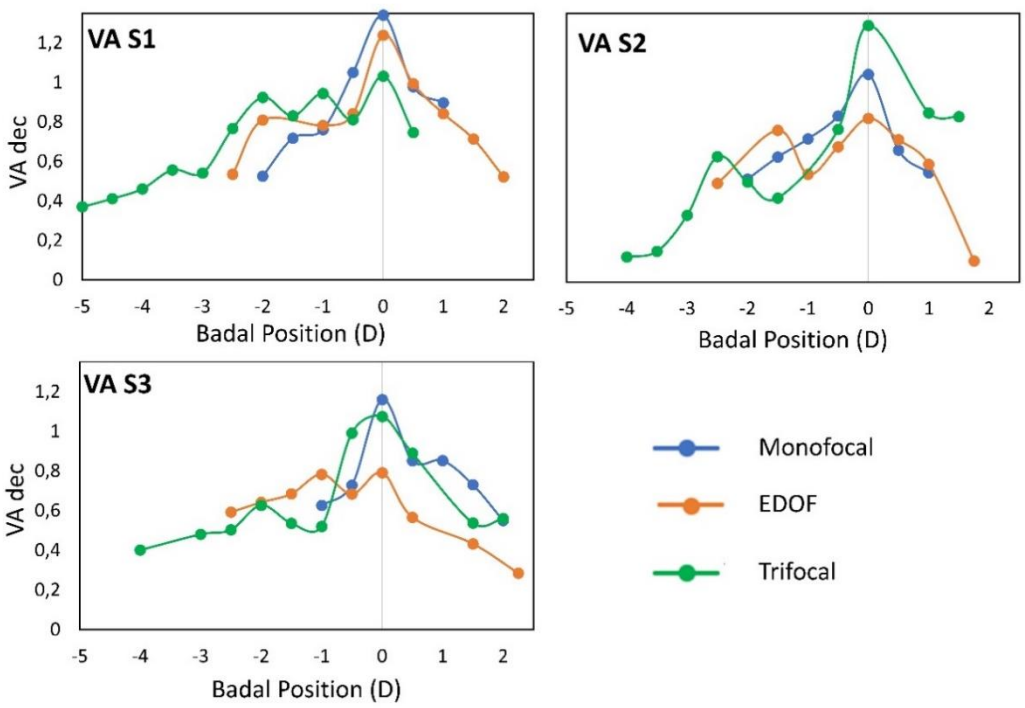

Figure 8.10. TF VA for 5 subjects with through the monofocal (blue lines), Isofocal (orange lines), and Trifocal (green lines) IOLs.

8.4. Discussion

In this study, we present the possibility of projecting non-0D real IOLs in the pupil's eyes through a Rassow telescope. The incorporation represents a new opportunity to validate AO and SimVis simulations. Although this comparison has been already done with 0D IOLs [77], there is not another system of AO that is equipped with a Deformable Mirror, a SLM, a channel for testing SimVis technology and a system to incorporate non-0D IOLs.

A comparison of Rassow telescope and VirtIOL have been done [242] in terms of contrast sensitivity function (CSF). Three designs of IOLs (monofocal, multifocal and EDF) were evaluated on twenty-one subjects with both devices. In this study, we also include computational calibrations to compare, not only between IOL's designs but with the expected performance of the lens.

In the theoretical configuration of Rassow telescope, rays arrive parallel to the IOL. It is important having account the difference of the performance of the IOL inside the eye, with rays arriving converging, and the performance of the IOL inside the Rassow telescope. In particular, the resulting spherical aberration can be the half when rays arrive parallel. This fact is especially relevant to those designs with a high amount of spherical aberration, such is EDOF lenses. Implementing a Rassow telescope system on an AO environment allows us to compensate for the difference of spherical aberration with an active element, such as a deformable mirror.

In addition, the implementation of a Rassow telescope on an AO system provides the possibility of cross validate the same lens with the different technologies that compose the system.

8.5. Conclusions

It has been demonstrated both computationally and experimentally that direct projection of an IOL I immersed a cuvette is not fully equivalent to the IOL implanted in the eye (after the cornea) or mapped in the visual simulators. However, the offset found in spherical aberration can be compensated with the deformable mirror in an Adaptive Optics system. This could be important when simulating certain refractive extended-depth-of-focus IOL designs that rely on spherical aberration to modulate the depth-of-field.

Chapter 9. Conclusions

In this thesis, two different Adaptive Optics systems have been used to explore different aspects of vision. One the one hand, fundamental questions regarding the optics of the eye and vision have been studied: interaction between chromatic and monochromatic aberrations, threshold to blur discrimination and adaptation to astigmatism.

On the other hand, Adaptive Optics systems, a critical tool to evaluate the optics of the eye and the impact of manipulating the optics on vision have been adapted for the purposes of the study, with new added capabilities. In particular, a new channel was designed, implemented and validated to measure non-0D IOLs immersed in a cuvette and optically projected onto the subject's eye. The results of this thesis have an impact on the evaluation and development of new optical corrections, in particular for presbyopia treatment,

The main accomplishments of this thesis are:

- Fundamental understanding of the interactions between chromatic and monochromatic aberrations. To investigate this question we have developed a new psychophysical paradigm allowing to test the perceptual impact of chromatic aberration on blue images (or equivalent defocus on green image), in the presence or absence of monochromatic aberrations measured and corrected in an AO system.

- Measurement of blur threshold discrimination for different pedestals references. Blur was induced by convolved images with the PSF of each subject or optically by using a Badal system to defocus the stimulus.

- Study of the perceptual impact of astigmatism induction in presbyopes wearing progressive lenses. For that, we evaluated perceived the best focus and visual acuity tasks under different amounts and angles of astigmatism in three groups of subjects: young emmetropic group, emmetropic presbyopic subjects wearing progressive lenses group and astigmatic presbyopic subjects wearing progressive lenses.

- Comparison of two visual simulators, Spatial Light Modulator and lathe-manufactured multi-zone surfaces, with six multifocal designs, both optically on-bench and psychophysically, through a perceptual scoring and visual acuity.

- Comparison of the performance of multifocal lenses mapped in the Spatial Light Modulator and SimVis visual simulators with that of the real intraocular lens immersed in a cuvette. This comparison was made objectively, through the correlation metric on through-focus double-pass retinal images and images of a stimulus in an artificial eye and psychophysically (through-focus visual acuity) in patients, with each simulator and the real projected IOL.

- Design and implementation of a new channel in the polychromatic AO system in order to characterize and in-eye projection of IOLs of different powers. The new channel was demonstrated on-bench and *in vivo* for 3 different designs of IOLs.

The main conclusions of the studies of this thesis are:

1. The presence of monochromatic optical aberrations protects vision against chromatic defocus, but adaptational mechanisms seem equally important in regulating contrast constancy and operate differentially across wavelengths. Specifically, the eye appears to be less sensitive to chromatic blur in blue stimuli that to pure defocus of the same magnitude in green stimuli, both under natural and correction of monochromatic aberrations. The results suggest neural adaption to chromatic blur in blue images.

2. The threshold of blur discrimination it is highly related to the optical quality of the subject.

3. Presbyopic patients wearing progressive lenses are adapted to astigmatism induced by their visual correction. In particular, presbyopes experience shifts in the best focus upon induced astigmatism and higher insensitivity to astigmatic induction, in terms of visual acuity. This higher insensitivity to astigmatism induction was found in all patients wearing progressive lenses (both emmetropes and astigmats) but was higher in patients with native astigmats. This study shows that the best focus correction in the presence of astigmatism is dependent on the refractive profile of the patient.

4. Visual simulators are excellent tools for evaluating vision under different visual corrections (particularly for presbyopia), that are mapped in Spatial Light Modulator, enabling rapid evaluation of different multifocal designs even prior to their manufacturing. We demonstrated that optical and visual performance through physical multifocal lathe-manufactured surfaces and well replicated with the Spatial Light Modulator.

5. Visual performance with multifocal IOLs can be predicted prior to implantation using programmable visual simulators. There was a large correspondence between the through-focus visual acuity obtained pre-operatively with the Spatial Light Modulator and SimVis simulators programmed to mimic a specific trifocal an IOL and that obtained post-operatively with the IOL implanted in the same patient.

6. A newly implemented channel for immersion and projection of IOLs of standard optical power allows new benchmarking for the different programmable simulators (deformable mirror, SLM and SimVis) in Adaptive Optics Simulator.

List of scientific activities

Publications included in this thesis

1. Clara Benedi-Garcia; Miriam Velasco-Ocana; Carlos Dorronsoro; Daniel Pascual; Martha Hernandez; Gildas Marin; Susana Marcos. Perceptual impact of astigmatism induction in presbyopes. Vision research. 165, pp. 143 - 151. Pergamon, 2019.
2. Maria Vinas; Clara Benedi-Garcia; Sara Aissati; Daniel Pascual; Vyas Akondi; Carlos Dorronsoro; Susana Marcos. Visual simulators replicate vision with multifocal lenses. Scientific reports. 9 - 1, pp. 1 - 11. 2019
3. Maria Vinas; Carlos Dorronsoro; Aiswaryah Radhakrishnan; Clara Benedi-Garcia; Edward Anthony LaVilla; Jim Schwiegerling; Susana Marcos. Comparison of vision through surface modulated and spatial light modulated multifocal optics. Biomedical optics express. 8 - 4, pp. 2055 - 2068. Optical Society of America, 2017.

Other publications

1. Susana Marcos; Mercedes Romero; Clara Benedi-Garcia; Ana Gonzalez-Ramos; Maria Vinas; Nicolas Alejandre; Ignacio Jimenez-Alfaro. Interaction of Monochromatic and Chromatic Aberrations in Pseudophakic Patients. Journal of Refractive Surgery. 36 - 4, pp. 230 - 238. SLACK Incorporated, 2020
2. Susana Marcos; Clara Benedi-Garcia; Sara Aissati; Ana Gonzalez-Ramos; Carmen M Lago; Aiswaryah Radhkrishnan; Mercedes Romero; Shirleka Vedhakrishnan; Lucie Sawides; Maria Vinas. VioBio lab adaptive optics: technology and applications by women vision scientist. Ophthalmic and Physiological Optics. 40 - 2, 2020.
3. Maria Vinas; Sara Aissati; Mercedes Romero; Clara Benedi-Garcia; Nuria Garzon; Francisco Poyales; Carlos Dorronsoro; Susana Marcos. Pre-operative simulation of post-operative multifocal vision. Biomedical Optics Express. 10 - 11, pp. 5801 - 5817. Optical Society of America, 2019.
4. Carlos Dorronsoro; Xoana Barcala; Enrique Gambra; Vyas Akondi; Lucie Sawides; Yassine Marrakchi; Victor Rodriguez-Lopez; Clara Benedi-Garcia; Maria Vinas; Eduardo Lage; others. Tunable lenses: dynamic characterization and fine-tuned control for high-speed applications. Optics express. 27 - 3, pp. 2085 - 2100. Optical Society of America, 2019.
5. Maria Vinas; Mercedes Romero; Sara Aissati; Juan Luis Mendez-Gonzalez; Clara Benedi-Garcia; Enrique Gambra; Vyas Akondi; Francisco Poyales; Carlos Dorronsoro; Susana Marcos; others. Comparison of multifocal visual simulations in patients before and after implantation of diffractive trifocal lenses. Investigative Ophthalmology & Visual Science. 59 - 9, pp. 252 - 252. The Association for Research in Vision and Ophthalmology, 2018.

Congress contributions

Personally presented

1. Clara Benedi-Garcia; Maria Vinas; Carmen Lago; Carlos Dorronsoro; Susana Marcos. Optical and visual quality of real intraocular lenses physically projected on the patient's eye. ARVO Investigative Ophthalmology & Visual Science. (Baltimore, USA/ Online), 2020. *Oral contribution.*
2. Clara Benedi-Garcia; Miriam Velasco-Ocana; Carlos Dorronsoro; Martha Hernandez; Gildas Marin; Susana Marcos. Perceived best focus and visual performance upon induction of astigmatism in presbyopes. ARVO Investigative Ophthalmology & Visual Science. (Vancouver, Canada), 2019. *Poster contribution.*
3. Clara Benedi-Garcia; Maria Vinas; Carlos Dorronso; Eli Peli; Stephen Burns; Susana Marcos. Impact of the interactions between mono- and chromatic aberrations on visual function. IX Workshop on Adaptive Optics for industry and medicine. (Murcia, Spain), 2018. *Poster contribution.*
4. Clara Benedi-Garcia, Maria Vinas, Carlos Dorronsoro, Mike Webster, Susana Marcos. Discriminación del emborronamiento en un sistema de óptica adaptativa. RNO Reunión Nacional de Óptica. (Castellón, Spain), 2018. *Oral contribution.*
5. Clara Benedi-Garcia; Maria Vinas; Carlos Dorronsoro; E Peli; Stephen A Burns; Susana Marcos. Impact of the interactions between mono-and chromatic aberrations on visual function. IONS International OSA Network for studients. (Paris, France), 2017. *Oral contribution*.
6. Clara Benedi-Garcia; Susana Marcos. Comparison between model and realistic eyes with through-focus intraocular lens. IONS International OSA Network for studients. (Valencia, Spain), 2015. *Oral contribution*.

Presented by collaborators

1. Sara Aissati; Maria Vinas; Clara Benedi-Garcia; Carlos Dorronsoro; Susana Marcos. Testing the effect of ocular aberrations on perceived Transverse Chromatic Aberration. ARVO Investigative Ophthalmology & Visual Science. (Vancouver, Canada), 2019. *Poster contribution.*
2. Alessandra Marie Carmichael Martins; Maria Vinas; Ana Gonzalez-Ramos; Clara Benedi-Garcia; Carlos Dorronsoro; Susana Marcos; Brian Vohnsen. Influence of the Stiles-Crawford effect of the first kind on visual acuity for decentered pupils. *Poster contribution*.
3. Susana Marcos; Sara Aissati; Clara Benedi-Garcia; Carlos Dorronsoro Enrique Gambra; Aiswaryah Radhakrishan; Maria Vinas; Michael Webster; Lucie Sawides. Visual Simulators: from understanding of vision mechanisms to applications in clinic. OSA Fall Vision Meeting (Washington, D.C., EEUU), 2019. *Oral contribution*.
4. Susana Marcos; Maria Vinas; Carlos Dorronsoro; Lucie Sawides; Enrique Gambra; Clara Benedi-Garcia; Sara Elaissati. Adaptive-Optics based visual simulators: from on-bench to wearable devices. OSA Imaging and Applied Optics Congress, (Orlando, USA), 2018. *Oral contribution*.
5. Maria Vinas; Mercedes Romero; Sara Aissati; Juan Luis Mendez-Gonzalez; Clara Benedi-Garcia; Enrique Gambra; Vyas Akondi; Francisco Poyales; Carlos

Dorronsoro; Susana Marcos. Comparison of multifocal visual simulations in patients before and after implantation of diffractive trifocal lenses. ARVO Investigative Ophthalmology & Visual Science. (Hawaii, EEUU), 2018. *Poster contribution.*

6. Susana Marcos; Clara Benedi; Maria Vinas; Carlos Dorronsoro; Stephen A Burns; Eli Peli. Visual benefit of correcting High Order Aberrations in blue or green light: an optical effect? ARVO Investigative Ophthalmology & Visual Science. (Hawaii, EEUU), 2018. *Poster contribution.*
7. Sara Aissati; Maria Vinas; Clara Benedi-Garcia; Carlos Dorronsoro; V Akondi; Susana Marcos. Double-pass technique to compare different visual simulators in an Adaptive Optics environment IONS International OSA Network for students. (Paris, France), 2017. *Poster contribution.*
8. Carlos Dorronsoro; Maria Vinas; Clara Benedi-Garcia; Sara Aissati; Vyas Akondi; Susana Marcos. Pre-surgical visual simulations of real multifocal lenses with different optical methods. ESCRS European Society of Cataract and Refractive Surgeons. (Lisbon, Portugal), 2017. *Oral contribution*.
9. Susana Marcos; Maria Vinas; Clara Benedi-Garcia; Sara Aissati; Vyas Akondi; Xoana Barcala; Enrique Gambra. Visual simulations of real multifocal lenses in a multi-channel Adaptive Optics system. ARVO Investigative Ophthalmology & Visual Science. (Baltimore, EEUU), 2017. *Oral contribution*.
10. Susana Marcos; Maria Vinas; A Radhakrishnan; Clara Benedi-Garcia; Sara Aissati; Enrique Gambra; Daniel Pascual; Vyas Akondi; JR Alonso-Sanz, Juan Luis Méndez, Xoana Barcala, Carlos Dorronsoro. Wearable See-thru Binocular Simulator of Multifocal and Monovision Presbyopic Corrections. Wavefront & Presbyopic Refractive Corrections. (San José, EEUU), 2017. *Oral contribution*.

Invited talks

Visual impact of the interaction between chromatic and monochromatic aberrations using Adaptive Optics. Webinar organized by Vision Sience committee of SEDOPTICA, 2019

Honours

ARVO International Travel Grant. These grants, from the Association for Research in Vision and Ophthalmology (ARVO), are awarded to PhD students attending and presenting their scientific work at the 2020 ARVO Annual Meeting (Baltimore, USA).

Other relevant information

Co-Author Book: *Descubriendo la luz. Editorial CSIC-Catarata, 2018. María Viñas, Sara Aissati, Xoana Barcala, Clara Benedí, Camilo Florián, Mario García, Juan Luis García, Juan Luis Méndez, Javier Nuño, Pablo Pérez. ISBN 978-84-00-10397-2*

Member of the IO-CSIC Student Chapter of the Optical Society of America (IOSA, https://sites.google.com/view/iosa-student-chapter-csic/home). Charges of Treasurer during 2017 and President during 2018. We organize internal seminars and talks and

participate in outreach programs, such as European Research Night, Week of Science, Ciencia en el Barrio or Ciudad Ciencia.

Teaching experience:

1. Practical course Adaptive Optics for Visual Optics and Biophotonics technologies. 2018
2. Theorical-practical course *Learning to teach in a fun way*. 2018
3. Course Introduction to research in Optics. 2018

Bibliography

[1] L. N. Thibos, A. Bradley, and X. Zhang, “Effect of ocular chromatic aberration on monocular visual performance,” *Optom. Vis. Sci.*, vol. 68, no. 8, pp. 599–607, 1991.

[2] H. A. Unterhorst and Alan Rubin, “Ocular aberrations and wavefront aberrometry: A review,” *African Vis. Eye Heal.*, vol. 74, no. 1, pp. 1–6, 2015.

[3] D. Atchison and G. Smith, *Optics of the Human Eye*. Butterworth-Heinemann, 2000.

[4] P. Artal, L. Chen, E. J. Fernández, B. Singer, S. Manzanera, and D. R. Williams, “Neural compensation for the eye’s optical aberrations,” *J. Vis.*, vol. 4, no. 4, pp. 281–287, 2004.

[5] L. Sawides, P. de Gracia, C. Dorronsoro, M. A. Webster, and S. Marcos, “Vision is adapted to the natural level of blur present in the retinal image,” *PLoS One*, vol. 6, no. 11, pp. 1–6, 2011.

[6] L. Chen, P. Artal, D. Gutierrez, and D. R. Williams, “Neural compensation for the best aberration correction,” *J. Vis.*, vol. 7, no. 10, pp. 1–9, 2007.

[7] M. A. Webster, “Visual Adaptation,” *Annu. Rev. Vis. Sci.*, vol. 1, no. 1, pp. 547–567, 2015.

[8] B. A. Wandell, *Foundations of vision*. Oxford University Press, 1995.

[9] “sonicasneuroblog.com.” .

[10] “https://med.libretexts.org/.” .

[11] “https://www.lifeder.com/.” .

[12] Kahle and Frotscher, “Ojo y anexos oculares,” in *Atlas de Anatomía con correlación clínica. Vol 3. Sistema nervioso y órganos de los sentidos.*, Madrid: Editorial Médica Panamericana, 2008, pp. 341–363.

[13] J. K. Bowmaker and H. J. Dartnall, “Visual pigments of rods and cones in a human retina.,” *J. Physiol.*, vol. 298, no. 1, pp. 501–511, 1980.

[14] Østerberg G, “Topography of the layer of rods and cones in the human retina,” *Acta ophthalmol*, vol. 13, no. S6, pp. 11–103, 1935.

[15] J. B. Jonas, U. Schneider, and G. O. H. Naumann, “Count and density of human retinal photoreceptors,” *Graefe’s Arch. Clin. Exp. Ophthalmol.*, vol. 230, no. 6, pp. 505–510, 1992.

[16] W. S. Stiles, B. H. Crawford, and J. H. Parson, “The luminous efficiency of rays entering the eye pupil at different points,” *Proc. R. Soc. London*, vol. Series B, no. 112, pp. 428–450, 1993.

[17] G. Westheimer, “Directional sensitivity of the retina: 75 Years of Stiles-Crawford effect,” *Proc. R. Soc. B Biol. Sci.*, vol. 275, no. 1653, pp. 2777–2786, 2008.

[18] Brian A. Wandell, *Fundations of Vision*. Prentice Hall, 1989.

[19] H. von Helmholtz, *Popular Scientific Lectures*. New York, 1885.

[20] J. Liang and D. R. Williams, “Aberrations and retinal image quality of the normal human eye,” *J. Opt. Soc. Am. A*, vol. 14, no. 11, p. 2873, 1997.

[21] A. Guirao, C. González, M. Redondo, E. Geraghty, S. Norrby, and P. Artal, “Average optical performance of the human eye as a function of age in a normal population,” *Investig. Ophthalmol. Vis. Sci.*, vol. 40, no. 1, pp. 203–213, 1999.

[22] S. Amano *et al.*, “Age-related changes in corneal and ocular higher-order wavefront aberrations,” *Am. J. Ophthalmol.*, vol. 137, no. 6, pp. 988–992, 2004.

[23] von F. Zernike, “Beugungstheorie des schneidenver-fahrens und seiner verbesserten form, der phasenkontrastmethode,” *Physica*, vol. 1, no. 7–12, pp. 689–704, 1934.

[24] L. N. Thibos, R. A. Applegate, J. T. Schwiegerling, and R. Webb, “Standards for reporting the optical aberrations of eyes,” *J. Refract. Surg.*, vol. 18, no. 5, pp. 652–660, 2002.

[25] P. Shaw-McMinn, “How to provide high-resolution vision: an introductory guide to prescribing iZon lenses,” vol. 143, no. 12, p. S1+, Aug. 2006.

[26] L. N. Thibos, X. Hong, A. Bradley, and X. Cheng, “Statistical variation of aberration structure and image quality in a normal population of healthy eyes,” *J. Opt. Soc. Am. A*, vol. 19, no. 12, p. 2329, 2002.

[27] A. Guirao and D. R. Williams, “A Method to Predict Refractive Errors from Wave Aberration Data,” *Optom. Vis. Sci.*, vol. 8, no. 1, pp. 36–42, 2003.

[28] L. N. Thibos, H. Xin, A. Bradley, and R. A. Applegate, “Accuracy and precision of objective refraction from wavefront aberrations,” *J. Vis.*, vol. 4, no. 4, pp. 329–351, 2004.

[29] J. Porter, H. M. Queener, J. E. Lin, K. Thorn, and A. Awwal, *Adaptive Optics for Vision Science: Principles, Practices, Design, and Applications*. 2005.

[30] R. Navarro and M. A. Losada, “Aberrations and relative efficiency of light pencils in the living human eye,” *Am. Acad. Optom.*, vol. 74, no. 7, pp. 540–547, 1997.

[31] J. C. He, S. Marcos, R. H. Webb, and S. A. Burns, “Measurement of the wave-front aberration of the eye by a fast psychophysical procedure,” *J. Opt. Soc. Am. A*, vol. 15, no. 9, p. 2449, 1998.

[32] J. Liang, B. Grimm, S. Goelz, and J. F. Bille, “Objective measurement of wave aberrations of the human eye with the use of a Hartmann–Shack wave-front sensor,” *J. Opt. Soc. Am. A*, vol. 11, no. 7, p. 1949, 1994.

[33] A. E. Shapiro, *The Optical papers of Isaac Newton. Volumen I: The optical papers (1670-1672)*. Cambridge (UK): Cambrigde University Press, 2010.

[34] R. E. E. Bedford and G. Wyszecki, “Axial Chromatic Aberration of the Human Eye,” *J. Opt. Soc. Am.*, vol. 47, no. 6, pp. 2–3, Jun. 1947.

[35] W. N. Charman and J. A. M. Jennings, “Objective measurements of the longitudinal chromatic aberration of the human eye,” *Vision Res.*, vol. 16, no. 9, pp. 999–1005, 1976.

[36] L. N. Thibos, A. Bradley, D. L. Still, X. Zhang, and P. A. Howarth, “Theory and

measurement of ocular chromatic aberration," *Vision Res.*, vol. 30, no. 1, pp. 33–49, 1990.

[37] L. Llorente, L. Diaz-Santana, Lara-Saucedo, and S. Marcos, "Aberrations of the Human Eye in Visible and Near Infrared Illumination," *Optom. Vis. Sci.*, vol. 80, no. 1, 2003.

[38] M. Vinas, C. Dorronsoro, D. Cortes, D. Pascual, and S. Marcos, "Longitudinal chromatic aberration of the human eye in the visible and near infrared from wavefront sensing, double-pass and psychophysics," *Biomed. Opt. Express*, vol. 23, no. 4, pp. 513–522, 2015.

[39] L. N. Thibos, M. Ye, X. Zhang, and A. Bradley, "The chromatic eye: a new reduced-eye model of ocular chromatic aberration in humans," *Appl. Opt.*, vol. 31, no. 19, p. 3594, 1992.

[40] P. Perez-Merino, C. Dorronsoro, L. Llorente, S. Durán, I. Jiménez-Alfaro, and S. Marcos, "In vivo chromatic aberration in eyes implanted with intraocular lenses," *Investig. Ophthalmol. Vis. Sci.*, vol. 54, no. 4, pp. 2654–2661, 2013.

[41] M. Vinas, C. Dorronsoro, N. Garzón, F. Poyales, and S. Marcos, "In vivo subjective and objective longitudinal chromatic aberration after bilateral implantation of the same design of hydrophobic and hydrophilic intraocular lenses," *J. Cataract Refract. Surg.*, vol. 41, no. 10, pp. 2115–2124, 2015.

[42] M. Vinas *et al.*, "In vivo measurement of longitudinal chromatic aberration in patients implanted with trifocal diffractive intraocular lenses," *J. Refract. Surg.*, vol. 33, no. 11, pp. 736–742, 2017.

[43] S. Winter, *Transverse Chromatic Aberration and Vision: Quantification and Impact across the Visual Field*. 2016.

[44] Y. U. Ogboso and H. E. Bedell, "Magnitude of lateral chromatic aberration across the retina of the human eye," *J. Opt. Soc. Am. A*, vol. 4, no. 8, pp. 1666–1672, 1987.

[45] P. Simonet and M. C. Campbell, "The optical transverse chromatic aberration on the fovea of the human eye.," *Vision Res.*, vol. 30, no. 2, pp. 187–206, 1990.

[46] S. Marcos, S. A. Burns, P. M. Prieto, R. Navarro, and B. Baraibar, "Investigating sources of variability of monochromatic and transverse chromatic aberrations across eyes," *Vision Res.*, vol. 41, no. 28, pp. 3861–3871, 2001.

[47] S. Aissati, M. Vinas, C. Benedi-Garcia, C. Dorronsoro, and S. Marcos, "Testing the effect of ocular aberrations in the perceived Transverse Chromatic Aberration," *Biomed. Opt. Express*, vol. 11, no. 8, pp. 4052–4068, 2020.

[48] R. A. Applegate, J. D. Marsack, R. Ramos, and E. J. Sarver, "Interaction between aberrations to improve or reduce visual performance," *J. Cataract Refract. Surg.*, vol. 29, no. 8, pp. 1487–1495, 2003.

[49] R. A. Applegate, C. Ballentine, H. Gross, E. J. Sarver, and C. A. Sarver, "Visual acuity as a function of Zernike mode and level of root mean square error.," *Optom. Vis. Sci.*, vol. 80, no. 2, pp. 97–105, Feb. 2003.

[50] S. Marcos, L. Sawides, E. Gambra, and C. Dorronsoro, "Influence of adaptive-optics ocular aberration correction on visual acuity at different luminances and contrast polarities," *J. Vis.*, vol. 8, no. 13, pp. 1–12, 2008.

[51] R. Montés-Micó, T. Ferrer-Blasco, and A. Cerviño, “Analysis of the possible benefits of aspheric intraocular lenses: Review of the literature,” *J. Cataract Refract. Surg.*, vol. 35, no. 1, pp. 172–181, 2009.

[52] P. de Gracia, C. Dorronsoro, E. Gambra, G. Marin, M. Hernández, and S. Marcos, “Combining coma with astigmatism can improve retinal image over astigmatism alone,” *Vision Res.*, vol. 50, no. 19, pp. 2008–2014, 2010.

[53] P. de Gracia, C. Dorronsoro, G. Marin, M. Hernández, and S. Marcos, “Visual acuity under combined astigmatism and coma: Optical and neural adaptation effects,” *J. Vis.*, vol. 11, no. 2, pp. 1–11, 2011.

[54] X. Cheng, A. Bradley, and L. N. Thibos, “Predicting subjective judgment of best focus with objective image quality metrics,” *J. Vis.*, vol. 4, no. 4, pp. 310–321, 2004.

[55] M. Vinas *et al.*, “Astigmatism impact on visual performance: Meridional and adaptational effects,” *Optom. Vis. Sci.*, vol. 90, no. 12, pp. 1430–1442, 2013.

[56] R. Sabesan, T. M. Jeong, L. Carvalho, I. G. Cox, D. R. Williams, and G. Yoon, “Vision improvement by correcting higher-order aberrations with customized soft contact lenses in keratoconic eyes,” *Opt. Lett.*, vol. 32, no. 8, p. 1000, 2007.

[57] S. Marcos, M. Velasco-Ocana, C. Dorronsoro, L. Sawides, M. Hernandez, and G. Marin, “Impact of astigmatism and high-order aberrations on subjective best focus,” *J. Vis.*, vol. 15, no. 11, pp. 1–12, 2015.

[58] L. Sawides, S. Marcos, S. Ravikumar, L. Thibos, A. Bradley, and M. Webster, “Adaptation to astigmatic blur,” *J. Vis.*, vol. 10, no. 12, pp. 22–22, 2010.

[59] M. Vinas, L. Sawides, P. de Gracia, and S. Marcos, “Perceptual Adaptation to the Correction of Natural Astigmatism,” *PLoS One*, vol. 7, no. 9, 2012.

[60] G. H. Guilino, “Design philosophy for progressive addition lenses,” *Appl. Opt.*, vol. 32, no. 1, p. 111, 1993.

[61] E. Villegas and P. Artal, “Comparison of aberrations in different types of progressive power lenses,” *Ophthalmic Physiol. Opt.*, vol. 24, no. 5, 2004.

[62] J. S. McLellan, S. Marcos, P. M. Prieto, and S. A. Burns, “Imperfect optics may be the eye’s defence against chromatic blur,” *Nature*, vol. 417, no. 6885, pp. 174–176, 2002.

[63] M. Smirnov, “Measurement of the Wave Aberration of the Human Eye,” *Biofizika*, vol. 6, pp. 776–795, 1961.

[64] A. W. Dreher, J. F. Bille, and R. N. Weinreb, “Active optical depth resolution improvement of the laser tomographic scanner,” *Appl. Opt.*, vol. 28, no. 4, p. 804, 1989.

[65] S. A. Burns, S. Marcos, A. E. Elsner, and S. Bara, “Contrast improvement of confocal retinal imaging by use of phase-correcting plates,” *Opt. Lett.*, vol. 27, no. 6, p. 400, 2002.

[66] G. Yoon, T. M. Jeong, I. G. Cox, and D. R. Williams, “Vision improvement by correcting higher-order aberrations with phase plates in normal eyes,” *J. Refract. Surg.*, vol. 20, no. 5, pp. 523–527, 2004.

[67] J. Liang, D. R. Williams, and D. T. Miller, “Supernormal vision and high-resolution

retinal imaging through adaptive optics," *J. Opt. Soc. Am. A*, vol. 14, no. 11, p. 2884, 1997.

[68] F. Vargas-Martín, P. M. Prieto, and P. Artal, "Correction of the aberrations in the human eye with a liquid-crystal spatial light modulator: limits to performance," *J. Opt. Soc. Am. A*, vol. 15, no. 9, pp. 2552–2562, Sep. 1998.

[69] H. Hofer, P. Artal, B. Singer, J. L. Aragón, and D. R. Williams, "Dynamics of the eye's wave aberration," *J. Opt. Soc. Am. A*, vol. 18, no. 3, p. 497, 2001.

[70] F. A. South, Y.-Z. Liu, and S. A. Boppart, "Correction of aberrations in the human eye using computational methods," *SPIE Newsroom*, vol. 101, no. 22, 2016.

[71] S. Marcos *et al.*, "Vision science and adaptive optics, the state of the field," *Vision Res.*, vol. 132, pp. 3–33, 2017.

[72] L. Sawides, E. Gambra, D. Pascual, C. Dorronsoro, and S. Marcos, "Visual performance with real-life tasks under Adaptive-Optics ocular aberration correction," *J. Vis.*, vol. 10, no. 5, p. 19, 2010.

[73] G.-Y. Yoon and D. R. Williams, "Visual performance after correcting the monochromatic and chromatic aberrations of the eye," *J. Opt. Soc. Am. A*, vol. 19, no. 2, p. 266, 2002.

[74] R. Sabesan and G. Yoon, "Visual performance after correcting higher order aberrations in Keratoconic eyes," *J. Vis.*, vol. 9, no. 5, pp. 1–19, 2009.

[75] P. A. Piers, E. J. Fenandez, S. Manzanera, S. Norrby, and P. Artal, "Adaptive optics simulation of intraocular lenses with modified spherical aberration," *Investig. Ophthalmol. Vis. Sci.*, vol. 45, no. 12, pp. 4601–4610, 2004.

[76] M. Vinas, C. Dorronsoro, V. Gonzalez, D. Cortes, A. Radhakrishnan, and S. Marcos, "Testing vision with angular and radial multifocal designs using Adaptive Optics," *Vision Res.*, vol. 132, pp. 85–96, 2016.

[77] M. Vinas *et al.*, "Visual simulators replicate vision with multifocal lenses," *Sci. Rep.*, vol. 9, no. 1, pp. 1–11, 2019.

[78] P. de Gracia, C. Dorronsoro, Á. Sánchez-González, L. Sawides, and S. Marcos, "Experimental simulation of simultaneous vision," *Investig. Ophthalmol. Vis. Sci.*, vol. 54, no. 1, pp. 415–422, 2013.

[79] A. Radhakrishnan, C. Dorronsoro, L. Sawides, and S. Marcos, "Short-term neural adaptation to simultaneous bifocal images," *PLoS One*, vol. 9, no. 3, 2014.

[80] A. Radhakrishnan, D. Pascual, S. Marcos, and C. Dorronsoro, "Vision with different presbyopia corrections simulated with a portable binocular visual simulator," *PLoS One*, vol. 14, no. 8, pp. 1–13, 2019.

[81] J. D. Marsack, L. N. Thibos, and R. A. Applegate, "Metrics of optical quality derived from wave aberrations predict visual performance," *J. Vis.*, vol. 4, no. 4, pp. 322–328, 2004.

[82] A. George Biddell, "On the diffraction of an object-glass with circular aperture," *Trans. Cambridge Philos. Soc.*, vol. 5, pp. 283–291, 1835.

[83] J. W. Goodman, *Introduction to Fourier Optics*, 2nd ed. New York: McGraw-Hill, 1998.

[84] F. Flamant, “Etude de la répartition de lumière dans l’image rétinienne d’une fente,” *Rev. d’Optique*, vol. 34, pp. 433–459, 1955.

[85] G. J. Burton and N. D. Haig, “Effects of the Seidel aberrations on visual target discrimination,” *J. Opt. Soc. Am. A*, vol. 1, no. 4, p. 373, 1984.

[86] P. Artal, “Calculations of two-dimensional foveal retinal images in real eyes,” *J. Opt. Soc. Am. A*, vol. 7, no. 8, p. 1374, 1990.

[87] E. Peli and A. Lang, “Appearance of images through a multifocal intraocular lens,” *J. Opt. Soc. Am. A Opt. Image Sci. Vis.*, vol. 18, no. 2, pp. 302–309, 2001.

[88] R. Legras, N. Chateau, and W. N. Charman, “Assessment of just-noticeable differences for refractive errors and spherical aberration using visual simulation,” *Optom. Vis. Sci.*, vol. 81, no. 9, pp. 718–728, 2004.

[89] L. Sawides, P. de Gracia, C. Dorronsoro, M. Webster, and S. Marcos, “Adapting to blur produced by ocular high-order aberrations,” *J. v*, vol. 11, no. 3, 2011.

[90] A. van Meeteren, “Calculations on the Optical Modulation Transfer Function of the Human Eye for White Light,” *Opt. Acta Int. J. Opt.*, vol. 21, no. 5, pp. 395–412, 1974.

[91] S. Marcos, S. A. Burns, E. Moreno-barriusop, and R. Navarro, “A new approach to the study of ocular chromatic aberrations,” *Vision Res.*, vol. 39, pp. 4309–4323, 1999.

[92] S. Ravikumar, “Effect of optical aberrations on image quality and visual performance,” School of Optometry, Indiana University, 2009.

[93] A. Bradley, R. Xu, H. Wang, M. Jaskulski, and N. Brink, “The Impact of IOL Abbe Number on Polychromatic Image Quality of Pseudophakic Eyes,” pp. 2271–2281, 2020.

[94] S. Marcos *et al.*, “Interaction of monochromatic and chromatic aberrations in pseudophakic patients,” *J. Refract. Surg.*, vol. 36, no. 4, pp. 230–238, 2020.

[95] S. Ravikumar, A. Bradley, and L. N. Thibos, “Chromatic aberration and polychromatic image quality with diffractive multifocal intraocular lenses,” *J. Cart. Refract. Surg.*, vol. 40, no. 7, pp. 1192–1204, 2014.

[96] C. W. G. Clifford *et al.*, “Visual adaptation: Neural, psychological and computational aspects,” *Vision Res.*, vol. 47, no. 25, pp. 3125–3131, 2007.

[97] M. A. Webster, “Adaptation and visual coding,” *J. Vis.*, vol. 11, no. 5, pp. 3–3, 2011.

[98] M. A. Webster, M. A. Georgeson, and S. M. Webster, “Neural adjustments to image blur,” *Nat. Neurosci.*, vol. 5, no. 9, pp. 839–840, 2002.

[99] O. Yehezkel, D. Sagi, A. Sterkin, M. Belkin, and U. Polat, “Learning to adapt: Dynamics of readaptation to geometrical distortions,” *Vision Res.*, vol. 50, no. 16, pp. 1550–1558, 2010.

[100] D. H. Owen, *The psychophysics of prior experience*. 1978.

[101] L. Sawides, “Correction and control of ocular aberrations with adaptive optics. Effects on Human Vision,” Universidad de Valladolid, 2013.

[102] C. Blakemore and F. W. Campbell, “Adaptation to spatial stimuli.,” *J. Physiol.*, vol. 200, no. 1, pp. 11P-13P, Jan. 1969.

[103] M. A. Webster and J. D. Mollon, “Adaptation and the Color Statistics of Natural Images,” vol. 37, no. 23, pp. 3283–3298, 1997.

[104] Y. Mizokami, C. Paras, and M. A. Webster, “Chromatic and contrast selectivity in color contrast adaptation.,” *Vis. Neurosci.*, vol. 21, no. 3, pp. 359–363, 2004.

[105] J. S. Werner and B. E. Schefrin, “Loci of achromatic points throughout the life span,” vol. 10, no. 7, 1993.

[106] P. B. Delahunt, M. A. Webster, L. E. I. Ma, and J. S. Werner, “Long-term renormalization of chromatic mechanisms following cataract surgery,” *Vis. Neurosci.*, vol. 21, no. 3, pp. 301–307, 2004.

[107] I. Fine, H. S. Smallman, P. Doyle, and D. I. A. Macleod, “Visual function before and after the removal of bilateral congenital cataracts in adulthood,” vol. 42, pp. 191–210, 2002.

[108] G. Fechner, *Elemente der Psychophysikin (translated to English in 1966, Elements of Psychophysics. Volume I).* 1851.

[109] K. Pesudovs and N. A. Brennan, “Decreased uncorrected vision after a period of distance fixation with spectacle wear.,” *Optom. Vis. Sci. Off. Publ. Am. Acad. Optom.*, vol. 70, no. 7, pp. 528–531, Jul. 1993.

[110] M. Mon-Williams, J. R. Tresilian, N. C. Strang, P. Kochhar, and J. P. Wann, “Improving vision: neural compensation for optical defocus,” *Proc. R. Soc. B Biol. Sci.*, vol. 265, no. 1390, pp. 71–77, 1998.

[111] M. Rosenfield, S. E. Hong, and S. George, “Blur Adaptation in Myopes,” *Optom. Vis. Sci.*, vol. 81, no. 9, pp. 657–662, 2004.

[112] E. Poulere, J. Moschandreas, G. A. Kontadakis, I. G. Pallikaris, and S. Plainis, “Effect of blur and subsequent adaptation on visual acuity using letter and Landolt C charts: differences between emmetropes and myopes.,” *Ophthalmic Physiol. Opt. J. Br. Coll. Ophthalmic Opt.*, vol. 33, no. 2, pp. 130–137, Mar. 2013.

[113] T. L. Alvarez, E. H. Kim, and B. Granger-Donetti, “Adaptation to Progressive Additive Lenses: Potential Factors to Consider,” *Sci. Rep.*, vol. 7, no. 1, p. 2529, 2017.

[114] K. Pesudovs, “Involvement of neural adaptation in the recovery of vision after laser refractive surgery.,” *J. Refract. Surg.*, vol. 21, no. 2, pp. 144–147, 2005.

[115] R. Sabesan and G. Yoon, “Neural Compensation for Long-term Asymmetric Keratoconic Eyes,” *Vis. Psychophys. Physiol. Opt.*, vol. 51, no. 7, 2010.

[116] P. Artal, “Visual performance and adaptation to changes in wave aberrations,” *J. Vis.*, vol. 4, no. 11, 2004.

[117] L. Sawides and M. Webster, “Adaptation to astigmatic blur,” *J. Vis.*, vol. 10(12), no. 22, pp. 1–15, 2010.

[118] A. R. Hughes, E. A. H. Mallen, and D. B. Elliott, “The Visual Impact of Lens-Induced Astigmatism is Linked to Habitual Axis,” *Optom. Vis. Sci.*, vol. 94, no. 2, p. 260—264, 2016.

[119] A. Ohlendorf, J. Tabernero, and F. Schaeffel, “Neuronal adaptation to simulated and optically-induced astigmatic defocus.,” *Vision Res.*, vol. 51, no. 6, pp. 529–534,

Mar. 2011.

[120] E. A. Villegas and P. Artal, “Spatially resolved wavefront aberrations of ophthalmic progressive-power lenses in normal viewing conditions,” *Optom. Vis. Sci.*, vol. 80, no. 2, pp. 106–114, 2003.

[121] W. W. Sprague, E. A. Cooper, S. Reissier, B. Yellapragada, and M. S. Banks, “The natural statistics of blur,” *J. Vis.*, vol. 16, no. 10, pp. 1–27, 2016.

[122] A. Seidemann and F. Schaeffel, “Effects of longitudinal chromatic aberration on accommodation and emmetropization,” *Vision Res.*, vol. 42, no. 21, pp. 2409–2417, 2002.

[123] S. A. Cholewiak, G. D. Love, and M. S. Banks, “Creating correct blur and its effect on accommodation,” *J. Vis.*, vol. 18, no. 9, pp. 1–29, 2018.

[124] M. Webster, Y. Mizokami, L. Svec, and S. Elliott, “Neural adjustments to chromatic blur,” *Spat. Vis.*, vol. 19, no. 2–4, pp. 111–132, 2005.

[125] R. Descartes, *L’Homme de René Descartes*, 2nd editio. Paris, 1677.

[126] T. Young, “The Bakerian Lecture. On the Mechanism of the eye,” *Philos. Trans. R. Soc.*, pp. 23–88, 1801.

[127] R. Martín Herranz, *Manual de optometría*. 2011.

[128] R. A. Weale, *A biography of the eye : development, growth, aging*. London: H.K. Lewis, 1982.

[129] W. N. Charman, “Developments in the correction of presbyopia I: Spectacle and contact lenses,” *Ophthalmic and Physiological Optics*, vol. 34, no. 1. pp. 8–29, 2013.

[130] W. N. Charman, “Developments in the correction of presbyopia II: Surgical approaches,” *Ophthalmic Physiol. Opt.*, vol. 34, no. 4, pp. 397–426, 2014.

[131] R. Gil-Cazorla, S. Shah, and S. A. Naroo, “A review of the surgical options for the correction of presbyopia,” *Br. J. Ophthalmol.*, vol. 100, no. 1, pp. 62–70, 2016.

[132] C. Benedi-Garcia *et al.*, “Perceptual impact of astigmatism induction in presbyopes,” *Vision Res.*, vol. 165, no. October, pp. 143–151, 2019.

[133] “gurulens.com.” .

[134] B. J. W. Evans, “Monovision: A review,” *Ophthalmic Physiol. Opt.*, vol. 27, no. 5, pp. 417–439, 2007.

[135] P. de Gracia, C. Dorronsoro, and S. Marcos, “Multiple zone multifocal phase designs,” *Opt. Lett.*, vol. 38, no. 18, pp. 3526–3529, 2013.

[136] H. W. Babcock, “The possibility of compensating astronomical seeing,” *Publ. Astron. Soc. Pacific*, vol. 65, no. 386, pp. 229–236, 1953.

[137] P. Marsh, D. Burns, and J. Girkin, “Practical implementation of adaptive optics in multiphoton microscopy,” *Opt. Express*, vol. 11, no. 10, p. 1123, 2003.

[138] P. Godara, A. M. Dubis, A. Roorda, J. L. Duncan, and J. Carroll, “Adaptive optics retinal imaging: Emerging clinical applications,” *Optom. Vis. Sci.*, vol. 87, no. 12, pp. 930–941, 2010.

[139] E. J. Fernández, “Adaptive Optics for Visual Simulation,” *ISRN Opt.*, vol. 2012, pp. 1–13, 2012.

[140] E. Moreno-Barriuso, S. Marcos, R. Navarro, and S. A. Burns, “Comparing laser ray tracing, the spatially resolved refractometer, and the hartmann-shack sensor to measure the ocular wave aberration,” *Optom. Vis. Sci.*, vol. 78, no. 3, pp. 152–156, 2001.

[141] M. Vinas, “Polychromatic Adaptive Optics to evaluate the impact of manipulated optics on vision,” Universidad Complutense de Madrid, 2015.

[142] C. Dainty, *Adaptive Optics for Industry and Medicine*. Imperial College Press, 2008.

[143] P. M. Prieto, E. J. Fernández, S. Manzanera, and P. Artal, “Adaptive optics with a programmable phase modulator: applications in the human eye,” *Opt. Express*, vol. 12, no. 17, p. 4059, 2004.

[144] Z. Zhang, Z. You, and D. Chu, “Fundamentals of phase-only liquid crystal on silicon (LCOS) devices,” *Light Sci. &Amp; Appl.*, vol. 3, pp. 1–10, 2014.

[145] P. de Gracia, “Vision under manipulated aberrations: towards improved multifocal corrections,” Universidad Complutense de Madrid, 2013.

[146] A. Radhakrishnan, “Presbyopia Corrections: Optical, Perceptual and Adaptational Implications Correcciones,” Universidad Complutense de Madrid, 2016.

[147] C. Dorronsoro *et al.*, “Portable simultaneous vision device to simulate multifocal corrections,” *Optica*, vol. 3, no. 8, pp. 918–924, 2016.

[148] C. Dorronsoro *et al.*, “Tunable lenses: dynamic characterization and fine-tuned control for high-speed applications,” *Opt. Express*, vol. 27, no. 3, p. 2085, 2019.

[149] V. Akondi, L. Sawides, Y. Marrakchi, E. Gambra, S. Marcos, and C. Dorronsoro, “Experimental validations of a tunable-lens-based visual demonstrator of multifocal corrections,” *Biomed. Opt. Express*, vol. 9, no. 12, p. 6302, 2018.

[150] “https://www.optotune.com/.” .

[151] R. Navarro, E. Moreno-Barriuso, S. Bará, and T. Mancebo, “Phase plates for wave-aberration compensation in the human eye,” *Opt. Lett.*, vol. 25, no. 4, p. 236, 2000.

[152] R. Kusel and B. Rassow, “Präoperative Abschätzung des mit Intraokularlinsen erreichbaren Sehvermögens,” *Klin. Monbl. Augenheilkd.*, vol. 215, no. 08, pp. 127–131, 1999.

[153] F. Schaeffel and H. Kaymak, “A rapid and convenient procedure to evaluate optical performance of intraocular lenses,” *Photonics*, vol. 1, no. 3, pp. 267–282, 2014.

[154] S. Marcos *et al.*, “VioBio lab adaptive optics : technology and applications by women vision scientists,” vol. 40, pp. 75–87, 2020.

[155] J. Ruiz-Alcocer, D. Madrid-Costa, S. García-Lázaro, C. Albarrán-Diego, and T. Ferrer-Blasco, “Visual simulation through an aspheric aberration-correcting intraocular lens in subjects with different corneal profiles using adaptive optics,” *Clin. Exp. Optom.*, vol. 96, no. 4, pp. 379–384, 2013.

[156] R. Sabesan, L. Zheleznyak, and G. Yoon, “Binocular visual performance and summation after correcting higher order aberrations,” *Biomed. Opt. Express*, vol. 3, no. 12, p. 3176, 2012.

[157] L. Hervella, E. A. Villegas, C. Robles, and P. Artal, “Spherical Aberration Customization to Extend the Depth of Focus With a Clinical Adaptive Optics Visual Simulator,” *J. Refract. Surg.*, vol. 36, no. 4, pp. 223–229, 2020.

[158] J. Tabernero, C. Otero, and S. Pardhan, “A comparison between refraction from an adaptive optics visual simulator and clinical refractions,” *Transl. Vis. Sci. Technol.*, vol. 9, no. 7, pp. 1–9, 2020.

[159] L. Hervella, E. A. Villegas, P. M. Prieto, and P. Artal, “Assessment of subjective refraction with a clinical adaptive optics visual simulator,” *J. Cataract Refract. Surg.*, vol. 45, no. 1, pp. 87–93, 2019.

[160] C. Dorronsoro *et al.*, “Portable simultaneous vision device to simulate multifocal corrections,” *Optica*, vol. 3, no. 8, p. 918, 2016.

[161] P. Studený, J. Hlaváček, R. Chaloupka, Veselý, and A. D. Baxant, “Virtiol – Simulation of vision guality with multifocal and edof intraocular lerses,” *Ces. a Slov. Oftalmol.*, vol. 74, no. 6, pp. 219–225, 2018.

[162] W. Brezna *et al.*, “Psychophysical vision simulation of diffractive bifocal and trifocal intraocular lenses,” *Transl. Vis. Sci. Technol.*, vol. 5, no. 5, 2016.

[163] H.-L. Liou and N. A. Brennan, “Anatomically accurate, finite model eye for optical modeling,” *J. Opt. Soc. Am. A*, vol. 14, no. 8, p. 1684, 1997.

[164] E. Gambra, “Accommodation: Optical Function and Crystalline Lens Imaging,” 2015.

[165] E. Gambra, L. Sawides, C. Dorronsoro, and S. Marcos, “Accommodative lag and fluctuations when optical aberrations are manipulated,” *J. Vis.*, vol. 9, no. 6, pp. 1–15, 2009.

[166] M. Vinas *et al.*, “Comparison of vision through surface modulated and spatial light modulated multifocal optics,” *Biomed. Opt. Express*, vol. 8, no. 4, p. 2055, 2017.

[167] M. Vinas *et al.*, “Pre-operative simulation of post-operative multifocal vision,” *Biomed. Opt. Express*, vol. 10, no. 11, pp. 5801–5817, 2019.

[168] F. C. Delori, R. H. Webb, and D. H. Sliney, “Maximum permissible exposures for ocular safety (ANSI 2000), with emphasis on ophthalmic devices,” *J. Opt. Soc. Am. A*, vol. 24, no. 5, p. 1250, 2007.

[169] American National Standard Institute, “American National Standard for Safe Use of Lasers, Z136.1-2007.” 2007.

[170] American National Standard Institute, “American National Standard for Safe Use of Lasers, ANSI Z136.1-2014,” *American National Standards Institute, Inc.* 2014.

[171] A. K. R. Choudhury, *Characteristics of light sources*. 2014.

[172] S. Raphael and D. I. A. MacLeod, “Mesopic luminance assessed with minimum motion photometry,” *J. Vis.*, vol. 11, no. 9, pp. 1–21, 2011.

[173] A. SM and C. P, “A minimum motion technique for judging equiluminance,” *Acad. Press London*, 1983.

[174] Z.-L. Lu and B. Dosher, *Visual Psychophysics. From laboratory to theory*. MIT Press books, 2014.

[175] S. Marcos and S. A. Burns, “On the symmetry between eyes of wavefront aberration and cone directionality,” *Vision Res.*, vol. 40, no. 18, pp. 2437–2447, 2000.

[176] M. Borgo, A. Soranzo, and M. Grassi, *MATLAB for Psychologist*, vol. 53, no. 9. Springer US, 2013.

[177] D. H. Brainard, “The psychophysics toolbox,” *Spat. Vis.*, vol. 10, no. 4, pp. 433–436, 1997.

[178] A. B. Watson and D. G. Pelli, “Quest: A Bayesian adaptive psychometric method,” *Percept. Psychophys.*, vol. 33, no. 2, pp. 113–120, 1983.

[179] W. J. Dixon and A. M. Mood, “A Method for Obtaining and Analyzing Sensitivity Data,” *J. Am. Stat. Assoc.*, vol. 43, no. 241, pp. 109–126, Mar. 1948.

[180] W. S. Geisler, “Eye movement statistics in humans are consistent with an optimal strategy General probabilistic framework of visual search task,” vol. 8, no. 2008, pp. 1–14, 2010.

[181] A. B. Watson and A. J. Ahumada, “Blur clarified: a review and synthesis of blur discrimination.,” *J. Vis.*, vol. 11, no. 5, pp. 1–30, 2011.

[182] S. Marcos, E. Moreno, and R. Navarro, “The depth-of-field of the human eye from objective and subjective measurements,” *Vision Res.*, vol. 39, no. 12, pp. 2039–2049, 1999.

[183] S. Ravikumar, L. N. Thibos, and A. Bradley, “Calculation of retinal image quality for polychromatic light,” *J. Opt. Soc. Am. A*, vol. 25, no. 10, p. 2395, 2008.

[184] A. van Meeteren, “Calculations on the optical modulation transfer function of the human eye for white light,” *Opt. Acta (Lond).*, vol. 21, no. 5, pp. 395–412, 1974.

[185] R. Legras, Y. Benard, and N. Lopez-Gil, “Effect of coma and spherical aberration on depth-of-focus measured using adaptive optics and computationally blurred images,” *J. Cataract Refract. Surg.*, vol. 38, no. 3, pp. 458–469, 2012.

[186] A. J. Aguila-carrasco, S. A. Read, and D. R. Iskander, “The effect of aberrations on objectively assessed image quality and depth of focus Robert Mont es-Mic o,” vol. 17, no. 2017, pp. 1–15, 2017.

[187] R. C. Bakaraju, K. Ehrmann, E. B. Papas, and A. Ho, “Depth-of-focus and its association with the spherical aberration sign. A ray-tracing analysis,” *J. Optom.*, vol. 3, no. 1, pp. 51–59, 2010.

[188] J. S. McLellan, P. M. Prieto, S. Marcos, and S. A. Burns, “Effects of interactions among wave aberrations on optical image quality,” *Vision Res.*, vol. 46, no. 18, pp. 3009–3016, 2006.

[189] F. J. Ruchker and D. Osorio, “The effects of longitudinal chromatic aberration and a shift in the peak of the middle-wavelength sensitive cone fundamental on cone contrast,” *Vision Res.*, vol. 48, no. 19, pp. 1929–1939, 2008.

[190] P. Artal, C. Li, E. J. Fernandez, B. Singer, S. Manzanera, and R. Williams, “Adaptive optics for vision : The eye’s adaptation to point spread function,” in *Journal of Refractive Surgery*, 2003.

[191] X. Cheng, L. Thibos, and A. Bradley, “Estimating visual quality from wavefront

aberration measurements," *J. Refract. Surg.*, vol. 19, no. 5, 2003.

[192] D. R. Iskander, "Computational aspects of the visual Strehl ratio," *Optom. Vis. Sci.*, vol. 83, no. 1, pp. 57–59, 2006.

[193] M. C. Rynders, R. Navarro, and M. A. Losada, "Objective measurement of the off-axis longitudinal chromatic aberration in the human eye," *Vision Res.*, vol. 38, no. 4, pp. 513–522, 1998.

[194] G. Wyszecki and W. S. Stiles, *Color Science: Concepts and Methods, Quantitative Data and Formulae*. Wiley, 2000.

[195] P. de Gracia, S. Marcos, A. Mathur, and D. A. Atchison, "Contrast sensitivity benefit of adaptive optics correction of ocular aberrations," *J. Vis.*, vol. 11, no. 12, pp. 1–10, 2011.

[196] F. W. Campbell, "The Depth of Field of the Human Eye," *Opt. Acta Int. J. Opt.*, vol. 4, no. 4, pp. 157–164, 1957.

[197] J. L. Pennebaker, William B., Mitchell, *JPEG. Still Image Data Compression Standard*. Springer US, 1993.

[198] F. A. A. Kingdom, J. Bell, C. Haddad, and A. Bartsch, "Perceptual scales for chromatic and luminance blur in noise textures," *J. Vis.*, vol. 15, no. 9, p. 6, 2015.

[199] G. Maiello, L. Walker, P. J. Bex, and F. A. Vera-Diaz, "Blur perception throughout the visual field in myopia and emmetropia," *J. Vis.*, vol. 17, no. 5, pp. 1–13, 2017.

[200] P. B. Kruger and J. Pola, "Stimuli for accommodation: Blur, chromatic aberration and size," *Vision Res.*, vol. 26, no. 6, pp. 957–971, 1986.

[201] S. M. Wuerger, H. Owens, and S. Westland, "Blur tolerance for luminance and chromatic stimuli," *J. Opt. Soc. Am. A*, vol. 18, no. 6, p. 1231, 2001.

[202] J. A. Solomon, "The History of Dipper Functions," *Orientations*, pp. 1–17, 2004.

[203] G. L. Mancil *et al.*, "Optometric clinical practice guideline. Care of the patient with presbyopia," *Am. Optom. Assoc.*, vol. 243 N, 2011.

[204] L. Sawides *et al.*, "Adaptation to astigmatic blur," *J. Vis.*, vol. 10, no. 12, pp. 1–15, 2010.

[205] R. I. Calver, M. J. Cox, and D. B. Elliott, "Effect of aging on the monochromatic aberrations of the human eye," *J. Opt. Soc. Am. A*, vol. 16, no. 9, pp. 2069–2078, Sep. 1999.

[206] C. Coe, A. Bradley, and L. Thibos, "Polychromatic Refractive Error from Monochromatic Wavefront Aberrometry," *Optom. Vis. Sci.*, vol. 91, no. 10, pp. 1167–1174, 2014.

[207] A. P. Venkataraman, A. Radhakrishnan, C. Dorronsoro, L. Lundström, and S. Marcos, "Role of parafovea in blur perception," *Vision Res.*, vol. 138, pp. 59–65, 2017.

[208] R. Dou and M. K. Giles, "Closed-loop adaptive-optics system with a liquid-crystal television as a phase retarder," *Opt. Lett.*, vol. 20, no. 14, p. 1583, 1995.

[209] G. D. Love, "Wave-front correction and production of Zernike modes with a liquid-crystal spatial light modulator," *Appl. Opt.*, vol. 36, no. 7, pp. 1517–1524, 1997.

[210] R. Martínez-cuenca, V. Durán, J. Arines, J. Ares, and Z. Jaroszewicz, “Closed-loop adaptive optics with a single element for wavefront sensing and correction,” *Opt. Lett.*, vol. 36, no. 18, pp. 3702–3704, 2011.

[211] L. N. Thibos and A. Bradley, “Used of liquid-crystal adaptive-optics to alter the refractive state of the eye,” *Optom. Vis. Sci.*, vol. 74, no. 7, pp. 581–587, 1997.

[212] S. Manzanera, P. M. Prieto, D. B. Ayala, J. M. Lindacher, and P. Artal, “Liquid crystal Adaptive Optics Visual Simulator : Application to testing and design of ophthalmic optical elements,” *Opt. Express*, vol. 15, no. 24, pp. 227–230, 2007.

[213] J. Tabernero, C. Schwarz, and E. J. Ferna, “Binocular visual simulation of a corneal inlay to increase depth of focus,” *Vis. Psychophys. Physiol. Opt.*, vol. 52, no. 8, pp. 5273–5277, 2011.

[214] S. Manzanera and P. Artal, “Minimum change in spherical aberration that can be perceived,” *Biomed. Opt. Express*, vol. 7, no. 9, pp. 3471–3477, 2016.

[215] C. Schwarz, S. Manzanera, P. M. Prieto, P. Piers, and P. Artal, “Binocular visual acuity for the correction of spherical aberration in polychromatic and monochromatic light,” *J. Vis.*, vol. 14, no. (2)8, pp. 1–11, 2014.

[216] L. Zhao, N. Bai, X. Li, L. S. Ong, Z. P. Fang, and A. K. Asundi, “Efficient implementation of a spatial light modulator as a diffractive optical microlens array in a digital Shack – Hartmann wavefront sensor,” *Appl. Opt.*, vol. 45, no. 1, 2006.

[217] A. Radhakrishnan, C. Dorronsoro, and S. Marcos, “Differences in visual quality with orientation of a rotationally asymmetric bifocal intraocular lens design,” *J. Cart. Refract. Surg.*, vol. 42, no. 9, pp. 1276–1287, 2016.

[218] C. Dorronsoro, A. Radhakrishnan, P. de Gracia, L. Sawides, and S. Marcos, “Perceived image quality with simulated segmented bifocal corrections,” *Biomed. Opt. Express*, vol. 7, no. 11, pp. 4388–4399, 2016.

[219] H. S. Abdul-rahman, M. A. Gdeisat, D. R. Burton, M. J. Lalor, F. Lilley, and C. J. Moore, “Fast and robust three-dimensional best path phase unwrapping algorithm,” *Appl. Opt.*, vol. 46, no. 26, pp. 6623–6635, 2007.

[220] D. G. Voelz, *Computational fourier optics: a MATLAB tutorial*. SPIE, 2011.

[221] C. Dorronsoro, L. Remon, J. Merayo-lloves, and S. Marcos, “Experimental evaluation of optimized ablation patterns for laser refractive surgery,” *Opt. Express*, vol. 17, no. 17, pp. 3349–3356, 2009.

[222] P. S. Kollbaum, M. E. Jansen, and M. E. Rickert, “Comparison of patient-reported visual outcome methods to quantify the perceptual effects of defocus,” *Contact Lens Anterior Eye*, vol. 35, pp. 213–221, 2012.

[223] C. Dorronsoro *et al.*, “Portable simultaneous vision device to simulate multifocal corrections,” *Optica*, vol. 3, no. 8, p. 918, 2016.

[224] W. H. Ehrenstein and A. Ehrenstein, “Psychophysical metods,” in *Modern Techniques in Neuroscience Research*, E. U. Windhorst, and H. Johansson, Ed. Springer, 1999, pp. 1211–1241.

[225] J. T. Holladay, “Proper method for calculating average visual acuity,” *J. Refract. Surg.*, vol. 13, 1997.

[226] E. LaVilla, M. Vinas, S. Marcos, and J. Schwiegerling, “Freeform Design of Multifocal Zone Plates,” in *Imaging and Applied Optics 2015*, 2015, p. FW3B.3.

[227] R. Davies and M. Kasper, “Adaptive Optics for Astronomy,” *Annu. Rev. Astron. Astrophys.*, vol. 50, no. 1, pp. 305–351, 2012.

[228] M. J. Booth, “Adaptive optical microscopy: The ongoing quest for a perfect image,” *Light Sci. Appl.*, vol. 3, no. January, pp. 1–7, 2014.

[229] A. Glasser and M. C. W. Campbell, “Presbyopia and the optical changes in the human crystalline lens with age,” *Vision Res.*, vol. 38, no. 2, pp. 209–229, 1998.

[230] C. Schwarz, P. M. Prieto, E. J. Fernández, and P. Artal, “Binocular adaptive optics vision analyzer with full control over the complex pupil functions,” *Opt. Lett.*, vol. 36, no. 24, p. 4779, 2011.

[231] M. Lombardo, S. Serrao, N. Devaney, M. Parravano, and G. Lombardo, “Adaptive optics technology for high-resolution retinal imaging,” *Sensors (Switzerland)*, vol. 13, no. 1, pp. 334–366, 2013.

[232] S. Bonora *et al.*, “Multi-actuator adaptive lens for wavefront correction in optical coherence tomography and two-photon excitation fluorescence microscopy (Conference Presentation),” in *Adaptive Optics and Wavefront control for biological systems II*, 2016, vol. 9717, p. 1.

[233] V. Akondi, C. Dorronsoro, E. Gambra, and S. Marcos, “Temporal multiplexing to simulate multifocal intraocular lenses: theoretical considerations,” *Biomed. Opt. Express*, vol. 8, no. 7, p. 3410, 2017.

[234] V. Akondi *et al.*, “Evaluation of the true wavefront aberrations in eyes implanted with a rotationally asymmetric multifocal intraocular lens,” *J. Refract. Surg.*, vol. 33, no. 4, pp. 257–265, 2017.

[235] D. Gatinel, C. Pagnoulle, Y. Houbrechts, and L. Gobin, “Design and qualification of a diffractive trifocal optical profile for intraocular lenses,” *J. Cataract Refract. Surg.*, vol. 37, no. 11, pp. 2060–2067, 2011.

[236] D. Gatinel and Y. Houbrechts, “Comparison of bifocal and trifocal diffractive and refractive intraocular lenses using an optical bench,” *J. Cataract Refract. Surg.*, vol. 39, no. 7, pp. 1093–1099, 2013.

[237] Z. Bouchal, V. Chlup, R. Čelechovský, P. Bouchal, and I. C. Nistor, “Achromatic correction of diffractive dispersion in white light SLM imaging,” *Opt. Express*, vol. 22, no. 10, p. 12046, 2014.

[238] R. Sabesan, K. Ahmad, and G. Yoon, “Correcting highly aberrated eyes using large-stroke Adaptive Optics,” *J. Refract. Surg.*, vol. 23, no. November, pp. 947–952, 2007.

[239] M. Aldaba, A. Giner, Guel, and J. Pujol, “Visual performance evaluation of a new multifocal intraocular lens design before implantation,” in *European Society of Cataract & Refreactive Surgeons*, 2014.

[240] D. Fernández, S. Barbero, C. Dorronsoro, and S. Marcos, “Multifocal intraocular lens providing optimized through-focus performance,” vol. 38, no. 24, pp. 5303–5306, 2013.

[241] D. Gatinel, C. Pagnoulle, Y. Houbrechts, and L. Gobin, “Design and qualification of

a diffractive trifocal optical profile for intraocular lenses," *J. Cataract Refract. Surg.*, vol. 37, no. 11, pp. 2060–2067, 2011.

[242] S. Wahl, C. Song, and A. Ohlendorf, "Comparison of two devices to simulate vision with intraocular lenses," *Clin. Ophthalmol.*, vol. 13, pp. 123–130, 2019.